



UNIVERSITÀ DEGLI STUDI DI NAPOLI
FEDERICO II

Scuola Politecnica e
delle Scienze di Base



Università degli Studi di Napoli Federico II
Dottorato di Ricerca in
Ingegneria Strutturale, Geotecnica e Rischio Sismico
THESIS FOR THE DEGREE OF DOCTOR OF PHILOSOPHY

**Structural behaviour and fragility evaluation
of existing prestressed concrete bridge decks
under traffic loads**

by
Giacomo Miluccio

Advisor: Prof. Fulvio Parisi



Scuola Politecnica e delle Scienze di Base
Dipartimento di Strutture per l'Ingegneria e l'Architettura

Dedication
or
Some quote

Structural behaviour and fragility evaluation of existing prestressed concrete bridge decks under traffic loads

Ph.D. Thesis presented
for the fulfilment of the Degree of Doctor of Philosophy
in Ingegneria Strutturale, Geotecnica e Rischio Sismico
by
Giacomo Miluccio

March 2023



Approved as to style and content by

Prof. Fulvio Parisi, Advisor

Università degli Studi di Napoli Federico II
Ph.D. Program in Ingegneria Strutturale, Geotecnica e Rischio Sismico
XXXV cycle - Chairman: Prof. Iunio Iervolino



www.dist.unina.it/dottorati-di-ricerca/dottorati

Candidate's declaration

I hereby declare that this thesis submitted to obtain the academic degree of Philosophiæ Doctor (Ph.D.) in Ingegneria Strutturale, Geotecnica e Rischio Sismico is my own unaided work, that I have not used other than the sources indicated, and that all direct and indirect sources are acknowledged as references. Parts of this dissertation have been published in international journals and/or conference articles (see list of the author's publications at the end of the thesis).

Napoli, March 9, 2023

Giacomo Miluccio

Abstract

Despite prior research on the seismic fragility of existing bridges, recent collapses highlight the need to evaluate their vulnerability under gravity loads. Following the collapse of the Morandi highway bridge in Genova in 2018, the Italian government announced new guidelines (GL) for prioritising safety checks and retrofit actions on existing bridges. Those guidelines provided new traffic load models (TLMs) that may be used for existing bridges in the event of non-compliant safety checks according to the Italian building code (NTC).

The initial purpose of this thesis is to examine a class of simply supported, beam-type prestressed concrete (PC) bridge decks built in Italy between 1970 and 1980. Based on data available in the literature and those collected on real bridges by the authors, a subset of random variables (RVs) was modelled through probability distributions, whereas other RVs were assumed to be statistically dependent upon the former RVs according to regression models. A sensitivity analysis was done in the first stage to identify the RVs that most impact the structural response. Those variables were then probabilistically modelled and propagated through fragility analysis to assess the conditional failure probability of the selected bridge decks given a traffic load intensity. The Monte Carlo sampling approach was then implemented in MATLAB, assuming geometric, material, and load properties as RVs as well as capacity model uncertainty, to randomly produce deck models and evaluate their traffic-load fragility. A fragility study was performed to examine the levels of vulnerability of existing Italian bridges under different load patterns according to GL and NTC provisions. In addition to a defined TLM, the sensitivity of fragility to bridge usage restrictions, such as reduced distance of external load lane from kerb or reduced number of lanes, was assessed to support decision-making by road management companies. Furthermore, using a European weigh-in-motion database and the convolution of fragility and hazard, the yearly failure probability of the selected bridges was computed. Analysis results demonstrate that structural fragility is greatly affected by the load pattern, indicating that more realistic vehicle models should be designed to attain the goal safety level required by current construction regulations. The complete process is incorporated in a software to simplify application and determine fragility for a single bridge or a portfolio of bridges. In addition, a safety cross section module is used to assess structural safety of individual case-study decks.

The thesis ends with a progressive collapse study of a 1:5 simply supported post tensioned PC bridge deck consisting of four beams, four cross girders, and a continuous RC slab. The analyses were carried out with the Extreme Loading for Structures software. The structural behaviour of a PC bridge deck is heavily impacted by the type of cross girder used. As a result, three types of cross girders are considered: (i) normal cross girders separated from the RC slab; (ii) prestressed cross girders separated from the RC slab; and (iii) normal cross girders connected to the RC slab. The results of the study reveal that cross girders can be employed as segmentation fuses in the bridge deck in some instances to bring the entire deck to a specific type of collapse. These analyses may also be used to create an experimental test on a PC bridge deck and validate the results in order to inform the design of bridge decks and cross girders.

Keywords: Existing prestressed concrete bridges, fragility analysis, new Italian bridge guidelines, bridge management, failure probability, progressive collapse.

Sintesi in lingua italiana

I recenti crolli dei ponti esistenti evidenziano la necessità di valutarne la vulnerabilità anche per carichi gravitazionali. A seguito del crollo del ponte Morandi a Genova nel 2018, il governo italiano ha annunciato nuove linee guida (LG). Le LG hanno fornito nuovi modelli di carico di traffico (MT) che possono essere utilizzati per i ponti esistenti in caso di verifiche di sicurezza non conformi agli standard delle norme tecniche per le costruzioni (NTC).

La tesi ha come primo scopo quello di esaminare la classe di impalcati da ponte in calcestruzzo armato precompresso (PC) del tipo a travi semplicemente appoggiate costruiti in Italia tra il 1970 e il 1980. Sulla base dei dati disponibili in letteratura e di quelli raccolti dagli autori su ponti reali, un sottoinsieme di variabili è stato modellato attraverso distribuzioni di probabilità, mentre si è ipotizzato che le restanti variabili fossero statisticamente dipendenti dalle precedenti secondo modelli di regressione. Inizialmente è stata definita un'analisi di sensibilità per identificare le variabili che maggiormente incidono sulla risposta strutturale. È stato quindi implementato in MATLAB l'approccio Monte Carlo per il campionamento delle variabili aleatorie, assumendo le geometrie, i materiali ed i carichi, nonché le incertezze del modello di capacità come tali, al fine di generare i modelli di impalcato e valutare la loro fragilità verso i carichi da traffico. È stato eseguito uno studio di fragilità per valutare la vulnerabilità dei ponti italiani esistenti verso i MT forniti da LG e NTC. Definito il MT, è stata valutato l'effetto delle restrizioni d'uso del ponte, come la distanza della corsia di carico più esterna dal marciapiede o il numero ridotto di corsie. Inoltre, utilizzando un database europeo di pesatura dinamica dei flussi di traffico ed applicando la convoluzione di fragilità e rischio, è stata calcolata la probabilità di collasso annuale dei ponti studiati. I risultati dell'analisi dimostrano che la fragilità è fortemente influenzata dal MT, indicando che dovrebbero essere definiti MT più realistici per raggiungere il livello di sicurezza richiesto dalle NTC. L'intera metodologia è stata quindi integrata in un software per semplificarne l'applicazione e determinare la fragilità di un singolo ponte o di una classe di ponti.

La tesi si conclude con un'analisi di collasso progressivo di un impalcato da ponte in PC post-teso in scala 1:5 semplicemente appoggiato con quattro travi, quattro traversi e una soletta continua in c.a. Le analisi sono state svolte con il software Extreme Loading for Structures. I risultati delle analisi mostrano che il comportamento strutturale è fortemente influenzato dalla tipologia di traversi utilizzati. Quindi, vengono considerati tre tipi di traversi: precompressi e non precompressi separati dalla soletta in c.a., e traversi non precompressi collegati alla soletta in c.a. I risultati dello studio rivelano che in alcuni casi i traversi possono essere impiegati come fusibili nell'impalcato da ponte per portare l'intero impalcato ad uno specifico meccanismo di collasso. Queste analisi possono anche essere utilizzate per la progettazione di un test sperimentale su un impalcato da ponte e convalidare i risultati ottenuti dalle analisi, al fine di aggiungere ulteriori dettagli per la progettazione degli impalcati da ponte e dei traversi.

Parole chiave: ponti in cemento armato precompresso, analisi di fragilità, nuove linee guida sui ponti, gestione dei ponti esistenti, probabilità di collasso, collasso progressivo.

Acknowledgements

This work was developed in the framework of PON INSIST (Sistema di monitoraggio INtelligente per la SICurezza delle infraSTruttute urbane) research project, which was funded by the Italian Ministry for Education, University and Research (Programma Operativo Nazionale “Ricerca e Innovazione 2014–2020”, Grant No. ARS01_00913).

The financial support by the Italian Consortium of University Laboratories of Earthquake and Structural Engineering (ReLUIIS) is also gratefully acknowledged.

List of Tables

Table 1. Traffic load model according to current Italian code.....	- 18 -
Table 2. Mechanical properties of steel by RD 2229/1939 (“RD 16/11/1939, n. 2229. Norme per l’esecuzione delle opere in conglomerato cementizio semplice od armato (in Italian)” 1939).	- 21 -
Table 3. Provisions of DM 30/05/1972 (Italian High Council of Public Works 1972) for prestressing steel.	- 23 -
Table 4. Provisions of DM 30/05/1972 (Italian High Council of Public Works 1972) for mild reinforcing steel.	- 23 -
Table 5. Distributions and statistics of independent RVs for periods 1960–1970 and 1970–1980.....	- 47 -
Table 6. Regression models.	- 50 -
Table 7. Summary of RV estimates used in sensitivity analysis.....	- 57 -
Table 8. Fragility parameters corresponding to flexural failure, shear failure, and ULS.-	66 -
Table 9. Mean, standard deviation and CoV of lognormal distributions representative of flexural demand and capacity.....	- 68 -
Table 10. Mean, standard deviation and CoV of lognormal distributions representative of <i>DCR</i>	- 69 -
Table 11. Fragility estimates derived through frequentist approach and convolution at multiple IM levels.	- 69 -
Table 12. Fragility curve parameters under varying mean value and CoV of $f_{p,01}$... -	71 -
Table 13. Fragility parameters, coefficient of determination and code-related fragility corresponding to NTC-TLM and GL-TLM under varying x_0	- 75 -
Table 14. Fragility parameters, coefficient of determination and code-related fragility corresponding to different codes and numbers of load lanes.	- 79 -
Table 15. Distributions and statistics of random variables.	- 101 -
Table 16. Loading scenarios considered for the case-study.....	- 103 -
Table 17. Fragility parameters, coefficient of determination and code-related fragility corresponding to loading scenarios.....	- 104 -
Table 18. Girder safety check results.....	- 106 -

List of Figures

Figure 1. Koenen’s settings for the steel bars tensioning.....	- 6 -
Figure 2. Freyssinet’s anchor system.....	- 8 -
Figure 3. Magnel’s anchor system.....	- 9 -
Figure 4. Colonnetti’s anchor system.....	- 11 -
Figure 5. Morandi’s anchor system.....	- 13 -
Figure 6. Traffic loads for Italian bridges implemented in the Normale of 1945 (Italian High Council of Public Works 1945).	- 13 -
Figure 7. Traffic loads for Italian bridges implemented in the Circ. CSLLPP 384/1962 (Italian High Council of Public Works 1962).	- 15 -
Figure 8. Traffic loads for Italian bridges implemented in the DM 02/08/1980 (Italian Ministry of Infrastructures and Transportation 1980).	- 16 -
Figure 9. Traffic loads for Italian bridges implemented in the DM 04/05/1990 (Italian Ministry of Infrastructures and Transportation 1990).	- 17 -
Figure 10. Longitudinal view of GL-TLMs (dimensions in m): (a) heavy, (b) medium and (c) light GL-TLM.	- 20 -
Figure 11. Vertical collapse mechanisms of bridge foundations: (a) undermining of pile; (b) buckling of pile; (c) penetration of friction pile tip; (d) undermining of footing base	- 29 -
Figure 12. Bridge bearings damage in Wenchuan earthquake: (a) Longwei Bridge, (b) Huilan ramp Bridge (Han et al. 2009).	- 35 -
Figure 13. Single span (a-b) and multi-span (c) masonry arch bridge collapse mechanisms.....	- 36 -
Figure 14. Static scheme for each decade: a) 1950s, b) 1960s, c) 1970s, d) 1980s (Galano et al. 2020).	- 40 -
Figure 15. Probability distributions for concrete compressive strength: (a) 1960–1970; (b) 1970–1980.....	- 42 -
Figure 16. Probability distribution for reinforcing steel yield strength: (a) 1960–1970; (b) 1970–1980.....	- 43 -
Figure 17. Probability distribution for conventional yield strength of prestressing steel.-	43 -
Figure 18. Cross sections of (a) half bridge deck and (b) longitudinal girder.	- 45 -
Figure 19. Probability distribution of girder length.	- 46 -
Figure 20. Flowcharts of (a) sensitivity analysis and (b) fragility analysis.	- 52 -
Figure 21. Deck cross section of bridge deck with traffic load lanes (first lane at x_0 from kerb).....	- 54 -
Figure 22. Sensitivity of bending moment capacity.....	- 58 -
Figure 23. Shear strength according to different capacity models.....	- 59 -

Figure 24. Sensitivity of shear capacity $V_{r,2}$	- 60 -
Figure 25. Sensitivity of demand-to-capacity ratios: (a) DCR_f ; (b) DCR_s	- 61 -
Figure 26. Simulated design: (a) increase in traffic load effects between NTC 2018 and Circ. CSLLPP 384/1962; (b) safety factor considering traffic loads provided by Circ. CSLLPP 384/1962.	- 64 -
Figure 27. Fragility curves associated with flexural and shear failure modes: (a) discrete distribution of prestressing ratio; (b) uniform distribution of prestressing ratio.	- 66 -
Figure 28. Collapse fragility curve of case-study bridges.....	- 67 -
Figure 29. Bending moment distributions: (a) capacity, (b) demand given $\square = 1$, (c) overlapping of capacity and demands corresponding to multiple load intensities... -	- 68 -
Figure 30. DCR distribution under varying IM level.	- 69 -
Figure 31. Traffic-load fragility curves under varying (a) mean value and (b) CoV of $f_{p,01}$	- 70 -
Figure 32. Comparison between fragility curves with or without consideration of model uncertainty (case of maximum number of load lanes and NTC-TLM).....	- 73 -
Figure 33. Fragility curves corresponding to the maximum number of load lanes: (a) NTC-TLM; (b) GL-TLM; (c) comparison between fragility curves under $0 \leq x_0 \leq 1$ m. -	- 74 -
Figure 34. Fragility curves corresponding to NTC-TLM under varying number of load lanes n_l : (a) $x_0 = 0$; (b) $x_0 = 1.0$ m; (c) $x_0 = 2.0$ m.	- 76 -
Figure 35. Fragility curves corresponding to heavy GL-TLM under varying number of load lanes n_l : (a) $x_0 = 0$; (b) $x_0 = 1.0$ m; (c) $x_0 = 2.0$ m.	- 77 -
Figure 36. Fragility curves corresponding to the maximum number of load lanes n_l and remaining load r_l under varying x_0 : (a) medium GL-TLM; (b) light GL-TLM.....	- 80 -
Figure 37. Median value of fragility curves under varying number of load lanes, transverse eccentricity and TLM: (a) $r_l = 1$; (b) $r_l = 0$	- 81 -
Figure 38. Dispersion of fragility curves under varying number of load lanes, transverse eccentricity and TLM: (a) $r_l = 1$; (b) $r_l = 0$	- 82 -
Figure 39. Main Q-BRIDGE GUI window.....	- 90 -
Figure 40. Data import and pre-processing GUI's window: (a) <i>User-Defined Probability Distributions</i> and (b) <i>User-Defined Regression Models</i> features.	- 92 -
Figure 41. Definition of the whole variables through the Uncertainty model GUI's module.....	- 94 -
Figure 42. Definition of the number of analysed models, the mean bridge and fragility analysis results through the <i>Fragility Analysis</i> GUI's module.	- 95 -
Figure 43. Type transversal bridge cross-section implemented in the Q-BRIDGE software.....	- 96 -
Figure 44. <i>Girder-Section Safety Check</i> module.....	- 97 -
Figure 45. Bridge deck and girder cross-section of the case study.	- 99 -

Figure 46. Fragility curves corresponding to: (a) NTC 2018-TLM with $x_0 = 0$ and $n_l = 3$, (b) GL – 5 axes – 440kN with $x_0 = 0$ and $n_l = 5$, (c) GL – 5 axes – 440kN with $x_0 = 1$ and $n_l = 5$, (d) GL – 3 axes – 260kN with $x_0 = 0$ and $n_l = 5$ - 103 -

Figure 47. GUI panel for deck, girder and prestressing cables geometries and materials adopted for girder safety check. - 105 -

Figure 48. GUI panel for girder safety check results for scenario n. 2. - 106 -

Figure 49. Top and bottom view of the simply supported post tensioned PC bridge deck. - 109 -

Figure 50. Mid-span beam cross section. - 111 -

Figure 51. Bridge deck and cross girders cross sections considering: (a) prestressed cross girders separated from RC slab; (b) cross girders separated from RC slab; (c) cross girders connected to RC slab. - 112 -

Figure 52. (a) Element generation for AEM, (b) spring distribution and area of influence of each pair of springs, (c) element shape, contact point and degrees of freedom ((K Meguro and Tagel-Din 1997; Kimiro Meguro and Tagel-Din 2002; Meguroi and Tagel-Din 2000; TAGEL-DIN and MEGURO 2000)..... - 114 -

Figure 53. Principal stress determination (K Meguro and Tagel-Din 1997; TAGEL-DIN and MEGURO 2000) - 117 -

Figure 54. Flow chart of applied element method analysis (TAGEL-DIN and MEGURO 2000). - 119 -

Figure 55. Numerical models: (a), (b) 1D and 2D FEM with SAP2000, (c) 3D FEM with Abaqus and (d) 3D AEM with ELS (Galano et al. 2023). - 121 -

Figure 56. ELS prestressed concrete beam model. - 122 -

Figure 57. ELS prestressed concrete bridge deck model. - 125 -

Figure 58. Constitutive models for concrete (ASI 2020; Maekawa and Okamura 1983)- 127 -

Figure 59. (a) specimens after casting, (b) geometry of the generic tested samples (longitudinal view and cross sections, measures are in mm)(Galano et al. 2023). - 128 -

Figure 60. Experimental-numerical comparison: force-displacement curves (Galano et al. 2023). - 129 -

Figure 61. Contours plots at ultimate response of the girders: (a) plastic hinges response for 1D FEAs, (b) stresses in the shells for 2D FEAs, (c) tension damages for 3D FEAs, (d) axial tensile strains in 3D AEAs (Galano et al. 2023)..... - 131 -

Figure 62. Numerical error coefficients and standard deviations related to each numerical model (Galano et al. 2023)..... - 132 -

Figure 63. Comparison between single beam and bridge deck (divided by the number of beams' deck) force-displacement response curves. - 133 -

Figure 64. PC bridge deck force-displacement response curve. - 135 -

Figure 65. RC slab sections to derive the bending moment envelope. - 136 -

Figure 66. PC bridge deck with prestressed cross girders separated from RC slab (a) force-displacement curve, (b) 3D model when the first drop (i.e., the first drop in the F_v - δ_v curve) occurs, (c) 3D model when the collapse occurs and (d) normalised F_v - δ_v and M - δ_v envelope curves. - 138 -

Figure 67. PC bridge deck with cross girders separated from RC slab (not prestressed) (a) force-displacement curve, (b) 3D model when the first drop (i.e., the first drop in the F_v - δ_v curve) occurs, (c) 3D model when the collapse occurs and (d) normalised F_v - δ_v and M - δ_v envelope curves. - 140 -

Figure 68. PC bridge deck with cross girders connected to RC slab (not prestressed) (a) force-displacement curve, (b) 3D model when the first drop (i.e., the first drop in the F_v - δ_v curve) occurs, (c) 3D model when the collapse occurs and (d) normalised F_v - δ_v and M - δ_v envelope curves. - 142 -

Contents

Abstract.....	i
Sintesi in lingua italiana.....	ii
Acknowledgements.....	iii
List of Tables	iv
List of Figures	v
1. Introduction.....	- 1 -
1.1. Framework and motivations of the study.....	- 1 -
1.2. Research objectives	- 3 -
1.3. Outline of the thesis	- 5 -
2. State-of-the-art on existing concrete bridges.....	- 6 -
2.1. Main types and technologies of concrete bridges	- 6 -
2.2. Evolution of technical codes for structural design and assessment	- 13 -
2.3. Evolution of standards and codes for materials and structural detailing of bridges.....	- 20 -
2.4. Failure modes and structural issues of existing bridges.....	- 23 -
3. Data collection and statistical analysis of existing roadway bridges.....	- 38 -
3.1. Statistical analysis of bridge types	- 38 -
3.2. Probability distributions and statistics of material properties	- 40 -
3.3. Probability distributions and statistics of geometric properties	- 44 -
3.4. Correlations between geometric properties.....	- 47 -
4. Structural performance assessment of existing prestressed concrete bridge decks under traffic loads	- 51 -
4.1. Structural modelling for fast simulations.....	- 53 -
4.2. Capacity modelling for bending and shear.....	- 55 -
4.3. Sensitivity analysis.....	- 56 -
4.4. Fragility analysis under code-based traffic loads.....	- 61 -
4.5. Fragility analysis under traffic loads according to new Italian guidelines	- 71 -
4.6. Development of software for fragility analysis and code-compliant safety checks of decks	- 86 -
4.6.1. Data import and pre-processing module	- 90 -
4.6.2. Uncertainty modelling module.....	- 93 -
4.6.3. Fragility Analysis module	- 94 -

4.6.4. Girder-Section Safety Check module.....	- 96 -
4.6.5. Application to a case-study bridge	- 99 -
5. Progressive collapse analysis of prestressed concrete bridge decks-	108
-	
5.1. Description of case study	- 108 -
5.2. Structural modelling via applied element method.....	- 113 -
5.3. Discussion of results.....	- 127 -
6. Conclusions and future perspectives	- 143 -
References	- 149 -

Introduction

1.1. Framework and motivations of the study

Bridges are a vital piece of civil infrastructure that must be maintained against different hazards in order to prevent socioeconomic losses caused by future damaging occurrences and ensure our society's sustainability and resilience. Nonetheless, the attainment of significant performance targets (such as life safety and collapse prevention) is hampered by a number of circumstances, including the presence of numerous bridges that are nearing or have already exceeded their nominal service life. Indeed, a large number of bridges were built beginning in the 1960s, which were a boom time for highway development in several nations, including the United States of America, France, Germany, and Italy. The first motorway in this latter nation, the "Autostrada del Sole," which connects Milan to Naples from north to south and is around 760 kilometres long, required the building of 853 bridges and 572 overpasses. Currently, one bridge every two kilometres marks the Italian infrastructure system, the majority of which are reinforced concrete (RC) and prestressed concrete (PC) constructions. In the last years, several bridge collapses were occurred in Italy. One of the most impactful failures is related to the Polcevera Viaduct, in Genoa (Italy). On August 14th, 2018, a portion of it collapsed killing 43 people. The bridge was constructed in 1967, and its collapse after 51 years of service served as a reminder of the bad state of infrastructure and maintenance of mid-century bridges in Italy. This bridge was the final section of the A10 highway, which connects Italy to the south of France. The viaduct was built to cross the valley of the Polcevera stream in order to increase city traffic and links with the commercial port. Thus, its collapse had an enormous impact on the economy and city life. Furthermore, other recent bridges failures in Italy must be noted as well. The bridge between Annone and Cesana Brianza, for example, fell on October 28th, 2016, when a vehicle carrying steel coils was passing, while the viaduct on the Fossano ring road collapsed unexpectedly on April 17th, 2017, in the absence of travelling loads (Clemente 2020). But not only Italy was affected by bridge failures, indeed many tragic events also hit China and USA for example. In this regard, another example is the 2007 catastrophic collapse of the I-35W Bridge in Minneapolis, Minnesota.

The bridge went into operation in 1967. It is a continuous truss-arched bridge with a total length of 581 metres and a width of 34.1 metres. Its greatest span was 139 metres long, and it transported 140,000 automobiles across the Mississippi River. The bridge collapse occurred during peak traffic hours. It included 117 automobiles, killed 13 people, and wounded 145 others. The bridge earned a "poor" condition grade in 1991 and again in 2006 (Salem and Helmy 2014). Inspectors' findings during the 2006 examination identified flaws such as inadequate weld details, corrosion, connection sway, fading paint, surface rust, and section loss in numerous parts, such as the main truss members, cross beams and rocker bearings (National Transportation Safety Board (NTSB) 2007). In China several disasters were happened in last years. On October 23, 2007, three heavily loaded vehicles caused a bridge in Baotou to topple and collapse (W. Peng et al. 2014). Moreover, the Chunhui bridge overpass in Shangyu, Zhejiang, China, fell on February 21, 2011. Four trucks crashed into the road, injuring three people (W. Peng et al. 2014). Several bridges were also damaged as a result of support disengagement caused by overweight vehicles travelling on one side. For example, on May 26, 2016, one-sided heavy cars triggered support disengagement on a bridge on the Shanghai Middle Ring Line; luckily, no collapse occurred (Ding 2016).

Therefore, several disasters, approximately 80% of which were caused by vehicle overloads and collisions, floods, and environmental degradation, have highlighted the presence of outdated transportation infrastructure and the consequent need for a major disaster risk reduction programme involving existing bridges (Cook et al. 2015; Deng et al. 2016; Wardhana and Hadipriono 2003). In this regard, a multi-scale approach is required in order to investigate the existing bridges by considering a regional scale (i.e., ten thousand bridges involved in the evaluation of their vulnerability subjected to different hazards) or a site-specific scale, where a specific case study is taken into account (for bridges with the most critical conditions). In this regard, some guidelines were developed to deal with this problem and in particular, in Italy, the Polcevera bridge collapse heightened public concern about the structural safety of existing bridges, prompting the High Council of Public Works to publish guidelines (abbreviated as GL hereafter) for risk-based classification, safety checks, and monitoring of existing bridges in April 2020. (Cosenza and Losanno 2021; Di Prisco 2019; Italian High Council of Public Works 2020; Nuti et al. 2020). On December 17,

2020, those guidelines became mandatory for Italian existing bridges, according to a ministerial decree (Italian Ministry of Infrastructures and Transportation 2020). GL provisions also introduced new traffic load models (TLMs) according to the Italian road code (Italian Ministry of Infrastructures and Transportation 1992), which provides different allowable vehicle classes on Italian roadways with corresponding maximum axles weight, gross vehicle weight and length. As opposed to modern code provisions (Comité Européen de Normalisation 2003; Italian Ministry of Infrastructures and Transportation 2018), GL (Italian High Council of Public Works 2020) include TLMs that were developed within a deterministic framework since no data from actual distributions of traffic loads were available for Italy. This resulted in different values of the corresponding partial safety factors depending upon the traffic control system imposed by the road management companies. Further details about the methodology and safety checks of Italian guidelines for existing bridges can be found in the paper by Cosenza and Losanno (Cosenza and Losanno 2021).

Therefore, the structural safety of existing bridges to traffic loading needs to be investigated, starting from a probabilistic analysis of decks and then moving to bearings and other components of the bridge structure. The assessment of existing bridges under traffic loads should take into account the following features:

- i. Traffic load conditions have been changing over time, so the structural design of bridges was carried out by assuming TLMs that are different from those prescribed by current code provisions.
- ii. Structural materials used in the past do not comply with modern building codes, hence requesting an appropriate modelling of their mechanical properties.

1.2. Research objectives

The first goal of this study is to investigate the structural fragility of existing Italian bridges subjected to traffic loads, based on code-conforming capacity models and analysis procedures (Italian Ministry of Infrastructures and Transportation 2018). Specifically, assuming code-conforming load patterns on the bridge deck, including GL provisions (Italian High Council of Public Works 2020) and limitations on the use of the carriageway to compare corresponding

safety levels, fragility is herein defined as the conditional probability of exceeding a damage state given the traffic load intensity. A class of simply supported, beam-type, PC bridges is considered, because they represent more than 90% of the Italian bridge stock (Borzi et al. 2015). Previous studies also reported that the time frame 1960–1980 is the period when the highest number of bridges were built due to the Italian economic growth and infrastructure development (see, e.g., (Borzi et al. 2015; Cardone et al. 2011; Pinto and Franchin 2010)). Therefore, based on available data collected by the authors on real case-study bridges, this study focuses on the traffic-load fragility of bridges built in the period 1970–1980. A sensitivity analysis was performed to assess the influence of different geometric and mechanical properties on the structural performance, whereas a validation of the simulated design process confirms the representativeness of adopted bridge models. The study is focused on the global structural behaviour of the deck with no consideration of local failure modes (e.g., slabs, bearings) and material deterioration. Furthermore, a preliminary evaluation of the unconditional collapse failure probability is discussed through the convolution of fragility and hazard. In that computation, traffic-load stochastic properties reported in the literature (Maljaars 2020) were adopted. Therefore, engineers, roadway management companies, and decision-makers may use the fragility models presented in this study in national/regional risk assessments of highway bridges. These assessments provide quantitative data for subsequent prioritisation schemes where the most crucial bridges are identified for more in-depth analysis and, if necessary, structural retrofitting.

Finally, using the applied element method (AEM), a 1:5 scaled simply supported bridge deck with post tensioned PC, four beams, four cross girders, and a continuous RC slab is modelled. This system's main benefit is its capability to track structural behaviour from the first loading phases to ultimate collapse in a manageable amount of CPU time. The 3D bridge deck model is implemented into the Extreme Loading for Structures (ELS) software in order to evaluate the influence of cross girders on the structural behaviour and collapse mechanism. Three different cross girder types are taken into account for a nonlinear analysis with displacement control: (i) prestressed cross girders separated from RC slab, (ii) cross girders separated from RC slab (not prestressed), (iii) cross girders connected to RC slab (not prestressed). Determining how the type of cross girders affects structural behaviour and collapse process is the purpose of this study.

These analyses may also be used to create an experimental test on a PC bridge deck and validate the results in order to add additional details to the design of bridge decks and cross girders to the current code provisions.

1.3. Outline of the thesis

This thesis is organized in five Sections. The first one introduces the framework and main goals of this study; the second chapter is based on the state of art of existing concrete bridges and describes the technologies of concrete bridges. In this regard, different techniques about prestressing, from first decades of 1900, are depicted. Furthermore, the evolution of technical codes for structural design and codes for materials and structural detailing of bridges in Europe is described with a focus on the Italian codes (from 1933 up to nowadays). Besides, in the final part of this chapter failure modes and structural issues of existing bridges are investigated by considering a literature review about main causes and consequences of bridge collapses. Then, the third Section is based on statistics about existing Italian bridges, indeed, in the first paragraph statistical analysis of bridge types is conducted. Therefore, based on literature review and data collected by authors the probability distributions and statistics of material and geometric properties are presented. In the end, the correlation (i.e., regression models) between geometric properties are evaluated. The fourth Section describes the modelling approach and capacity models used in order to carry out sensitivity and fragility analyses. In this regard, the sensitivity analysis is conducted to identify the random variables that most impact the structural response, which were then taken into account in the fragility analysis for the ultimate limit state. Therefore, fragility analyses are carried out by adopting code-based traffic loads and traffic loads according to new Italian guidelines. In these paragraphs using a European weigh-in-motion database and the convolution of fragility and hazard, the yearly failure probability of chosen bridges is computed. The whole methodology is, then, implemented in a software that is described in the last paragraph of the fourth chapter. The last Section of this thesis presents a progressive collapse analysis of a 1:5 simply supported post tensioned PC bridge deck. The case study is depicted in the first paragraph, whereas the structural modelling is described in the second one. In the end, the analyses and discussion of results are reported in the last paragraph.

State-of-the-art on existing concrete bridges

2.1. Main types and technologies of concrete bridges

The first proposal to have the prestressed concrete was made by P.H. Jackson in 1886, who obtained a patent for the reinforcement of vaulted reinforced concrete elements with tensioned parts (US patent 375-999, San Francisco, California, (Billington 1976)).

In 1888 W. Dohrung presented a patent (DRP 53-548, Berlin, Germany) which provided for a prestressing on the bench, with the aim of increasing the resistance of floor rafters through the pretension of the reinforcement, made up of steel wires. Probably the first proposal for the construction of prefabricated concrete parts.

In 1906 M. Koenen, again in Berlin, carried out tests on the concrete reinforcement under tension (Figure 1). In 1907, Koenen attempted to carry out an experimental verification based on Dohrung's ideas.

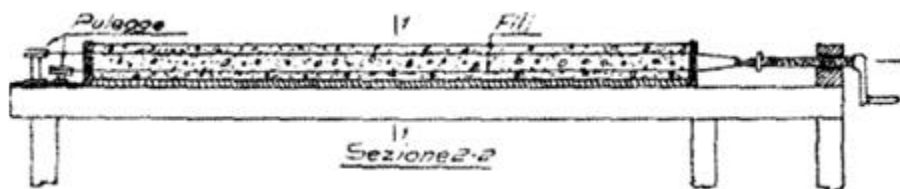


Figure 1. Koenen's settings for the steel bars tensioning.

Such studies were carried out by several other figures and new patents were published. However, there were no practical applications and the technique was not successful. This is because much of the prestress impressed on the moving elements is lost over time. At that time, the first prestressed elements that were designed, worked well in the initial phase, but over time they showed cracks and sometimes broke. This is because low strength steel is used on the prestressing elements, which it was impossible to apply great prestress. Furthermore, slow phenomena such as shrinkage and creep were not yet known. All over time and in many cases the prestress was almost zero after a few months (Billington 1976).

In 1919 K. Wettstein produced thin concrete slabs with high tensioned piano strings.

Even without knowing in advance the slow phenomena in concrete and steel, Wettstein was the first subject to use high-strength steel under heavy stress (Sanabra-loewe and Capellà-Ilovera 2014). The process of using piano strings for prestressing was then later resumed by Ewald Hoyer in 1939, who used it in the joists of prefabricated floors.

The fundamental concepts necessary for the sequential success and development of prestressing were established by the studies and research of the French engineer Eugène Freyssinet. He was the first to theorize that the use of high-strength steel was necessary for successful prestressing. Already in 1924 he used the prestressing technique to reduce the elongation of the tie rods used in large-span warehouses. Subsequently, in 1928 he patented a prestressing system with steel tensions higher than 400 MPa (Billington 1976; Sanabra-loewe and Capellà-Ilovera 2014). Freyssinet was studying the causes of stress decreases in prestressed parts over time (falls and losses), through his research on shrinkage and creep, allowing the application of prestress in structural concrete. Freyssinet also developed a system for anchoring the prestressing wires using a wedge system. He designed and built his first reinforced concrete bridge in 1941 on the Marne River in Luzancy (France), where he used his prestressing and anchoring system (Billington 1976). The system patented by Freyssinet is a type of mobile anchor, with wedge action and can be used for both wires and strands. In the case of wires, the anchor is designed for the simultaneous locking of several wires in number of 2, 3, 12 and 18 and consists of two parts: the cylinder (female cone, Figure 2a (1)) and the wedge (male cone, Figure 2b (2)). The cylinder is drowned in the concrete at the point where the cable comes out, pressed by a hydraulic jack whose dual purpose is to tension the wires and at the same time press the female cone into the concrete. The cone is pushed into the cylinder by pressure, tightening the threads after tensioning the cable (Figure 2b). The cylinder has a double steel spiral on the internal and external surfaces, the cone has longitudinal grooves that form the seat of the wires and is perforated in the centre, to allow to inject the cable (Figure 2a).

In the case of strands (12 strands of Ø12.4 or 12 strands of Ø15.2 mm), steel blocks are used as anchors (Figure 2c). The anchoring consists of an anchoring plate combined with a truncated cone-shaped element, into which the jacket, the

anchor head and the special truncated conical wedges (for clamping the strands) are inserted.

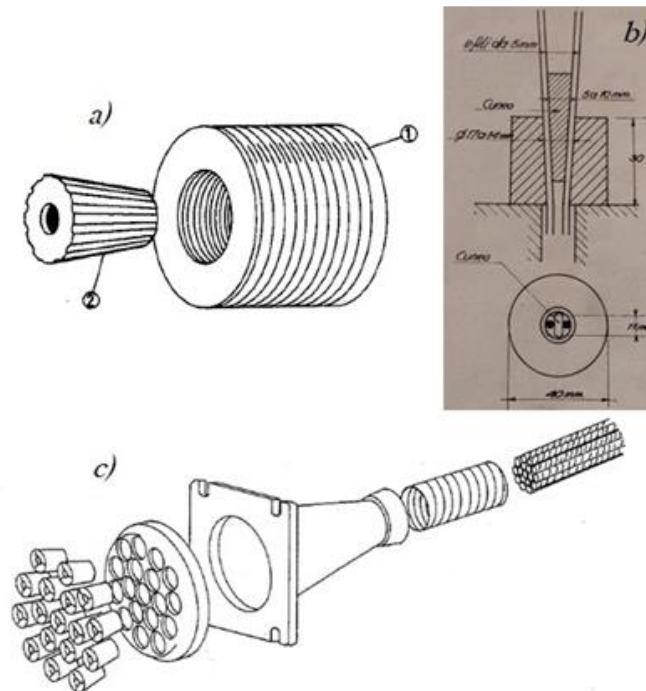


Figure 2. Freyssinet's anchor system.

The founder of Zeiss-Dywidag, Franz Dischinger registered a patent in 1928 about PC. In 1934, Dischinger registered another patent for a system of prestressed bridge beams using intertwined and large-diameter steel cables arranged in a parabolic configuration, positioned outside the beam. The external positioning allowed to adjust the prestressing tension over time (Sanabra-loewe and Capellà-llovera 2014).

After Freyssinet's studies, several inventions and contributions to the development of prestressing emerged, mainly through German engineers. Indeed, in 1938 the first externally PC bridge was built in Aue, Germany (Sanabra-loewe and Capellà-llovera 2014).

Between 1940 and 1942, Gustave Magnel, from Belgium, developed a prestressing process and he built the first continuous beam bridge, in PC (on the river Maas, in Sclayn) (Sanabra-loewe and Capellà-llovera 2014).

The Magnel' system was developed to build a mobile anchor, with wedge action and can be used for wires. It consists of a distribution plate (Figure 3) in-built with the concrete of the beam and perforated to allow the wires to pass. Above this plate there is another one, called sandwich plate (Figure 3). The wires, after

being pulled, are fixed to it with steel wedges. Therefore, the wires are passed between the internal groove of the plate and the external one of the wedges. The spacing of the wires along the cable is ensured by appropriate mild steel grids (Figure 3), reinforced in the bending positions of the harmonic steel in order to resist the transverse component of the pre-stress. With this system it is possible to form cables with a large number of wires (e.g. Cables with 64 wires of 7 mm) and rotate the distribution plate at the desired angle.

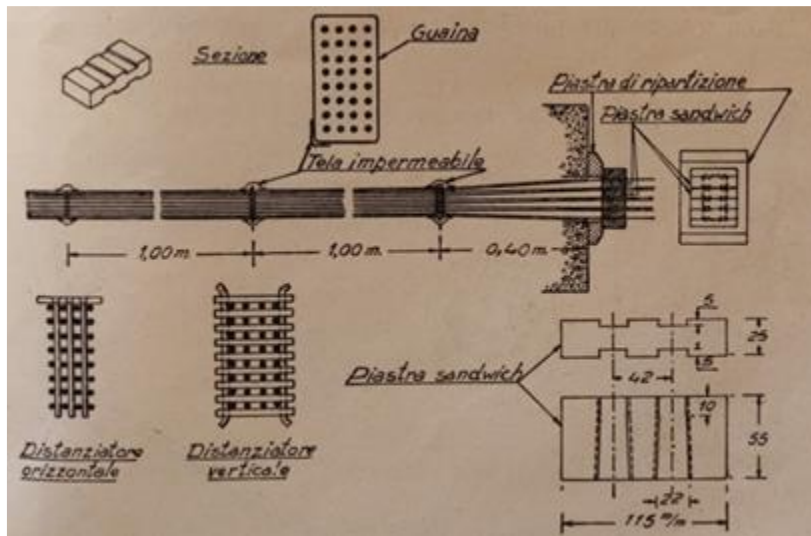


Figure 3. Magnel's anchor system.

After the Second World War, the development of PC gained great momentum through its application in various bridges and large structures. The collaboration between engineers and companies has given rise to various prestressing processes. New types of prestressing steels have also favoured the development of various prestressing processes.

In 1950 U. Finsterwalder built the first PC bridge with the cantilever method, a construction process that quickly spread around the world, becoming one of the most practical to overcome large spans in regions with difficult conditions for shoring (Billington 1976). After 1956, the development of prestressing was characterized by an increase in the capacity of prestressing steel and also by the rationalization of the methods of execution.

As mentioned, the development of the prestressing technique led to a rapid increase in the number of patents proposed by different researchers and designers. These mostly concerned the prestressing technology, i.e. the tensioning and anchoring equipment of the prestressing reinforcement.

The systems for anchoring harmonic steel to concrete can be classified according to one of the following criteria:

- Based on mobility:
 - Fixed anchors: allow only the anchoring of the prestressing reinforcement;
 - Mobile anchors: allow the tensioning and anchoring of the pre-compression reinforcement. In some cases, they also allow tensioning in several successive instants;
- Based on the action exercised:
 - Wedge anchors: they use wedge elements to fit the reinforcement to special support cylinders;
 - Direct support anchors: the prestressing reinforcement itself, specially prepared, is used for anchoring;
 - Winding anchors: a system consisting of winding steel elements allows the reinforcement to be anchored to the concrete.
- Based on the stretched element:
 - Anchors for wires;
 - Anchors for strands;
 - Anchors for bars;

In Italy, the first real applications of prestressing concerned mostly concrete pipes. The Vannini company, specializing in the production of PC pipes, presented in 1933 a new patent for the production of prestressed pipes by using wires that spiral around the circumference. In June 1939 the S.C.A.C. (*Società Cementi Armati Centrifugati*) developed a type of concrete piles in which the prestress was obtained by inserting high tension wires along the height of the pole.

The first Italian patent for reinforced concrete beams with pretensioned wires belongs to Gustavo Colonnetti. In 1939 he wrote a series of articles on the potential development and application of prestressing in Europe and in June of the same year, he gave a lecture at the Sorbonne in Paris on states of compulsion. In December of the same year he filed his first patent, followed by another in January 1940. While basing himself on ideas already present in other European patents, Colonnetti proposed some original solutions. First, he designed an arch beam by suggesting aligning the lower core points of the maximum positive moment sections with the upper ones of the maximum negative moment sections and the centres of mass of any zero moment sections. This alignment then makes it coincide with the line of action of the resultant of previously tensioned cables.

Thus, in the formed beam, the working conditions of an arch without thrust were created, with the pressure curve entirely contained in the core of the section. The goal was to obtain the optimal working conditions for each material, each one stressed according to its mechanical characteristics and with the beam working as a whole as a thrust-free arch.

A further peculiarity of the Colonnetti patent was the lack of adhesion between the concrete and the prestressing cables. Unlike Dischinger, Colonnetti positioned the cables inside the concrete, protecting them with insulating material to prevent contact with the concrete. In this way, after casting, the cables were free and their tensioning could take place when the concrete shrinkage was almost completed. Colonnetti proposed to insulate the cables with thin metal sheets, or tar, bitumen or plastic cements based on rubber, oil or fibers to be spread directly on the cables.

Colonnetti also proposed a simple anchoring system based on the wedge principle, similar to the one proposed by Freyssinet (Figure 4).

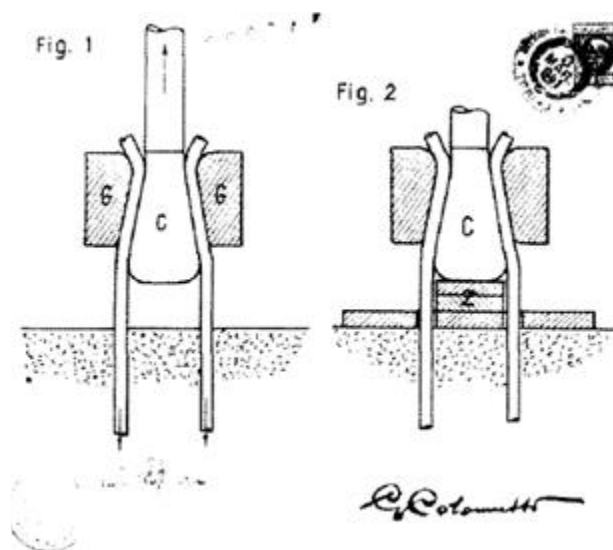


Figure 4. Colonnetti's anchor system.

Despite the significant contributions made by Colonnetti, in the following years his patent there were no major developments in prestressing technology in Italy and this mainly due to the absence of raw materials. The post-war situation limited the purchase of high-strength steels and the monopoly created by the long-term agreements previously signed by other nations made it even more complicated.

Despite this, Colonnetti's work stimulated new patents, such as Luigi's

Magistretti, Augusto De Fant and Franco Mattiazzo, mainly with regard to the technology of tensioning and anchoring cables in beams.

In 1941, in the laboratory of Construction and Institute of Bridges of the Politecnico di Milano, Luigi Stabilini conducted load tests on partially pretensioned Varese type floor joists. In the same year, S.A.C.A.P. was founded. under the strong push of Eng. Giovanni Agnelli.

In 1942 the S.C.A.C. bought the rights to the Hoyer patent for the beams, building the first industrial plant for pre-tensioning (in Monterotondo), using the Ultracem type of cement supplied by Italcementi's Civitavecchia branch.

In February 1944 Riccardo Morandi registered his first patent for the production of prestressing cables using low voltage electric current. It can be defined as the incipit of the subsequent development that led to the birth of prominent figures in the panorama of the design and construction of works in PC in Italy. The Morandi's patent was about a type of mobile anchor, with a wedge action and can be used for strands.

In the M5 system, the anchoring consists of two grooved parts: perforated metal plate and conical pin, both in steel. The plate reports the load on the concrete. In each hole there are two wires that are blocked with wedge pins provided with housing for the wires. The threads are pulled four at a time and it is possible to carry out the catch after some time from the pull (Figure 5).

The anchor has also been adapted to a division into groups of three wires which are locked in a cylinder with a hole by means of a pin. The cylinders transmit the stress to the concrete through a perforated steel plate so as to be able to compose cables each consisting of groups of three wires.

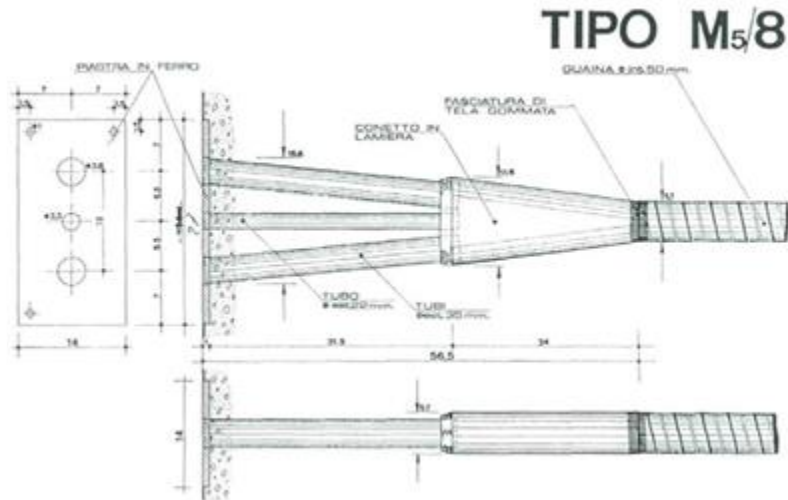


Figure 5. Morandi's anchor system.

2.2. Evolution of technical codes for structural design and assessment

The Italian codes for bridge loads start from Normale n.8 of 15/09/1933 (Italian High Council of Public Works 1933). The bridges were designed to allow the transfer of military vehicles, which were modelled through the scheme that corresponds to the howitzer 305/17 with a total weight of 92t. After the Second World War all the military loads were abolished with the Normale of 1945 (Italian High Council of Public Works 1945). As consequence of that, all bridges were designed for civil traffic loads. In this regard, a continuous row of trucks, composed by alternately 8t and 4t axes with equal spacing of 3m was considered. Besides, a steamroller of 18t was defined. Figure 6 describes the load conditions of Normale 1945:

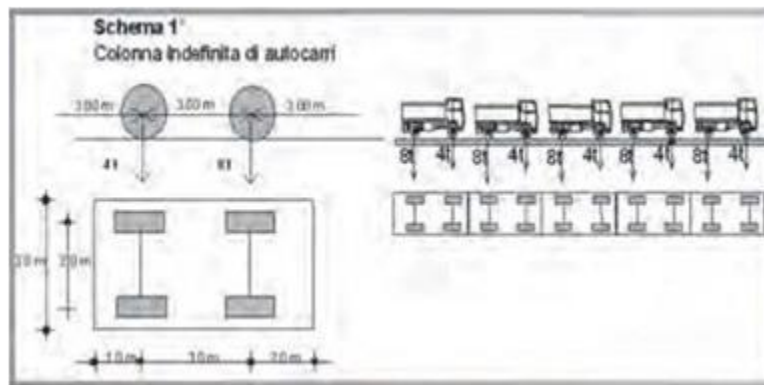


Figure 6. Traffic loads for Italian bridges implemented in the Normale of 1945 (Italian High Council of Public Works 1945).

The first technical Italian code for PC structures was written in the 1947. The Legislative decree of the provisional Head of State (D.C.P.S.) n.1416 of 20th December of 1947 was about procedures, controls and provisions for the PC structures.

Therefore, the Italian regulation Circ. CSLLPP 384/1962 (Italian High Council of Public Works 1962) provided the TLMs to design bridges in Italy. The following categories of bridges were considered: Category I bridges, opened to both military and civil vehicles; and Category II bridges, opened only to civil vehicles. Most of bridges were designed against military vehicles according to the following TLM: a military lane, considering load types (LTs) denoted as LT4, LT5 or LT6, as listed below; one or more regular truck lanes (LT1) and pedestrians on the sidewalks (LT3). The load type LT2 was only considered for Category II bridges. LTs were associate with vehicle types or pedestrians as follows:

- LT1: multiple 2-axles truck load of 120 kN with width equal to 3.11 m (Figure 7a);
- LT2: single 2-axles steamroller load of 180 kN with width equal to 3.11 m (Figure 7b);
- LT3: uniformly distributed load of 4 kN/m²;
- LT4: multiple 6-axles military load of 615 kN with width equal to 3.5 m (Figure 7c);
- LT5: multiple 6-axles military load of 320 kN with width equal to 3.5 m (Figure 7d);
- LT6: single 6-axles military load of 745 kN with width equal to 3.5 m (Figure 7e).

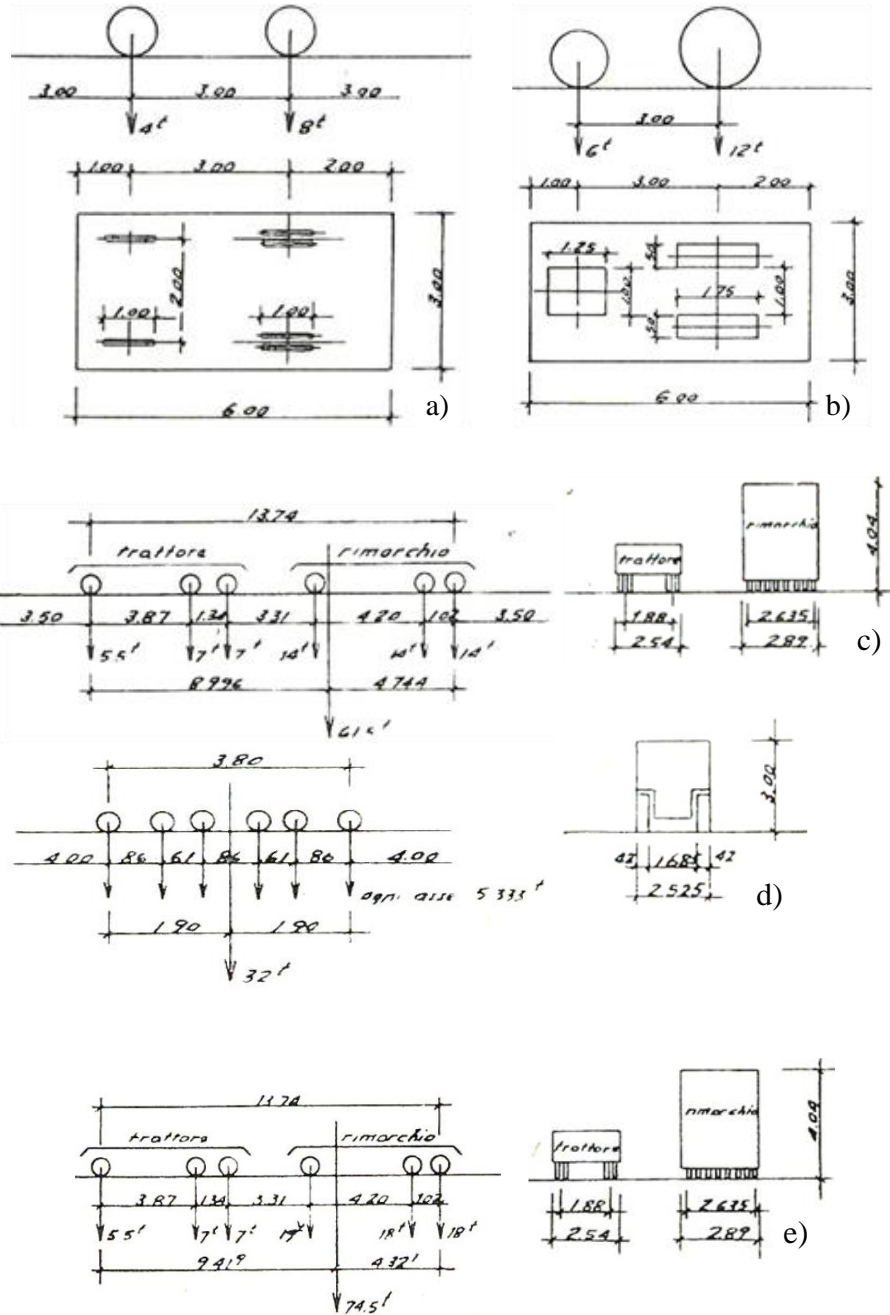


Figure 7. Traffic loads for Italian bridges implemented in the Circ. CSLP 384/1962 (Italian High Council of Public Works 1962).

For all Italian bridges designed between 1980 and 1990, the DM 02/08/1980 (Italian Ministry of Infrastructures and Transportation 1980) was adopted. Three bridges' categories were defined and six TLMs were implemented. The loads conditions are described as follows:

- Scheme q1a: uniformly distributed load depending on the bridge length;

- Scheme q1b: uniformly distributed load depending on the bridge length (smaller than scheme q1a);
- Scheme q1c: isolated towing with 3 axes of 55t (Figure 8a);
- Scheme q1d: isolated truck with 3 axes of 31t (Figure 8b);
- Scheme q1e: isolated load of 1t on the square area with side length of 0.7 m;
- Scheme q1f: uniformly distributed load of 0.4 t/m²;

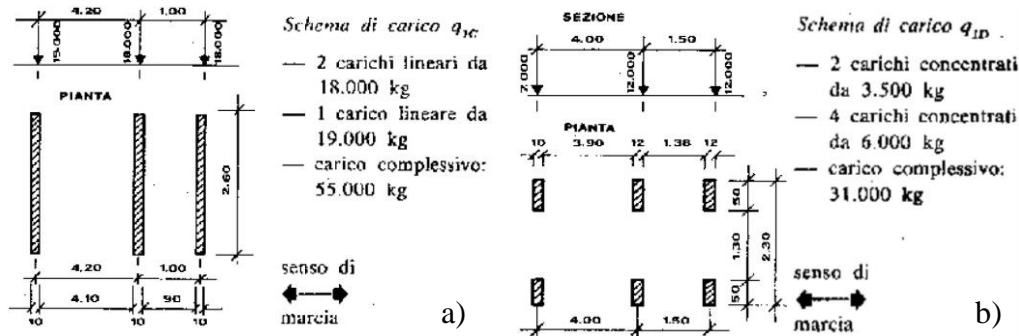


Figure 8. Traffic loads for Italian bridges implemented in the DM 02/08/1980 (Italian Ministry of Infrastructures and Transportation 1980).

Bridges that belong to the first Category are opened to all of six TLMs, Category II includes all bridges designed for q1b, q1d, q1e and q1f loads, whereas Category III of bridges takes into account pedestrian walkways. Moreover, depending on the bridge class those loads could be combined each other in order to define the worst load conditions.

Then, the High Council of Public Works in May 1990 released an update of the technical code for the design, execution and test of roadway bridges (Italian Ministry of Infrastructures and Transportation 1990). In this code was introduced the main load of 60t classified as scheme q1a:

- Scheme q1a: 3 axes of 60t (Figure 9);
- Scheme q1b: uniformly distributed load of 3 t/m;
- Scheme q1c: isolated load of 10 t on the square area with side length of 0.3 m;
- Scheme q1d: isolated load of 1t on the square area with side length of 0.7 m;
- Scheme q1e: uniformly distributed load of 0.4 t/m²

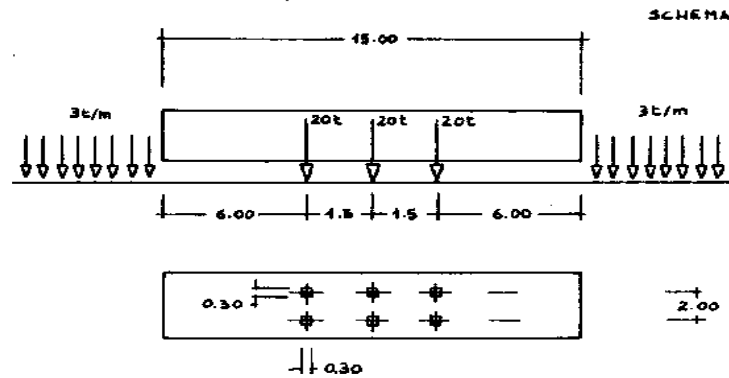


Figure 9. Traffic loads for Italian bridges implemented in the DM 04/05/1990 (Italian Ministry of Infrastructures and Transportation 1990).

RC bridges were designed according to RD 2229/1939 (“RD 16/11/1939, n. 2229. Norme per l’esecuzione delle opere in conglomerato cementizio semplice od armato (in Italian)” 1939), which was replaced by DM 30/05/1972 (Italian High Council of Public Works 1972), DM 29/07/1974 (Italian High Council of Public Works 1974), DM 16/06/1976 (Italian High Council of Public Works 1976), DM 27/07/1985 (Italian High Council of Public Works 1985) and DM 14/02/1992 (Italian High Council of Public Works 1992) to include RC, PC and steel structures. As a common feature, all those codes adopted the permissible stress design (PSD) method, assuming nominal loads and a linear elastic behaviour for all structural materials. However, in the 1990 were introduced the limit state approach in addition to the permissible stress design (PSD) approach.

The recent Italian regulations (i.e., the DM 14/01/2018 (Italian Ministry of Infrastructures and Transportation 2018), NTC 2018 hereafter) are based on the design approach of Eurocodes and provide TLMs for road bridges. Table 1 outlines the TLM prescribed by NTC 2018 (Italian Ministry of Infrastructures and Transportation 2018), including the spacing and axles distribution for each lane (Comité Européen de Normalisation 2003). Moreover, a uniform distributed load of 2.5 kN/m^2 is considered in the remaining part of the carriageway width (r_l) to be loaded when relevant. The NTC-TLMs consider the maximum number of notional lanes (n_l) depending on the carriageway width.

Table 1. Traffic load model according to current Italian code.

Lane	Number of axles	Total axle load Q_k [kN]	Distributed load q_k [kN/m ²]
1	2	300	9
2	2	200	2.5
3	2	100	2.5

Then, in Italy, after the Polcevera bridge collapse in Genoa (Italy) in 2018, significantly increased the public attention on the structural safety of existing bridges, leading to the publication of guidelines for risk-based classification, safety checks and monitoring of existing bridges by the High Council of Public Works in April 2020 (Cosenza and Losanno 2021; Di Prisco 2019; Italian High Council of Public Works 2020). According to Ministerial Decree n.578 issued on 17 December 2020 (Italian Ministry of Infrastructures and Transportation 2020), GL were enforced as mandatory provisions consistent with the 2018 Italian building code (Italian Ministry of Infrastructures and Transportation 2018). GL (Italian High Council of Public Works 2020) introduced a multi-level approach for prioritization of safety evaluations and retrofit interventions on existing bridges by means of a simplified, multi-hazard risk assessment.

GL provisions also introduced new traffic load models (TLMs) according to the Italian road code (Italian Ministry of Infrastructures and Transportation 1992), which provides different allowable vehicle classes on Italian roadways with corresponding maximum axles weight, gross vehicle weight and length. As opposed to modern code provisions (Comité Européen de Normalisation 2003; Italian Ministry of Infrastructures and Transportation 2018), GL (Italian High Council of Public Works 2020) include TLMs (here denoted as GL-TLMs) that were developed within a deterministic framework since no data from actual distributions of traffic loads were available for Italy. This resulted in different values of the corresponding partial safety factors depending upon the traffic control system imposed by the road management companies. Further details about the methodology and safety checks of Italian guidelines for existing bridges can be found in the paper by Cosenza and Losanno (Cosenza and Losanno 2021).

GL-TLMs should have been proposed to provide equal safety levels of those prescribed by NTC (Italian Ministry of Infrastructures and Transportation 2018).

Nonetheless, no comprehensive study has yet validated GL-TLMs from a probabilistic standpoint, for instance through a comparison between failure probabilities associated with GL-TLMs and NTC-TLMs. Before GL became mandatory provisions in Italy, existing bridges were assessed according to NTC-TLMs. In case of non-compliant safety levels, NTC (Italian Ministry of Infrastructures and Transportation 2018) and their commentary included in Circ. 7/2019 (Italian Ministry of Infrastructures and Transportation 2019) permitted the implementation of limitations on the use (e.g., reduced number or different position of lanes) and/or allowable vehicles (e.g., limitation of gross vehicle weight, but no further details were given) in order to meet required safety levels, i.e., a target failure probability $P[C] = 10^{-5}$ – 10^{-7} depending on the consequence class of the structure (Comité Européen de Normalisation 2003). In this context, GL provisions include new TLMs based on different vehicle classes of the Italian stock to be properly regulated by road management agencies. GL-TLMs were not characterized according to a stochastic framework, so deterministic values inferred from the Italian road code (Italian Ministry of Infrastructures and Transportation 1992) were assigned to each TLM to make a clear distinction between different vehicle classes.

As described above, Level I reliability method (Comité Européen de Normalisation 2004a, 2006) is currently adopted in NTC (Italian Ministry of Infrastructures and Transportation 2018) through partial safety factors calibrated for structural design of constructions. By contrast, GL provisions (Italian Ministry of Infrastructures and Transportation 2019) are based on a Level II first order reliability method (FORM) to account for reduced reliability index for existing structures as per fib Bulletin 80 (Allaix et al. 2016). Reduced partial safety factors can be obtained for a given value of target reliability β_0 over the residual service life of the bridge (t_{ref}) (Cosenza and Losanno 2021).

Four different TLMs are provided by GL to be representative of different vehicle classes (Italian High Council of Public Works 2020):

- Heavy GL-TLM: load pattern representative of heavy lorry, which is modelled through 5 axles with resulting load of 440 kN over a total length of 11 m (Figure 10a) plus a uniformly distributed load of 9 kN/m².
- Medium GL-TLM: load pattern representative of a bus, which is modelled through 3 axles with resulting load of 260 kN over a total

length of 9 m (Figure 10b) plus a uniformly distributed load of 7.5 kN/m².

- Light GL-TLM: load pattern representative of light lorry, which is modelled through 2 axles with resulting load of 75 kN over a total length of 6 m (Figure 10c) plus a uniformly distributed load of 4.2 kN/m².
- Very light GL-TLM: load pattern representative of vans and cars, which are modelled with a uniformly distributed load of 2.5 kN/m².

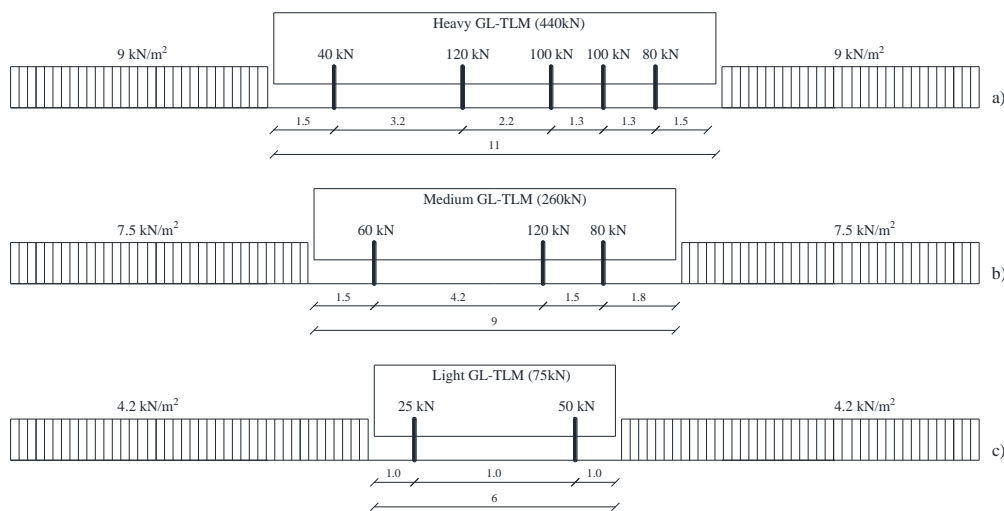


Figure 10. Longitudinal view of GL-TLMs (dimensions in m): (a) heavy, (b) medium and (c) light GL-TLM.

In contrast to NTC (Italian Ministry of Infrastructures and Transportation 2018) and EN 1991-2 (Comité Européen de Normalisation 2003), distributed loads in GL-TLMs can be only applied outside the silhouette of vehicles corresponding to the concentrated loads. In addition to this, the maximum number of traffic lanes considered by GL provisions (Italian High Council of Public Works 2020) depend solely on the carriageway width and should be defined to assume either different types of vehicles (e.g., heavy lorry and car) or a single type of vehicle (e.g., heavy lorry) over all lanes with nominal width equal to 3.0 m. It is worth to mention that NTC-TLM is assumed to have a 5% probability of exceedance in 1000 years, whereas no similar considerations are available in the GL provisions.

2.3. Evolution of standards and codes for materials and structural detailing of bridges

Dealing with material properties, RD 2229/1939 (“RD 16/11/1939, n. 2229. Norme per l’esecuzione delle opere in conglomerato cementizio semplice od

armato (in Italian)” 1939) only prescribed a concrete mixture with cement unit weight by volume of 300 kg/m³ in order to obtain a minimum value of concrete cubic compressive strength (R_{ck}) of 12 MPa and 16 MPa for RC and PC structures, respectively. Such minimum requirement was updated by DM 30/05/1972 (Italian High Council of Public Works 1972), which prescribed $R_{ck} \geq 30$ MPa for PC structures. A simplified safety check in terms of ultimate bending capacity was allowed, assuming a minimum global safety factor of 1.75. In this respect, design codes did not prescribe partial safety factors for material properties and loads.

Through the years, mild reinforcing steel was regulated according to different classes under varying tensile properties. RD 2229/1939 (“RD 16/11/1939, n. 2229. Norme per l’esecuzione delle opere in conglomerato cementizio semplice od armato (in Italian)” 1939) prescribed three classes: mild, semi-hard ad hard steel with ultimate deformation (ε_u) higher than 0.20, 0.16 and 0.14 respectively. The hardest is the steel the bigger is minimum yielding stress (f_y), indeed, mild steel must have f_y higher than 230 MPa, whereas the hard steel must have f_y at least equal to 310 MPa. Moreover, a minimum reinforcing steel ratio (ρ_s) related to the concrete area (A_c) was prescribed. In this regard, a ρ_s higher than 0.5% and 0.8% was defined if A_c was less than 0.2 m² and higher than 0.8 m², respectively. Table 2 summarizes the provisions of RD 2229/1939 (“RD 16/11/1939, n. 2229. Norme per l’esecuzione delle opere in conglomerato cementizio semplice od armato (in Italian)” 1939).

Table 2. Mechanical properties of steel by RD 2229/1939 (“RD 16/11/1939, n. 2229. Norme per l’esecuzione delle opere in conglomerato cementizio semplice od armato (in Italian)” 1939).

Steel class	Yielding stress (f_y) [MPa]	Ultimate tensile stress (f_t) [MPa]	Ultimate deformation (ε_u) [%]
Mild	≥ 230	$\geq 420; \leq 500$	≥ 20
Semi-hard	≥ 270	$\geq 500; \leq 600$	≥ 16
Hard	≥ 310	$\geq 600; \leq 700$	≥ 14

In the Italian Moradi's license, described in Section 2.1 there were some limitations on steels used in structures prestressed with this method. Indeed, the ε_u and ultimate tensile stress (f_t) must have higher than 0.035 and 1721 MPa, respectively, whereas the tensile stress at 1% of steel deformation must have higher than 682 MPa and lower than $0.95 f_t$.

Starting from DM 30/05/1972 (Italian High Council of Public Works 1972) the prestressing steel was regulated and some provisions were defined. In this regard, prestressing steel was regulated in the form of wires, strands, and bars for use in both post-tensioned and pre-tensioned structures. No strength acceptance limits were defined for prestressing steel because a qualification process of the manufacturer was required. In this regard, the f_t had to be defined through the "Italian Institution of Standardization" (UNI). This contributed to explain the reason for a limited number of available tensile tests on prestressing steel over the last decades.

DM 30/05/1972 (Italian High Council of Public Works 1972) provided limitations of mechanical properties for the prestressing steel related to the f_t . Indeed, the yielding stress must have included between $0.75 f_t$ and $0.95 f_t$. Besides, the ultimate deformation was related to the type of prestressing steel, for example ε_u higher than 0.07 was defined for bars.

Provisions and classes of mild steel were defined in DM 30/05/1972 (Italian High Council of Public Works 1972) as well. Five steel classes were considered, two of which are for smooth bars and the remaining three for corrugated bar. Moreover, in PC structures, a minimum reinforcing steel ratio (ρ_s) of 0.25% was prescribed, calculated as the ratio of the total reinforcing steel area A_s over the tension area of the concrete (i.e., web area plus section enlargement at the tension side). Table 3 and Table 4 summarize the provisions of DM 30/05/1972 (Italian High Council of Public Works 1972) for prestressing and mild steel.

Table 3. Provisions of DM 30/05/1972 (Italian High Council of Public Works 1972) for prestressing steel.

Yielding stress (f_y) [MPa]	Stress at 0.2% of steel deformation ($f_{0.2}$) [MPa]	Stress at 1% of steel deformation (f_l) [MPa]	Ultimate tensile stress (f_t) [MPa]
$\geq 0.75f_t; \leq 0.95 f_t$	$\geq 0.8f_t; \leq 0.95f_t$	$\geq 0.8f_t; \leq 0.95f_t$	To be evaluated according to UNI- conforming material tests

Table 4. Provisions of DM 30/05/1972 (Italian High Council of Public Works 1972) for mild reinforcing steel.

Strength class	Type of bar	Yielding stress (f_y) [MPa]	Ultimate tensile stress (f_t) [MPa]	Ultimate deformation (ϵ_u) [%]
FeB22	Smooth	≥ 220	≥ 340	≥ 24
FeB32	Smooth	≥ 320	≥ 500	≥ 23
A38	Ribbed	≥ 380	≥ 460	≥ 14
A41	Ribbed	≥ 410	≥ 500	≥ 14
FeB44	Ribbed	≥ 440	≥ 550	≥ 12

With the D.M. 30/05/1974 (Italian High Council of Public Works 1974) were introduced slight differences respect than previous code, in particular the steel A41 was removed and the A38 steel was called FeB38 with the same proprieties. Moreover, in PC structures, a minimum reinforcing steel ratio of 0.1% was prescribed.

2.4. Failure modes and structural issues of existing bridges

The presence of an outdated transportation infrastructure and the consequent need for a major disaster risk reduction programme involving existing bridges

have been dramatically spotlighted by several disasters, approximately 80% of which triggered by vehicle overloads and collisions, floods, and environmental degradation (Cook et al. 2015; Deng et al. 2016; Wardhana and Hadipriono 2003). In Italy, the Polcevera bridge collapse in Genoa (Italy) in 2018 significantly increased the public attention on the structural safety of existing bridges. Despite the large number of studies on the seismic vulnerability of existing bridges (e.g., (Banerjee and Shinozuka 2008; Borzi et al. 2015; Cardone et al. 2011; GARDONI et al. 2003; Monteiro et al. 2019; Mosleh et al. 2020; Pinto and Franchin 2010)), a continuously increasing number of bridges are approaching their design service life, calling for proper maintenance and special repair due to aging and deterioration of materials. Corrosion of reinforcing steel may be addressed as one of the most popular causes of damage to reinforced concrete and PC structural members (Belletti, Vecchi, et al. 2020; Conti et al. 2020; Pelle et al. 2022; Vereecken et al. 2021). In this regard, in the last decades seismic performance of bridges has been extensively studied, involving a number of topics such as nonlinear modelling, performance-based design, probabilistic assessment and structural fragility (Borzi et al. 2015; Cardone et al. 2011; Ozsarac et al. 2021; Perdomo et al. 2022).

During the last few years, a growing interest has been paid in first-order reliability methods for safety assessment of existing bridges (Allaix et al. 2016; Gino et al. 2021). Moreover, other researchers recently investigated the experimental behaviour of full-scale PC beams, which are recognised to be critical components for existing bridges (Belletti, Rodríguez, et al. 2020; Botte et al. 2021; Huber et al. 2018).

According to (LeBeau and Wadia-Fascetti 2007) bridge collapses are usually associated with serious economic and life losses. In addition to casualties and loss of lives, the disruption in the service results in tremendously adverse effects on economic growth (Cook et al. 2015; Diaz et al. 2009; SMITH 1976). For example, the failure of the Quebec Bridge in 1907 caused 75 deaths during construction (Pearson and Delatte 2006), and the failure of the Silver Bridge in 1967 killed 46 people during service (Harik et al. 1990; Lichtenstein 1993). In 2007, Tuojiang Bridge catastrophically collapsed during construction, resulting in 64 deaths and 22 injuries as well as a direct economic loss of about 39.747 million yuan (W. Peng et al. 2017).

Thanks to the Wardhana and Hadipriono (Wardhana and Hadipriono 2003) research it has been showed that in the United States, between 1989 and 2000, a total of 503 bridge collapses were reported, causing huge losses to the nation. Wardhana and Hadipriono (Wardhana and Hadipriono 2003) investigated 503 bridge failures in the United States and obtained the principal characteristics of bridge failures from the aspects of structural type, material type, service age, type of failure, and time of failure. Based on Wardhana and Hadipriono (Wardhana and Hadipriono 2003) research, Lee et al. (G. C. Lee et al. 2013) collected 1062 bridge failures and analysed the correlation between bridge failure and structural type, material type, service age, type of failure, and time of failure. Therefore, a more comprehensive condition of bridge failures in the United States was obtained. Xu et al. (Xu et al. 2016) analysed the statistical characteristics of 302 collapsed bridges in China, including time of failure, casualties, location, life, span, and bridge type. That study provided a comprehensive reference of the current situation of bridge failures in China.

Among the above scholars, Wardhana and Hadipriono (Wardhana and Hadipriono 2003) and Lee et al. (G. C. Lee et al. 2013) divided the damage degree of the bridge failures into distress, partial collapse, and total collapse. Distress represents the unserviceability of a structure or its component that result in a collapse. It is a particular structure's condition, in which there are some deformations, but the bridge is still alive and useable. According to Wardhana and Hadipriono (Wardhana and Hadipriono 2003) a "Partial collapse" means that some primary members of a span or multiple spans have undergone severe deformation and so travelling on the bridge could be dangerous for people. While a total collapse means that all primary members of a span or multiple spans have undergone severe deformation, so no travel lanes are passable. Thanks to many observations reported it is showed that more than 80% is made up of total or partial collapse, while less than 20% reported a distress failure (G. Zhang et al. 2022).

On the other hand, bridge types were divided into beam bridge, arch bridge, cable bridge, culvert, truss, floating bridge, and pedestrian bridge. Xu et al. (Xu et al. 2016) only studied total collapsed bridges, and classified bridge types into beam bridge, arch bridge, cable-stayed bridge, and suspension bridge.

In this regard, as reported by Deng et al., (Deng et al. 2016) and Xu et al., (Xu et al. 2016) bridge structural types mainly include beam, arch, cable-stayed, and

suspension bridge. According to Zhang et al. (G. Zhang et al. 2022) beam bridges represent the dominant type of failed bridges with more than 45% occurrences. This phenomenon is closely related to the wide applications of beam bridges. For instance, as reported by Lee et al., (G. C. Lee et al. 2013) and Liu et al., (Liu et al. 2017) beam bridges accounted for over 60% and 70% of the total number of existing bridges in the United States and China, respectively. Moreover, many studies confirmed that steel truss bridges are more vulnerable than other structural types because steel truss bridges produced 29% of the failures while they occupied less than 1% of the total number of existing bridges in the United States (G. C. Lee et al. 2013; Wardhana and Hadipriono 2003).

As concern the Lee et al., (G. C. Lee et al. 2013) and Wardhana and Hadipriono (Wardhana and Hadipriono 2003) and Xu et al., (Xu et al. 2016)'s studies, the service age of a bridge plays a fundamental role in the bridge's collapse. In this regard, the service age is defined as the time from the date when the bridge is completely built to the time when the bridge has failed (G. Zhang et al. 2022). (G. Zhang et al. 2022) shows that in the United States bridges service age have reached 30 years, and more than 50% of failed bridges has a service age of 50 years, whereas in China most failed bridges served no more than 30 years with an average service life of fewer than 25 years.

Another important aspect that is worth to mention is the usage of bridge. According to Lee et al., (G. C. Lee et al. 2013) and Liu et al., (Liu et al. 2017) and Wardhana and Hadipriono (Wardhana and Hadipriono 2003) there are many types of uses for a bridges, that are: highway bridge, roadway bridge, railway bridge, pedestrian bridge, and highway-railway dual functioned bridge. As concern (G. Zhang et al. 2022) observations, highway bridge was the dominant type of failed bridges with more than 70% occurrences, while railway bridge failures ranked with less than 25% failed bridges. That's because the number of bridges built was much higher than that of other types and there were more highway bridge failures (G. C. Lee et al. 2013; Liu et al. 2017). In addition to the difficulty of vehicle management, the probability of overload is higher.

Wardhana and Hadipriono (Wardhana and Hadipriono 2003) categorized the principal causes of bridge failures as internal causes (design error, construction mistake, and lack of maintenance), and external causes (hydraulic, overload, and collision). Based on the research of Wardhana and Hadipriono (Wardhana and Hadipriono 2003) and Deng et al. (Deng et al. 2016) further analysed the

correlation between the causes of bridge failures and structural type and found that floods, earthquakes, and overloads caused the most failures of beam bridges and masonry arch bridges. In addition, collisions, wind, and fatigue contributed to the failures of beam bridges, flexible long-span bridges, and steel truss bridges, respectively. Indeed, the collapse of the original Tacoma Narrows Bridge in 1940 promoted research in the field of bridge aerodynamics-aeroelastic and a physical phenomenon known as aeroelastic flutter (Billah and Scanlan 1991).

According to Frangopol et al., (Frangopol et al. 2001) “the circle of a bridge’s life” concerns different phases such as: the design, construction, service, and demolition. The risk of failure concerns the last 3 phases). In fact, Zhang 2022 (G. Zhang et al. 2022) demonstrates that “bridge failures mainly occurred during the service phase with more than 60% occurrences, while less than 40% failed during construction and few failed during demolition in most investigations. In this regard, (G. Zhang et al. 2022) claim that the possible reason is that the most bridge failures occurred in recent decades bridges in the United States are in the midst of large-scale maintenance, while bridges in China were in the midst of large-scale construction.

In order to better understand what can cause a bridge collapse, it is fundamental understand that it is usually a very complex process which is the result from a combined effect of many different factors. Thus, it is crucial to discover the main causes of a bridge collapse. In this regard, there are two wide categories: natural factors and human factors. The natural factors are linked to natural disasters (e.g., flood, scour, earthquakes, landslides, debris flows and so on). The critical issue of a natural disaster is that it is most of the times unpredictable and so can cause serious damages to a bridge’s structure. The natural disaster, such as in this case floods, account for nearly half of the bridge collapses in United States (Wardhana and Hadipriono 2003), whereas scour, construction and supervision mistake and collisions accounts for 15% (each one) of total collapses (Wardhana and Hadipriono 2003). Moreover, the main causes of a bridge failure are classified into principal causes and specific causes by Fu et al., (Z. Fu et al. 2012) and Lee et al., (G. C. Lee et al. 2013). Principal causes can be divided into internal causes and external causes or natural factors and human factors. Internal causes are design error, construction mistake, lack of maintenance, material defect, etc. According to Lee et al., 2013; Wardhana and Hadipriono (Wardhana and Hadipriono 2003), internal causes usually require detailed failure investigations,

such as material test, an inspection of design, construction, and maintenance documents, structural calculation, etc. External causes include natural disasters such as earthquake, flood, fire, and wind, and extreme loads such as collision and overload. (Wardhana and Hadipriono 2003). (G. Zhang et al. 2022) shows that the proportion of construction mistake and hydraulic were the highest, followed by collision and overload, while the proportion of design errors was the least.

Witzany et al. (Witzany et al. 2008) and Hong et al. (Hong et al. 2012) describes a flood as a heavy precipitation, usually leads to flooding, which may cause phenomena such as scour, erosion, river convergence, insufficient embedment depth, protection works-induced overfall or hydraulic jump, softened bedrock, sand mining, debris impact or abrasion on bridge foundations, etc. A combination of these phenomena can cause dramatic reductions in the bridge's strength and stability. Biezma and Schanack, (Biezma and Schanack 2007) showed that a huge number of bridges were destroyed by hydraulic, in particular flood and scour as Deng et al., (Deng et al. 2016), Hong et al., (Hong et al. 2012) and Montalvo et al., (Montalvo et al. 2020) have showed. On the other hand, according to AASHTO scour is a phenomenon in which the level of the river's riverbed becomes lower due to water erosion, and it cause an exposure of bridge foundation. According to Lee et al., (G. C. Lee et al. 2013) and Wardhana and Hadipriono (Wardhana and Hadipriono 2003) scour is defined as the erosion or removal of a streambed or bank material from bridge foundations caused by flowing water, usually considered as long term bed degradation, contraction, and local scour. The more scour's depth increase, the more lateral resistance of soil supporting the foundation is reduced, leading the increase of lateral deflection of the foundation head (Daniels et al. 2007; Lin et al. 2010). Moreover, the bending buckling of the foundation may occur when the critical scour's depth is reached, under the combined effect of the dead load of bridge superstructures and the traffic load. (Hughes et al. 2007; Walton et al. n.d.). Bridge scour includes four main categories: local scour, contraction scour, general scour, and channel migration. According to a review by Lin et al. (Lin et al. 2014), failure modes of bridges caused by bridge scour can be subcategorized into four main types: vertical failure, lateral failure, torsional failure, and bridge deck failure. As shown in Figure 11, pile buckling, inadequate bearing capacity of shallow foundations, friction pile penetration, undermining of pile toes, are four main categories that may be used to classify vertical failure of bridges brought on by scour (Lin et al.

2014). In this regard, between 1993 and 1996 the United States experienced 2 catastrophic floods with 171 bridge failures in these 2 years alone. It makes the proportion of bridge failures caused by floods far higher than other natural causes (G. C. Lee et al. 2013; Wardhana and Hadipriono 2003).

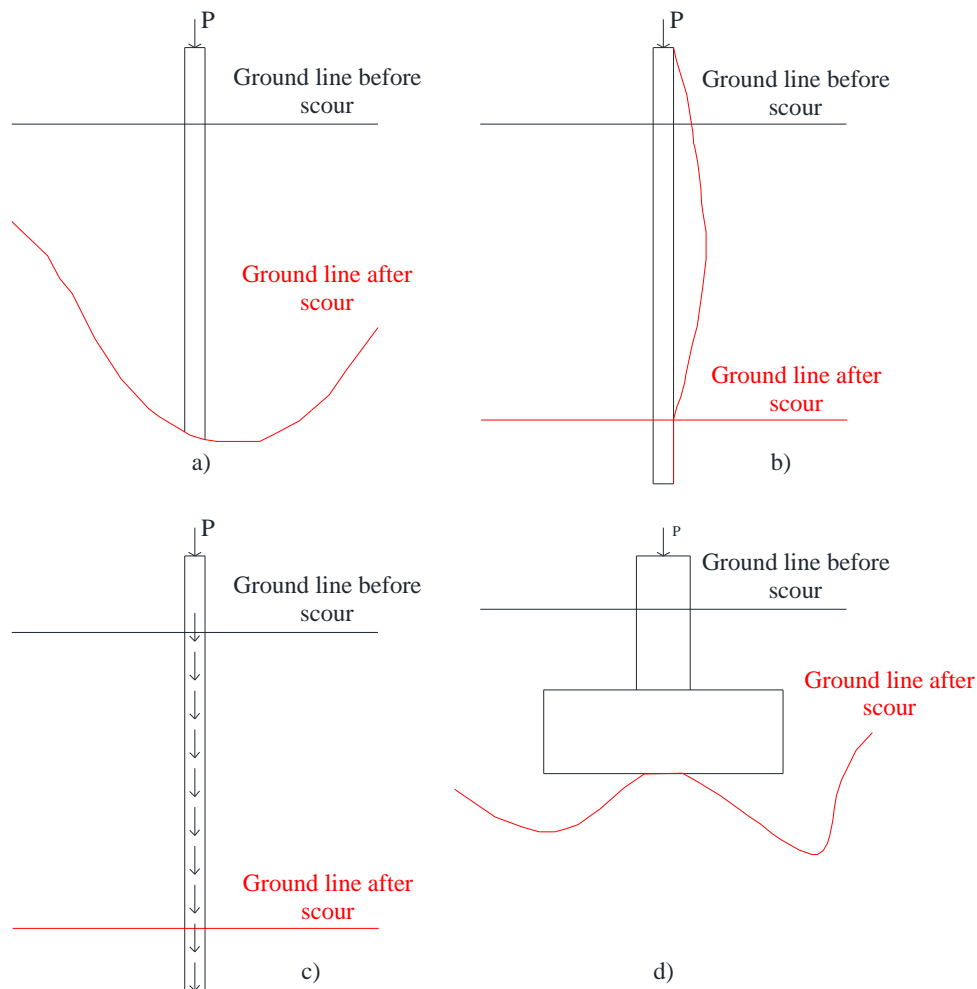


Figure 11. Vertical collapse mechanisms of bridge foundations: (a) undermining of pile; (b) buckling of pile; (c) penetration of friction pile tip; (d) undermining of footing base

In order to protect bridges from hydraulics, designers should select proper bridge sites, arrange bridge span properly, and ensure adequate foundation depth. On the other side the bridge regulation and protection should be improved. Other implementation must occurred with bridge maintenance work, that should be strengthened, and foundation scouring maintenance, which should be included in the preventive maintenance category. Studies confirmed that about 163 bridge failures were caused by collision Lee et al., (G. C. Lee et al. 2013) which a total collapse dominated approximately 39% while partial collapse dominated approximately 60%.

Another natural factors that cause bridge's collapse are earthquakes. They lead to vertical and horizontal ground motions that can cause the failure of bridge substructures (Wang et al. 2013; Warn and Whittaker 2008; Yang and Lee 2007). Both vertical and horizontal ground motions may cause the soil's liquefaction at the bridge foundations, which can reduce the load-carrying capacity of the foundations and lead to bridge collapse (Hashimoto and Chouw 2003; Wang et al. 2013). Due to the seismic effect, bridge columns or piers tend to fail in three modes, namely, flexural failure (Bhattacharya et al. 2008; Lou and Zerva 2005; M. J. N. Priestley 1988), shear failure (Ghobarah and Ali 1988; Hwang et al. 2000) and crushing failure (S. J. Kim et al. 2011; PAPAZOGLU and ELNASHAI 1996).

According to Kunnath et al. (Kunnath et al. 2008) and Kim et al. (S. J. Kim et al. 2011) vertical ground motion causes significant fluctuating axial forces in bridge columns or piers, which may induce outward buckling or crushing of the columns or piers. It also can cause significant amplification of the bending moment at the bridge midspan, which may lead to the bending failure of the bridge deck (Kunnath et al. 2008; Veletzos and Restrepo 2011). The horizontal ground motion mainly contributes to the shear failure of bridge columns or piers (M. J. Nigel Priestley et al. 1994; Sun et al. 2012).

Moreover, a secondary event that can be triggered by earthquake or heavy rain are landslides (Cui et al. 2009). These events are a natural phenomena which are linked to water saturation, earthquake, or volcanic eruption, and it may result in the downward and outward movement of slope-forming materials including rock, soil, artificial fill, or a combination of these materials (Iverson 2000). These materials will lead to severe damage or even collapse of the bridge when hitting it.

Many studies focused on slow-moving landslides (i.e., landslides with a velocity almost equal to 0.6 mm per day). In this case, the foundations of the structures situated on the top of the slopes are affected by differential displacements (Fotopoulou and Pitilakis 2017a, 2017b). Nevertheless, heavy damage is also induced by the earthflow impact on the structures situated at the toe of the slope due to the high velocity of the flow-type landslides (i.e., up to 30 m/s). In addition, objects such as debris, rocks and cars can be carried by the flow and crash into the buildings (Mavrouli et al. 2014). In this regard, a debris flow has a tremendous impact force that drags all obstacles in its way, such as large stones.

It also has severely erosive effects. In fact, when a flow impacts a bridge, the damage could be devastating (Takahashi 1978).

Another natural factors that cause bridge's collapse are hurricanes and typhoons. They are tropical cyclones that are caused by low pressure systems. They moved with wind waves which raise the water level to an elevation and it can strike the superstructure of bridges along the coast. Bridge decks may be knocked off the pile caps due to the impulsive vertical and horizontal forces generated by the storm waves riding on high surges (Q. Chen et al. 2009; Robertson et al. 2007). These damages are the result of a vibration, that is usually caused by three different types of oscillations: flutter, buffeting, and vortex-induced oscillation (Ge and Tanaka 2000; Scanlan 1998). Thus, both aerostatic and aerodynamic forces lead to large displacements and stresses that exceed the bridge structures, leading to a collapse of bridges (Cheng et al. 2002; Scanlan 1998). As reported by Padgett et al. (Ataei and Padgett 2013), Chen et al. (Q. Chen et al. 2009) and Ataei and Padgett (Ataei and Padgett 2013) deck unseating has been found to be the predominant failure mode during hurricane events for simply-supported multi-span coastal bridges without supplemental restraints. During this natural phenomena the uplift force caused by the wave and air trapped underneath the bridge deck may overcomes the gravity load and the restrain forces of the bridge deck itself and thus, the deck will be unseated. There is another element that contribute to a bridge's collapse: the impact of barges, oil drilling platforms, and other types of debris (Padgett et al. 2008).

Last but not least, wind could induce aerostatic and aerodynamic instability problems for flexible long-span bridges. In detail, there are two types of aerostatic instability according to the modes of static instability: the torsional divergence and lateral-torsional buckling (Boonyapinyo et al. 1994; Cheng et al. 2002).

We also write about human factors, that may cause a bridge collapse. They include imperfect design and construction method, collision, vehicle overloading, fire, terrorist attack, lack of inspection and maintenance and may also result in bridge collapses. In many cases, poor design and the inappropriate construction methods can lead to bridge collapse in the construction phase (e.g. the collapse of the West Gate Bridge in Australia in 1970) while the failure of the Kutai-Kartanegara Bridge in Indonesia in 2011 was due to an imperfect connection design and questionable material selection that overstress in the

connections of the bridge (KAWAI et al. 2014). So, in order to avoid these types of bridge collapses strict process control and proper supervision must be followed, so it will be reducing the probability of this type of bridge failure.

Accidental collisions represent another human factor that may cause bridge collapse. They occur between vehicles and bridge superstructures and between vessels and bridge piers or columns. During the collision, a very large lateral force is transmitted to the impacted bridge structures (Consolazio and Cowan 2005; Fan et al. 2011). This large impact force may cause very high local pressure and so damage to bridge components. Thus, collision can cause serious damages to local structural components but also lead to progressive collapse of multi-span bridges. Many researchers have studied the mechanisms of bridge progressive collapse due to the accidental loss of supports for beam bridges, in order to prevent progressive collapses. Lu and Zhang (Lu and Zhang 2013) have studied the failure process of the Jiujiang Bridge caused by a vessel impact and pointed out that the progressive failure of three consecutive spans resulted from the separation of structural elements and the centrifugal force of the falling bridge deck. (G. Zhang et al. 2022) showed that in the USA, vehicles have hit about 61% of overpasses.

Fires on bridges are commonly due to the collision of vehicles (Bai et al. 2006; Payá-Zaforteza and Garlock 2012) and more or less 3% of total bridge's collapses are relating to them (Wardhana and Hadipriono 2003). According to Payá-Zaforteza and Garlock (Payá-Zaforteza and Garlock 2012) fire can reach very high temperatures (800–900°C) within the fire initiation and then the temperature can rise to 1,000°C or higher in the first 30 min. The rapid temperature increasing creates large thermal gradients in the structural members and cause spalling of the concrete and local buckling of steel members (G.-F. Peng et al. 2008). Fires can also lead to a reduction in the strength and stiffness of materials, which can further lead to partial or full collapse of bridges (Astaneh-Asl 2008; Bai et al. 2006).

According to the increasing automotive market, vehicle overloading has become a common cause of a bridge collapse (G. Fu and Hag-Elsafi 2000). Especially truck overloading tiring out the bridge components ((Biezma and Schanack 2007; Wardhana and Hadipriono 2003)). With an increasing traffic volume, the truckloads exceeded the limitations, resulting in bridge failures, and it affects especially older bridges. This type of bridge failures is common in the United

States and European countries (G. C. Lee et al. 2013). In this regard, the fatigue damage of steel bridges is accelerated by the overloads (Biezma and Schanack 2007). In this scenario beam bridges are the dominant structural type of failure caused by overloads. The live load effect accounts for a large proportion of the total effect, which causes beam bridges vulnerable to overloads. Lee et al. (G. C. Lee et al. 2013) studied 135 bridge failures caused by overloads, in which steel bridge failures dominated approximately 64% while concrete bridge failures dominated approximately only 11%.

Also terroristic attacks can configure a bridge collapse, as a human factor. In fact, due to their accessibility and potential impacts on human lives and economic activities (Z. Yi et al. 2014a), transportation infrastructures have been considered as attractive targets for terrorist attack. The safety of critical bridges under blast loading has become a public concerned a topic of interest for many researchers due to the increase in terrorist attacks in recent years. Numerical simulations were carried out on three-span simply-supported highway bridges to evaluate the blast effect on it and the failure mechanisms of main bridge components (Z. Yi et al. 2014b). Yi et al. (Z. Yi et al. 2014b) described four different bridge's component failures: (i) pier: eroding of pier bottom concrete, shearing of a pier from the footing, rebar severance, breakage of pier, spalling of concrete surface, and formation of plastic hinges; (ii) bent beam: local failure of concrete under bearings, crushing of concrete, and shear failure; (iii) stringer: collapse, and yielding of the steel; (iv) deck: crushing under high pressure, dislocation under the effect of the blast wave, and collapse due to loss of support. In this regard, as demonstrated by Ghali and Tadros (Ghali and Tadros 1997) progressive collapse may occur under the effect of a blast, as reported in the failure of a multi-span bridge on the Northumberland Strait in Canada.

Moreover, as a result of human activities, lack of inspection and maintenance can cause bridges collapse. As it is known, bridges are constantly subject to natural factors and live loads. They can cause the deterioration of the bridge structure and it influenced by various factors including material properties and mechanical and environmental stressors (S. Kim et al. 2013; Kong and Frangopol 2005). Thus, a good maintenance program which includes regular inspection and proper rehabilitation will reduce the deterioration process of bridges and help detect potential structural problems before they develop into serious disasters (Biezma and Schanack 2007; Estes and Frangopol 2001).

In the framework of human mistakes, some bridge collapses are related to design errors. According to Lee et al., (G. C. Lee et al. 2013) design error is related to bridge failures caused by defects in design theory and carelessness of designers, in which are difficult to find the errors before the completion of the bridge and verify the causes after its failure. For instance, the Tacoma Bridge's collapse was caused by an insufficient understanding of the consequences of the wind when it impacts the bridge (Billah and Scanlan 1991). Also, the collapse of the I-35W Bridge was due to insufficient understanding, in the case about the fatigue of truss bridge joints. In addition, also structural calculation errors or blind application of codes by designers caused by a lack of experience and knowledge will lead to bridge failure. It was the case of the Chirajara Bridge in Colombia, that collapsed under construction due to insufficient design of the bearing capacity of the lower beam of the bridge tower (Pujol M.E.; Monical, J.D.; and Schultz, A.E. n.d.). The purpose of bearings is to transmit forces and provide relative motion between components of the superstructure and substructure. Depending on the bearing type, different bearings are damaged during earthquakes; some examples include anchor bolts being pulled out or sheared and movement of elastomeric bearings. The unseating of spans, which happens when the bridge superstructure is permanently displaced from its position atop the substructure, can be attributed to bearing failure (Di Sarno et al. 2019). Due to their relatively low bearing seat lengths, certain older bridges are far more susceptible to unseat (Di Sarno et al. 2019). Unseating can cause one or more spans to completely collapse or result in girders shifting out of place and resting on the pier cap.

Reinforced concrete bridges suffered only minimal damage in recent Italian earthquakes as those that hit the city of L'Aquila in 2009 and Emilia in 2012 (Kawashima et al. 2010). This was mostly due to inadequate maintenance. Therefore, deck bearings and drainage systems were the most impacted components (Di Sarno et al. 2019).

Highways A24 and A25, two significant throughways that link Italy's east and west coasts, pass through the L'Aquila earthquake-affected region in 2009. Most bridge decks are made composed of one-span, prestressed precast, simply supported components that rest on bearings atop RC piers. Many of these supports were unbolted and could withstand lateral loads by depending only on friction. Bearings and gaps were made to allow for deck thermal deformations

but not to withstand horizontal and vertical seismic loads or displacements (Di Sarno et al. 2019). Following the L'Aquila earthquake in 2009, these roads were closed for inspection and reopened a few days later. While there was typically little structural damage to the bridges, certain interventions were required to fix damage brought on by pounding, movement, or bearing failure. The lack of internal connections during the seismic event caused each segment and each pier to respond independently, resulting in relative displacements between the deck segments and their supports. (Di Sarno et al. 2019)

During 2008 Wenchuan earthquake many bridges were affected by severe damages due to bearings. Figure 12 shows a bearing failure of Longwei Bridge in Beichuan County due to a lack of connection between bridge structure components and rubber bearing (Figure 12a). On the other hand, Figure 12b depicts a too high deformation of bearing (i.e., 15cm) in the Huilan Bridge in Mianzhu City (Han et al. 2009). In the first case, the deck collapses as a result of the bearings being in a "floating" condition and being unable to endure lateral or longitudinal relative movement between the pier cap and the deck.



Figure 12. Bridge bearings damage in Wenchuan earthquake: (a) Longwei Bridge, (b) Huilan ramp Bridge (Han et al. 2009)

Investigations by Fu et al., (Z. Fu et al. 2012), Yi et al., (R. Yi et al. 2015), Zhao et al., (Zhao et al. 2017) and Zhou and Zhen, (Liu et al. 2017) showed that a huge number of bridges collapsed under construction. most of the bridge failures are caused by human factors such as unreasonable construction technology, structure calculation errors, illegal construction, equipment operation mistakes, etc. (Correia et al. 2019; Liu et al. 2017; Pereira et al. 2020; Zhao et al. 2017). In this case, for example, workers do not adopt or change without any authorizations the construction scheme, which probably leads to bridge failures.

The failure mechanism of masonry arch bridges was the object of many studies and researches. For instance, Heyman (Heyman 1982) had established a four-hinge collapse mechanism by considering the following assumptions: (i) the masonry in the arch has no tensile strength; (ii) the masonry in the arch is incompressible; and (iii) sliding between masonry units is not allowed. Clemente et al. (1995) extended Heyman's theory and theorizes that there must be at least five hinges with a symmetric structural geometry under symmetric loading. After that, many researchers (Baggio and Trovalusci 1998; Gilbert 2007; Livesley 1992; Orduña and Lourenço 2005) proposed a combined failure mode with hinges and sliding. In a multi-span arch bridge, the subsequent failure of adjacent spans and eventually the collapse of the entire bridge may be caused by the unbalanced force resulting from the local failure of a key structural component in one span (Starossek 2007). Figure 13 shows the main types of collapse mechanisms of a single span and multi-span masonry arch bridge.

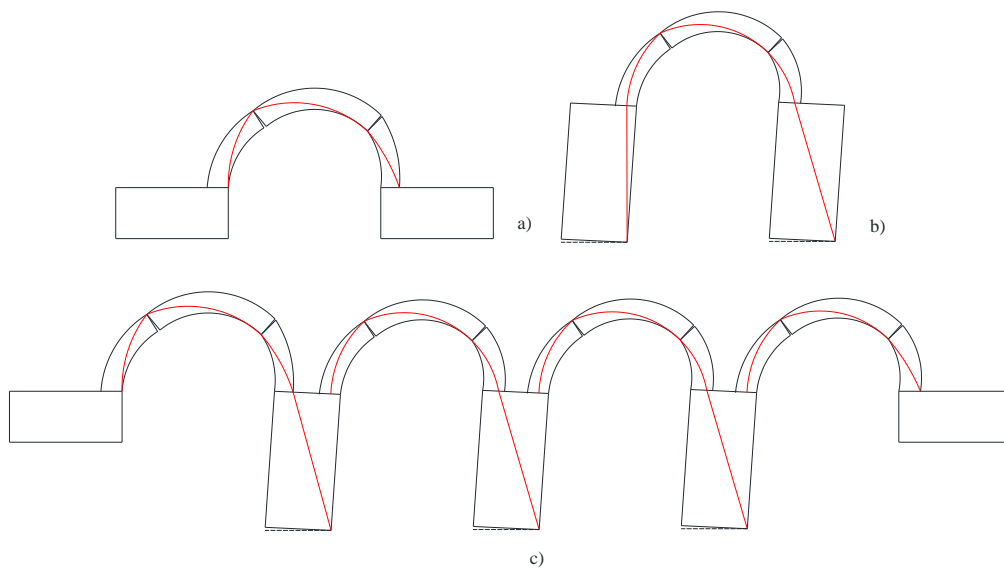


Figure 13. Single span (a-b) and multi-span (c) masonry arch bridge collapse mechanisms.

On the other hand, in the case of steel truss bridge a critical structural member or connection, such as an eye bar, a vertical member, a gusset plate, etc. may cause the failure of the entire bridge (S.-B. Lee 1996). Indeed, the collapse of the Sungsoo, Grand Bridge across the Han River in Seoul, Korea, as reported by Lee (S.-B. Lee 1996), was caused by the fracture of a vertical structural member and the consequential pulling out of the suspended truss. Another example is given by the collapse of the I-35 W Bridge in Minnesota. Many studies have shown that the beginning of the collapse was because of the failure of the gusset plate

U10, which led to the progressive collapse of the main truss in a brittle manner due to the lack of redundancy in the truss (Astaneh-Asl 2008; Hao 2010). Therefore, we can conclude that it is fundamental for steel truss bridges to have a sufficient level of structural redundancy and maintenance of safety and serviceability.

Data collection and statistical analysis of existing roadway bridges

Differently from past codes, the most recent Italian regulations are provided by NTC2018 (Italian Ministry of Infrastructures and Transportation 2018) both in terms of TLMs and design provisions according to Eurocodes. NTC 2018 (Italian Ministry of Infrastructures and Transportation 2018) are based on the semi-probabilistic design method (i.e., Level I reliability method), controlling the variability in loads and material properties through partial safety factors in order to meet a target failure probability (Comité Européen de Normalisation 2004a, 2006; Italian Ministry of Infrastructures and Transportation 2018). Conversely, this study makes use of a full probabilistic (Level III) reliability method (Comité Européen de Normalisation 2006), assuming geometric and material properties, permanent loads and capacity model error (ME) as random variables (RVs) and code-based TLMs. In order to develop a consistent comparison between fragility levels corresponding to different provisions.

3.1. Statistical analysis of bridge types

Most of the existing bridges on the Italian road network were built starting from the economic growth following the end of the Second World War. In the following decades, reinforced concrete and prestressed concrete were widely used, also following the global technological development (Borzi et al. 2015; Pinto and Franchin 2010; “Strade & Autostrade. La messa in sicurezza dei ponti italiani.” 2021).

The useful life for structures of this type, designed before the advent of the most modern regulations, can be estimated at 50 years (De Matteis et al. 2018, 2019). Consequently, most of the existing bridges in the absence of adequate maintenance interventions, are currently reaching this conventional limit and may not meet the safety requirements compliant with current regulations (Cosenza and Losanno 2021; Santarsiero et al. 2021). In Italy, between 2013 and 2018 six bridges were collapsed: Carasco (2013), Annone (2016), Ancona (2017), Fossano (2017), Bologna (2018) and Genoa (2018) (Di Prisco 2019). Four of these bridges were built in PC.

The tragic events that have taken place over the years have clearly highlighted the vulnerability of the existing infrastructures, with particular attention to the works in PC to adherent cables, which may have hidden defects related to the technology. The evolution of traveling loads and exposure to atmospheric elements, combined with sometimes insufficient maintenance interventions, have contributed to aggravating the condition of several existing structures (Crespi et al. 2020; Morgese et al. 2020).

Galano et al (Galano et al. 2020) analysed many studies and reports (Associazione italiana tecnico-economica del cemento. 1929, 1962; Associazione nazionale italiana cemento armato precompresso. 1956, 1962, 1966, 1970, 1974; Morandi 1954; Zorzi 1981) in order to evaluate the main types of PC bridges in Italy during four decades from 1950 to 1990 ('50-'60, '60-'70, '70-'80, '80-'90). 772 PC, single and multi-span, bridges were analysed. Most of the sources belong to the AITEC associations (Italian Technical-Economic Cement Association) and ANICAP (Italian National Association of Prestressed Reinforced Concrete), which over the years have collected numerous data on reinforced concrete structures progressively made in Italy. These sources have been made available by the libraries of various departments of the University of Naples Federico II and by the AICAP Association.

The static structure with a simply supported beam was observed as the most widely used static scheme for PC bridges over the total time period. Indeed, an overall percentage of 66% (510 bridges) was evaluated. Previous studies (Borzi et al. 2015) showed how the percentage of structures simply supported was even more significant (about 90%). Probably due to the different sources examined. Moreover, the study of Galano et al (Galano et al. 2020) shows a significant presence of portal/frame bridges (23% of the total works, or 179 bridges) and continuous girder bridges (about 7%, equal to 53 works). On the other hand, the total percentage relating to bridges with different static schemes is negligible; trestle bridges, with Gerber saddles, arched and stays with stays account for a total of less than 3% (30 works).

The same trend was also found on the statistics for the single decade considered. Figure 14 (Galano et al. 2020) depicts the most used bridges' static scheme in Italy from 1950 to 1990.

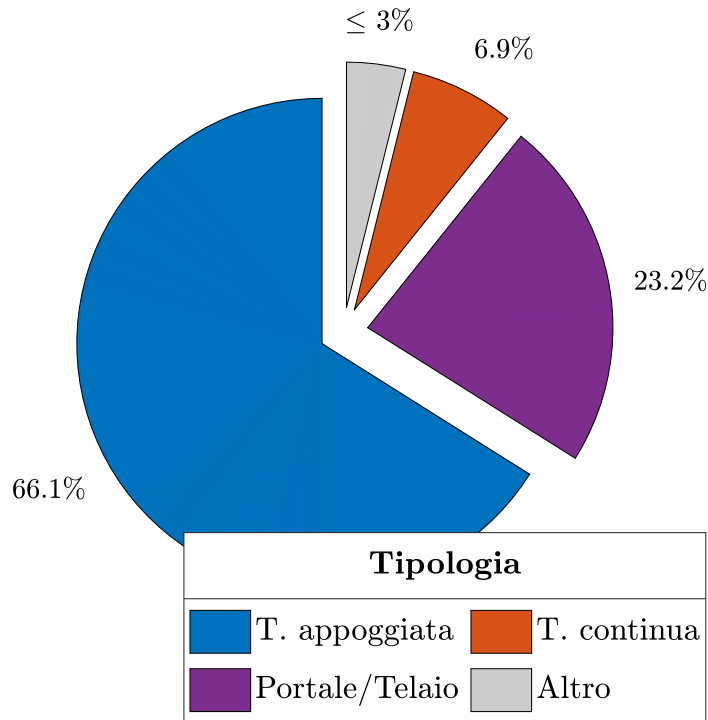


Figure 14. Static scheme for each decade: a) 1950s, b) 1960s, c) 1970s, d) 1980s (Galano et al. 2020).

3.2. Probability distributions and statistics of material properties

Based on data available in the literature (Borzi et al. 2015) and those collected on real bridges by the authors of this study, a subset of RVs was modelled through probability distributions, whereas other RVs were assumed to be statistically dependent upon the former RVs according to regression models. To that aim, the authors examined the following information on PC girder bridges built in the period 1970–1980:

- data on geometric properties.
- experimental data on mechanical properties of concrete (100 specimens), reinforcing steel (65 specimens), and prestressing steel (21 specimens).

Case-study bridges have different locations in Italy and were built by different construction companies to be representative of the selected class of bridges. In the following sections, probability distributions and regression models are described, differentiating between RVs modelled as statistically independent features and those predicted starting from their knowledge. The discussion

includes a comparative analysis of experimental data on mechanical properties of concrete and reinforcing steel related to PC bridges that were constructed in the decades 1960–1970 and 1970–1980, because of the evolution in Italian codes across those periods.

As described in (Castaldo et al. 2019; Castaldo, Gino, et al. 2018; Gino et al. 2021), uncertainties can be divided in two different groups, namely, aleatory and epistemic uncertainties. In this study, epistemic uncertainties related to the bridge deck analysis method are not taken into account, so they will be implemented in future studies. By contrast, aleatory uncertainties were duly considered.

The database of material properties was based on laboratory test results collected by the authors. Two different distributions were fitted to data on concrete compressive strength f_c and yield strength of reinforcing steel f_y , differentiating between data sets related to the periods 1960–1970 and 1970–1980. Figure 15a and Figure 15b show three alternative probability distributions fitted to experimental data of periods 1960–1970 and 1970–1980, respectively, to model the uncertainty in f_c , namely normal, lognormal and Weibull distributions. Based on best fitting outcomes, the lognormal distribution with mean value $f_{cm} = 34.7$ MPa and coefficient of variation $\text{CoV} = 24.4\%$ was assumed for the period 1960–1970. Those statistics changed to $f_{cm} = 38.5$ MPa and $\text{CoV} = 11.4\%$ for the period 1970–1980, thus highlighting an improved quality of concrete. The same procedure was applied to derive a probability distribution for yield strength f_y of reinforcing steel (Figure 16a and Figure 16b). Best fitting produced a lognormal distribution with mean value $f_{ym} = 436$ MPa and $\text{CoV} = 6.4\%$ for the period 1960–1970, which changed to $f_{ym} = 451$ MPa and $\text{CoV} = 7.2\%$ in the period 1970–1980.

A probability distribution was also fitted to experimental data on the conventional yield strength of prestressing steel $f_{p,01}$ for bridges built in the period 1970–1980, fitting a lognormal distribution with a mean value and CoV equal to 1665 MPa and 2.5%, respectively (Figure 17). Despite the limited amount of data available on such a mechanical property, these statistics agree well with different studies available in the literature (e.g., (Jacinto et al. 2012; Wiśniewski et al. 2012)).

The effectiveness of the above-mentioned distributions was tested through the Kolmogorov-Smirnov (KS) test, assuming a significance level of 5%. The one-sample Kolmogorov-Smirnov test is a nonparametric test of the null hypothesis that the population cdf of the data is equal to the hypothesized cdf. The two-sided

test tests the null hypothesis against the alternative that the population cdf of the data is not equal to the hypothesized cdf. The test statistic is the maximum absolute difference between the empirical cdf calculated from x and the hypothesized cdf: The algorithm ("MATLAB and Statistics Toolbox Release R2022b. The MathWorks Inc., Natick, Massachusetts" 2022) decides to reject the null hypothesis by comparing the p-value (is the probability of observing a test statistic as extreme as, or more extreme than, the observed value under the null hypothesis) with the significance level. More details about KS test can be found in (Marsaglia, G., W. Tsang 2003; Massey 1951; Miller 1956).

The null hypothesis (i.e., the hypothesis that the data is distributed as the selected probability distribution) was never rejected because the p-value was always found to be higher than 0.05. Nonetheless, a lognormal distribution was assumed in line with current Italian codes for existing bridges (Italian High Council of Public Works 2020; Italian Ministry of Infrastructures and Transportation 2020).

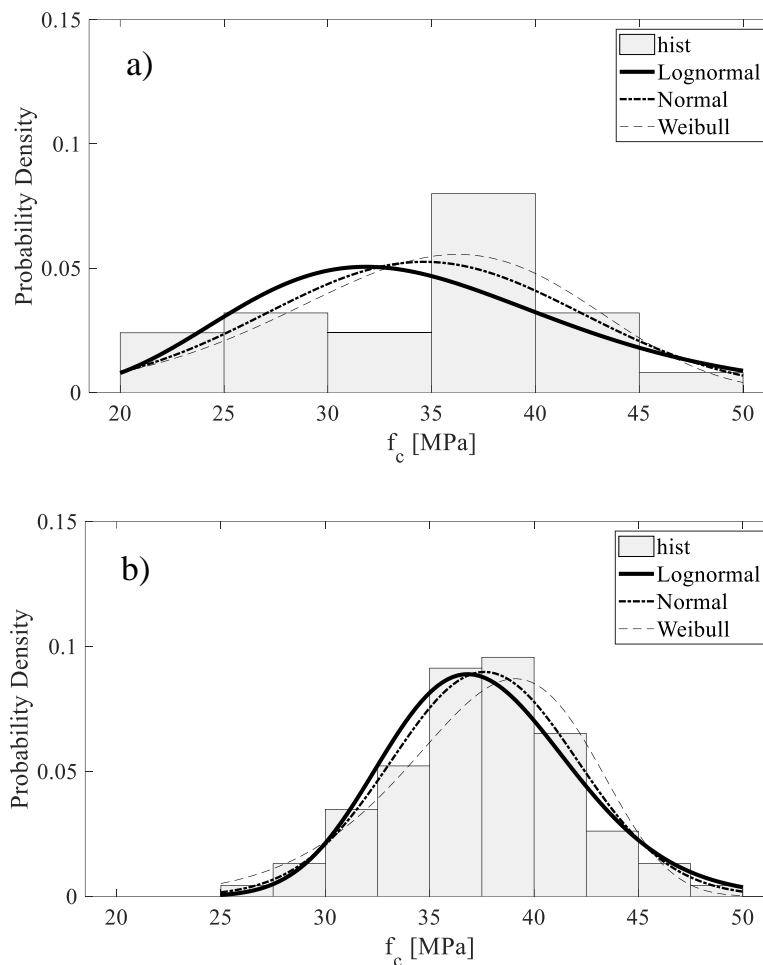


Figure 15. Probability distributions for concrete compressive strength: (a) 1960–1970; (b) 1970–1980.

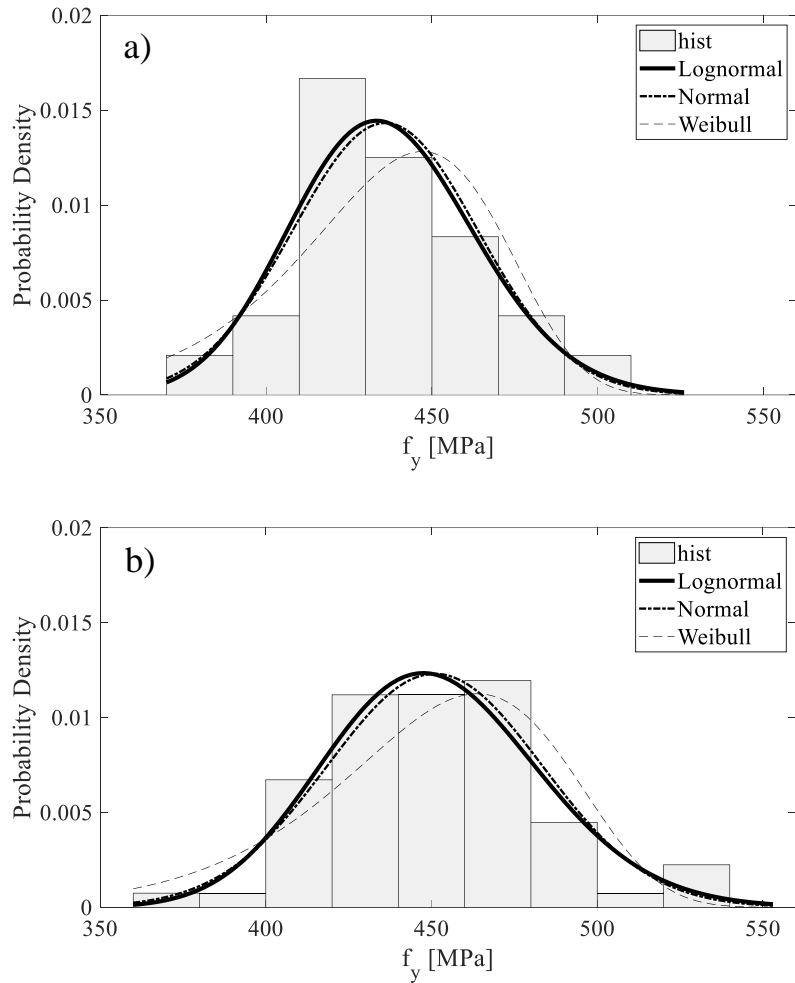


Figure 16. Probability distribution for reinforcing steel yield strength: (a) 1960–1970; (b) 1970–1980.

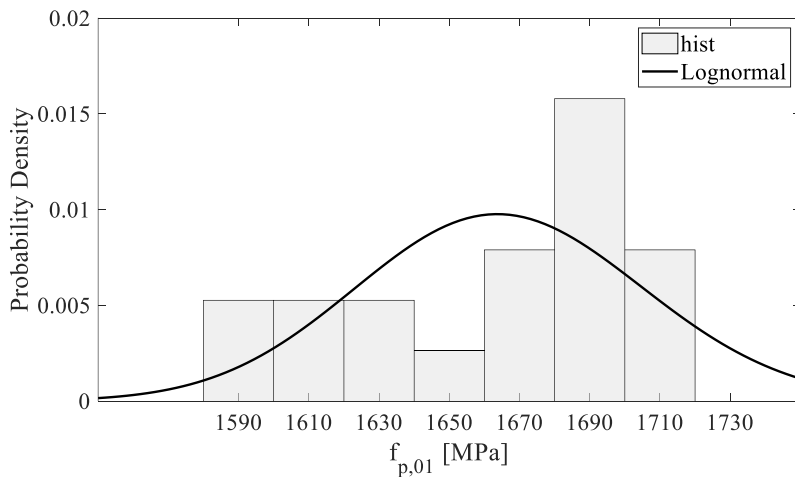


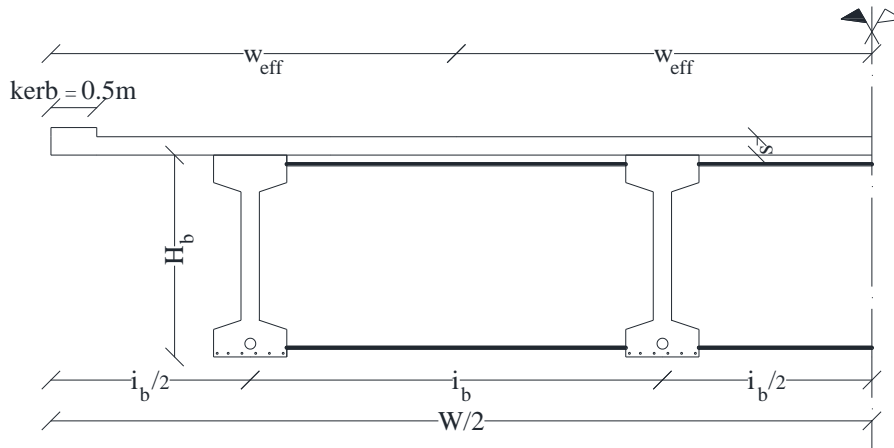
Figure 17. Probability distribution for conventional yield strength of prestressing steel.

The different values of material properties (especially concrete strength due to different regulations that changed from RD 2229/1939 (“RD 16/11/1939, n. 2229. Norme per l’esecuzione delle opere in conglomerato cementizio semplice

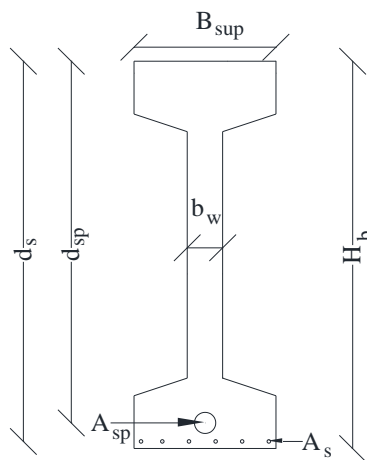
od armato (in Italian)” 1939) to DM 30/05/1972 (Italian High Council of Public Works 1972) in 1972), in addition to the lack of data on prestressing steel before 1970 (no test results available before that period), led the authors to assume different RVs for the two timeframes (i.e., 1960–1970 and 1970–1980), retaining only the period 1970–1980 for subsequent analysis. Nonetheless, particularly in the case of prestressing steel, the experimental data considered above does not include the effects of material deterioration because laboratory tests were performed at the time of construction of the real bridges. In this respect, corrosion effects should be simulated in future studies, because their impact on structural performance and fragility could be significant according to previous studies (e.g., (Belletti, Vecchi, et al. 2020)).

3.3. Probability distributions and statistics of geometric properties

Geometric properties were defined for simply supported PC bridge decks built during the whole timeframe 1960–1980 due to a common structural system and design practice, which did not undertake relevant changes. Throughout that period, beam-type decks were designed according to PSD method under the same TLMs (i.e., those provided by Circ. CSLLPP 384/1962 (Italian High Council of Public Works 1962)). This motivated the authors not to distinguish between the two decades, hence aggregating all data for uncertainty modelling of geometric parameters in order to obtain a larger data set. The cross sections of the deck and longitudinal girders are respectively shown in Figure 18a and Figure 18b, highlighting the most relevant geometric properties considered in the analysis.



(a)



(b)

Figure 18. Cross sections of (a) half bridge deck and (b) longitudinal girder.

The span length L and width W of the deck were assumed as main independent RVs. Based on data available in the literature (Borzi et al. 2015) and those collected by the authors on case-study bridges, the histogram of the bridge span length was derived. Approximately half of the existing bridges have a span length between 30 m and 35 m, as depicted in Figure 19. A lognormal distribution was assumed for L , with mean value equal to 33.2 m and $CoV = 13.6\%$. The distribution was truncated at 15 m and 45 m to obtain realistic values of bridge length in subsequent probabilistic simulation. The KS test was performed in order to demonstrate the effectiveness of lognormal distribution and the null hypothesis was rejected with a significance level of 5%. Regarding the deck width W , a probability mass function (PMF) with three values equal to 8.5, 12.25 and 16 m having the same probability of occurrence was assumed. The slab thickness (denoted by s) was modelled through a uniform distribution with mean value and CoV equal to 0.25 m and 12%, respectively, in the range [0.2 m, 0.3 m].

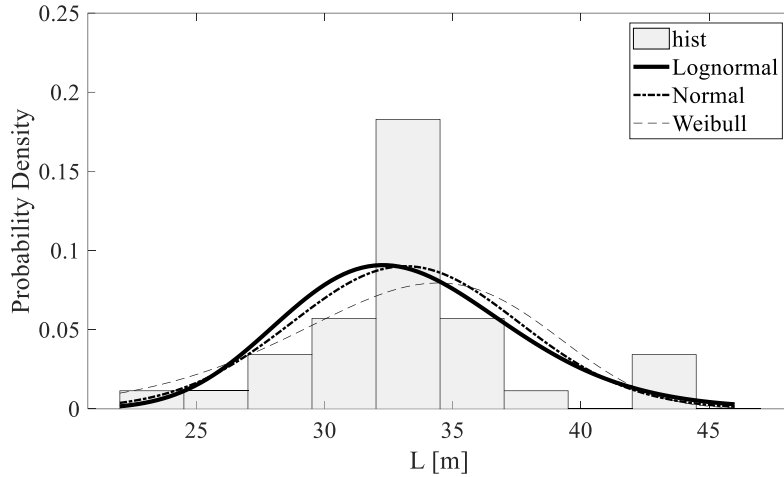


Figure 19. Probability distribution of girder length.

The transverse reinforcement ratio $\rho_{sw} = A_{sw}/p$ (namely, the ratio between the transverse reinforcement area A_{sw} and distance p between stirrups at girder ends) and prestressing ratio of the tendons $\sigma_{sp}/f_{p,01}$ (namely, the ratio between the prestressing stress σ_{sp} and $f_{p,01}$) were considered as additional independent RVs. The former was modelled through a uniform distribution between 300 mm²/m (corresponding to 8-mm-diameter stirrups with 330 mm spacing as per minimum code requirement) and 1130 mm²/m (corresponding to 12-mm-diameter stirrups with 200 mm spacing as maximum recorded value). The prestressing ratio was modelled in two different ways as follows: (i) uniform distribution between 40% and 60%; (ii) PMF with 3 equally probable values equal to 40%, 50% and 60%. In this work, degradation of prestressing steel is not taken into account. The residual stress levels σ_{sp} take into account average values of relaxation losses due to concrete creep, shrinkage and relaxation of steel under tension (Comité Européen de Normalisation 2004a). Assuming a maximum initial prestress level equal to $0,80f_{p,01}$ and 25% relaxation losses, an upper bound of $\sigma_{sp}/f_{p,01}$ equal to 60% is obtained. Lower values (i.e., 40% and 50%) are representative of a combination of lower initial pre-stress level and/or more significant relaxation losses.

Dealing with probabilistic modelling of loads, the weight per unit volume of reinforced concrete (γ_c) was modelled through normal distribution with mean and CoV equal to 25 kN/m³ and 5%, respectively, in order to account for variability in structural permanent loads (G_{Ik}). Non-structural permanent loads per unit area (g_{2k}) were modelled via a normal distribution with mean value and CoV equal to 2 kN/m² and 10%, respectively.

The set of independent RVs is listed in Table 5, providing their distributions, mean μ and CoV.

Table 5. Distributions and statistics of independent RVs for periods 1960–1970 and 1970–1980.

Category	RV	1960–1970		1970–1980		Distribution
		μ	CoV [%]	μ	CoV [%]	
Materials	f_c [MPa]	34.70	24.40	38.50	11.40	Lognormal
	f_y [MPa]	436.00	6.40	451.00	7.20	Lognormal
	$f_{p,01}$ [MPa]	–	–	1665.00	2.50	Lognormal
Geometry	L [m]	33.20	13.60	33.20	13.60	Lognormal
	W [m]	8.50,	–	8.50,	–	PMF
		12.25,	–	12.25,	–	
		16.00	–	16.00	–	
	s [m]	0.25	12.00	0.25	12.00	Uniform
	ρ_{sw} [mm ² /m]	715.00	34.00	715.00	34.00	Uniform
	$\sigma_{sp}/f_{p,01}$ [%]	50.00	12.00	50.00	12.00	Uniform
	$\sigma_{sp}/f_{p,01}$ [%]	40, 50, 60	–	40, 50, 60	–	PMF
Loads	γ_c [kN/m ³]	25.00	5	25.00	5	Normal
	g_{2k} [kN/m ²]	2.00	10	2.00	10	Normal

3.4. Correlations between geometric properties

Data available on real case-study bridges allowed the authors to observe some statistical (expected) dependence of some geometric properties on those discussed in Section 3.3. Thus, regression models were developed in order to model RVs conditioned upon independent RVs. The following dependent variables were considered:

- number of longitudinal girders, n_b ;
- height of longitudinal girder, H_b ;
- gross area of girder cross section, A_b ;
- width of girder top flange, B_{top} ;
- distance of equivalent total prestressing area from top of girder cross section, d_{sp} ;
- geometric ratio of prestressing steel ρ_{sp} multiplied by d_{sp} , i.e., $\rho_{sp} \cdot d_{sp}$.

A linear regression model for the number of longitudinal girders was derived as follows:

$$n_b = 0.33W \quad (1)$$

with a coefficient of determination $R^2 = 0.51$ and rounding the number of girders to the closest integer number. The regression model was set to have a number of girders between 2 and 8. After that n_b is estimated, the transverse girder-to-girder distance is calculated as $i_b = W/n_b$. It can be noted that for each girder the effective width w_{eff} is equal to i_b , according to geometric limitation given in Eurocode 2 (Comité Européen de Normalisation 2004a). A bivariate regression was fitted to data on the girder height H_b as follows:

$$H_b = 0.28i_b + 0.03L \quad (2)$$

with $R^2 = 0.81$ describing the accuracy of the fitting. Eq. (2) provides higher values of H_b under increasing span length of the bridge and on-centre distance of longitudinal girders, or equivalently the deck width given the number of girders. As expected, increasing n_b would proportionally reduce H_b . This latter variable was set within the range $[L/20, 3.2 \text{ m}]$.

Geometric data also allowed the authors to develop the following quadratic regression model for prediction of girder gross sectional area A_b given H_b ($R^2 = 0.84$):

$$A_b = 0.43 + 0.06H_b^2 \quad (3)$$

Eq. (3) allows the computation of girder self-weight per unit length G_{Ik} as effective sectional area $A_{b,eff} = A_b + w_{eff} \cdot s$ multiplied by the concrete unit weight γ_c , where $w_{eff} \cdot s$ denotes the effective slab area of the bridge deck.

The width of the top girder flange B_{top} was evaluated in order to define the prestressing steel area A_{sp} given ρ_{sp} . It is worth mentioning that both ρ_{sp} and ρ_s are defined in terms of tension area of the concrete cross section (i.e., web area plus section enlargement on the tension side). Hence, B_{top} was correlated to other RVs through the following multivariate regression model:

$$B_{top} = 0.34H_b + 0.02G_{Ik} - 0.02H_b G_{Ik} + 0.002G_{Ik}^2 \quad (4)$$

with $R^2 = 0.71$. The regression model was set to have a maximum value equal to 1.2 m.

The distance d_{sp} of the prestressing steel reinforcement centroid from the top of the girder cross section was conditioned upon H_b through the following linear regression model ($R^2 = 0.97$):

$$d_{sp} = 0.98H_b \quad (5)$$

The prestressing steel ratio (ρ_{sp}) multiplied by d_{sp} , $\rho_{sp} \cdot d_{sp}$, is obtained adopting a correlation with L :

$$\rho_{sp} d_{sp} = 8.16 \times 10^{-5} L + 1.85 \times 10^{-5} L^2 \quad (6)$$

with $R^2 = 0.88$ and a minimum value of $\rho_{sp} = 0.7\%$ as provided by data.

The Pearson correlation coefficient $\rho_{X,Y}$ between each outcome variable Y and its predictor X was also computed for each regression model. This coefficient is evaluated as the ratio between covariance of variables $\text{COV}(X,Y)$ and the product of the standard deviations of two variables σ_X and σ_Y . Thus, $\rho_{X,Y}$ turns out to be a normalised covariance that is a measure of linear correlation between two data sets. The correlation coefficient falls in the range $[-1,1]$, with 0 and ± 1 indicating no correlation and perfect correlation (i.e., all data belonging to a linear trend line in a scatter plot), respectively.

All regression models described above are characterised by some variability, which is another source of uncertainty referred to as model error (ME) and is the ratio between observed and predicted data. Each ME was considered as a normally distributed RV with zero mean and standard deviation σ_{ME} . Thus, the error of each regression model was added to the conditional mean value predicted through one of Eqs. (1)–(6), when randomly generating each RV conditioned upon another. In Table 6, the regression models used in this study are summarised together with their predictors (i.e., independent variables), coefficient of determination, bound values and correlation coefficient(s). It can be observed that R^2 and $\rho_{X,Y}$ are rather close to unity, apart from the regression model defined by Eq. (1) that is affected by higher dispersion of data. In all cases, $\rho_{X,Y}$ highlights a positive correlation between variables.

Table 6. Regression models.

Outcome variable	Predictor(s)	Equation	R^2	Lower bound	Upper bound	$\rho_{X,Y}$
n_b	W	1	0.51	2	8	0.64
H_b	i_b, L	2	0.81	$H_b \geq L/20$	3.2 m	$\rho_{i_b, H_b} = 0.72$ $\rho_{L, H_b} = 0.64$
A_b	H_b	3	0.84	–	–	0.88
B_{top}	H_b, G_{1k}	4	0.71	–	1.2 m	$\rho_{H_b, B_{top}} = 0.61$ $\rho_{G_{1k}, B_{top}} = 0.82$
d_{sp}	H_b	5	0.97	–	–	0.99
$\rho_{sp} d_{sp}$	L	6	0.88	$0.007d_{sp}$	–	0.94

The following deterministic variables were assumed:

1. concrete cover equal to 30 mm;
2. girder web thickness equal to 0.2 m;
3. bottom flange thickness equal to 0.3 m;
4. geometric ratio of longitudinal reinforcing steel $\rho_s = 0.1\%$;
5. Young's modulus of steel equal to 200 GPa.

Such properties were settled as deterministic variables according to values suggested by the code provisions during the period of construction selected in this study. This assumption was justified by low variability of those properties (based on the data collected by the authors) and/or negligible sensitivity of the structural behaviour to such properties (based on a preliminary sensitivity analysis performed by the authors). Specifically, variables 1, 3 and 5 are characterised by both low variability and minor influence on the structural performance of the selected bridge decks. Even though variables 2 and 4 would affect the structural response more significantly, they are characterized by a very small variability according to the collected data.

Structural performance assessment of existing prestressed concrete bridge decks under traffic loads

Based on the modelling of uncertainties, loads and structural capacity of the deck, fragility analysis was performed to assess the conditional probability of exceeding ULS in at least one edge girder, according to a single-component reliability-based safety assessment as per current Italian codes and guidelines.

The methodology was developed through the following steps:

- (i) derivation of statistics, probability distributions and regression models for material and geometric properties, based on data available in the literature and others collected on real bridges built in the period 1970–1980;
- (ii) geometric and capacity modelling of bridge decks, according to the current Italian code (Italian Ministry of Infrastructures and Transportation 2018);
- (iii) sensitivity analysis, which was based on the generation of capacity models using statistics of material and geometric properties, followed by structural analysis to identify the modelling variables that mostly influence the performance of bridge decks under traffic loading;
- (iv) fragility analysis, which was based on the random generation and analysis of capacity models to assess the conditional probability of exceeding ULS of bridge decks under varying traffic load intensity.

All these steps were fully implemented in MATLAB (“MATLAB and Statistics Toolbox Release R2022b. The MathWorks Inc., Natick, Massachusetts” 2022), delineating the flowcharts shown in Figure 20a and Figure 20b for sensitivity and fragility analyses, respectively. It is worth mentioning that the sensitivity analysis was carried out by considering the TLMs proposed by NTC2018 (Italian Ministry of Infrastructures and Transportation 2018).

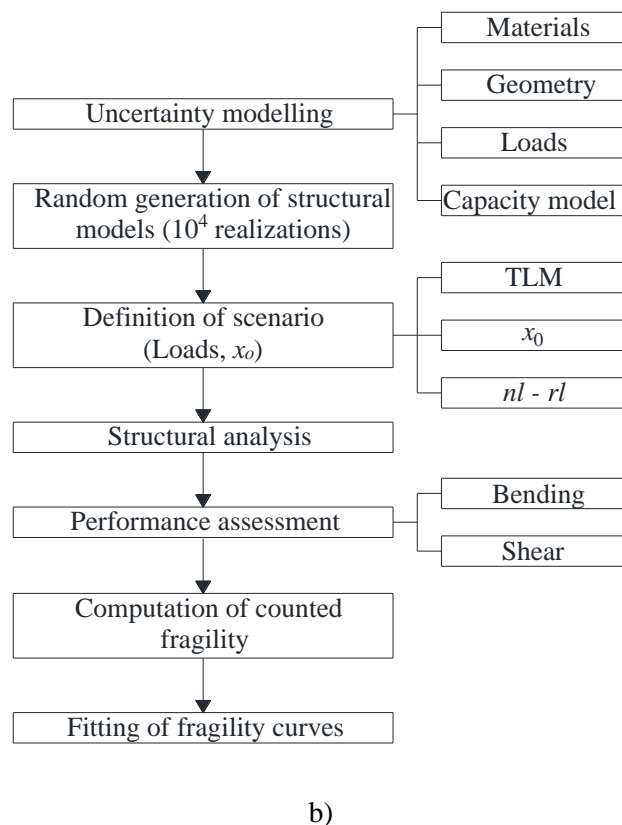
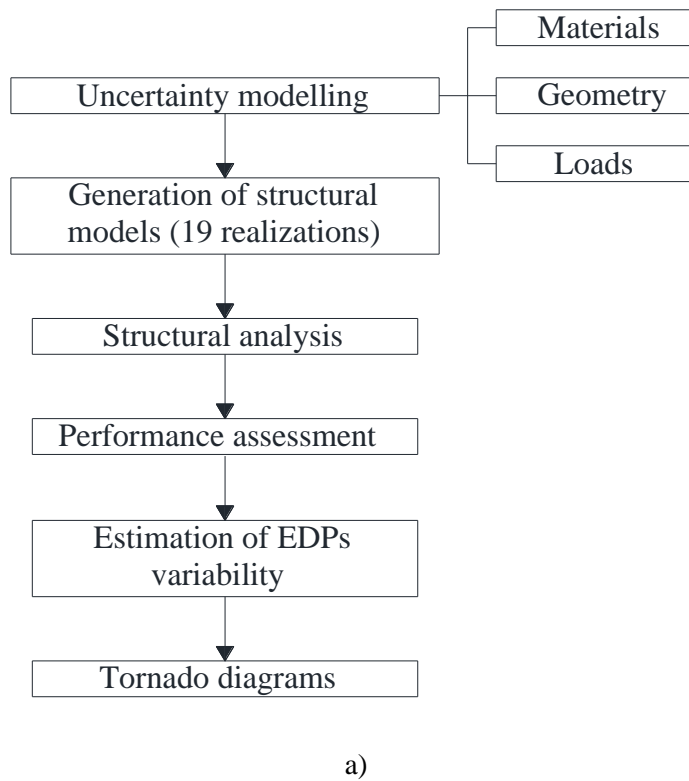


Figure 20. Flowcharts of (a) sensitivity analysis and (b) fragility analysis.

For each bridge deck model, structural analysis is performed to predict maximum internal forces (particularly bending moment and shear force) in the edge girder

under a given TLM (either NTC-TLM or GL-TLM).

This study aims to evaluate the influence of different TLMs and bridge usage limitations on analytically derived structural fragility and target failure probability $P[C]$.

Based on the variables defined through either probability distributions or regression models, in the following sections the structural analysis procedure to evaluate the effects of loads on bridge decks via engineering demand parameters (EDPs) and structural performance via demand-to-capacity ratios (DCRs) are depicted. Moreover, the assumptions for capacity modelling of the bridge deck are illustrated.

4.1. Structural modelling for fast simulations

A rigid deck cross-section was assumed according to previous finite element analyses carried out on fragility analysis case study bridges. Thus, strength demand on girders under traffic loads was evaluated according to Courbon-Engesser formulation (Cestelli Guidi n.d.; Raithel 1977, 1978). Moreover, this assumption can be adopted because fragility analysis was performed up to the ultimate limit state of the edge girder without simulating the subsequent behaviour nor the damage propagation and resulting redistribution of loads throughout the deck. This method was adopted to find the most adverse traffic load effects on the edge girder of the deck under each load pattern of interest. The presence of cross girders (usually from 3 to 5 along the deck) along with a continuous RC top slab usually provide a significant contribution towards nearly rigid sectional behaviour of existing bridge decks. This outcome can be confirmed through a grillage numerical model providing more accurate results in bridge deck analysis (Cosenza and Losanno 2021). After that a set of bridge deck models was randomly sampled, traffic loads were imposed according to either NTC-TLM or GL-TLM in order to assess strength demand. A geometric limitation on the position of the first notional lane was also taken into account through a clear distance from the kerb, hereafter indicated as x_0 (Figure 21).

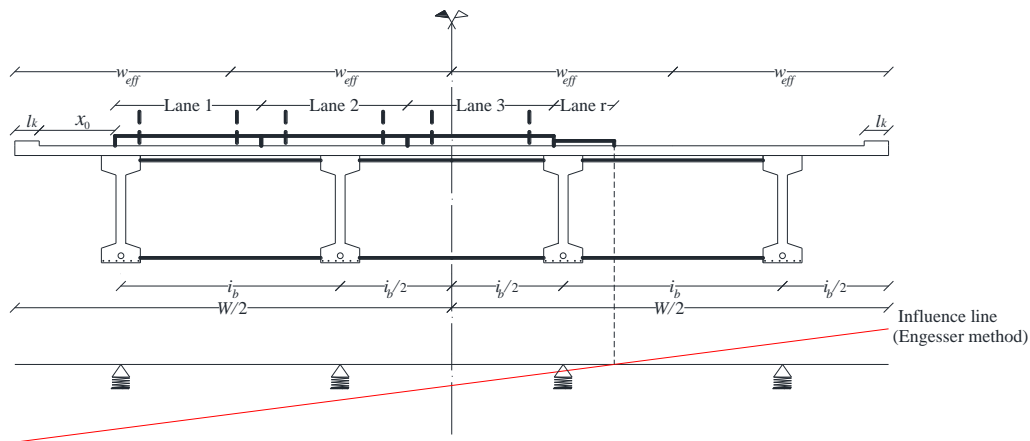


Figure 21. Deck cross section of bridge deck with traffic load lanes (first lane at x_0 from kerb)

In addition to this, an upper bound to the number of lanes n_l was also considered, that is, the maximum number of lanes was set equal to the maximum considerable number in design conditions (Comité Européen de Normalisation 2003; Italian Ministry of Infrastructures and Transportation 2018). Based on geometric statistics of the selected bridges, the authors found that, even in case GL provisions are applied (i.e., no limit to the maximum number of load lanes (Deng et al. 2016), the maximum n_l considered for the largest deck geometry would be equal to 3. A load pattern with $n_l = 1$ was also applied to evaluate the strength demand reduction on longitudinal girders in case of single traffic lane, which establishes the minimum usability of the bridge.

The remaining load area (Comité Européen de Normalisation 2003; Italian Ministry of Infrastructures and Transportation 2018) was multiplied by a factor r_l to consider either its use ($r_l = 1$) or not ($r_l = 0$) in order to evaluate its influence on structural fragility. Differently from NTC, GL provisions do not specify whether the remaining area should be subjected to loading or not, so a uniform load of 2.5 kN/m^2 was assigned to that part of the deck.

Even if those bridges were mainly designed according to a permissible stress design (PSD) approach, stress analysis of the bridge deck would require a comprehensive knowledge of the construction and prestressing stages, which cannot be assumed for a whole class of bridges. Thus, based on such assumptions, ULS was supposed to be attained through deck analysis under each load pattern when either flexural or shear capacity was achieved.

A fully automated procedure was implemented in MATLAB (“MATLAB and Statistics Toolbox Release R2022b. The MathWorks Inc., Natick, Massachusetts” 2022) in order to generate the bridge model and to automatically identify the traffic load pattern that produced the maximum strength demand on the edge girder through structural analysis, given the TLM, n_l , x_0 and r_l .

4.2. Capacity modelling for bending and shear

Flexural and shear capacity models are introduced in this study to evaluate the load-bearing capacity of the edge girder at ULS, as representative of the bridge structural behaviour according to current codes for girder bridges.

The following assumptions were made for computation of the ultimate bending moment resistance M_r of the girder cross section (Comité Européen de Normalisation 2004a; Italian Ministry of Infrastructures and Transportation 2018):

- 1) plane cross sections and perfect steel-concrete bond after flexural deformation;
- 2) ultimate compressive strain of concrete equal to 0.35%;
- 3) uniform compressive stress distribution (i.e., stress block) and zero tensile strength of concrete;
- 4) reinforcing and prestressing steel with elastic-perfectly plastic behaviour.

Prestressing steel area A_{sp} and reinforcing steel area A_s were lumped in their respective centroids. The flexural capacity of girder cross section was evaluated according to the following expression:

$$M_r = \left(A_{sp} f_{p,01} + A_s f_y \right) d^* \quad (7)$$

where d^* is the internal lever arm.

Due to a low value of A_{sp} according to available data, yielding strain was always achieved even neglecting the initial, residual strain in prestressing steel.

As far as shear capacity V_r is concerned, three different formulations were considered as per Eurocode 2 (Comité Européen de Normalisation 2004a). The first capacity model (providing $V_{r,1}$) refers to RC beam members in cracked configuration without proper shear reinforcement. The second capacity model

(providing $V_{r,2}$) retains for PC beam members in uncracked configuration, i.e., assuming a linear elastic behaviour. The third capacity model (providing $V_{r,3}$) is suited for cracked RC elements with transverse reinforcement based on a strut-and-tie resisting mechanism. The second capacity models is reported in equations 8:

$$V_{r,2} = 0.7b_w d \sqrt{f_{ct}^2 + \sigma_{cp} f_{ct}} \quad (8)$$

where: b_w is the girder web width; d is the distance of reinforcing steel rebar from the top compression side (equal to girder height minus concrete cover); f_{ct} is the concrete tensile strength calculated according to code provisions (Comité Européen de Normalisation 2004a; Italian Ministry of Infrastructures and Transportation 2018); and σ_{cp} is the average compressive concrete stress due to the residual prestressing action σ_{sp} .

4.3. Sensitivity analysis

A sensitivity analysis was performed to define the influence of different RVs on the structural response, which is measured through the following EDPs: bending moment M_E , shear force V_E , and corresponding $DCRs$.

According to the flowchart shown in Figure 20a sensitivity analysis was carried out considering three different values for each independent RV defined as $\mu - \sigma$, μ , and $\mu + \sigma$, where σ is the standard deviation. It is worth noting that $\mu - \sigma$ and $\mu + \sigma$ were replaced by the minimum and maximum values of the yield stress of the prestressing steel, due to a limited amount of data. The variables used in the sensitivity analysis together with their values are summarised in Table 7, considering $\mu^- = \mu - \sigma$ and $\mu^+ = \mu + \sigma$ as the lower and upper bounds, respectively.

Table 7. Summary of RV estimates used in sensitivity analysis.

RV	μ	μ^-	μ^+
L [m]	33.2	28.7	37.7
W [m]	12.5	8.5	16.0
s [m]	0.25	0.2	0.3
$f_{p,01}$ [MPa]	1650	1580	1720
f_c [MPa]	28.6	34.1	42.9
f_y [MPa]	451	418.5	483.5
ρ_s [%]	0.2	0.1	0.3
ρ_{sw} [mm ² /m]	715	300	1130
$\sigma_{sp}/f_{p,01}$ [%]	50	40	60

In detail, the following independent RVs were considered:

- bridge span length, L ;
- concrete compressive strength, f_c ;
- prestressing steel yield stress, $f_{p,01}$;
- reinforcing steel yield stress, f_y ;
- girder height, H_b ;
- ratio of transversal reinforcing steel, ρ_{sw} .

Regarding the prestressing ratio, the discrete probability distribution model with equally probable values of 40%, 50% and 60% was chosen. The geometric percentage of reinforcing steel ρ_s was defined through a PMF with equally probable values of 0.1%, 0.2% and 0.3%.

Other RVs defined through a PMF (i.e., deck width w , prestressing ratio ρ_{sp} , and geometric percentage of mild longitudinal steel reinforcement ρ_s) were evaluated, assuming the three values that characterize each variable.

In the sensitivity analysis, the RVs obtained through regression models were implemented without considering their model error, hence assuming their conditional mean value.

After that all variables were defined, the set of mean values of each variable was assumed to define the so called “mean bridge”. Therefore, 19 bridge models including the mean bridge were generated through MATLAB software (“MATLAB and Statistics Toolbox Release R2022b. The MathWorks Inc., Natick, Massachusetts” 2022), varying the values of each RV one by one. Therefore, the loads were automatically applied on each geometric configuration

of the bridge deck, afterwards computing both flexural and shear capacities of edge girders. In that way, the influence of each parameter and its variability on the structural response was singled out.

Following the procedure presented above, the sensitivity of the bridge models was evaluated considering the variability in their capacity and response in comparison with the mean bridge. According to, e.g., Parisi et al. (Parisi et al. 2019), the sensitivity S_{vR} of an output variable R to all variables v under study (i.e., RVs) can be graphically represented through a tornado diagram, which shows the following sensitivity measure:

$$S_{vR} = \frac{R_{v = \mu + \sigma} - R_{v = \mu - \sigma}}{R_{v = \mu}} \quad (11)$$

Eq. (11) establishes that S_{vR} is the difference (referred to as swing) between the output variable values and corresponding to the upper and lower bounds of v , normalised to the value associated with the mean of v . Thus, the tornado diagram turns out to be a bar plot with input variables v on the vertical axis and S_{vR} on the horizontal axis, ordering the input variables from top to bottom as their bar length (i.e., swing) reduces.

The variability in flexural capacity Mr is graphically represented by the tornado diagram in Figure 1Figure 22, where only input variables that produced $S_{vR} > 0.5\%$ are plotted.

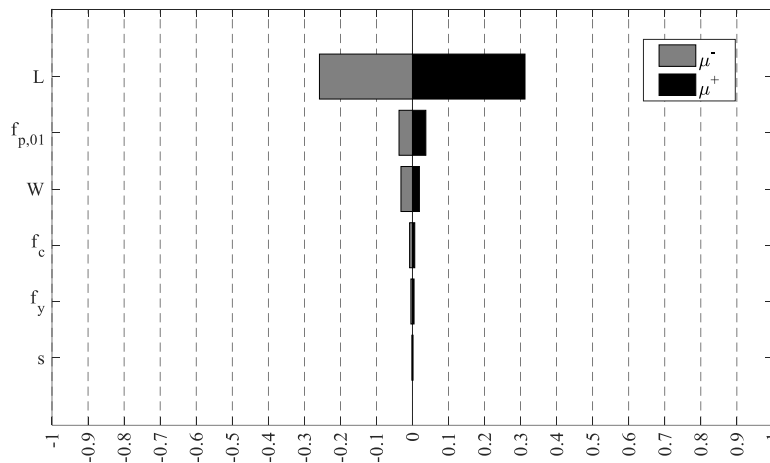


Figure 22. Sensitivity of bending moment capacity.

For the geometry under study, there is no evidence of sensitivity to the residual prestressing stress σ_{sp} , because low prestressing steel ratios result in steel strains

greater than yield steel strain according to the stress–strain relationship of steel. The tornado diagram in Figure 22 confirms that span length L is one of the most relevant parameters ($S_{vR} \approx \pm 30\%$) because it has a major impact on both H_b and ρ_{sp} that directly affect M_r . A $\pm 5\%$ variation in M_r was found under varying $f_{p,01}$ and W .

The sensitivity of shear capacity V_r was also assessed to evaluate the influence of different capacity models under varying prestressing ratio $\sigma_{sp}/f_{p,01}$ (i.e., 40%, 50%, 60%) and transverse reinforcement ratio ρ_{sw} . Figure 23 shows the variability in shear capacity of the mean bridge.

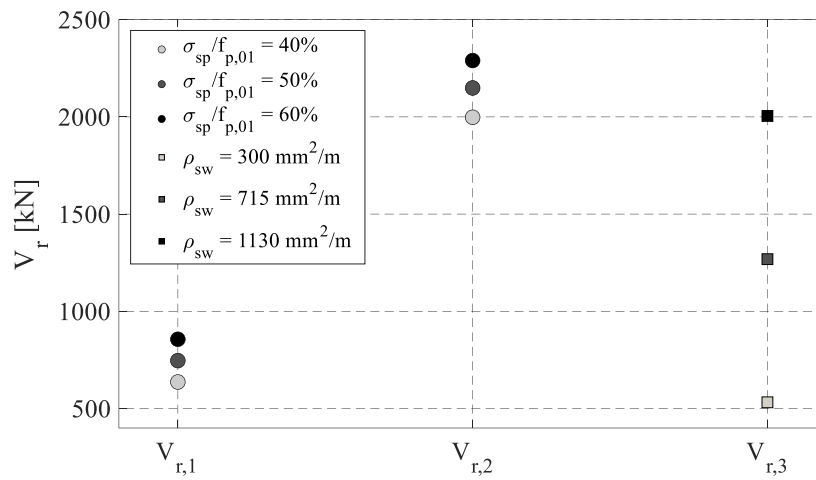


Figure 23. Shear strength according to different capacity models.

Analysis results show that $V_{r,1}$ significantly underestimates the shear capacity of PC bridge girders due to limited amount of reinforcing steel ρ_s and corresponding contribution from dowel action. The second shear capacity model leads to $V_{r,2}$ that increases with prestressing ratio, providing the maximum capacity estimates over the three models under consideration. The third capacity model leads to $V_{r,3}$ that only provides a value of capacity approaching $V_{r,2}$ in case of transverse reinforcement equal to the upper bound value. This analysis underlines that the shear capacity model for PC elements in uncracked condition and average residual prestress tends to provide the most accurate estimate for the class of bridges under study. The tornado plot on the sensitivity of shear capacity $V_{r,2}$ is shown in Figure 24. In addition to the span length L , the prestressing ratio produced a variability in shear capacity of $\pm 8\%$. A similar trend is observed for the sensitivity to concrete compressive strength f_c (with $S_{vR} \approx \pm 6\%$) due to direct correlation with tensile strength.

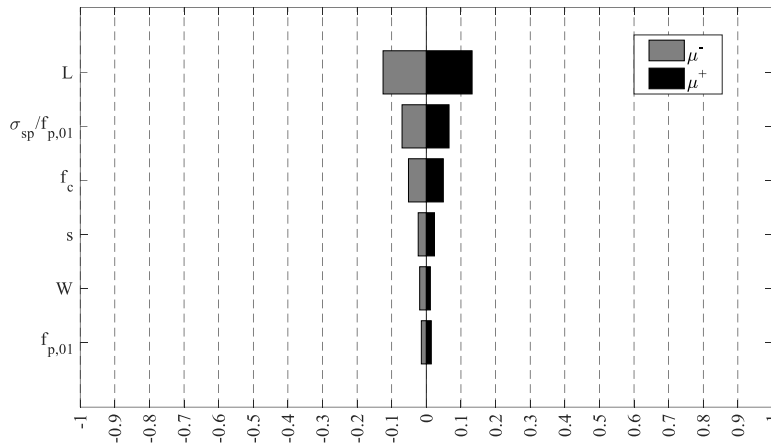
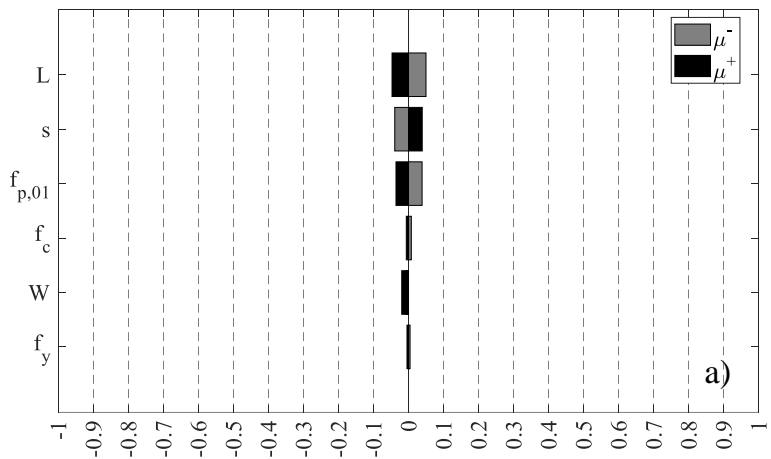


Figure 24. Sensitivity of shear capacity $V_{r,2}$.

Tornado plots were also obtained in terms of both flexural and shear DCR s (Figure 25), defined as $DCR_f = M_E/M_r$ and $DCR_s = V_E/V_r$, respectively. Flexural DCR (Figure 25a) had a certain sensitivity (around $\pm 5\%$) of the structural response to the span length L , slab thickness s , and yield strength of prestressing steel $f_{p,01}$. Shear DCR (Figure 25b) had a higher sensitivity to the prestressing ratio, which was found to be approximately $\pm 10\%$.



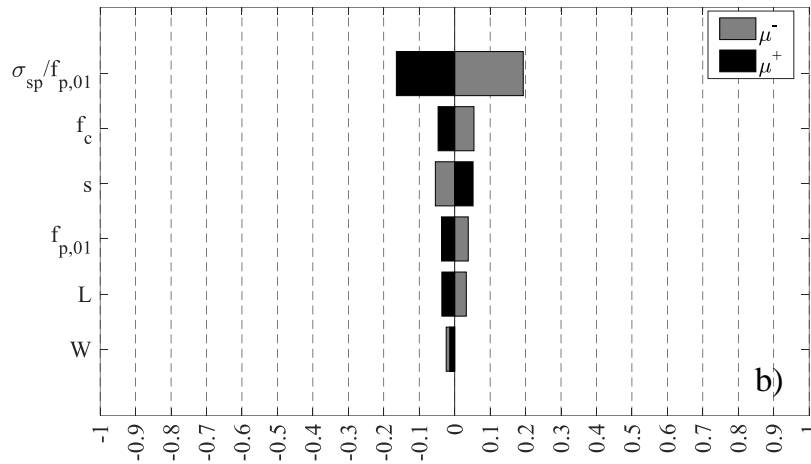


Figure 25. Sensitivity of demand-to-capacity ratios: (a) DCR_f ; (b) DCR_s .

Other variables, such as concrete compressive strength, deck width and yield strength of prestressing steel, had a lower impact on structural response. An increase in s produces an increase in both flexural and shear DCR_s , due to additional slab self-weight. Sensitivity analysis demonstrated that only shear capacity model $V_{r,2}$ can be retained and that the variability in reinforcing steel ratio ρ_s can be neglected in fragility analysis, allowing the use of a deterministic value equal to 0.1%.

4.4. Fragility analysis under code-based traffic loads

Fragility analysis was carried out according to the flowchart shown in Figure 20b. Based on statistics and probability distributions presented in Section 3, N_{sim} realizations of RVs were randomly generated through Monte Carlo sampling, assuming $N_{sim} = 10^4$. It is worth mentioning that this value of N_{sim} is enough to derive the range of probability of interests (see following Sections) with high accuracy. In this regard, other sampling techniques could be adopted, such as Latin Hypercube sampling Method (LHS). The LHS simulation considers N hyperplanes, where N is the number of RVs considered, and each of them is divided into several equally probable intervals N_{sim} (i.e., number of samples defined). In this way, N_{sim} hypercubes are created and for each of them, a value of each RV is randomly sampled.

Regression models were then used to generate statistically dependent variables, considering the model error of each regression equation. The magnitude of traffic loads was defined through an intensity measure (IM) denoted as α and defined

as the ratio between the incremental and its design value according to NTC 2018. Structural analysis of each set of 10^4 deck models was carried out under varying α from 0 to 2.5 with step of 0.01. Such multiplier α was applied to a code-compliant TLM both in terms of distributed and tandem loads for each lane, in accordance with NTC 2018 (Italian Ministry of Infrastructures and Transportation 2018) (see Section 2.2). For each deck model, both flexural and shear capacities were computed and processed in terms of $DCRs$.

The output of fragility analysis was the conditional probability of exceeding ULS (i.e., $DCR \geq 1$) given IM, assuming the following limit state function:

$$DCR = \max \left\{ DCR_f, DCR_s \right\} \quad (12)$$

Fragility was thus defined as $P[DCR \geq 1 | IM = im]$, where im indicates a value assigned to IM, and hence the load multiplier α applied to the TLM. Given the large number of model realizations and corresponding analysis results, an index function $I_{DCR|IM}(\theta)$ was used to count the number of failure cases and to estimate the traffic-load fragility of the bridge class under study. In detail, θ is a real vector that includes the RVs defined into a region Ω and $I_{DCR|IM}$ is a Bernoulli-type variable that was assumed to be:

$$\begin{aligned} I_{DCR|IM}(\theta) &= 0 && \text{if } DCR < 1 \\ I_{DCR|IM}(\theta) &= 1 && \text{if } DCR \geq 1 \end{aligned} \quad (13)$$

Therefore, the traffic-load fragility was numerically estimated as the expected value of $I_{DCR|IM}(\theta)$ according to the following equation:

$$P[DCR \leq 1 | IM = im] \approx \frac{\sum_{i=1}^{N_{sim}} I_{DCR|IM}(\theta)}{N_{sim}} \quad (14)$$

After that counted fragilities were computed over the whole range of IM levels, fragility curves were fitted through a lognormal distribution to allow a continuous modelling of traffic-load fragility and its possible convolution with hazard models in future probabilistic risk assessments.

It is worth noting that Eq. (14) directly provides the traffic-load fragility because the bridge deck analysis according to Engesser method is not affected by convergence issues nor instability phenomena, allowing the computation of *DCRs* in all cases. By contrast, previous studies (e.g.(Castaldo, Palazzo, et al. 2018)) show that collapse cases should be carefully processed in fragility assessments based on nonlinear structural analysis. In such a more general case, ULS can be exceeded in two possible conditions that need to be considered in fragility computation: (1) $DCR \geq 1$ (hereafter C1 case), and (2) dynamic instability (Shome and Cornell 2000) resulting in very large *DCR* values or loss of analysis convergence (hereafter C2 case). According to (Jalayer et al. 2017) and the total probability theorem, the probability of exceeding collapse (i.e., event denoted by C) should be computed as follows:

$$P[C|IM=im]=P[C|IM=im,C_1] \times (1-P[C_2|IM=im]) + P[C_2|IM=im] \quad (15)$$

where $P[C|IM=im,C_1]$ is the conditional probability calculated according to Eq. (14) and $P[C_2|IM=im]$ is the probability of collapse condition C2 due to numerical instability (Shome and Cornell 2000). In this work, the methodology adopted for bridge deck analysis produces $P[C_2|IM=im]=0$, so Eq. (15) turns out to be equal to Eq. (14).

In order to assess if the proposed model variables are consistent with the original design provisions, the bridges under study were assumed to be subjected to TLMs defined by Circ. CSLLPP 384/1962 (Italian High Council of Public Works 1962) and were checked according to DM 30/05/1972 (Italian High Council of Public Works 1972). This modus operandi was motivated by the fact that Circ. CSLLPP 384/1962 (Italian High Council of Public Works 1962) and DM 30/05/1972 (Italian High Council of Public Works 1972) were the Italian codes in force at the time of construction for the selected bridges in terms of TLMs and safety check provisions, respectively. Specifically, Circ. CSLLPP 384/1962 provided the TLMs for bridge analysis, whereas DM 30/05/1972 was the Italian code of reference for capacity modelling and safety checking of bridges. Stress-based safety checks according to PSD would require a comprehensive knowledge of the construction and prestressing stages significantly affecting internal stress distributions, which cannot be assumed for a whole class of bridges. Alternatively, at the time of construction a simplified design check against ultimate condition could be carried out in order to provide a minimum value of

safety factor $SF_{DM.1972}$ equal to 1.75, calculating $SF_{DM.1972}$ as the ratio between bending moment capacity and demand (i.e., $SF_{DM.1972} = M_{r,DM.1972}/M_{E,Circ.1962}$). The original design process was thus validated over 10^3 model realizations that were randomly generated using Monte Carlo sampling. Traffic loads according to both past and current Italian codes, i.e., Circ. CSLLPP 384/1962 (Italian High Council of Public Works 1962) and NTC 2018 (Italian Ministry of Infrastructures and Transportation 2018), were adopted to assess bending moments $M_{E,Circ.1962}$ and $M_{E,NTC2018}$, respectively. Bending moment capacity $M_{r,DM.1972}$ was calculated by assuming a maximum concrete compressive strength $\sigma_{c,am} = 0.55R_c$ and yield steel strength f_y according to past code provisions.

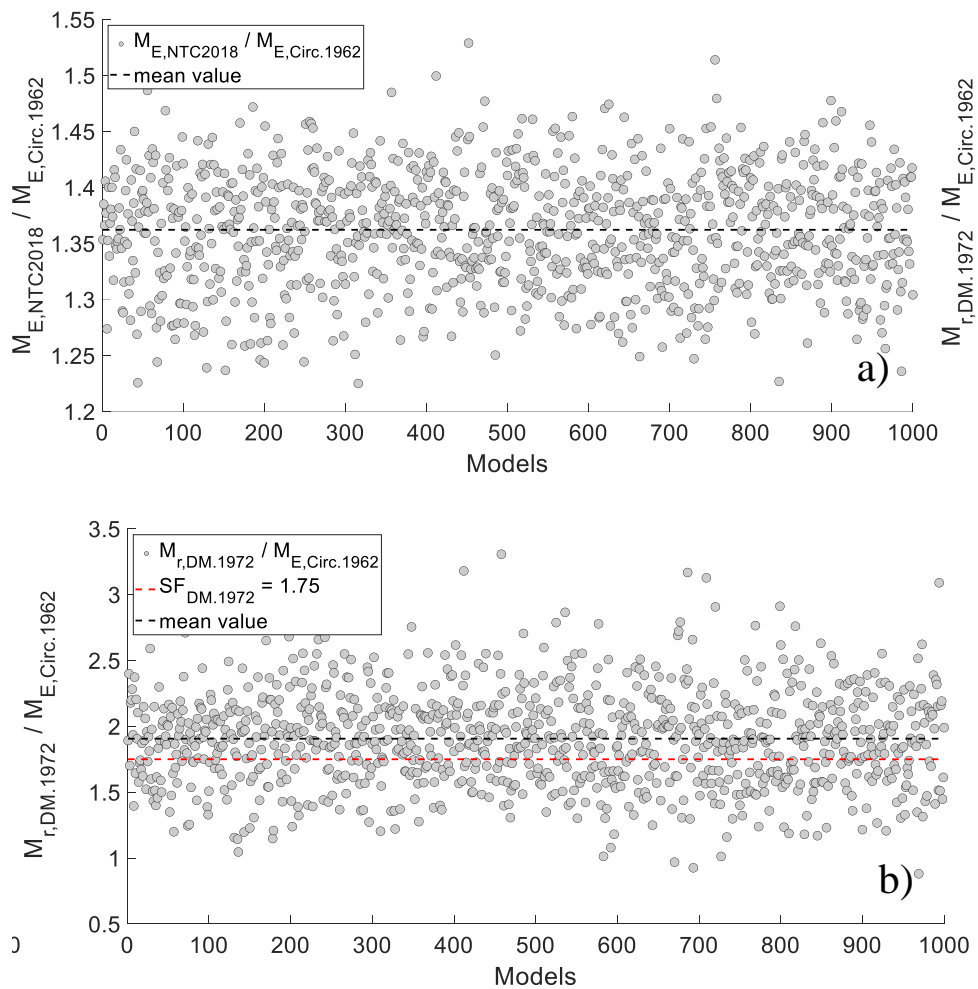
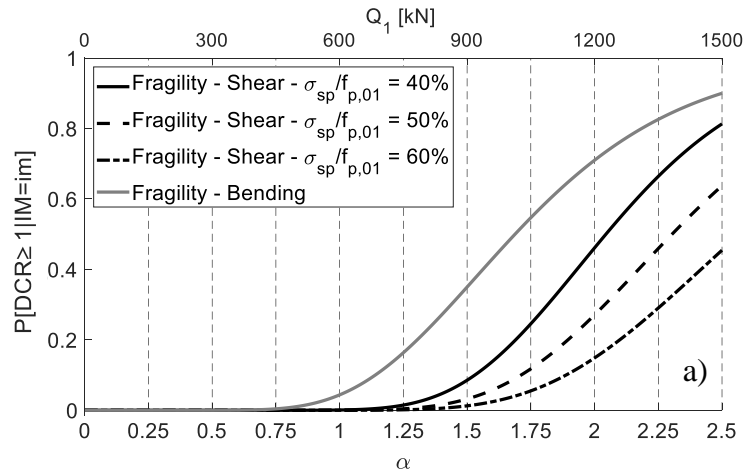


Figure 26. Simulated design: (a) increase in traffic load effects between NTC 2018 and Circ. CSLLPP 384/1962; (b) safety factor considering traffic loads provided by Circ. CSLLPP 384/1962.

Different effects of TLMs provided by Circ. CSLLPP 384/1962 (Italian High Council of Public Works 1962) and NTC 2018 (Mosleh et al. 2020) are shown in

Figure 26a in terms of ratio between $M_{E,NTC2018}$ and $M_{E,Circ.1962}$. This ratio falls in the range [1.2,1.5] with mean value of 1.36, demonstrating a significant increase in traffic load effects associated with current code provisions. Figure 26b shows a mean safety factor $SF_{DM,1972,m} = 1.91$, which is greater than minimum value of 1.75, with a few cases resulting in a safety factor close to unity. This outcome confirms the representativeness of the randomly generated bridge models and their compliance with past Italian codes in force at the time of their construction. Additional data will be collected by the authors to further improve the accuracy of model variables.

Then, fragility curves associated with flexural and shear failure modes were first derived separately, considering either deterministic values (Figure 27a) and uniformly distributed values (Figure 27b) of prestressing ratio. In Figure 27, the lower x-axis indicates the selected IM (i.e., α), whereas the upper x-axis provides the corresponding first-lane tandem load $Q_1 = \alpha Q_{1d}$, being $Q_{1d} = 600$ kN the design load on first lane. Figure 27 shows a higher fragility of the case-study bridges in terms of flexural failure.



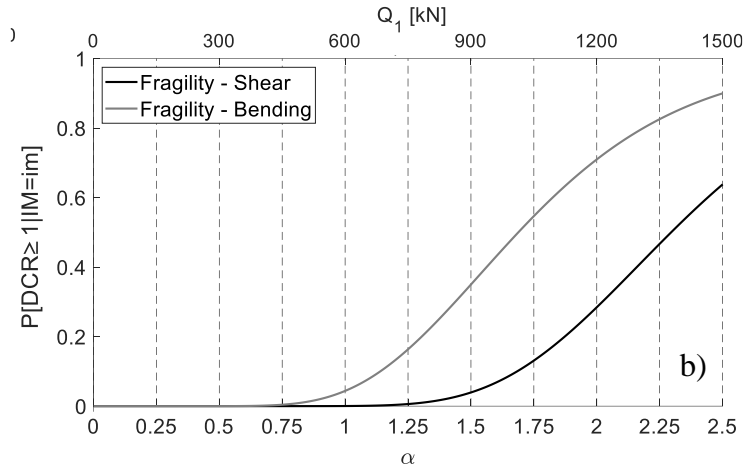


Figure 27. Fragility curves associated with flexural and shear failure modes: (a) discrete distribution of prestressing ratio; (b) uniform distribution of prestressing ratio.

Indeed, the median value η of the flexural fragility curve is lower than that of the shear fragility curve, regardless of the prestressing ratio. This means that the attainment of ULS is governed by flexural failure. As shown in Figure 27a, shear fragility significantly reduces under increasing prestressing ratio. Table 8 outlines the median value η , dispersion β (i.e., the logarithmic standard deviation) and R^2 of each fragility curve, evidencing that the lognormal distribution fits very well the fragility points as demonstrated by R^2 very close to unity.

Table 8. Fragility parameters corresponding to flexural failure, shear failure, and ULS.

Failure mode/damage level	η	β	R^2
Flexural failure	1.69	0.31	
Shear failure ($\sigma_{sp}/f_{p,01} = 40\%$)	2.04	0.23	
Shear failure ($\sigma_{sp}/f_{p,01} = 50\%$)	2.30	0.23	0.99
Shear failure ($\sigma_{sp}/f_{p,01} = 60\%$)	2.57	0.24	
Shear failure ($\sigma_{sp}/f_{p,01}$ uniformly distributed)	2.30	0.24	
ULS	1.68	0.30	0.99

Figure 28 shows the fragility curve of the case-study bridges for the ULS, which is almost totally overlapped to that associated with flexural failure mode. However, the median value and dispersion are slightly different from those related to the flexural fragility curve because of a very rare occurrence of shear failure in some model realizations. Table 8 shows that the selected bridges have a median collapse traffic load multiplier equal to 1.68 with dispersion $\beta = 0.30$. It is also found that the conditional probability of collapse given design traffic

load (corresponding to $\alpha = 1$) is $4.4 \cdot 10^{-2}$. Further studies are needed to assess the unconditional failure probability of collapse, namely, the failure probability derived as a convolution of fragility and traffic-related hazard. Based on fragility analysis results, realizations of bending moment capacity M_r , demand M_E and DCR_f were fitted through a lognormal distribution (Figure 29a–c).

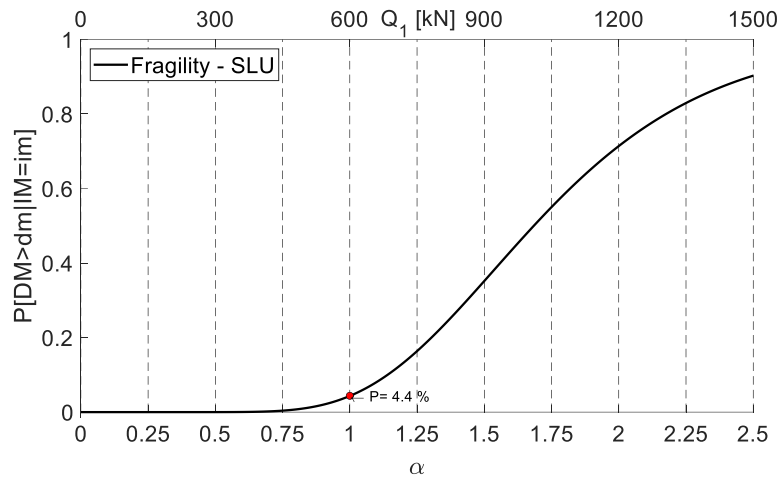
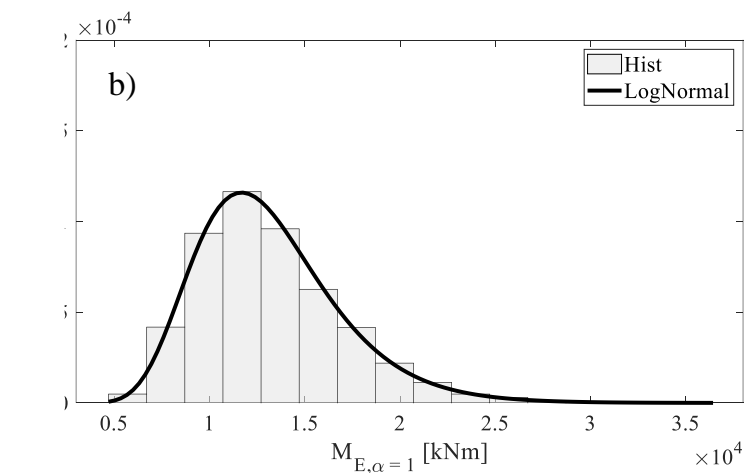
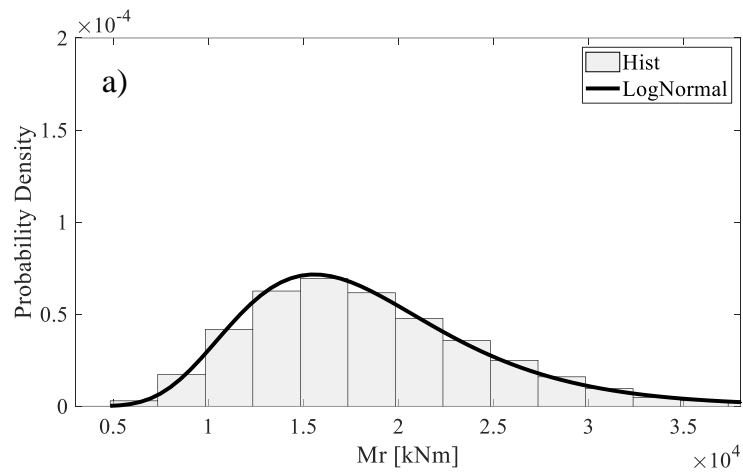


Figure 28. Collapse fragility curve of case-study bridges.



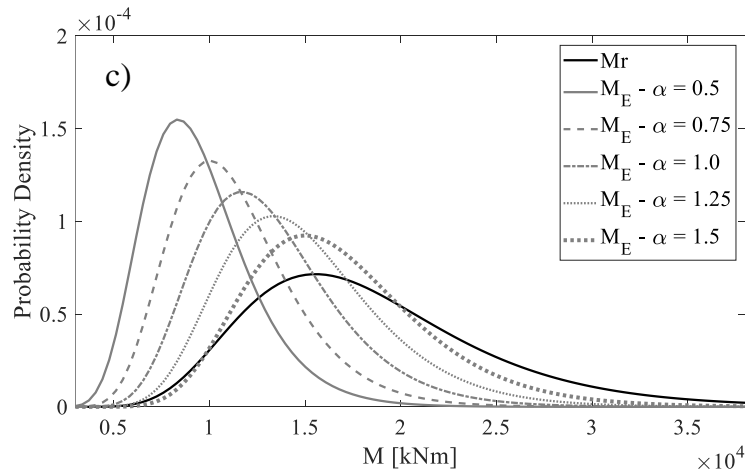


Figure 29. Bending moment distributions: (a) capacity, (b) demand given $\square = 1$, (c) overlapping of capacity and demands corresponding to multiple load intensities.

Five different values of IM were chosen (i.e., 0.5, 0.75, 1, 1.25 and 1.5) to derive corresponding demand and *DCR* distributions. As outlined in Table 9, bending moment demand distributions are characterised by $CoV \approx 30\%$. A slightly higher value of coefficient of variation is found for M_r , i.e., $CoV = 34.8\%$, however ensuring $M_r > M_E$ under any IM level. *DCR* distributions were derived through the same procedure (Figure 30), evidencing $CoV \approx 20\%$ (Table 10). In the case $\alpha = 1$, a mean value $\mu = 0.74$ was obtained with $\mu + \sigma = 0.89$. The probability of exceeding ULS given IM can be calculated as the area below the corresponding distribution under *DCR* ranging in the interval $[1, +\infty]$, namely, through a convolution of demand and capacity.

Table 9. Mean, standard deviation and CoV of lognormal distributions representative of flexural demand and capacity.

Bending moment	μ [kNm]	σ [kNm]	CoV
$M_E (\alpha = 0.50)$	$9.5 \cdot 10^3$	$2.9 \cdot 10^3$	30.1%
$M_E (\alpha = 0.75)$	$11.4 \cdot 10^3$	$3.3 \cdot 10^3$	29.4%
$M_E (\alpha = 1.00)$	$13.2 \cdot 10^3$	$3.8 \cdot 10^3$	28.9%
$M_E (\alpha = 1.25)$	$15.0 \cdot 10^3$	$4.3 \cdot 10^3$	28.5%
$M_E (\alpha = 1.50)$	$16.8 \cdot 10^3$	$4.7 \cdot 10^3$	28.5%
M_r	$18.5 \cdot 10^3$	$6.4 \cdot 10^3$	34.8%

Table 10. Mean, standard deviation and CoV of lognormal distributions representative of *DCR*.

α	μ	σ	CoV
0.50	0.53	0.10	19.5%
0.75	0.64	0.13	19.9%
1.00	0.74	0.15	20.2%
1.25	0.84	0.17	20.5%
1.50	0.95	0.20	20.7%

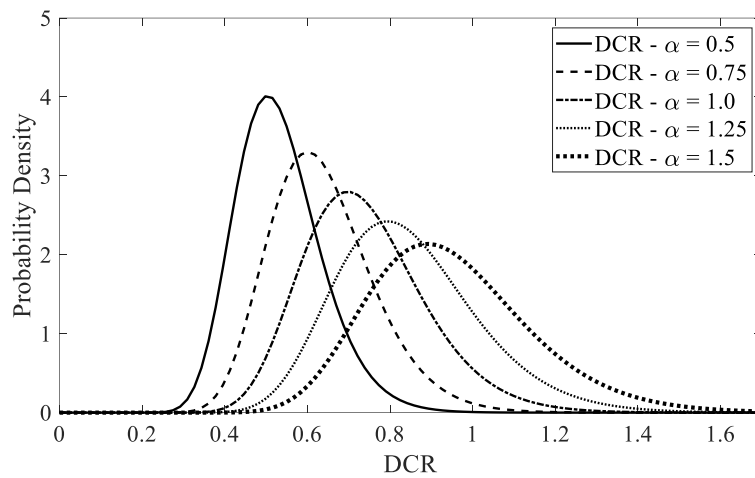


Figure 30. *DCR* distribution under varying IM level.

Table 11 allows a comparison between conditional failure probabilities obtained through frequentist approach (i.e., fragility curves presented above) and convolution (i.e., numerical integration of *DCR* distributions), highlighting that values very close to each other are obtained especially for higher values of α . This confirmed the appropriate number of realizations to obtain an accurate value of traffic-load fragility through a frequentist approach.

Table 11. Fragility estimates derived through frequentist approach and convolution at multiple IM levels.

α	Frequentist approach	Convolution
0.50	$4.00 \cdot 10^{-5}$	$4.70 \cdot 10^{-4}$
0.75	$4.10 \cdot 10^{-3}$	$8.80 \cdot 10^{-3}$
1.00	$4.40 \cdot 10^{-2}$	$5.70 \cdot 10^{-2}$
1.25	$1.63 \cdot 10^{-1}$	$1.83 \cdot 10^{-1}$
1.50	$3.5 \cdot 10^{-1}$	$3.75 \cdot 10^{-1}$

Therefore, fragility analysis results led the authors to assess the influence of conventional yield stress $f_{p,01}$ on flexural fragility. According to sensitivity analysis, $f_{p,01}$ is indeed the mechanical parameter that mostly influence bending capacity M_r but only a few experimental data were collected on real bridges, due to lack of available tensile tests on prestressing steel. In fragility analysis, the authors assigned $f_{p,01}$ a lognormal distribution with mean value and coefficient of variation equal to $\mu_{f_{p,01}} = 1665$ MPa and $\text{CoV}_{f_{p,01}} = 2.5\%$, respectively. In order to shed more light on the influence of $f_{p,01}$, the authors carried out an additional fragility analysis to investigate its sensitivity to different values of $\text{CoV}_{f_{p,01}}$ (i.e., 2.5%, 5% and 7.5%) given $\mu_{f_{p,01}} = 1665$ MPa. Such values of CoV are deemed adequately representative of tensile strength variation in both reinforcing and prestressing steel (Castaldo et al. 2019; Jacinto et al. 2012). The corresponding parametric fragility curves are shown in Figure 16 and their parameters are outlined in Table 9, showing almost no sensitivity of traffic-load fragility to CoV.

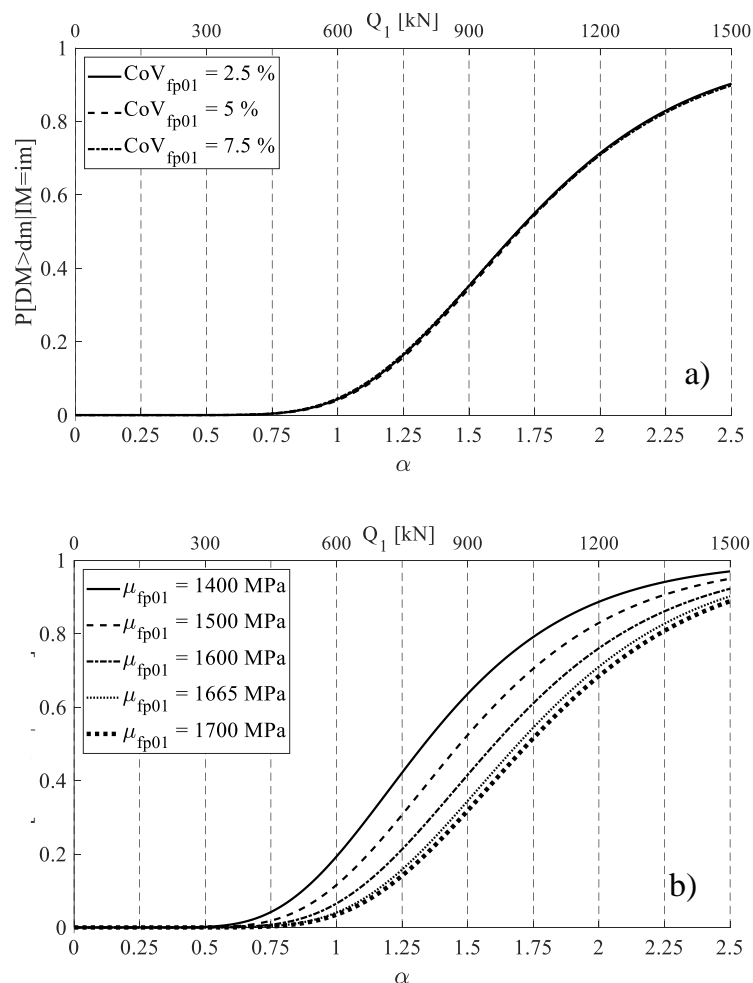


Figure 31. Traffic-load fragility curves under varying (a) mean value and (b) CoV of $f_{p,01}$.

According to such an outcome, a further sensitivity analysis was carried out by assuming different values of $\mu_{fp,01}$ (i.e., 1400, 1500, 1600, 1665 and 1700 MPa) given $\text{CoV}_{fp,01} = 2.5\%$. The corresponding parametric fragility curves are shown in Figure 31b. Median value η varies from 1.34 (corresponding to $f_{p,01} = 1400$ MPa) to 1.73 (corresponding to $f_{p,01} = 1700$ MPa), confirming the key role of prestressing steel tensile strength in determining the structural (flexural) capacity of the case-study bridges. Given a distribution of prestressing steel strength, Figure 31 allows one to have a sufficiently accurate estimate of the bridge fragility under code-compliant traffic loads.

Table 12. Fragility curve parameters under varying mean value and CoV of $f_{p,01}$.

Variable	$\mu_{fp,01}$	$\text{CoV}_{fp,01}$	η	β	R^2
$\text{CoV}_{fp,01}$	1665 MPa	2.5%	1.69	0.31	0.99
	1665 MPa	5.0%	1.69	0.31	
	1665 MPa	7.5%	1.69	0.30	
$\mu_{fp,01}$	1400 MPa	2.5%	1.34	0.33	
	1500 MPa	2.5%	1.47	0.32	
	1600 MPa	2.5%	1.60	0.31	
	1665 MPa	2.5%	1.69	0.31	
	1700 MPa	2.5%	1.73	0.30	

4.5. Fragility analysis under traffic loads according to new Italian guidelines

Based on the procedure described in Section 4.4, another fragility analysis was carried out to derive fragility curves under TLMs proposed by new Italian guidelines (Italian High Council of Public Works 2020). The IM (denoted as α) was assumed to range from 0 to 5 with step of 0.01 and the performance of each sample bridge deck was measured via *DCR* related to the edge girder.

In each fragility plot, the upper x-axis provides the corresponding first-lane tandem load $Q_l = \alpha Q_{ld}$. If α is set to 1, then the design traffic load of the selected bridge provisions is defined, namely, $Q_{ld} = 600$ kN in case of NTC-TLM and $Q_{ld} = 440$ kN in case of heavy GL-TLM. As discussed before, this study aimed at investigating the sensitivity of traffic-load fragility to the following parameters: (i) traffic load model, i.e., TLM, (ii) limitation of the transverse eccentricity, i.e. $0 \leq x_0 \leq 2.0$ m, (iii) number of lanes, i.e. $1 \leq n_l \leq 3$, and (iv) presence or lack of remaining uniform load, i.e. $r_l = 1$ or $r_l = 0$.

As described in the last Section, bridge decks analysed are much more vulnerable to the flexural failures than shear ones, thus, the uncertainties related to flexural capacity model have been taken into account while neglecting those related to shear capacity.. According to experimental data from the literature (Elsharkawy et al. 2013; Harajli n.d.; Hussien et al. 2012; Vu et al. 2010; X. Zhang et al. 2017), 16 PC beams were considered in terms of experimental flexural capacity compared to its theoretical counterpart provided by Equation 7. The model error θ was defined as the ratio between the experimental and theoretical strength values for each specimen (Castaldo, Gino, et al. 2018), namely $\theta = M_{r,exp}/M_{r,th}$. As suggested in a previous study (Castaldo, Gino, et al. 2018), a lognormal probability distribution of θ was derived and characterised by a mean value $\mu_\theta = 0.99$ and logarithmic standard deviation $\sigma_\theta = 0.15$, or equivalently, coefficient of variation $CoV_\theta = 15\%$. Therefore, Equation 15 was applied in order to derive the logarithmic standard deviation (or dispersion, β) of each fragility curve:

$$\beta = \sqrt{\beta_{al}^2 + \beta_{ep}^2} \quad (15)$$

where β_{al} is the logarithmic standard deviation associated with aleatory uncertainties (representative of the inherent variability of geometric and material properties, as well as loads) and β_{ep} is the logarithmic standard deviation associated with epistemic uncertainties that turns out to be the standard deviation of the model error θ , hence resulting in $\beta_{ep} = \sigma_\theta$.

In order to evaluate the sensitivity of fragility analysis, in Figure 32, the fragility curve previously derived in Section 4.4 without considering model uncertainty for the ULS under NTC-TLM is compared to that newly derived by accounting for model uncertainty.

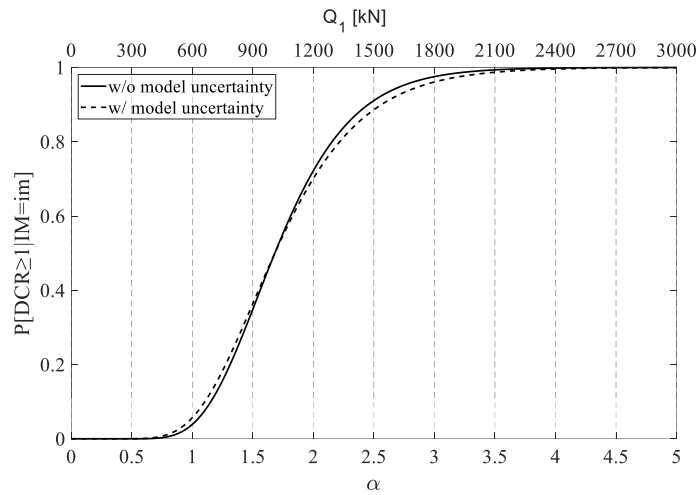
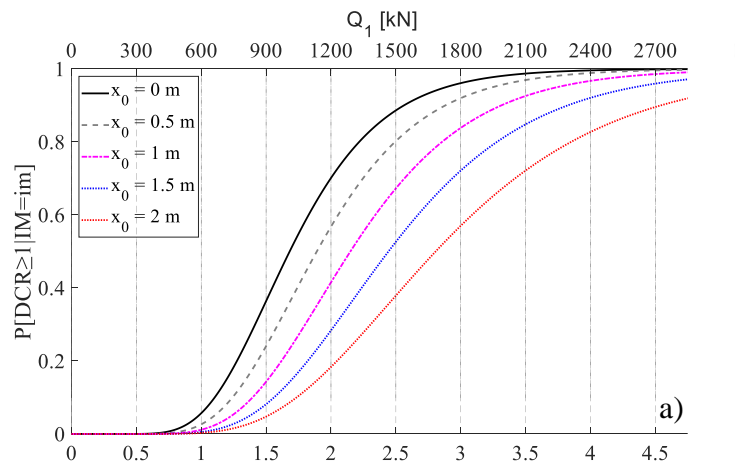


Figure 32. Comparison between fragility curves with or without consideration of model uncertainty (case of maximum number of load lanes and NTC-TLM).

The two curves shown in Figure 32 present the same median value equal to 1.68 but their dispersion is equal to 0.33 and 0.29 depending on whether model uncertainty is considered or not, respectively. The two curves are very close to each other, highlighting a relatively low influence of the uncertainty associated with the flexural capacity model on traffic-load fragility.

Figure 33 shows fragility curves obtained for different values of x_0 by assuming the maximum number of load lanes (i.e., the value of n_l that maximizes strength demand) and $r_l = 1$. It is noted that, in case of NTC-TLM, the condition $x_0 = 0$ would provide an NTC-conforming load distribution (considered in Section 4.4).



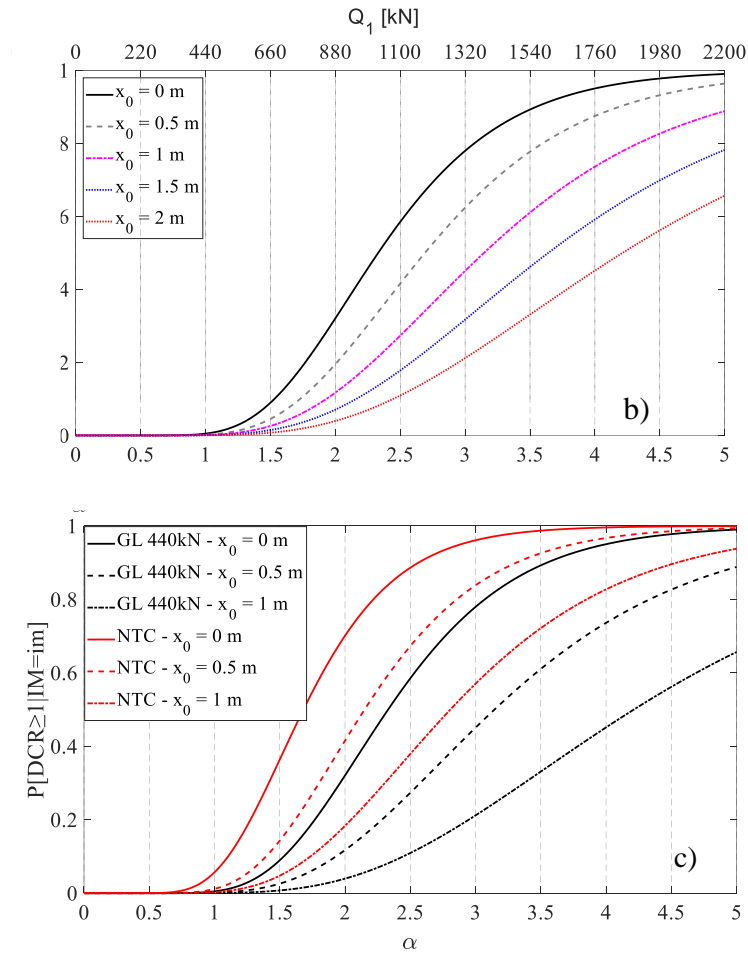


Figure 33. Fragility curves corresponding to the maximum number of load lanes: (a) NTC-TLM; (b) GL-TLM; (c) comparison between fragility curves under $0 \leq x_0 \leq 1$ m.

Figure 33a and Figure 33b highlight a major effect of maximum transverse eccentricity under both NTC-TLM and heavy GL-TLM. A significant reduction of traffic-load fragility can be observed when a limitation on the maximum eccentricity of the first load lane is applied. In case GL-TLM is considered (Figure 33b), the rate of fragility reduction under increasing x_0 is higher than that observed under the other load pattern (i.e., NTC-TLM) due to the assumption of equal traffic loads on different lanes (Figure 33c). Fragility curves corresponding to heavy GL-TLM always provide a lower conditional probability of failure than those related to NTC-TLM because of the following motivations: (i) lower value of the tandem load in case of heavy GL-TLM (i.e., 440 kN instead of 600 kN) and (ii) different distribution of tandems (i.e., 5 axles over 11 m instead of 2 axles with 1.2 m spacing). This occurs even if the same uniformly distributed load is assumed in both traffic load models (i.e., 9.0 kN/m^2).

Table 13 outlines the median value η , dispersion β , and coefficient of

determination R^2 of fragility curves, as well as the code-related fragility level (i.e., the conditional probability of collapse associated with design traffic loads, and hence $P[C|H] = P[C|\alpha = 1]$), given the traffic load model under varying x_0 . The assumption of a NTC-conforming load pattern with $x_0 = 0$ led to $P[C|\alpha = 1] = 5.7 \cdot 10^{-2}$, whereas fragility reduces to $4.9 \cdot 10^{-3}$ (hence becoming approximately 10 times lower) in the case of heavy GL-TLM. If x_0 is increased from 0 to 1.0 m, $P[C|\alpha = 1]$ reduces to $1.2 \cdot 10^{-2}$ and $1.3 \cdot 10^{-3}$ under NTC-TLM and GL-TLM, respectively. This shows that decisions about the deck usage can directly produce significant benefits in terms of traffic-load fragility. For both $P[C|\alpha = 1]$ and η , the ratio between NTC- and GL-related values reduces under increasing x_0 .

Table 13. Fragility parameters, coefficient of determination and code-related fragility corresponding to NTC-TLM and GL-TLM under varying x_0 .

Traffic load scenario			η	β	R^2	$P[C \alpha = 1]$
Provisions	x_0 [m]	n_l				
NTC	0	3	1.68	0.33	0.99	$5.7 \cdot 10^{-2}$
NTC	0.5	3	1.89	0.33		$2.6 \cdot 10^{-2}$
NTC	1.0	3	2.15	0.34		$1.2 \cdot 10^{-2}$
NTC	1.5	3	2.44	0.35		$5.3 \cdot 10^{-3}$
NTC	2.0	3	2.81	0.38		$3.0 \cdot 10^{-3}$
GL	0	3	2.33	0.33		$4.9 \cdot 10^{-3}$
GL	0.5	3	2.69	0.35		$2.1 \cdot 10^{-3}$
GL	1.0	3	3.15	0.38		$1.3 \cdot 10^{-3}$
GL	1.5	3	3.64	0.41		$8.0 \cdot 10^{-4}$
GL	2.0	3	4.21	0.42		$3.0 \cdot 10^{-4}$

Figure 34 and Figure 35 show the sensitivity of fragility curves to the number of load lanes n_l , considering three different values of x_0 (i.e., 0, 1.5 and 2.0 m) with and without consideration of a uniform load on the remaining area (i.e., $r_l = 1$ or $r_l = 0$, respectively).

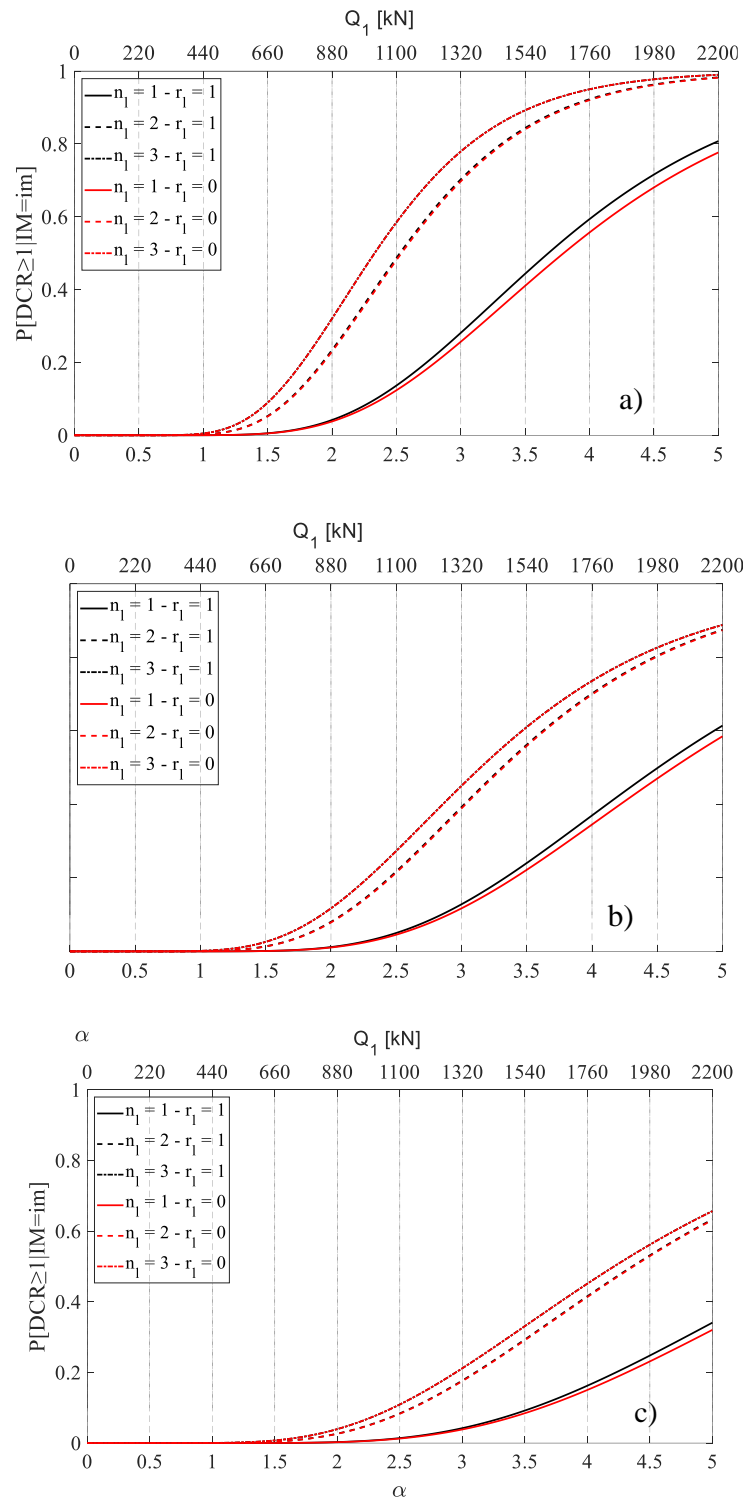


Figure 34. Fragility curves corresponding to NTC-TLM under varying number of load lanes n_i : (a) $x_0 = 0$; (b) $x_0 = 1.0$ m; (c) $x_0 = 2.0$ m.

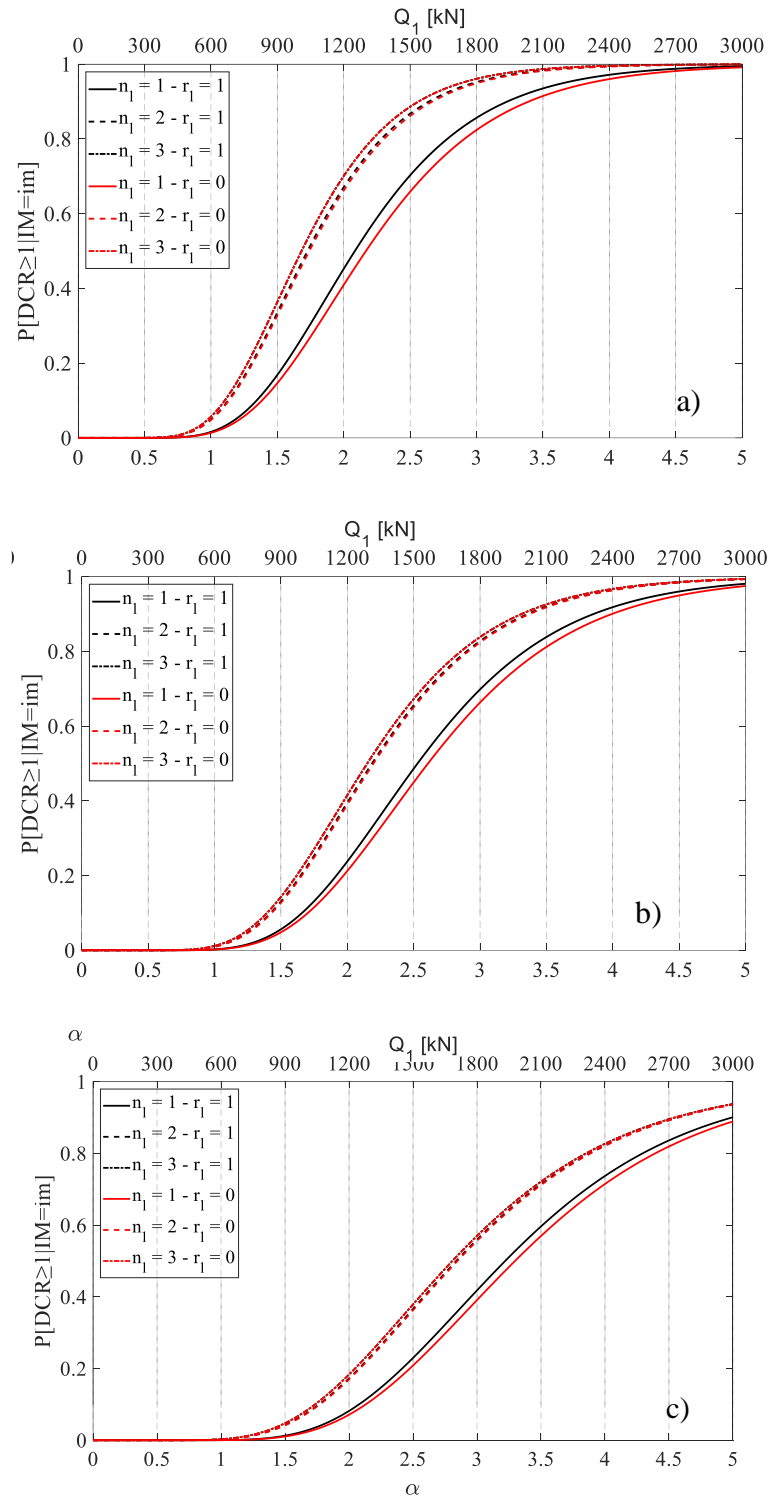


Figure 35. Fragility curves corresponding to heavy GL-TLM under varying number of load lanes n_l : (a) $x_0 = 0$; (b) $x_0 = 1.0$ m; (c) $x_0 = 2.0$ m.

Both Figure 34 and Figure 35 demonstrate that fragility decreases with a lower number of lanes even if a significant reduction is obtained only if $n_l = 1$. Especially in case of NTC-TLM, a slight difference arises between $n_l = 2$ and n_l

= 3 because most of deck geometries require a maximum number of notional lanes equal to 2. The influence of the remaining load area (i.e., $r_l = 1$ or $r_l = 0$) seems negligible unless $n_l = 1$ is considered. Table 5 outlines the fragility curve parameters and $P[C|\alpha = 1]$ under the different patterns of Figure 34 and Figure 35. As explained above, in case the GL-TLM is considered, $P[C|\alpha = 1]$ reduces at higher rate by limiting the number of lanes (e.g., $n_l < 3$).

Table 14. Fragility parameters, coefficient of determination and code-related fragility corresponding to different codes and numbers of load lanes.

Scenarios	η	β	R^2	$P[C \alpha = 1]$
NTC - $x_0 = 0 - nl = 1 - rl = 1$	2.08	0.34	0.99	$1.6 \cdot 10^{-2}$
NTC - $x_0 = 0 - nl = 1 - rl = 0$	2.17	0.35		$1.4 \cdot 10^{-2}$
NTC - $x_0 = 0 - nl = 2 - rl = 1$	1.73	0.33		$5.0 \cdot 10^{-2}$
NTC - $x_0 = 0 - nl = 2 - rl = 0$	1.74	0.33		$4.8 \cdot 10^{-2}$
NTC - $x_0 = 0 - nl = 3 - rl = 1$	1.68	0.33		$5.7 \cdot 10^{-2}$
NTC - $x_0 = 0 - nl = 3 - rl = 0$	1.68	0.23		$5.7 \cdot 10^{-2}$
NTC - $x_0 = 1.0 \text{ m} - nl = 1 - rl = 1$	2.53	0.33		$2.4 \cdot 10^{-3}$
NTC - $x_0 = 1.0 \text{ m} - nl = 1 - rl = 0$	2.61	0.33		$2 \cdot 10^{-3}$
NTC - $x_0 = 1.0 \text{ m} - nl = 2 - rl = 1$	2.19	0.34		$9.8 \cdot 10^{-3}$
NTC - $x_0 = 1.0 \text{ m} - nl = 2 - rl = 0$	2.20	0.33		$9.3 \cdot 10^{-3}$
NTC - $x_0 = 1.0 \text{ m} - nl = 3 - rl = 1$	2.15	0.34		$1.2 \cdot 10^{-2}$
NTC - $x_0 = 1.0 \text{ m} - nl = 3 - rl = 0$	2.15	0.34		$1.2 \cdot 10^{-2}$
NTC - $x_0 = 2.0 \text{ m} - nl = 1 - rl = 1$	3.22	0.34		$3.1 \cdot 10^{-4}$
NTC - $x_0 = 2.0 \text{ m} - nl = 1 - rl = 0$	3.30	0.34		$2.3 \cdot 10^{-4}$
NTC - $x_0 = 2.0 \text{ m} - nl = 2 - rl = 1$	2.84	0.37		$2.4 \cdot 10^{-3}$
NTC - $x_0 = 2.0 \text{ m} - nl = 2 - rl = 0$	2.85	0.37		$2.3 \cdot 10^{-3}$
NTC - $x_0 = 2.0 \text{ m} - nl = 3 - rl = 1$	2.81	0.34		$3.0 \cdot 10^{-3}$
NTC - $x_0 = 2.0 \text{ m} - nl = 3 - rl = 0$	2.81	0.38		$3.0 \cdot 10^{-3}$
GL - $x_0 = 0 - nl = 1 - rl = 1$	3.68	0.35		$1.1 \cdot 10^{-4}$
GL - $x_0 = 0 - nl = 1 - rl = 0$	3.80	0.36		$1.1 \cdot 10^{-4}$
GL - $x_0 = 0 - nl = 2 - rl = 1$	2.53	0.32		$2 \cdot 10^{-3}$
GL - $x_0 = 0 - nl = 2 - rl = 0$	2.54	0.32		$1.9 \cdot 10^{-3}$
GL - $x_0 = 0 - nl = 3 - rl = 1$	2.33	0.33		$4.9 \cdot 10^{-3}$
GL - $x_0 = 0 - nl = 3 - rl = 0$	2.33	0.33		$4.9 \cdot 10^{-3}$
GL - $x_0 = 1.0 \text{ m} - nl = 1 - rl = 1$	4.51	0.36		$1.3 \cdot 10^{-5}$
GL - $x_0 = 1.0 \text{ m} - nl = 1 - rl = 0$	4.62	0.36		$1.3 \cdot 10^{-5}$
GL - $x_0 = 1.0 \text{ m} - nl = 2 - rl = 1$	3.31	0.36		$4.3 \cdot 10^{-4}$
GL - $x_0 = 1.0 \text{ m} - nl = 2 - rl = 0$	3.32	0.36		$4.1 \cdot 10^{-4}$
GL - $x_0 = 1.0 \text{ m} - nl = 3 - rl = 1$	3.15	0.38		$1.3 \cdot 10^{-3}$
GL - $x_0 = 1.0 \text{ m} - nl = 3 - rl = 0$	3.15	0.38		$1.3 \cdot 10^{-3}$
GL - $x_0 = 2.0 \text{ m} - nl = 1 - rl = 1$	5.86	0.39		$2.6 \cdot 10^{-6}$
GL - $x_0 = 2.0 \text{ m} - nl = 1 - rl = 0$	6.00	0.39		$2.5 \cdot 10^{-6}$
GL - $x_0 = 2.0 \text{ m} - nl = 2 - rl = 1$	4.36	0.40		$1.3 \cdot 10^{-4}$
GL - $x_0 = 2.0 \text{ m} - nl = 2 - rl = 0$	4.37	0.40	$1.3 \cdot 10^{-4}$	
GL - $x_0 = 2.0 \text{ m} - nl = 3 - rl = 1$	4.21	0.35	$3.5 \cdot 10^{-4}$	
GL - $x_0 = 2.0 \text{ m} - nl = 3 - rl = 0$	4.21	0.42	$3.5 \cdot 10^{-4}$	

Assuming the same set of bridge models, fragility analysis was also carried out under medium GL-TLM (i.e., 260 kN representative of a bus) and light GL-TLM (i.e., 75 kN representative of a light lorry) under varying x_0 , assuming $n_l = 3$ and $r_l = 1$ as shown in Figure 36a and Figure 36b, respectively. In both cases of medium and light GL-TLM, it can be noted that fragility is significantly lower than that associated with heavy GL-TLM. This shows a key role of decision-making when setting traffic load limitations on existing bridges. In case of light GL-TLM, the code-related fragility turns out to be $P[C|\alpha = 1] = 8 \cdot 10^{-7}$ with a median value of load factor α resulting in $\eta = 7.17$ under $x_0 = 0$. On the other hand, a medium GL-TLM yields $P[C|\alpha = 1] = 2.25 \cdot 10^{-4}$ and a median value $\eta = 3.19$. Due to the very low values of code-related fragility (i.e., $P[C|\alpha = 5] = 0$), the case of very-light GL-TLM (e.g., vans and cars) is not discussed hereafter.

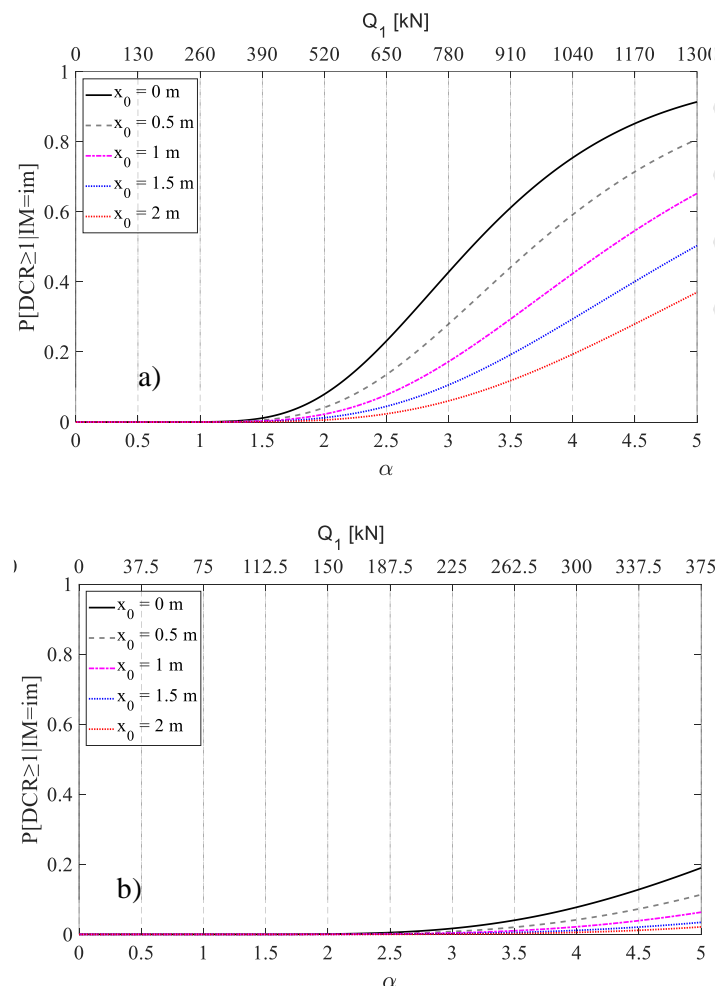


Figure 36. Fragility curves corresponding to the maximum number of load lanes n_l and remaining load r_l under varying x_0 : (a) medium GL-TLM; (b) light GL-TLM.

All fragility curves presented in this work are characterised by a coefficient of

determination very close to unity (i.e., $R^2 = 0.99$), indicating a very good fitting of the lognormal distribution function to each set of fragility points.

Based on the number of load lanes, values of the transverse eccentricity and remaining load area, a number of 30 scenarios (i.e. 3 values of n_l x 5 values of x_0 x 2 values of r_l) were generated for each of the 4 TLMs (i.e., NTC-TLM, heavy GL-TLM, median GL-TLM and light GL-TLM). For each of the 120 loading scenarios (=30 x 4), 10^4 model realizations for each value of load intensity measure (501 values of α) were considered thus providing a total number of 6.01×10^6 structural analyses. Figure 37 and Figure 38 show the variability of fragility curves median values and dispersions among all different scenarios through 3D bar plots, respectively.

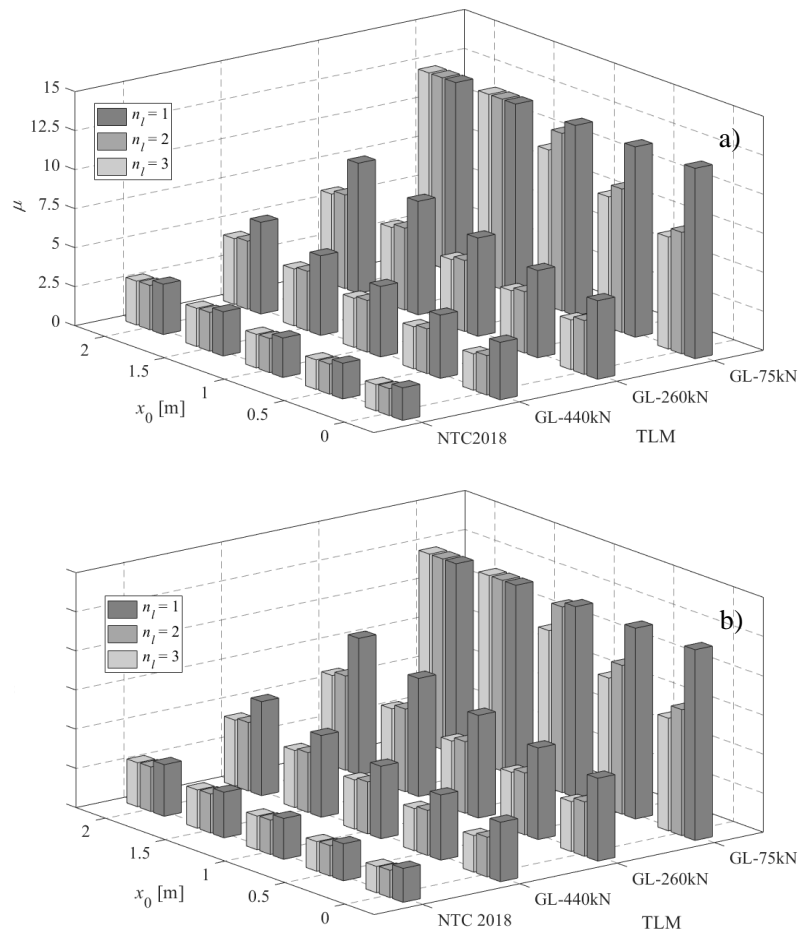


Figure 37. Median value of fragility curves under varying number of load lanes, transverse eccentricity and TLM: (a) $r_l = 1$; (b) $r_l = 0$.

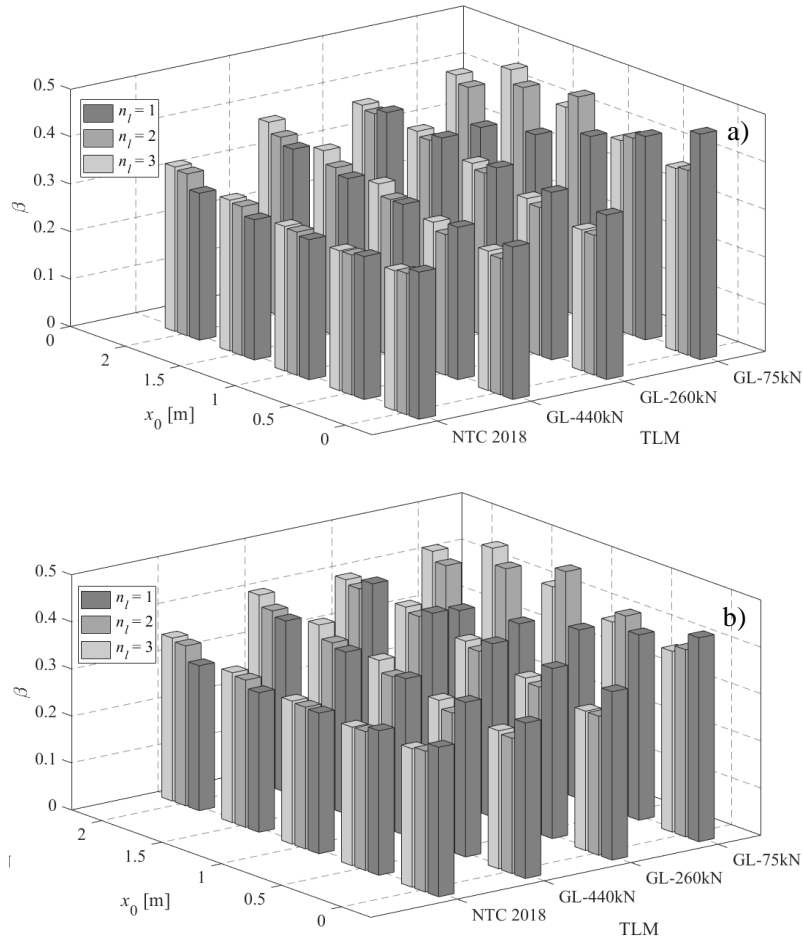


Figure 38. Dispersion of fragility curves under varying number of load lanes, transverse eccentricity and TLM: (a) $r_l = 1$; (b) $r_l = 0$.

Figure 37 underlines a higher fragility (i.e., lower median values) under the NTC-TLM in comparison with fragility levels associated with GL-TLMs. By contrast, the light GL-TLM produces highest median values. A slight variability is observed for each TLM between scenarios with n_l equal to 2 and 3, whereas n_l equal to 1 provides a significant increase of medians unless NTC-TLM is considered. The remaining load influence can be observed by comparing Figure 37a and Figure 37b with each other: only the scenarios with $n_l = 1$ show a slight increase in traffic-load fragility under $r_l = 0$.

Figure 38 highlights that dispersion of fragility curves falls in the range [0.29,0.47], reaching slightly lower values in case of NTC-TLM.

Based on the fragility analysis results, it is able to derive the failure probability conditioned on code-based TLM (i.e. $P[C]_{TLM}$). It can be calculated by multiplying the fragility (i.e., $P[C/H]_{TLM}$) and traffic-related hazard (i.e., $P[H]$), as follows:

$$P[C]_{TLM} = P[C|H]_{TLM} \times P[H] \quad (16)$$

While $P[C/H]_{TLM}$ was the subject of the present study, $P[H]$ would require a probabilistic model of traffic loads on existing bridges. It is noted that, in line of principle, H is the event that the traffic load (both distribution and magnitude) occurs on the bridge deck, so $P[H]$ is the probability of occurrence of both traffic load pattern and first-lane load intensity Q_I (or equivalently the load factor α). This is because ratios between loads on different lanes may change under varying α . In this respect, future probabilistic models for traffic loads on Italian bridges are likely to be used for calibration of partial safety factors by keeping the current code-based TLMs. This would imply only a revision of design traffic load values (i.e., Q_I in fragility models presented in this study), allowing ease of use when setting up TLMs in engineering practice. Nonetheless, traffic load data sets for existing Italian bridges are being collected, so hazard models are still to be developed. Therefore, this section provides some preliminary considerations about collapse risk based on traffic load models available in the literature.

A reference value of $P[H]$ is that assigned to NTC-TLM, which is defined as characteristic value with 5% probability of exceedance in 50 years, and hence a return period of 1000 years (Comité Européen de Normalisation 2003). Therefore, in order to estimate the mean annual rate of occurrence of the NTC-TLM, $P[H]$ can be assessed as the ratio between 0.05 and 50 years. Fragility analysis under NTC-TLM led to $P[C/\alpha = 1]_{NTC} = 5.7 \cdot 10^{-2}$, resulting in $P[C]_{NTC} = 5.7 \cdot 10^{-5}$ that matches the upper bound of the failure probability range assumed for design of new bridges, i.e., between 10^{-7} and 10^{-5} depending on the consequence class of the bridge³¹.

Some considerations on traffic load statistics are provided in order to shed some light on the collapse probability of existing PC bridge decks under real traffic loads in comparison with $P[C]_{NTC}$. In order to develop probabilistic models of traffic loads and properly tune TLMs with corresponding safety factors in an amended version of GL provisions, WIM systems could provide very useful data on vehicles moving on critical infrastructures (S.-Z. Chen et al. 2018, 2019a, 2019b; J. Kim and Song 2019). Considering the cumulative frequencies obtained through an early application of a WIM system and reported in Maljaars (Maljaars 2020), traffic load properties are considered representative of unmodified traffic composition since no special derailment systems were applied to divert illegal

vehicles. The data collected are referred to one month observation in 2018. Assuming that traffic loads are described by a stationary stochastic model, the monthly frequency can be adopted as annual frequency.

Assuming that traffic loads properties reported in Maljaars (Maljaars 2020) are constant between fast and slow lanes (conservative assumption because most of heavy vehicles pass on slow lanes (Maljaars 2020), Maljaars (Maljaars 2020) found a cumulative frequency of exceeding a 440 kN vehicle total weight $P[GVW > 440kN] = 9 \times 10^{-2}$, i.e. approximately one vehicle out of ten (Maljaars 2020). The conditional failure probability $P[C/H]_{TLM}$ derived under heavy GL-TLM traffic load model with $n_l = 3$ and $x_0 = 0$ was equal to $4.9 \cdot 10^{-3}$, resulting into a collapse probability $P[C]_{GL,440kN} = 4.4 \cdot 10^{-4}$. This assumption of uniform traffic load distribution across different lanes may be overly conservative, thus providing $P[C]_{GL,440kN} > P[C]_{NTC}$.

Since GL-TLMs are intended to be representative of congested traffic with no clear distance between vehicles, an additional term can be implemented for traffic hazard conditioned on congestion state (i.e., a very low distance between the rear and front axles of two consecutive vehicles). $P[H]$ can be calculated as probability that the gross vehicle weight (GVW) higher than threshold $\overline{GVW} = 440$ kN (e.g. \overline{GVW}) given that distance d between two heavy vehicles is less than $\overline{d} = 16$ m, multiplied by $P[d < \overline{d}]$, as follows:

$$P[H] = P[GVW > \overline{GVW} | d < \overline{d}] P[d < \overline{d}] \quad (17)$$

If $P[d < \overline{d}] = 1 \cdot 10^{-2}$ is assumed according to Maljaars (Maljaars 2020), $P[C]_{TLM}$ turns out to be $4.4 \cdot 10^{-6}$.

In case limitations on traffic loads are combined with limitations on the use of the bridge (i.e., $x_0 > 0$ and/or $n_l < 3$), a further reduction of $P[C]_{TLM}$ can be obtained. This can also be intended as a provisional measure applied by some road management companies in order to limit the effects of traffic loads on edge girders in case of limited deck capacity or local damage (Cosenza and Losanno 2021).

If the heavy GL-TLM is retained for only one lane ($n_l = 1$), $P[C/H]_{GL,440kN}$ reduces to $1.1 \cdot 10^{-4}$ and $P[C]_{GL,440kN}$ is accordingly equal to $9 \cdot 10^{-6}$. In a similar way, if the condition $x_0 = 0.5$ m is assumed, $P[C/H]_{GL,440kN}$ and $P[C]_{GL,440kN}$ turn

to be equal to $2.1 \cdot 10^{-3}$ and $1.9 \cdot 10^{-4}$, respectively. A further assumption of hazard conditioned on congested traffic according to Equation 17 further reduces $P[C|H]_{GL,440kN}$ and $P[C]_{GL,440kN}$ to $9 \cdot 10^{-6}$ and $1.9 \cdot 10^{-8}$, respectively.

Cumulative frequencies reported in Maljaars (Maljaars 2020) for lower intensity traffic loads, i.e., medium and light loads according to corresponding GL-TLMs, would provide annual collapse failure probabilities always lower than 10^{-6} even without any restriction to allowable vehicle classes.

As for the conditional failure probability, the unconditional collapse failure probability $P[C]$ can be derived. It is calculated as the convolution of fragility (i.e., $P[C|H]$) and traffic-related hazard (i.e., $P[H]$), as follows:

$$P[C] = \sum_i P[C | \alpha = \alpha_i, TLM] \times P[\alpha = \alpha_i | TLM] \quad (18)$$

where α is the IM described above and TLM is the conventional load model assigned to traffic.

Based on the fragility curves derived under heavy GL-TLM with $n_l = 3$ and $x_0 = 0$ (i.e., in line with the assumption of uniform load pattern on bridge deck), collapse probability turns out to be $P[C] = 5.8 \cdot 10^{-4}$. Moreover, the congested traffic hypothesis can be implemented as described above, leading to $P[C] = 5.8 \cdot 10^{-6}$. This highlights that the annual probability of collapse associated with $GVW = 440$ kN under actual traffic loads ranges between 10^{-6} and 10^{-4} , including the value $P[C]_{NTC} = 5.7 \times 10^{-5}$. The range of collapse probability $[10^{-6}, 10^{-4}]$ indicates an annual collapse rate between approximately one deck out of 500,000 bridges and one deck out of 5000 bridges. This outcome is deemed in line with the annual failure rate reported by Cook et al. (Cook et al. 2015), i.e., one total collapse over 5000 bridges and 1.2 total collapse over 50,000 bridges due to overloads only.

Both $P[C]_{GL,440kN}$ and $P[C]_{NTC}$ fall in the range $[10^{-6}, 10^{-4}]$, delineating a lower bound to target failure probability for design of new roadway PC bridges. Such outcomes highlight the need to start planning retrofit interventions and revising target failure probability for existing bridges (Cosenza and Losanno 2021).

Even if any probabilistic model of the traffic load would be region-specific or even site-specific, these considerations demonstrate that both traffic and usage limitations can properly reduce the collapse probability of existing bridges. The proposed fragility curves can allow road management companies to properly set

limitations in terms of maximum number of lanes and distance from the kerb, in order to provide a target safety level once the allowable vehicle class is selected.

4.6. Development of software for fragility analysis and code-compliant safety checks of decks

As discussed before, bridges are one of the most vulnerable components of a road network subjected to multiple hazards. Many studies were focused on seismic fragility evaluation due to damages and subsequent financial losses related to earthquake shaking that have hit many existing bridges. The probability to exceed a limit state given a certain level of seismic intensity is an indicator of bridge damage and it can be used by management companies as decision-making tool.

Several techniques were developed to derive as-built bridges fragility curves: empirical (i.e., based on empirical data), analytical (i.e., obtained through numerical models) and hybrid, which is obtained through a combination of empirical data (e.g., earthquake damages) and analysis results.

The uncertainties definition is one of the most important and critical issues in the fragility framework. Indeed, the demand and capacity definition are strictly related to the uncertainties definition (epistemic and aleatory) (Aviram et al. 2008; R. and G. 2022).

In literature, some tools were developed in order to derive seismic fragility curves for piers of a specific bridge or bridge classes without investigating the bridge deck. In this regard, bridge fragility functions lists are included in a fragility functions manager tool developed by Silva et al. (Silva V, Crowley H 2014). In this software, the user is able to add owner fragility functions that are not included in it. Stefanidou (Stefanidou 2017) implemented the methodology - proposed by Stefanidou and Kappos (Stefanidou and Kappos 2017) - in ad-hoc software in order to derive fragility curves for a bridge-specific seismic performance. In that study, single-component analysis and system analysis are performed to define the component capacity and demand, respectively. Moreover, all structure properties were taken into account (i.e., deck type, pier-to-deck connection, etc...) to define the bridge model through OpenSees software (McKenna, F., Fenves, G.L. and Scott 2003) and the software can include different types of bridges.

More recently, Stefanidou and Kappos (Stefanidou et al. 2022) developed an online-platform to include the previous defined bridge-specific fragility analysis

for as-built and retrofitted bridges by considering an extended database of bridge components and fragility curves. Limit state thresholds of piers, bearings and abutments for as-built and retrofitted bridges are evaluated in a specific module of the platform, it allows a nonlinear pushover analysis on a fully parametrised inelastic model. Last but not least, the limit state thresholds estimation of components is based on a closed-form relationship studied by Stefanidou and Kappos (Stefanidou and Kappos 2021).

Baltzopoulos et al. (Baltzopoulos et al. 2018) developed a graphical user interface that uses the OpenSees finite element platform to perform nonlinear dynamic analysis of single-degree-of-freedom oscillators (DYANAS). The definition of the required analysis parameters and seismic input are one of the main advantages of DYANAS. The types of dynamic analysis frameworks supported are incremental, multiple-stripe and cloud. Moreover, simultaneous consideration of pairs of uncoupled dynamic systems gives the possibility for intensity measures to refer to bidirectional ground motion.

Werner et al. (Werner et al. 2006) developed REDARSTM 2, a software to carry out different types of seismic risk analyses that includes a guidance tool to define pre and post-earthquake decisions. This software is able to take into account deterministic and probabilistic analyses in order to evaluate a pre-earthquake strategies (e.g., new design criteria) and a post-earthquake response. In this regard, potential consequences induced by earthquake and response strategies can be estimated from REDARS 2.

In the seismic risk assessment framework, Marco Tobol (Torbol 2011) developed a C++ object-oriented software in order to implement a dataset of fragility curves derived from his study. The fragility analysis included different bridge classes, considering uncertainties about soil conditions, number of spans and level of skewness.

In the framework of seismic bridge fragility, the study conducted by Khosravikia (Khosravikia 2020) characterizes the seismic demand and derive the vulnerability and risk (i.e., as structural damage repair cost) at structural and regional scales of highway bridges. This study combines machine learning techniques with structural analysis (i.e., considering bridges nonlinear models) and earthquake engineering by considering uncertainties in design, detailing practises, ground motion and local soil conditions. A Monte Carlo simulation and repair cost

analysis was carried out to derive the damage and losses for various earthquake scenarios. Then, fragility functions were developed by taking into account different bridge classes.

In the end, an open-source web application, based on Python language, named ShakeRisk was developed by authors to derive the risk, resilience and reliability of civil infrastructure by implementing artificial intelligence, systems engineering, structural and earthquake engineering. Moreover, user-friendly software to implement a preliminary design of seismically isolated bridges was developed by Manos et al., (Manos et al. 2012). In this regard, the typical overpass configurations, studied by Kappos and Moschonas (Kappos A 2006), were considered. The software is able to quickly define the bearing scheme, the seismic conditions and common steel laminated elastomeric bearing sections (Faravelli 2001; M.C. Kunde and R.S. Jangid 2003). The decision-making system and the related software are based on different codes (American Association of State Highway and Transportation Official (AASHTO). 2001; Comité Européen de Normalisation 2004b), engineering judgments and laboratory tests.

Bridges collapses are also related to flood events as highlighted by Wardhana and Hadipriono (Wardhana and Hadipriono 2003). In this regard, damages due to water pressure, corrosion, debris and scour are very common for bridges. Few studies have investigated the bridge piers behaviour under natural hazards and implemented them into a tool. Lee et al., (J. Lee et al. 2016) proposed a methodology to evaluate the fragility of bridges subjected to flood by considering a first-order reliability method (FORM) to reduce the time cost for deriving flood fragility curves. In this framework, a Python-based tool was developed by the authors to couple FERUM (Finite Element Reliability Using MATLAB) (i.e., a reliability analysis software) and a finite element analysis software (i.e., ABAQUS) to implement the methodology.

Based on the above literature review, it is worth underlying that several tools and software were developed to derive bridge fragility under natural hazards (i.e., earthquake shaking and flood events). On the other hand, there is a lack of fragility evaluation of bridges under man-made hazards. In this regard, the main goal of this study is the development of user-friendly MATLAB (“MATLAB and Statistics Toolbox Release R2022b. The MathWorks Inc., Natick, Massachusetts” 2022) based software to implement the methodology described in Section 4. For the first time, a tool to evaluate the fragility of bridge deck under

traffic loads was developed. Among several advances, this software and study behind it can allow quick safety checks and fragility analysis of existing bridge decks under different traffic load models. Road management companies will benefit from that software to make a risk-informed classification of their bridge portfolios, and subsequently, to perform detailed inspections and structural safety checks. Different modules were defined to derive single-bridge (intra-structure variability) or bridge classes (inter-structures variability) fragility curves under different code-conforming traffic load models (TLMs) (Italian High Council of Public Works 2020; Italian Ministry of Infrastructures and Transportation 2018). The methodology proposed was taken into account by considering fully parametrised simply supported, beam-type, bridges. Reinforced and prestressed concrete bridges were implemented in the software. Moreover, two different modules allow the user to define owner probability distributions and regression models (based on user data) that can be used to define the bridge model. Moreover, user-defined girder safety check was implemented in an additional module. The user is able to define all parameters of the girder deck model. Then, a code-conforming or user-defined TLM can be set, and the girder safety check can be carried out.

The basic structure of the GUI and its main window are shown in Figure 39. The software allows carrying out both a multi-level fragility analysis of RC or PC simply supported beam-type bridge deck under different TLMs and a deterministic analysis of the single deck. The multi-level analysis is used to derive fragility curves for a portfolio of bridges or a specific bridge through a bridge-class fragility analysis or a bridge-specific fragility analysis, respectively. In this regard, the software can be useful for road management companies in order to analyse an entire class fragility as well as for a civil engineer for a specific bridge. Four modules are implemented and described in the following sub-sections: *Data import and pre-processing*, *Uncertainty modelling*, *Fragility Analysis* and *Girder-Section Safety Check*.

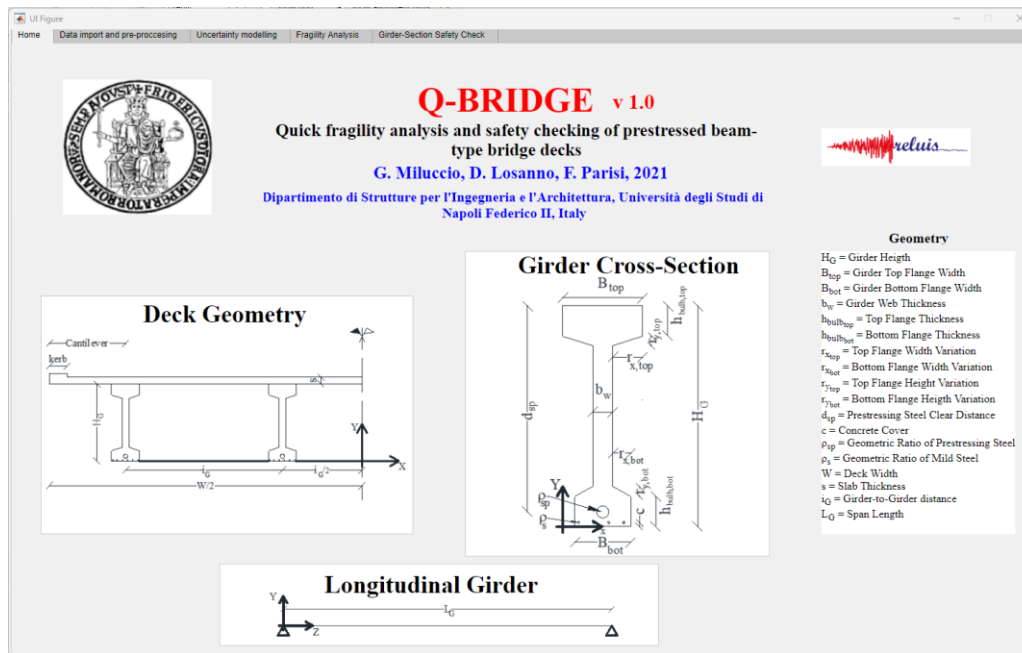


Figure 39. Main Q-BRIDGE GUI window

4.6.1. Data import and pre-processing module

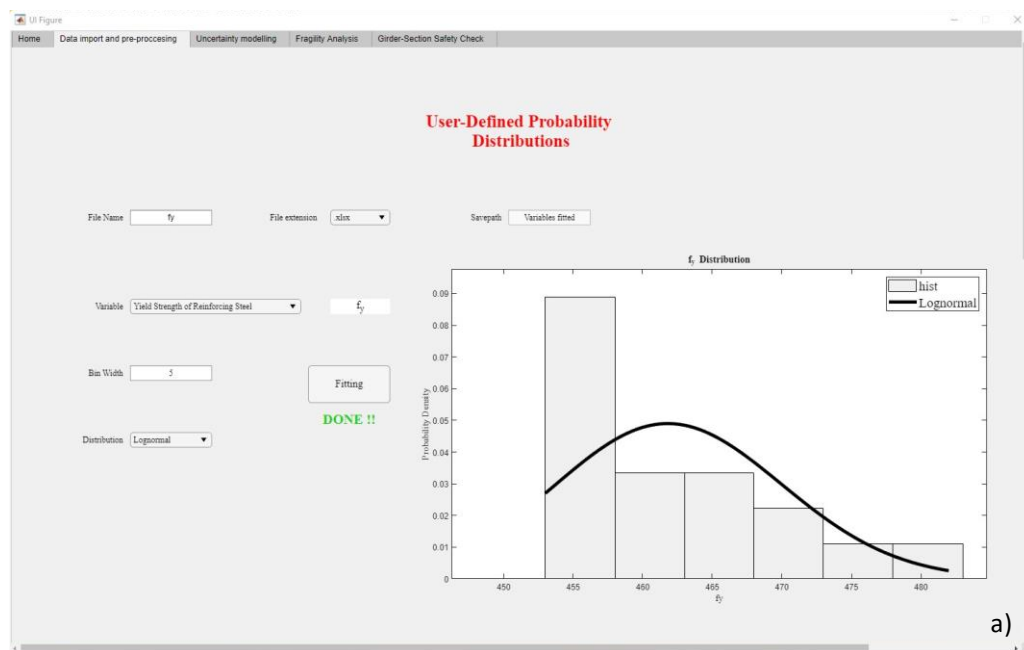
The simply supported bridge deck model is fully parametrised through the *Uncertainty modelling* module. All variables can be also derived through the *Data import and pre-processing* module allowing the implementation of empirical or literature user data of a certain variable (e.g., girder length) to derive a probability distribution or a regression model based on that data. Then, these models would be saved and could be used in the *Uncertainty modelling* module for the specific variable. Moreover, input variables could be saved and used at a later time with different case studies. Several code conforming TLMs, according to previous sections, can be used to carry out fragility analysis for different range of intensity measure (IM). The fragility outputs can be also saved as plots or data to define a comparison of the same bridge class (or specific bridge) under different TLMs.

In the framework of specific bridge, the *Girder Safety Check* module was developed for deterministic analysis. Based on the simply supported bridge deck model proposed in this work, all parameters are defined as deterministic and their values are user-defined. The girder cross section (and bridge deck) can be set as RC or PC. In the last case, cables distributions can be defined along the girder with many options and parameters, allowing the user to generate a fully detailed girder cross section. Moreover, a user-defined TLM is allowed in addition to the code conforming TLMs. In this regard, the user can also simulate specific traffic

conditions on the bridge deck such as bridge load test.

The first module of the GUI comprises three sub-modules and is related to the derivation of fragility curves for a bridge class or a specific bridge. Therefore, a bridge-class fragility analysis or a bridge-specific fragility analysis can be carried out. The bridge deck model is fully parametrised, and each variable can be set through a pre-defined or user-defined (i.e., based on empirical or literature data) probability distribution and regression model. Therefore, code conforming TLMs and intensity measure ranges can be defined by the user to derive bridge deck fragility curves under different traffic loads conditions. The description of each sub-module is here depicted in order to completely describe all features referred to the fragility analysis procedure.

The first out of three sub-modules includes the possibility of generating user-defined variables to implement in the *Uncertainty modelling* sub-module. In this regard, all parameters included in the simply supported, beam-type, bridge deck model such as: girder length (L_G), concrete compressive strength (f_c) or girder height (H_G) can be derived. The user can take empirical data from real case studies (i.e., from tests on a real bridge or from a bridges portfolio) and derive probability distributions and regression models based on them. Figure 40a and Figure 40b show the two features that can be used to generate each variable: the User-Defined Probability Distributions and the User-Defined Regression Models.



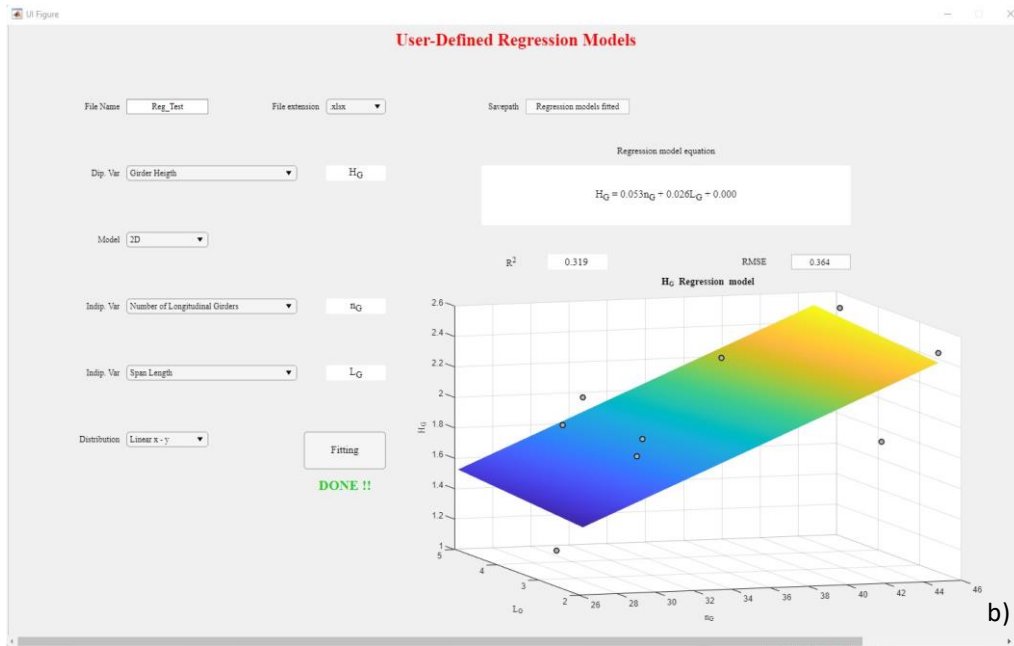


Figure 40. Data import and pre-processing GUI’s window: (a) *User-Defined Probability Distributions* and (b) *User-Defined Regression Models* features.

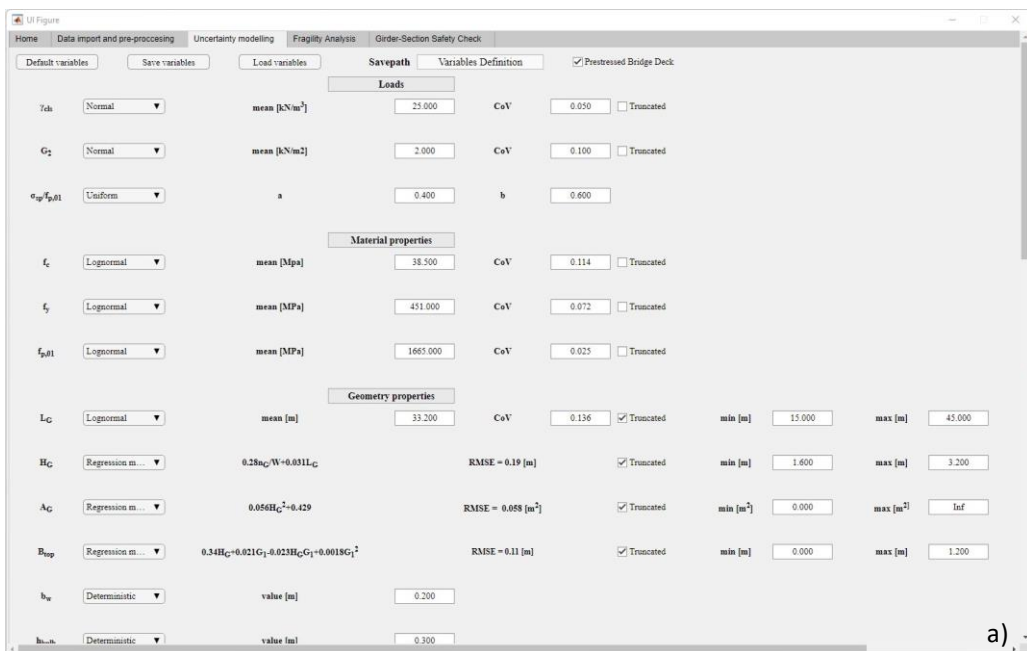
The software reads the data from Excel files and using MATLAB (“MATLAB and Statistics Toolbox Release R2022b. The MathWorks Inc., Natick, Massachusetts” 2022) applications is able to generate probability distributions and regression models. Based on the probability distributions depicted in Section 3.2 the main probability distributions that characterize the bridge deck model variables can assume a normal, lognormal, Weibull and uniform distribution. Therefore, those are implemented as options that can be chosen from the user to generate its own variable. Then, the histogram bins width has to be set to build the histogram of inserted data and plot the probability distribution of the chosen variable.

On the other hand, the *User-Defined Regression Model* feature allows the user to define its own regression model for each variable. Mono-dimensional and bi-dimensional regression models are implemented in the current GUI release. In this regard, the dependent variable and one (mono-dimensional) or two (bi-dimensional) independent variables have to be chosen to generate the regression model. Moreover, three and nine different options can be selected for a mono-dimensional and bi-dimensional regression models, respectively. In this regard, a linear, quadratic and cubic relationship can be set between the dependent and independent variables. Then, the plot and corresponding equation of the user-defined regression model is shown in the GUI boxes.

All user-defined variables and corresponding probability distributions and regression models parameters (i.e., mean, median, standard deviation and coefficient of variation for the probability distributions and equation and coefficients for the regression models) are saved in a specific folder to be used in the *Uncertainty modelling* sub-module.

4.6.2. Uncertainty modelling module

This module allows to define all variables that are included in the bridge deck model. Normal, lognormal and uniform probability distributions can be chosen. Those are defined through their mean and CoV when normal and lognormal distributions are selected, whereas the minimum and maximum values have to be set with the uniform distribution. Moreover, variables can be also defined as deterministic parameters, thus, a single value is required. On the other hand, if the selected variable has been previously derived through the *Data import and pre-processing* module, the *User-Defined Probability Distribution* and *User-Defined Regression Model* options can be selected. In this regard, the user-defined variable parameters are automatically loaded into the *Uncertainty modelling* module. In addition, the default variable option allows the user to set all variables as defined in Section 3. This aspect can be useful if the user would like to change only some parameters of the entire deck model or the traffic loads conditions considering the same bridge deck model implemented in this study. Figure 41a and Figure 41b show the variables considered in the software underlying the different options that can be chosen for each of them.



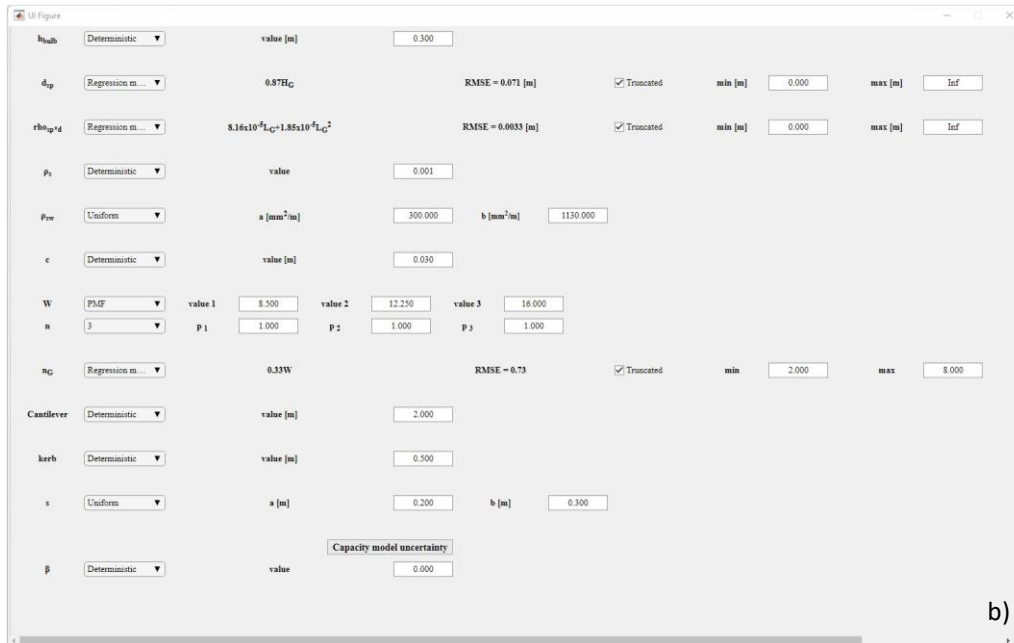


Figure 41. Definition of the whole variables through the Uncertainty model GUI's module.

As reported in Figure 41a this module allows to define if the simply supported, beam-type, bridge deck will be a prestressed concrete or a reinforced concrete deck. This characteristic can be chosen by the user through the checkbox *Prestressed Bridge Deck* (Figure 41a). In this regard, if the checkbox is checked, a PC bridge deck will be defined. On the other hand, if the RC bridge deck is chosen, all variables related to the prestressing steel are not taken into account.

In addition, the Truncated option can be set for the variables defined through probability distributions (i.e., normal and lognormal) and regression models. For those cases, a range within is set minimum and maximum values. Thus, the variables will be truncated beyond these values.

4.6.3. Fragility Analysis module

Then, the *Fragility Analysis* module is the last sub-module to carry out the fragility analysis and derive fragility analysis curves. Figure 42 shows the GUI for this module.

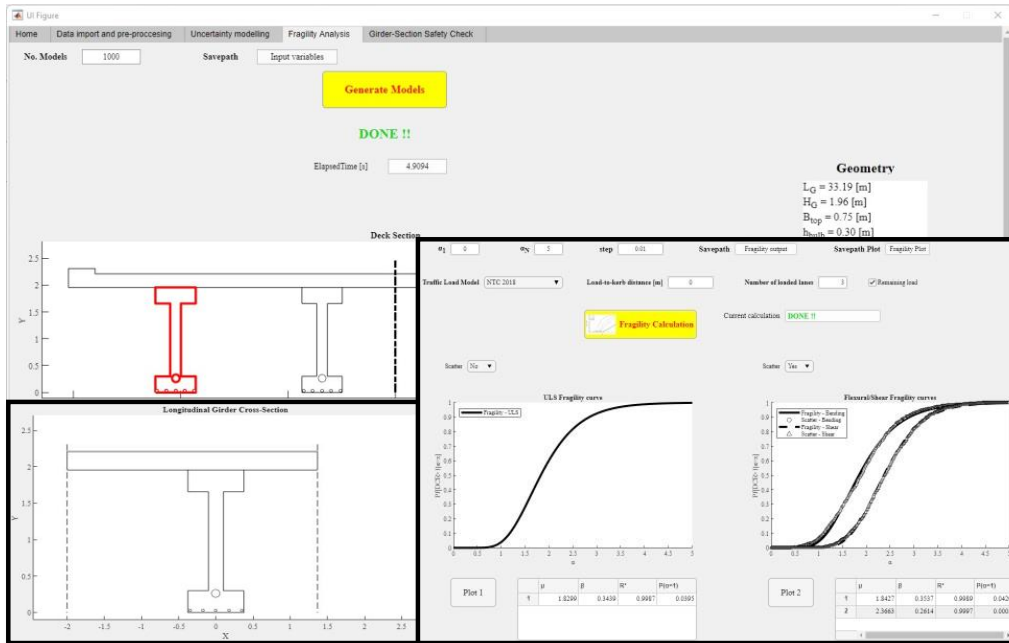


Figure 42. Definition of the number of analysed models, the mean bridge and fragility analysis results through the *Fragility Analysis* GUI’s module.

Based on the variables defined in the *Uncertainty modelling* module and number of models defined here, the simply supported, beam-type, bridge deck models can be generated. Thus, the Monte Carlo method is considered in order to randomly generate the previously defined models. Therefore, the “mean bridge”, is shown and the mean values are depicted (Figure 42). Then, the TLMs proposed by Italian code DM2018 (Italian Ministry of Infrastructures and Transportation 2018) and new Italian Guidelines for risk-based classification, safety checks and monitoring of existing bridges (Italian High Council of Public Works 2020) can be defined by the user. In this regard, the geometric limitation on the first notional lane position can be also set by defining its clear distance from the kerb (x_0) (Figure 43). In addition to this, the maximum number of lanes (according to the code conforming TLM that has been chosen) can be defined. Moreover, the remaining load area factor is checked or not through a checkbox (Figure 43) to consider its influence in the fragility analysis.

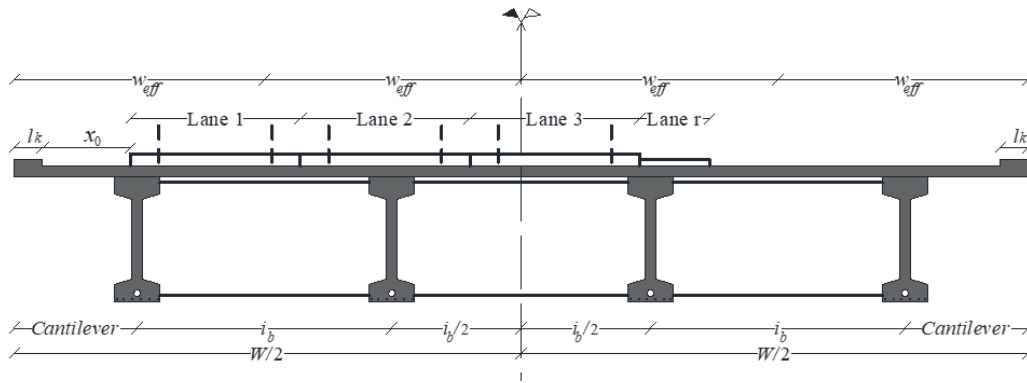


Figure 43. Type transversal bridge cross-section implemented in the Q-BRIDGE software.

Based on the fragility analysis procedure described in Section 4.4 the fragility is derived through the frequentist approach. Therefore, the fragility is derived as the conditional probability of exceeding ultimate limit state (ULS) given IM, where the IM is defined as the ratio between the incremental tandem load and its nominal value given the TLM. In this regard, the ULS is defined as $DCR \geq 1$. The IM range must be set through the minimum (α_I) and maximum (α_N) value of IM before the fragility analysis can be started, as well as the IM step. Then, the fragility analysis of simply supported, beam type, bridge deck models can be carried out through the *Fragility Calculation* button.

This module allows also to plot the fragility curves obtained and corresponding parameters (i.e., median and standard deviation) (Figure 43). In this regard, two plots can be generated: (i) the ULS and (ii) flexural/shear fragility curves. Moreover, the code-related fragility level (i.e., the conditional probability of collapse associated with design traffic loads) is also depicted.

4.6.4. Girder-Section Safety Check module

In the end, in order to carry out a simply supported, beam type, bridge deck safety check the *Girder-Section Safety Check* module can be used. In this module, the assumption of transversely rigid deck cross section (in accordance with Engesser (Cestelli Guidi n.d.; Raithel 1977, 1978) formulation) is made in order to derive the transverse load distribution and carry out deck analysis. Based on that, the edge girder is considered as the most stressed element in the deck, thus, the safety check is conducted on it. The module allows to choose each cross-section along the girder to be checked by defining its cross-section location (i.e., defined as the Z-axis coordinate). Figure 44a and Figure 44b show the entire module organization by depicting all inputs and outputs.

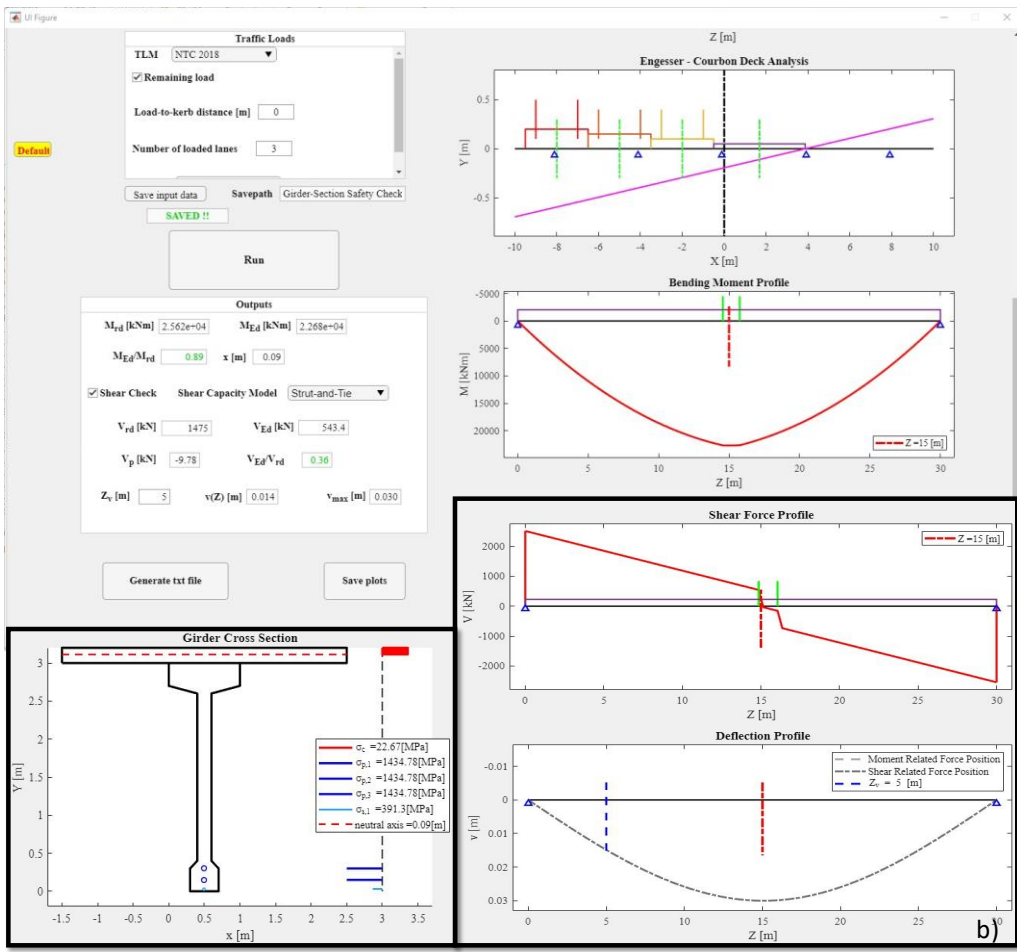
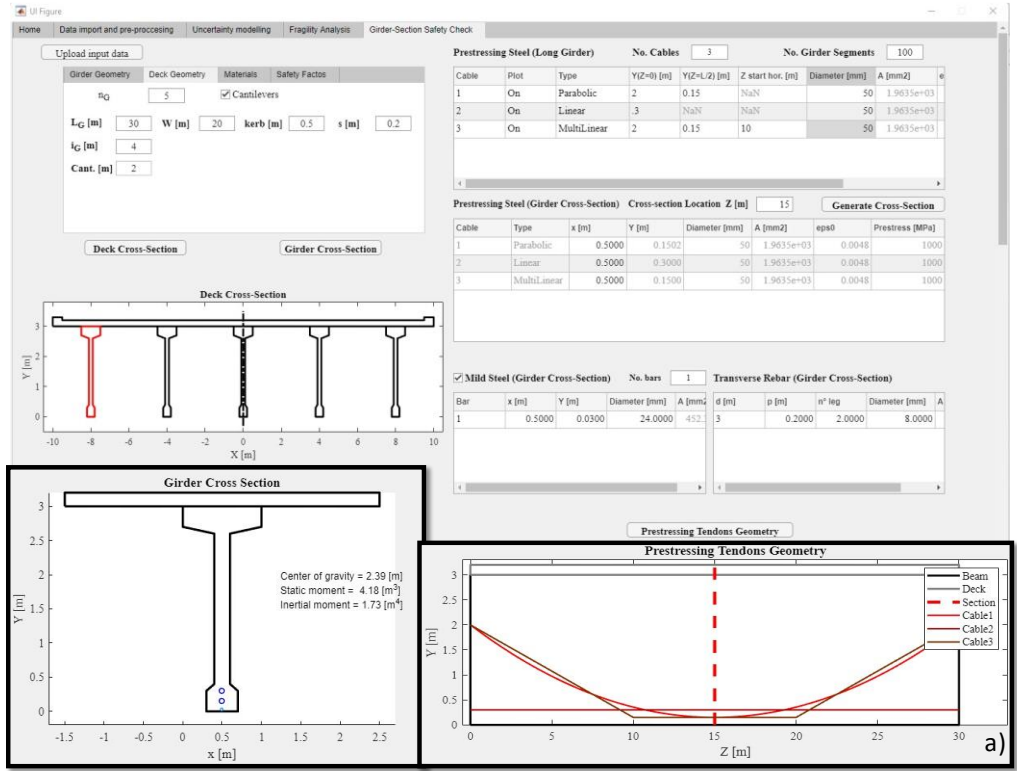


Figure 44. Girder-Section Safety Check module.

Three different girder cross-sections can be chosen: default (i.e., a typical PC bridge girder cross section, with a wide bottom flange for prestressing cables), T-shape and rectangular shape. Their geometries are fully parametrised to implement the own cross section in the software.

The geometry of the simply supported, beam type, bridge deck can be fully defined by the user that can chooses the number of girders in the deck as well. All materials properties and safety factors related with them are user-defined, thus, no code-provisions are implemented in this regard.

The software allows to define both RC and PC bridge deck by defining the number of prestressing cables in the girder cross-section (i.e., with zero prestressing cables a RC girder is considered). Therefore, the GUI was developed to allow the user to define his own cross-section by implementing the prestressing cables geometry. In this regard, three type of cables can be set: parabolic, linear (i.e., horizontal cable) and MultiLinear (i.e., composed by two diagonal and one horizontal sections, at the end and mid of the girder, respectively). The cables diameter and initial prestress can be also defined. Then, the coordinates of each defined cables are generated when the cross-section location is set. In this way, the user is able to carry out the safety check of different cross-sections of the same girder (i.e., with the same geometry and materials) by changing the cross-section location only (i.e., the software is able to derive the cables positions along the girder). Moreover, the mild steel can be defined in the girder cross-section by setting the number of reinforcing bars, their diameter and location in the cross-section. In addition, the user can choose the transversal reinforcements as well. Then, the deck cross-section, girder cross-section and prestressing tendons geometry plots can be generated.

In the module, the traffic loads panel allows the user to define the traffic loads conditions on the bridge deck. In this regard, the traffic loads defined in the fragility analysis module and previous Sections are also considered in this module. The algorithm implemented in the software evaluates the worst condition for the traffic loads position on the transversal bridge deck cross-section and along the edge girder by maximizing the stresses in the cross-section chosen for the safety check. Moreover, the user is able to define the own traffic loads condition through the *user-defined traffic loads* option. Thus, the number of load axles, their positions (i.e., on the bridge deck transversal cross-section and along the edge girder) and loads can be defined by the user. Therefore, the

software is able to simulate both an exercise traffic condition and a specific load condition such as a load test conducted on the bridge.

All outputs are shown on both plots and results panel. The formers show the load distributions on the transversal bridge deck and stresses and deformed shape along the edge girder. On the other hand, the numerical outputs are shown in the results panel, by highlining the safety check result for the cross-section defined. In this regard, a flexural and shear check is done. The last is defined by adopting three different shear capacity models suggested by Eurocode and described in Section 4.2. In the end, a report of the whole analysis can be generated (in .txt format) and all plots can be saved.

4.6.5. Application to a case-study bridge

In order to test the software, a single-bridge fragility analysis and the girder safety check of a real case study is carried out under different traffic loads conditions. The selected bridge is an Italian existing simply supported prestressed concrete, beam-type, bridge. The bridge deck is composed by 5 pre-tensioned girders with an interaxle spacing and a mean span of 3.31 m and 21.7 m, respectively. The girders have a height equal to 1.30m and are pre-tensioned with 28 tendons. The bridge deck and girder cross-section are shown in Figure 45.

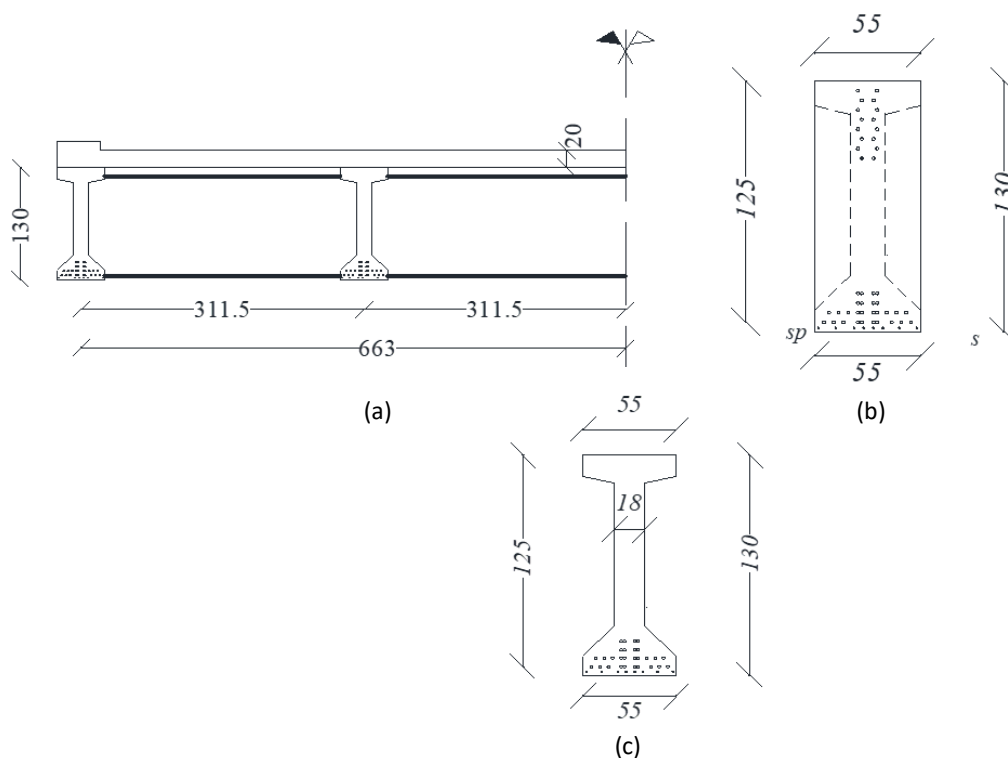


Figure 45. Bridge deck and girder cross-section of the case study.

Fragility curves for the case study were derived by using the *Fragility Analysis* module described above. The bridge geometry as well as prestressing steel parameters were settled as deterministic variables due to their low variability in a single bridge analysis. On the other hand, material properties and girder span were considered as variables by taking into account the data collected by the authors. In this regard, the concrete compressive strength (f_c), prestressing steel and mild steel yielding strength ($f_{p,01}$ and f_y) and girders span length (L_G) probability distributions were derived by using the *User-defined variable generator* sub-module. As suggested in Section 3.2 lognormal distribution was chosen as representative of these variables. Parameters distributions (i.e., mean and coefficient of variation) of variables were shown in Table 15.

Table 15. Distributions and statistics of random variables.

Category	Random variable	Statistics			Distribution
		Symbol [units]	μ	CoV [%]	
Loads	Weight per unit volume of RC	γ_c [kN/m ³]	25.00	5.0	Normal
	Non-structural permanent loads	g_{2k} [kN/m ²]	2.00	10.0	Normal
	Prestressing ratio	$\sigma_{sp}/f_{p,01}$ [%]	50.00	12.0	Uniform
Material properties	Concrete compressive strength	f_c [MPa]	30.29	13.8	Lognormal
	Yield strength of mild steel	f_y [MPa]	461.95	1.8	Lognormal
	Yield strength of prestressing steel	$f_{p,01}$ [MPa]	1772.64	2.4	Lognormal
Geometry properties	Girder length	L_G [m]	21.70	2.0	Lognormal
	Girder height	H_G [m]	1.30	-	Deterministic
	Girder gross area	A_G [m ²]	0.19	-	Deterministic
	Girder top flange width	B_{top} [m]	0.55	-	Deterministic
	Girder web thickness	b_w [m]	0.18	-	Deterministic
	Bottom flange thickness	h_{bulb} [m]	0.11	-	Deterministic
	Prestressing steel clear distance	d_{sp} [m]	1.20	-	Deterministic
	prestressing steel ratio multiplied by d_{sp}	$\rho_{sp} \cdot d_{sp}$ [m]	0.02	-	Deterministic
	Geometric ratio of mild steel	ρ_s	0.01	-	Deterministic
	Transverse reinforcement ratio	ρ_{sw}	243.00	-	Deterministic
	Concrete cover	c [m]	0.05	-	Deterministic
	Deck Width	W [m]	13.25	-	Deterministic
	Number of longitudinal girders	n_G [m]	5.00	-	Deterministic
	Cantilever	-	0.00	-	Deterministic
	Kerb length	$kerb$ [m]	0.50	-	Deterministic
Slab thickness	s [m]	0.20	-	Deterministic	
Model uncertainty	Capacity model uncertainty	β	0.15	-	Deterministic

As shown in Table 15 the biggest variability is related to the concrete

compressive strength distribution, indeed a mean value of 30.29 MPa and a coefficient of variation (CoV) equal to 13.8% were obtained. On the other hand, the remaining variables have a CoV around 2% that leads to a very small variability of these parameters. Moreover, the remaining parameters were set as deterministic (Table 15), thus, the whole variability of the fragility curves will be mainly related to the concrete compressive strength, that is a realistic framework in a real case study (i.e., in a specific bridge, the main variability is related to the materials, and much more to the concrete due to the fact that the prestressing steel and mild steel have a controlled manufacturing).

Then, the *Fragility Analysis* sub-module was used to generate 1000 bridge models (based on the previous defined variables) and carry out the fragility analysis in order to derive bridge fragility curves under different traffic loads conditions.

At this point, the traffic loads conditions must be set. The IM range was defined by setting the minimum (α_I) and maximum value (α_N) of IM equal to 0 and 5, respectively. Then, the step between α_I and α_N was set equal to 0.01 (i.e., 500 analyses for each bridge model). Thus, three (out of 5) different TLMs were considered for this case study: NTC2018 (TLM 1), GL – 5 axes – 440kN (TLM 2) and GL – 3 axes – 260kN (TLM 3). These TLMs were proposed by Italian code DM2018 (Italian Ministry of Infrastructures and Transportation 2018) and new Italian Guidelines (Italian High Council of Public Works 2020). In this regard, the geometric limitation on the first notional lane position (i.e., the Load-to-kerb distance x_0 in the GUI) was set equal to 0 (no geometric limitation) for all TLMs and 1m for the TLM 3 (i.e., to highlight the effects of geometric limitations on the bridge fragility). Moreover, the number of loaded lanes was set equal to 3 for TLM 1 (i.e., maximum number of lanes n_l) and 5 for TLM 2, 3 and 4. For all scenarios the remaining load was set as active. Thus, in the case studio both traffic loads and geometric limitations were taken into account in order to derive the bridge specific fragility curves. The elapsed time to carry out the fragility analysis for each loading scenario (500000 analyses: 1000 bridge models multiplied for 500 IM steps) is about 3 minutes, underlying a very contained time effort to obtain the fragility curves. Table 16 summarizes the loading scenarios considered.

Table 16. Loading scenarios considered for the case-study.

Scenario	TLM	Load-to-kerb distance [m]	Number of loaded lanes
1	NTC 2018	0	3
2	GL – 5 axes – 440kN	0	5
3	GL – 5 axes – 440kN	1	5
4	GL – 3 axes – 260kN	0	5

The fragility analysis results were depicted in Figure 46 and summarized in Table 3. Two plots can be observed in Figure 46. In the first one, the fragility curve for ULS is shown, whereas the second one shows two different fragility curves for the flexural/shear failure mechanisms. The further results discussion is focused on the ULS fragility curves.

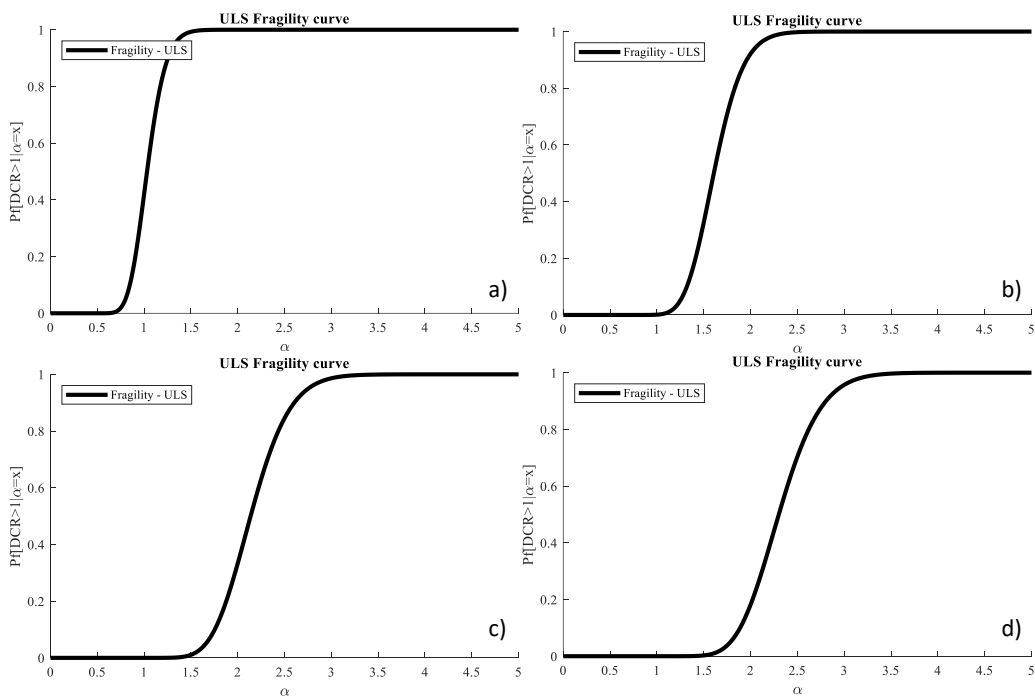


Figure 46. Fragility curves corresponding to: (a) NTC 2018-TLM with $x_0 = 0$ and $n_l = 3$, (b) GL – 5 axes – 440kN with $x_0 = 0$ and $n_l = 5$, (c) GL – 5 axes – 440kN with $x_0 = 1$ and $n_l = 5$, (d) GL – 3 axes – 260kN with $x_0 = 0$ and $n_l = 5$.

Table 17. Fragility parameters, coefficient of determination and code-related fragility corresponding to loading scenarios.

Scenario	μ	β	R^2
1	1.03		
2	1.61		
3	2.14	0.15	1
4	2.30		

The fragility curves show a highest fragility for TLM 1 with fragility curve median value (μ) equal to 1.03, instead of 2.30 when the traffic loads limitations (i.e., TLM 4) were considered. Moreover, the geometric limitations of the bridge led the fragility curves to a median value equal to 2.14, that corresponds to increase the traffic loads of 100% to reach the same fragility when no limitations (TLM 1) are applied. In all scenarios a standard deviation (β) equal to 0.15 was observed, representative of a very small variability in the fragility curves.

In the end, the *Girder-Section Safety Check* module was used in order to carry out the edge girder safety check (i.e., the most stressed girder assuming a transversely rigid bridge deck). In this regard, the material and loads partial safety factors were set according to the DM2018 (Italian Ministry of Infrastructures and Transportation 2018).

Geometrical and material properties of the entire bridge deck and girders were set according to the mean values of the variables shown in Table 15. The 28 prestressing cables were modelled through four cables (i.e., one cable for each layer shown in Figure 45) that have an equivalent area according to the total area of cables at each layer. Figure 47 shows the deck, girder and prestressing cables geometries and materials adopted in the GUI module.

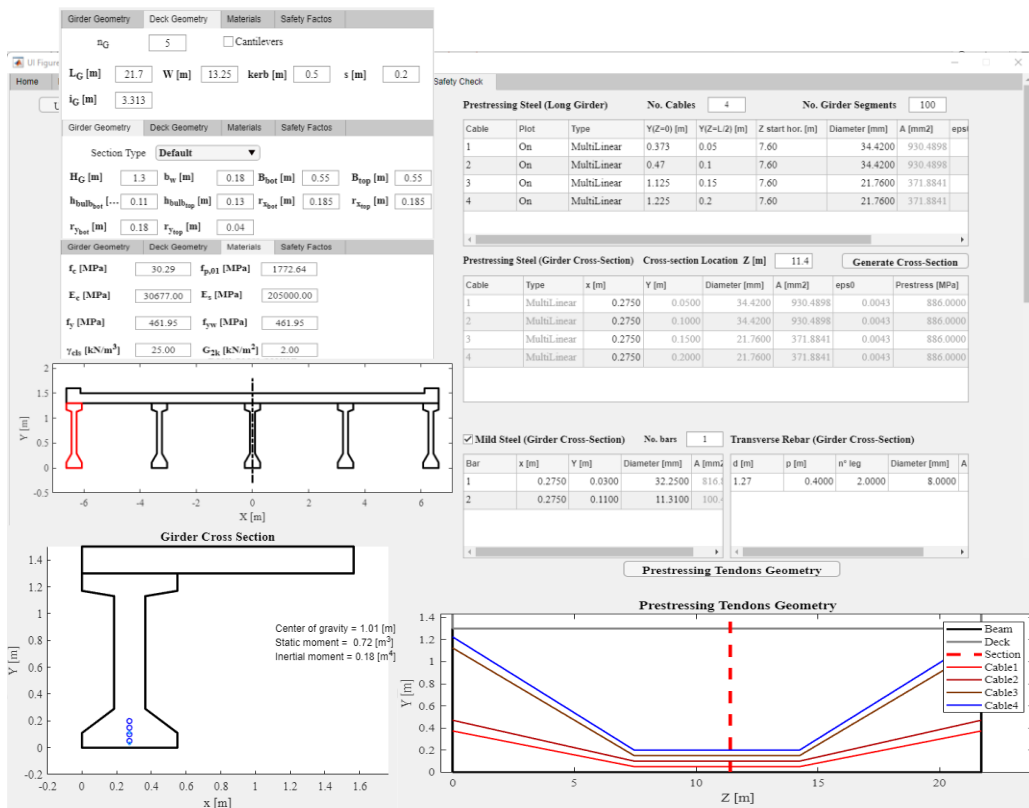
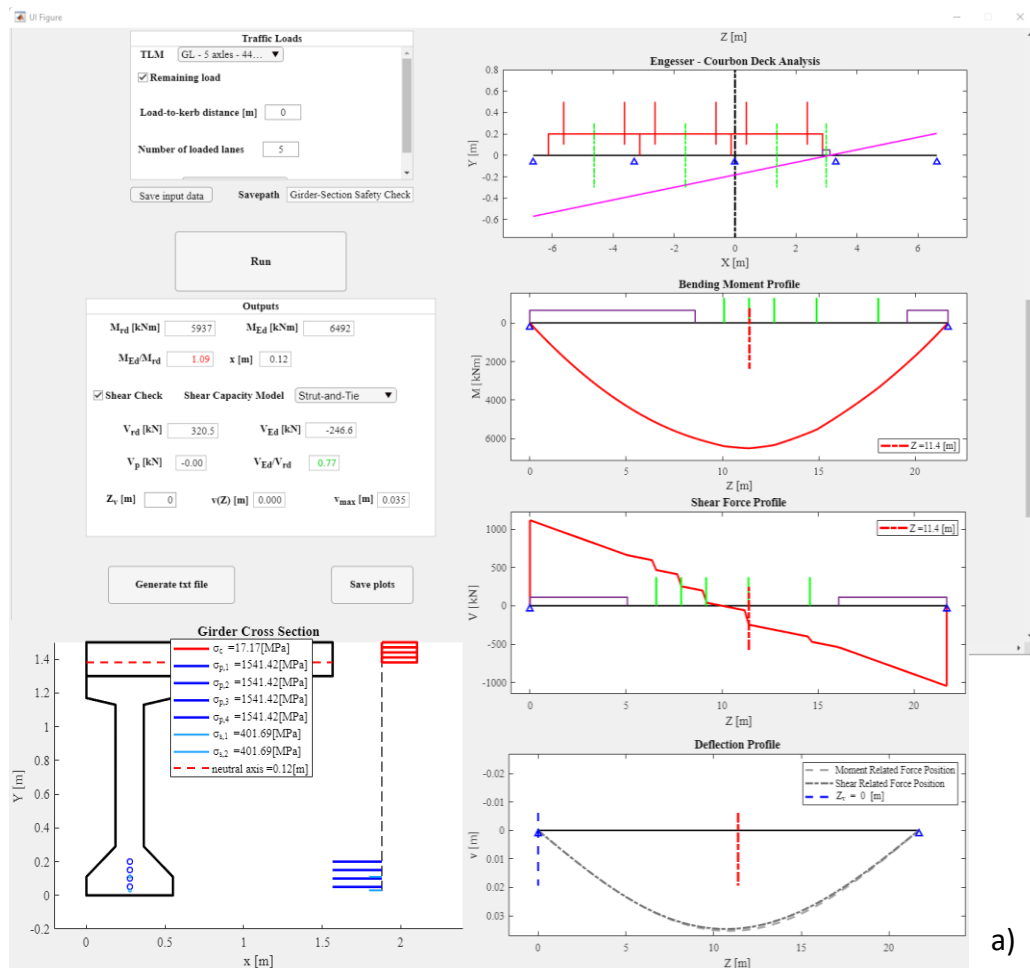


Figure 47. GUI panel for deck, girder and prestressing cables geometries and materials adopted for girder safety check.

Then, the edge girder safety check was carried out by taking into account all scenarios shown in Table 16. In this regard, the mid span cross section was considered since these types of bridges deck are much more vulnerable to the flexural stresses (as described in Section 4.4). The software application allows to show the Engesser-Courbon deck analysis results by depicting the traffic loads distributions and influence line on the bridge deck. Moreover, the bending moment and shear distributions along the edge girder were plotted by showing the loads distributions on it. In addition, the girder cross-section is showed with the concrete and steel (either prestressing and mild) tensions and neutral axis position reached during the analysis to define the ultimate bending moment of the girder. Table 18 summarizes results for all scenarios considered and Figure 48 shows the Q-BRIDGE GUI's windows for scenario n. 2.



a)

Figure 48. GUI panel for girder safety check results for scenario n. 2.

Table 18. Girder safety check results.

Scenario	M_E/M_r	V_E/V_r
1	1.65	1.31
2	1.09	0.80
3	0.97	0.67
4	0.92	0.64

The *Outputs* panel in Figure 48 shows all results derived from the analysis. In this regard, as presented in Table 18 the traffic loads proposed by DM2018 (Italian Ministry of Infrastructures and Transportation 2018) led to a flexural stress ratio of 1.65 underlying that the edge girder is not verified. If the GL – 5 axes – 440kN traffic loads are considered the stress ratio is equal to 1.09 without any geometric limitations. In these cases the edge girder did not satisfy the safety check against the bending moment. When a *Load-to-kerb distance* equal to 1m

is adopted, the stress ratio reaches the value of 0.97. The last scenario that was considered is related to a traffic loads limitation: GL – 3 axes – 260kN. In this case the safety check is satisfied with a stress ratio equal to 0.92. Then, the shear check is considered as well, and three different shear capacity models suggested by Eurocode and implemented in can be adopted: the *Strut and Tie*, *Uncracked* and *Cracked* models. The software is able to automatically carry out the shear distribution along the edge girder by maximizing the shear stress on the cross-section that the user would be check. In the case-study the cross-section at 1.50m from the support is considered. Table 18 shows that the edge girder suffers much more for the bending than the shear, indeed, the value of the shear *DCR* exceed 1 with the NTC 2018-TLM only (1.31). The lower value of shear *DCR* (0.64) is reached when the GL – 3 axes – 260kN-TLM is applied.

Progressive collapse analysis of prestressed concrete bridge decks

Analyses described in Section 4 were carried out in order to provide to road management companies a tool for quick fragility evaluation. Moreover, the Engesser method was implemented, thus the failure of the first structural element (i.e., the most stressed girder) was considered. In this Chapter a more refined 3D bridge model is considered to carry out progressive collapse analysis to investigate the real collapse of a case study bridge. Moreover, different cross girder types are taken into account in order to investigate their influence on the structural behaviour and to support design of an experimental test.

5.1. Description of case study

As case study, 1:5 scaled simply supported post tensioned PC bridge decks with four beams, four cross girders and a continuous RC slab was considered. The deck has a total length and width equal to 6.6m and 1.92m, respectively, with a total height of 440 mm, which the slab thickness is 60mm. The cross girders have an interaxle of 2.1 m and are considered at both headers of the deck and at 1.05m from the midspan. Figure 49 shows the deck geometry from top (Figure 49) and bottom (Figure 49) views.

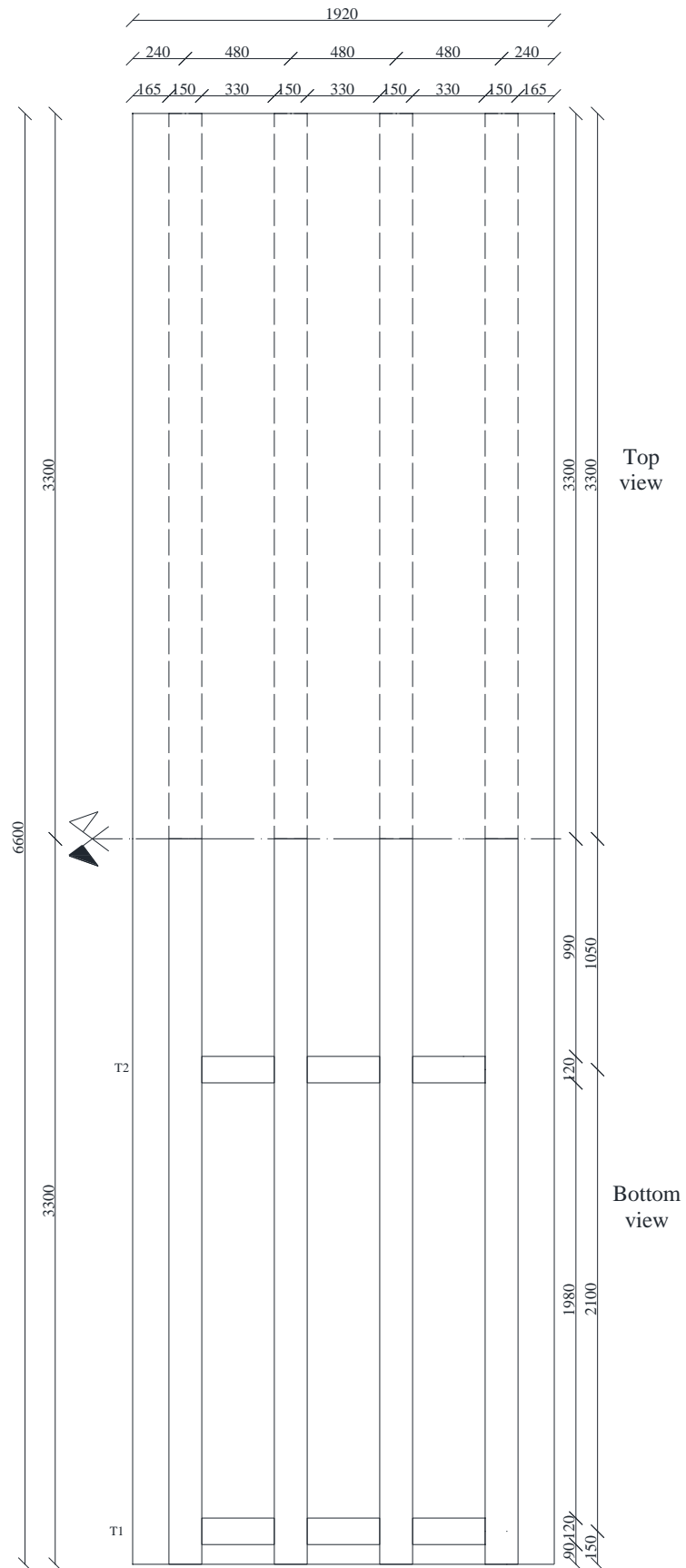


Figure 49. Top and bottom view of the simply supported post tensioned PC bridge deck.

The girder geometry was derived by Galano et al. (Galano et al. 2023) that conducted a four-point bending test on a 1:5 scaled simply supported post-tensioned scaled PC beam. Each girder has a T-shaped cross section (by considering the effective width (Comité Européen de Normalisation 2004a)), with web and top flange widths of 150 and 480 mm, respectively, and a total height of 440 mm, which 60mm are the RC slab thickness; the total length is equal to 6.6 m. The girder web presents equally spaced reinforcing bars with nominal diameter equal to 8 mm and concrete cover of 30 mm. The shear reinforcement is composed by vertical stirrups with nominal diameter of 8 mm and 100 mm longitudinal spacing. The girder is prestressed with two seven-wire tendons with an equivalent area of 150 mm² each one. The clear distance from the top flange of the midspan cross section is equal to 407 mm for the upper tendon and 342 mm for the bottom tendon; at the terminal cross sections these two distances are equal to 281 mm and 111 mm, respectively. On the other hand, the RC slab presents an 8 mm 200x200 welded mesh. Figure 50 shows the girder cross section and its reinforcements and prestressing steel.

Then, as described in the following sections, the cross girders play a fundamental role in the collapse of bridge deck as well as in the type of collapse. Thus, different types of cross girders were considered in this study in order to evaluate different behaviour of bridge deck. In particular, the cross girder could be considered as the element that allows to define the bridge deck cross section as rigid if it is accurately designed (Cestelli Guidi n.d.; Raithel 1977, 1978).

Therefore, the first type of cross girder has a rectangular cross section with height and width equal to 350mm and 120mm, respectively, and a total length (calculated as the clear distance between two consecutive beam webs) of 330mm. Thus, the cross girder has a clear distance from the slab of 30mm. In this way slab and cross girder are separated and no interaction is considered between them. The cross girder presents two reinforcing bars at bottom and upper side of cross section with a nominal diameter of 8mm and a concrete cover of 30mm. Moreover, the shear reinforcement is composed by four vertical stirrups with nominal diameter of 8 mm along the cross girder's length (equal to 93 mm of spacing). This type of cross girder is prestressed with one horizontal tendon with an equivalent area of 150 mm². The clear distance from the top side of the cross section is equal to 125 mm and it is continuous through the beams.

The second type of cross girder has the same geometry of the first one, but it is not prestressed. In this regard, a sensitivity analysis on behaviour of bridge deck due to the prestressing of cross girder is allowed. On the other hand, the third and last type of cross girder considered has different geometry and reinforcements. Therefore, a rectangular cross section with a width equal to 120mm and a total height of 380mm is considered. As described before, also the beam's web has a total height of 380mm, thus, the upper side of cross girder section and bottom side of RC slab correspond. The cross girder has two reinforcing bars at bottom side of cross section with a nominal diameter of 8mm and a concrete cover of 30mm and other two bars of 8mm diameter in the RC slab. Moreover, four vertical stirrups with nominal diameter of 8 mm along the cross girder's length are considered as shear reinforcement. In order to allow the perfect connection between cross girder and slab (that is the aim of the third cross girder type) the stirrups are extended in the RC slabs. The aim of this type of cross girder is the evaluation of bridge deck behaviour varying the connection between cross girders and RC slab.

It is worth noticing that for all types of cross girders the longitudinal reinforcing bars are continuous through the beams in order to establish a connection between cross girders and beams. Moreover, all cross girders are considered as casted together with beams.

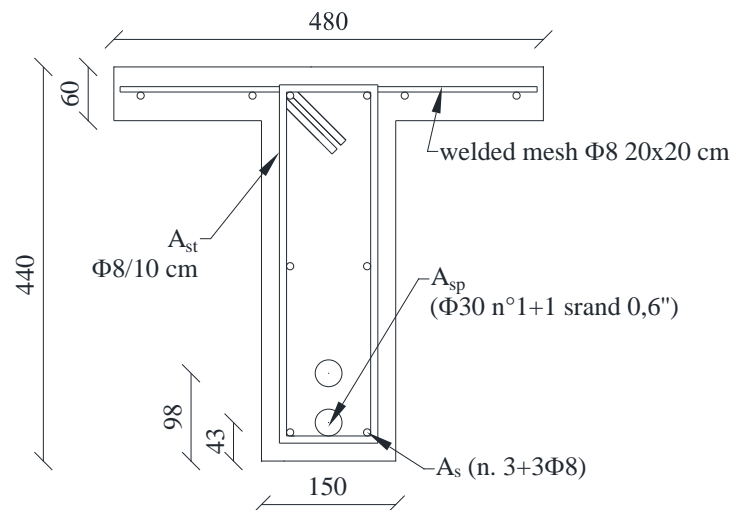


Figure 50. Mid-span beam cross section.



Figure 51. Bridge deck and cross girders cross sections considering: (a) prestressed cross girders separated from RC slab; (b) cross girders separated from RC slab; (c) cross girders connected to RC slab.

Based on the study conducted by Galano et al (Galano et al. 2023) the concrete has been designed for a compressive stress of 28 MPa. Then, the mean value of the compressive stress obtained from the concrete cubic samples has been found equal to 30 MPa (Galano et al. 2023).

The strands were tested showing an average value of the ultimate tensile stress equal to 1929 MPa, a conventional yielding stress (i.e. stress at 0.1% of tensile strain) equal to 1720 MPa and an elastic modulus of 203,400 MPa .

In Galano et al. (Galano et al. 2023) two specimens, with the same geometry and reinforcements, but with different levels of initial prestressing force were tested. Galano et al. consider the initial prestress for each tendon in the first specimen equal to 150 kN (or 1000 MPa), whereas each tendon in the second specimen, it was set at 75 kN (or 500 MPa). The two samples are thus indicated as S1-HP

(Specimen 1 - High Prestress) and S2-LP (Specimen 2 - Low Prestress). The initial prestressing forces in the bottom and top tendons for S1-HP were decreased to 111 kN (-26%) and 104 kN (-31%), respectively, owing to early deformation of the strand anchorages, friction, creep, and shrinkage, and to 36.3 kN (-52%) and 51.6 kN (-31%) for S2-LP. On the other hand, in the simply supported post tensioned PC bridge decks the S1-HP was considered as beams.

5.2. Structural modelling via applied element method

The Finite Element Method (FEM) has been used mostly for failure analysis of reinforced concrete structures. The FEM, on the other hand, makes the assumption that elements are connected by nodes, and these nodes cannot separate while the analysis is taking place. Moreover, to ensure connection between components, the transition from big to small size elements in FEM should be done using particular meshing techniques. These issues result from: (i) the transition layer may cause the number of components to rise and (ii) the meshing procedure is complicated because elements must be joined through boundaries. Additionally, the separation of the elements at the node site causes a stress singularity at the fracture tip.

Okamura et al (1990) (Okamura and Maekawa 1990) discrete crack methods make the assumption that the position and direction of fracture propagation are known before the study and numerous more techniques were created in order to address these issues. One of these is the Rigid Body and Spring Method (RBSM), developed by Kawai in 1980 (Kawai 1980). The primary benefit of this method is that, in comparison to FEM, it simulates the cracking process using a technique that is relatively simple. On the other hand, the principal drawback is that, according to Kikuchi et al. (1992) (Kikuchi et al. 1992), crack propagation primarily depends on the shape, size, and arrangement of the elements.

In the Applied Element Method (AEM) it is assumed that the two elements are connected by pairs of normal and shear springs placed at contact locations, spaced evenly around the edges of the components (Figure 52) (K Meguro and Tagel-Din 1997; Kimiro Meguro and Tagel-Din 2002; TAGEL-DIN and MEGURO 2000). As consequence of that, even if two elements share only a portion of the same surface (partially overlapped elements), in AEM, connectivity springs are generated. On the other hand, partial connectivity could

be included in FEM, however, this would require more nodes and elements to be taken into account at the locations of contacts, which would result in more degrees of freedom (DOFs), more complexity in the formulation of the elements, and a longer build time for the models. In AEM, loads, strains, deformations, and failure of a specific area of the structure are totally represented by each spring. The key benefit of this technology is its ability to reliably and accurately track structural behaviour from the early loading phases to final collapse in a manageable amount of CPU time (K Meguro and Tagel-Din 1997; Kimiro Meguro and Tagel-Din 2002; TAGEL-DIN and MEGURO 2000).

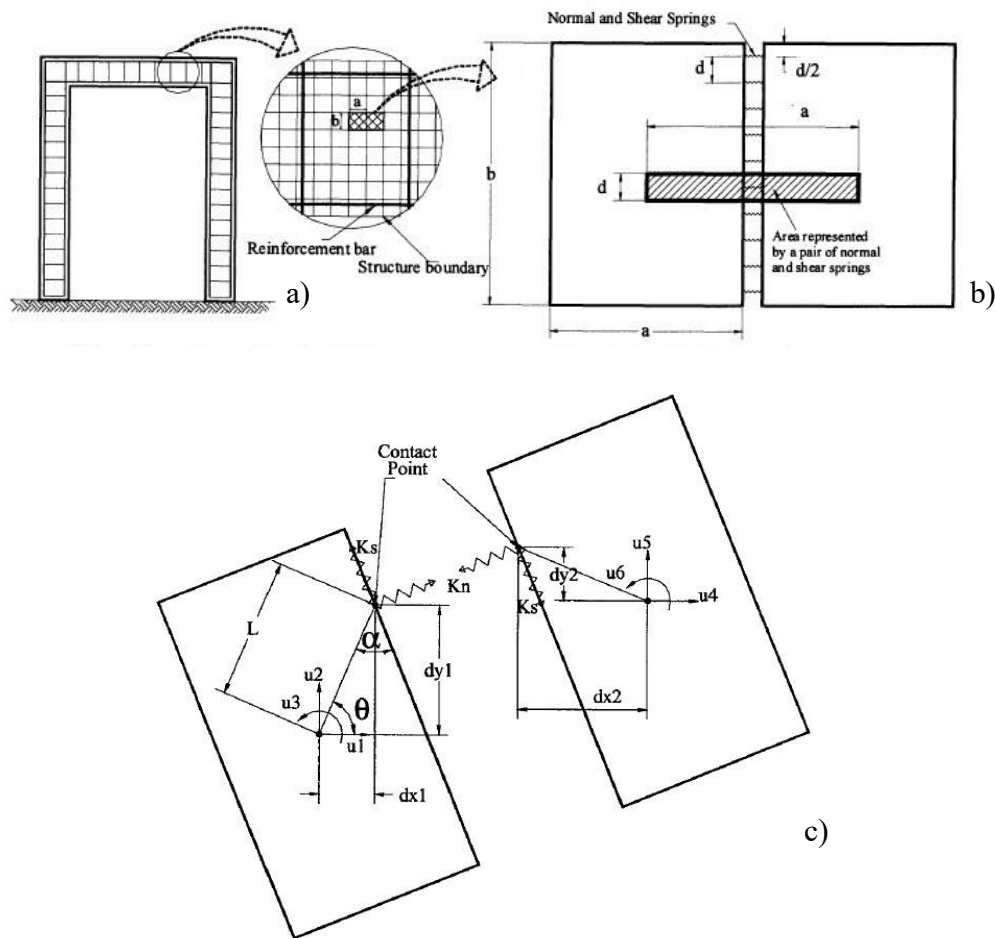


Figure 52. (a) Element generation for AEM, (b) spring distribution and area of influence of each pair of springs, (c) element shape, contact point and degrees of freedom ((K Meguro and Tagel-Din 1997; Kimiro Meguro and Tagel-Din 2002; Meguroi and Tagel-Din 2000; TAGEL-DIN and MEGURO 2000)

Poisson's ratio effects, which are typically ignored in approaches based on rigid body elements, are also successfully addressed (K Meguro and Tagel-Din 1997; Meguroi and Tagel-Din 2000). Moreover, the AEM can predict failure loads and

follow complex nonlinear behaviour such fracture initiation, propagation, and opening and closing (K Meguro and Tagel-Din 1997). The geometrical stiffness matrix does not need to be determined in the AEM, in contrast to previous approaches.

As showed in Figure 52, the structure of the AEM is separated into small elements. A pair of normal and shear springs are believed to link two items at certain locations along their edges. The following equation shows how the spring stiffness is determined (Kimiuro Meguro and Tagel-Din 2002):

$$K_n = \frac{EdT}{a} \quad K_s = \frac{GdT}{a} \quad (19)$$

where a is the length of the representative area, d is the distance between springs, T is the element thickness, E is the material Young's modulus, and G is the material shear modulus. Each spring is supposed to reflect the stiffness of a volume with the dimensions d , T , and a , according to equation 19. Rebar stiffness is added to the material stiffness determined by Equation 19 when reinforcement is present.

For each element in the two-dimensional model, three DOFs are taken into account, which represent the element's rigid body motion. This results in a stiffness matrix that is rather small (size: 6x6). Even though they move like rigid bodies and their shape doesn't change, components can deform internally thanks to spring deformations (the element assembly is deformable). By unitarily displacing one DOF while maintaining the other DOFs stationary, stiffness matrix components can be calculated. The forces required to produce this configuration are represented by the stiffness matrix components, which are equal to the contributions of the element's surrounding springs added together. The contact spring's contribution to DOFs u_1 , u_2 , and u_3 is

$$\begin{aligned} A &= \sin(\theta + \alpha) \\ B &= \cos(\theta + \alpha) \\ C &= \sin(\alpha) \\ D &= \cos(\alpha) \end{aligned}$$

$$K_{1/4} = \begin{bmatrix} A^2 K_n + B^2 K_s & -K_n AB + K_s AB & BA^2 K_s LC - AK_n LD \\ -K_n AB + K_s AB & A^2 K_s + B^2 K_n & BA^2 K_n LD + AK_s LC \\ BA^2 K_s LC - AK_n LD & BA^2 K_n LD + AK_s LC & L^2 D^2 K_n + L^2 C^2 K_s \end{bmatrix} \quad (20)$$

where each term is shown in Figure 52. One-fourth of the element stiffness matrix is shown in equation 20. Then, by adding together the contributions of each spring in the system, the global stiffness matrix, K , is discovered. One set of normal and shear springs are used to create a stiffness matrix at an arbitrary contact point (Figure 52). Thus, the location of the contact point and the stiffness of the normal and shear springs also affect the element stiffness matrix in this formulation (K Meguro and Tagel-Din 1997; Kimiro Meguro and Tagel-Din 2002; Meguroi and Tagel-Din 2000). Moreover, assuming the degrees of freedom to be at the centroid of the blocks, it should be noted that the number of springs has no effect on the size of the global stiffness matrix.

Models for spring failure make the assumption that the spring under consideration has no stiffness (K Meguro and Tagel-Din 1997). Therefore, in light of the stress situation surrounding the element, the stiffness matrix that was produced is an average stiffness matrix for the element.

According to the load condition and material type of each spring, spring stiffness is estimated for each spring. The modelling of diagonal cracking is one of the key issues with using rigid parts to represent reinforced concrete. It is incorrect to apply Mohr-failure Coloumb's criteria, which were derived using normal and shear springs with normal and shear stresses rather than primary stresses. This assumption causes a structure's resistance to increase and its fracture behaviour to behave incorrectly (K Meguro and Tagel-Din 1997). Thus, the following method, described by Meguro 1998 (K Meguro and Tagel-Din 1997) is used to identify the main stresses at each spring location. In Figure 53, the deformation of the normal and shear springs attached at the contact point is used to calculate the shear and normal stress components (τ and σ) at the point (A). The normal stresses in locations (B) and (C) are used to determine the secondary stress (σ_2) (equation 21).

$$\sigma_2 = \frac{x}{a} \sigma_B + \frac{(a-x)}{a} \sigma_c \quad (21)$$

Then, the tension resistance of concrete is compared with this principal stress value, (σ_p) (equation 22) and the normal and shear spring forces are redistributed in the following increment when σ_p surpasses the critical value of tension resistance by applying the shear and normal spring forces in the opposite direction.

$$\sigma_p = \frac{(\sigma_1 + \sigma_2)}{2} + \sqrt{\left(\frac{(\sigma_1 + \sigma_2)}{2}\right)^2 + (\tau)^2} \quad (22)$$

In the following increment, the redistributed forces are transferred as a force and a moment to the element centroid (K Meguro and Tagel-Din 1997). In order to follow the proper fracture propagation, the redistribution of spring forces at the crack position is crucial. The normal spring redistributes the entire force so that there is no tension stress at the crack faces. Shear springs at the site of tension cracking could have some resistance after the cracking due to the friction and interlocking between the crack faces, but the shear stiffness is considered to be zero at this point. Thus, a redistributed value (a residual shear strength) is used to take friction and interlocking effects into account. Mohr-failure Coulomb's criterion is used to determine compression shear failure for springs that are subjected to compression. Shear force is transferred and shear stiffness is supposed to be zero in subsequent increments when the spring achieves the compression shear failure. The following equation may be used to compute the local crack's inclination angle to the element edge direction shown (Figure 53) (TAGEL-DIN and MEGURO 2000):

$$\tan(2\beta) = \left(\frac{2\tau}{\sigma_1 + \sigma_2}\right) \quad (23)$$

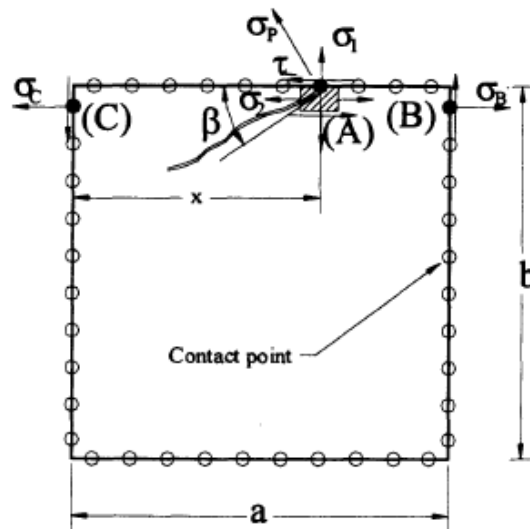


Figure 53. Principal stress determination (K Meguro and Tagel-Din 1997; TAGEL-DIN and MEGURO 2000)

As described in Meguro et al. (2000) (TAGEL-DIN and MEGURO 2000), there are two major ways to depict the occurrence of the fractures. The first is to divide

the element into two segments, each of which has three DOFs. Thus, tension stresses are redistributed at the major tension stress plane and zero shear plane. In this regard, four main advantages can be observed (TAGEL-DIN and MEGURO 2000): (i) accurate redistribution of tension stress, (ii) accurate crack direction inside the element, (iii) simulation of shear transfer and softening after the evaluation of the crack width, (iv) accurate simulation of shear type failure. Even though these advantages, the number of elements grows excessively, thus, the time of analysis increases and the spring stiffness at cracked elements cannot be predicted with the same precision as before the crack. The simple fact that each spring cannot replicate a specific location as it was before to breaking is the cause. Moreover, if the elements after cracking have a low aspect ratio, numerical inaccuracies will occur. On the other hand, it can be assumed that the cracks inside the element is associated with failure of attached springs (TAGEL-DIN and MEGURO 2000). This implies that if a spring meets the criteria for failure, the spring force is re-allocate and the failed springs' stiffness is set to zero. This efficient approach has the benefit of not requiring any fancy rendering to depict the cracking. The angle (β) tends to be zero in cases when shear stresses are not the main force. This suggests that the crack is parallel to the edge of the element, and great precision is thus anticipated. The biggest drawback of this method is that it is impossible to determine the fracture width precisely. This suggests that it is impossible to reproduce effectively post fracture behaviour factors like shear transfer and shear softening with accuracy that depend on the crack width. Furthermore, if the fracture plane is not parallel to the edges of the elements, proper simulation of compression shear failure is also impossible.

Figure 54 depicts the numerical technique's flowchart. For reinforcement bars and concrete springs, stresses and strains are computed for each increase and the failure criteria is examined in tensioned spring cases. The new tangent stiffness is computed for compression springs and steel springs using the chosen material model. At each increment, the global matrix is built, and the spring stiffness matrices are formed. Meguro 2000 (TAGEL-DIN and MEGURO 2000) should be consulted for further information on the analysis's progression in the elastic case.

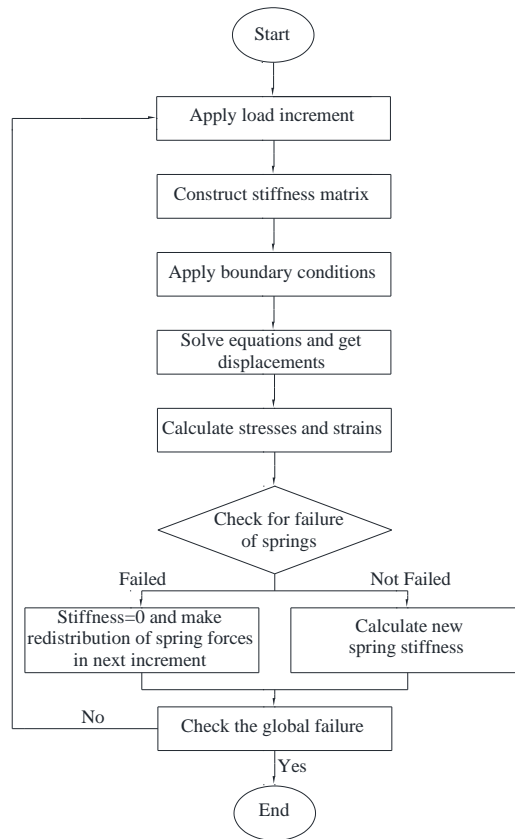


Figure 54. Flow chart of applied element method analysis (TAGEL-DIN and MEGURO 2000).

Meguro and Tangel-Din (1997) (K Meguro and Tagel-Din 1997) carried out two distinct analyses utilizing 20 and 10 springs connecting each pair of neighbouring element faces to examine the effects of the number of connecting springs. Therefore, he derived that adding more base elements causes the error to decrease while the CPU time increases and when there are 5 or more base elements, the error is reduced to less than 1%. Even though the CPU time for 10 springs is approximately half that of 20 springs, the outcomes are same.

Moreover, the AEM was further verified for evaluations of large deformations under dynamic loading conditions (Kimiuro Meguro and Tagel-Din 2002). The fact that an AEM formulation does not require a geometric stiffness matrix, results in a simpler numerical process than the complex one used by FEM. The correctness of AEM formulation in the context of reinforced concrete structures with springs that are subject to nonlinear constitutive material laws was examined in subsequent research works (Kimiuro Meguro and Tagel-Din 2001; TAGEL-DIN and MEGURO 2000). The results confirmed the viability of AEM once

again because it was feasible to precisely predict the failure behaviour, including fracture start and propagation, under monotonic and cyclic loads.

Galano et al. (Galano et al. 2023) conducted experimental testing on two distinct PC beams (detailed in Section 5.1) that created the basis for the simply supported PC bridge deck modelling. As a result, reporting the numerical modelling of girders studied by Galano et al. (Galano et al. 2023) might be valuable. In that study, both PC girders' (described in Section 5.1) numerical models were created using the finite element method (FEM) and the AEM, respectively. One-, two-, and three-dimensional finite element studies as well as 3D applied element analysis were carried out. 3D FEAs and AEAs were conducted using Abaqus FEA (Smith 2009) and Extreme Loading for Structures© (ELS) (ASI 2020) whilst 1D and 2D FEAs were conducted using SAP2000 (I. Computer and structures)

The 1D FEAs employed two different sorts of objects: "tendon" for the prestressing steel and "frame" for the concrete girder (Figure 59a). The single structural element was meshed using two-node components. It was possible to sketch the T-shaped cross section and the longitudinal rebars within using SAP2000's section designer. The two tendons were then given a cross-sectional area of 150 mm². Then the prestress to the two tendon components was applied through both the force and the stress approaches.

Then, the concrete girder was modelled in the 2D models using a four-node formulation multi-layered non-linear shell element (Figure 59b). The longitudinal rebar and concrete were separated into several layers. The single concrete shell element could respond nonlinearly due to the material characteristics (Galano et al. 2023), whereas the layers of rebar were represented using elastic-plastic with hardening models (Galano et al. 2023). Given the concrete girder's T-shaped cross section, two areas—the flange and the web—were modelled, meshes, and joined. The same "tendon" object and material's parameters utilised for the 1D studies were used to simulate the prestressing steel (Figure 59b).

The Concrete Damage Plasticity Model (CPDM), a continuum, plasticity-based damage model, was used to model concrete in Abaqus (Smith 2009). CPDM assumes two basic failure mechanisms: (i) tensile cracking and (ii) concrete crushing. Two hardening factors, the tensile equivalent plastic strain and the

compressive equivalent plastic strain, govern the development of the yield (or failure) surface. Galano et al. (Galano et al. 2023) go into further depth on the material modelling in Abaqus. For concrete elements, the eight-node brick element with reduced integration(C3D8R) from the Abaqus library was utilised. It is a linear brick element with one integration point (i.e., located in the middle of the element) with the same shape functions of C3D8 element (Lapidus, L. and Pinder 1982). Both regular and prestressed steel were modelled using two-node truss elements (element T3D2 in the Abaqus library) (Figure 59c). The embedded approach was thought to simulate the ideal bonding situation between the surrounding concrete and the interaction between rebars (longitudinal bars and stirrups) or tendon and concrete. Temperature-based approach was used to apply the prestress to the tendons (Galano et al. 2023).

Then, the AEM beam’s model was the same adopted for the PC bridge deck, and it is described in the following lines.

Details about material modelling were provided in (Galano et al. 2023).

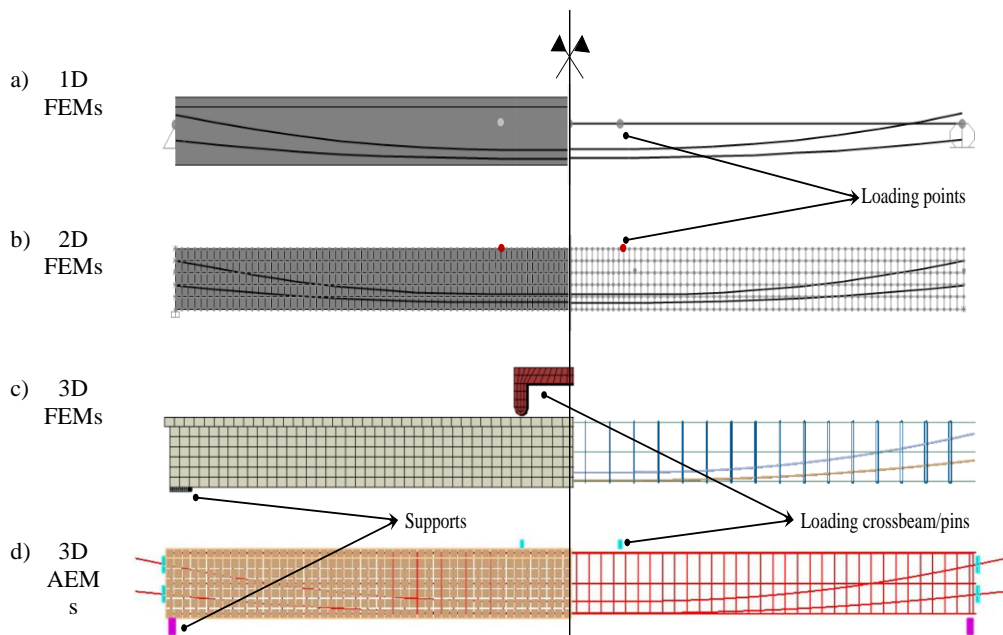


Figure 55. Numerical models: (a), (b) 1D and 2D FEM with SAP2000, (c) 3D FEM with Abaqus and (d) 3D AEM with ELS (Galano et al. 2023).

On the other hand, according to case study described in Section 5.1, the progressive collapse analysis of 1:5 scaled simply supported post tensioned PC bridge decks with four beams, four cross girders and a continuous RC slab was accomplished by using nonlinear modelling with the objective of producing

capacity curves and defining performance levels that represent the damage process and the observed unique failure types. The bridge deck numerical model was defined through Extreme Loading for Structure© (ELS) (ASI 2020) software that fully implements the AEM method in a user-friendly graphical interface.

The geometrical model of bridge deck was made up of PC beams, cross girders, RC slab, supports and plate elements (in order to apply loads). The post tensioned PC beams models have a rectangular section with 150mm and 380mm of width and height, respectively, and a total length of 6.6m. It is worth mentioning that the T-shaped cross section (described in Section 5.1) is derived by considering the RC slab and the effective width (Comité Européen de Normalisation 2004a). Therefore, the PC beam and RC slab have two different models. Then, each beam was meshed with 50x3x7 elements, along x, y and z global axes respectively, resulting in 1050 elements with dimensions equal to 132x50x54 mm. The reinforcing bars and stirrups were implemented through the “RFT Tool” proposed by ELS in order to arrange them as described in previous Section. This tool allows to draw each bar as a line and stirrups with a closed shape (e.g., rectangular shape) and assign them materials and nominal diameters. Then, all reinforcements were drawn and included in each beam taking care to respect the 30mm concrete cover. The prestressing steel was also modelled through the ELS “RFT Tool” by considering two tendons with an equivalent area of 150mm² for each seven wires tendon. Therefore, the “RFT Tool” allows to apply the prestress by considering the equivalent prestress force on the modelled tendon, thus, each strand was prestressed by applying a 128 kN force directly to it. Then, as for reinforcing bars and stirrups, the prestressing steel was included into the beam taking care of right position. To properly redistribute the prestressing forces, two steel plates were taken into account at each beam head. Modelling these plates as rigid and highly resistant prevented them from having an impact on the bridge deck's structural behaviour. Figure 56 shows the ELS beam model with the prestressing steel and reinforcing bars.

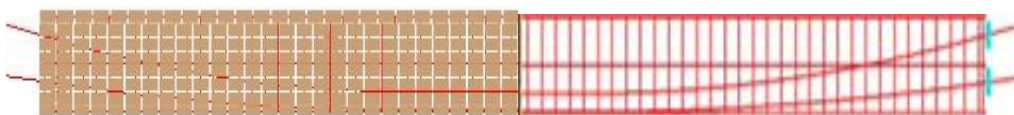


Figure 56. ELS prestressed concrete beam model.

The RC slab was then modelled as a single element with dimensions of 1.92m in width, 60mm in thickness, and 6.6m in total length. In order to have the same

section for each beam, this width was taken into account (i.e., considering the effective width, all beams have the same cross section). As a consequence of meshing the RC slab model with $47 \times 36 \times 1$ along the x, y, and z global axes, 1692 elements with dimensions of 140x53x60 mm were produced. Therefore, when modelling the reinforcements in the slab the custom RFT Tool was employed, leading to a welded mesh made up of bars with a nominal diameter of 8mm and a 200x200mm spacing.

Then, the cross girders were modelled in three different ways to define the three types defined in Section 5.1. The first two type cross girders present the same geometry, with a rectangular cross section with 120 mm of width and 350 mm of height (i.e., separated from the RC slab). The cross girders were modelled with a total length (calculated as the clear distance between two consecutives beam webs) of 330mm. The first two type of cross girders were meshed with $3 \times 3 \times 6$ elements along the x, y, and z global axes, thus, 54 elements with dimensions of 40x110x58 mm were produced.

The reinforcing bars were implemented through the “Girder RFT Tool” that allows to automatically define longitudinal bars and stirrups by setting the following parameters:

1. Concrete cover of top, bottom and side bars
2. Number, material and area of top, bottom and side bars
3. Number of branches, spacing, nominal diameter and material of stirrups

These parameters were defined on the cross section and the software extrude the reinforcements along the longitudinal axis of the element. It is worth underlying that the same reinforcing bars or stirrups along the longitudinal axis of the element is required to use the “Girder RFT Tool” (i.e., no variation of stirrups spacing or branches or longitudinal bars position is allowed with this tool). In this regard, two reinforcing bars at bottom and upper side of cross section with a nominal diameter of 8mm and a concrete cover of 30mm were considered. On the other hand, the shear reinforcement was composed by four vertical stirrups with nominal diameter of 8 mm along the cross-girder’s length (equal to 93 mm of spacing). Moreover, the first type of cross girder is also prestressed, thus, a prestressing bar with an area of 150mm^2 was modelled through the custom RFT Tool.

The third type of cross girders differ from the others because its geometry. Indeed, the cross section is characterized by a rectangular shape with a width and height equal to 120mm and 380mm, respectively. Thus, this type of cross girder has upper side of cross section that corresponds with the bottom side of RC slab. The cross girder presents two reinforcing bars at bottom side of cross section with a nominal diameter of 8mm and a concrete cover of 30mm and other two bars of 8mm diameter in the RC slab. Moreover, four vertical stirrups with nominal diameter of 8 mm along the cross girder's length were considered as shear reinforcement. In order to allow the perfect connection between cross girder and slab (that is the aim of the third cross girder type) the stirrups are extended in the RC slabs. Both longitudinal bars and stirrups were modelled through the custom RFT Tool of ELS (ASI 2020). The third type of cross girders were meshed with 3x3x6 elements along the x, y, and z global axes, thus, 54 elements with dimensions of 40x110x63 mm were produced.

In the bridge deck model, the boundaries conditions were assumed to be applied by modelling proper items. In particular, the supports were defined through rigid and high resistant elements (continuous under the entire deck width) placed at beam heads and fixed to the ground (Figure 57). In this regard, the analysis will focus on the bridge deck structural response, thus, the support behaviour was not taken into account. The interface between beams and supports were modelled through a bearing material (ASI 2020). Moreover, horizontal displacements were not allowed for the left beam-support interface (i.e., hinge constraint), whereas the right one release them (i.e., carriage constraint). On the other hand, two rigid plates were modelled on top of the edge beam in order to apply the vertical loads on bridge deck. Besides, these plates were constrained with respect to the horizontal displacements in order to admit displacements along the load direction only.

Figure 57 shows the ELS PC bridge deck model.

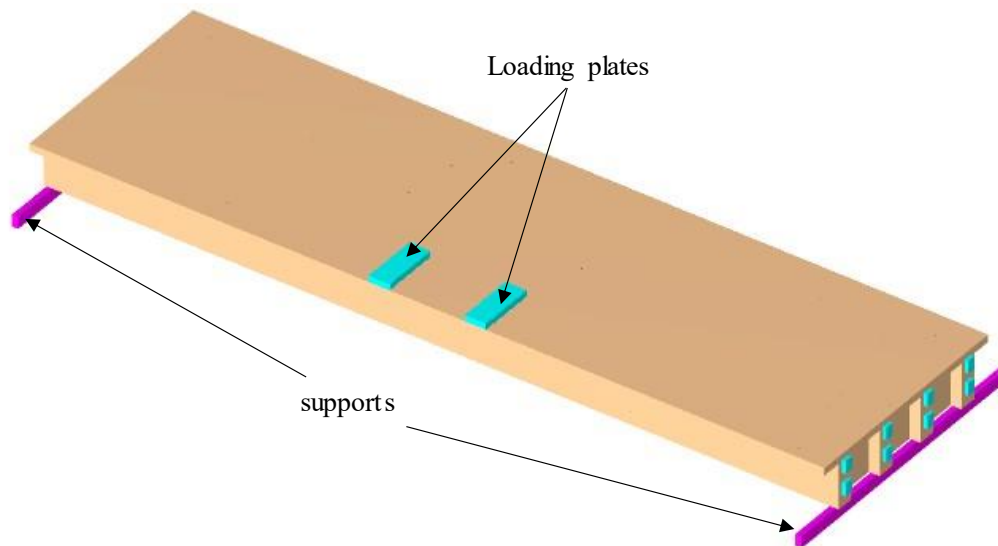


Figure 57. ELS prestressed concrete bridge deck model.

The Maekawa compression model (Maekawa and Okamura 1983) (illustrated in Figure 58a) is used to model concrete under compression. The initial Young's modulus, the fracture parameter, and the compressive plastic strain are the three parameters utilised in this model to define the envelop for compressive stresses and compressive strains. While the plastic strain indicates the degree of residual plastic deformations under compression, the fracture parameter indicates the extent of internal concrete damage. The strain value at the spring site is used to get the tangent modulus. In order to prevent negative stiffness at peak loads, spring stiffness is taken as a minimal value. Due to this, there is a discrepancy between the estimated stress and the stress that emerges from the spring strain. Thus, the following loading phase redistributes these unbalanced stresses by applying the redistributed force values in the opposite direction (ASI 2020).

When tension is applied to concrete springs, spring stiffness is taken for the initial stiffness up until the cracking point. The minimum stiffness for springs under stress is established after cracking. The redistributed force values are then applied in the opposite direction in the following loading stage to redistribute the residual stresses (ASI 2020). In ELS software it is assumed that until concrete begins to break, the relationship between shear stress and shear strain will stay linear. Concrete is considered as fractured when stresses exceed the strength limit depicted in Figure 54b. Both the normal and shear stresses drop to zero in tensioned concrete. The shear stress-shear strain relationship for compressed concrete, on the other hand, follows the curve depicted in Figure 54b and is restricted to a certain value based on the compressive stresses. The residual shear

strength factor, which is dependent on aggregate interlock and friction at the fracture surface, determines the degree of shear stress decrease. Concrete will fail according to the Mohr-Coulomb failure envelope when normal compressive forces and shear stresses are combined. The failure envelope is considered to be linear when concrete is exposed to normal tensile stresses, with a limiting normal strength of f_t when the shear stress is zero (ASI 2020). A concrete's residual shear strength is taken into account after cracking. In this regard, the shear stress transmitted at the fracture surface after a brittle material crack is significantly influenced by the surface roughness of the crack as well as the normal forces acting on it (ASI 2020). When the crack surface is exposed to compressive stresses, the shear transfer has a fairly significant value for crack surfaces with a highly corrugated shape, such as normal-strength concrete with high aggregate interlocking, whereas the shear transfer has a very small value for smooth crack surfaces. The ratio of the residual shear strength to the initial shear strength value is represented by the residual shear strength factor (ASI 2020). Based on the configuration of the fracture surface it varies from zero to unity. However, the residual shear strength is ignored in the ELS (ASI 2020) when the broken surface is exposed to tensile normal stresses.

The mild steel uniaxial behaviour was implemented as an elastic – plastic with hardening model (Galano et al. 2023), whereas the prestressing steel uniaxial response was given by manufacturing, thus, a stress-strain relationship was imported in ELS software (Galano et al. 2023).

A fundamental role in the ELS material model is played by the separation strain, that is defined as the strains at which adjacent components completely separate from one another at the connecting face (ASI 2020). When the resulting strain of the matrix springs exceeds the separation strain value, the components separate. All springs between neighboring sides, including reinforcement bar springs, are removed when the separation strain for reinforced concrete is attained. The components will behave as two separate rigid bodies that interacted if they come into contact once again. It should be remembered that steel reinforcing bars are cut when their maximal tension is reached or when the separation strain of the matrix springs (concrete springs) is reached (ASI 2020). Each material has a separation strain that is determined by its ultimate strain and by whether the loading is monotonic (in which case open fractures tend to remain open) or cyclic (in which case open cracks may close).

In the ELS bridge deck model, concrete with a 30 MPa of initial Young's modulus, 12.5 MPa of shear modulus and 30 MPa compressive strength was used. The tensile strength of concrete was considered equal to 1.5 MPa. In addition, a separation strain equal to 0.2 (as suggested by ELS manual (ASI 2020)) and a residual shear strength factor equal to 1 were set. On the other hand, mild steel was assumed with a yield and ultimate strength equal to 450 MPa and 540 MPa, respectively and a Young's modulus of 210 GPa. The prestressing steel model was derived from tensile tests on tendons (Galano et al. 2023) and produced equivalent yield stresses (i.e., stress at 0.1% of residual strain) of 1782 MPa, ultimate tensile stresses of 1969 MPa, and a Young's modulus of 203.4 GPa.

The concrete constitutive models and related values were entirely set basing on the study conducted by Galano et al (2023) (Galano et al. 2023).

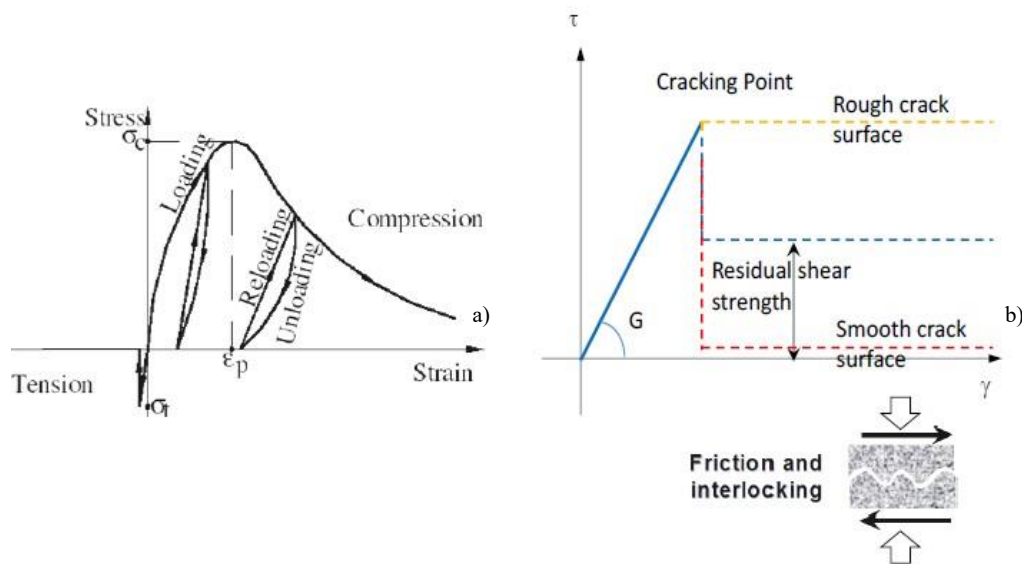


Figure 58. Constitutive models for concrete (ASI 2020; Maekawa and Okamura 1983)

5.3. Discussion of results

Galano et al. (Galano et al. 2023) conducted experimental tests on two different PC beams (described in Section 5.1 and 5.2) that have laid the foundation for the simply supported PC bridge deck analysis. Thus, it could be useful to report the main results of that study in order to better understand the bridge deck analysis results. For this purpose, a briefly overview of the test setup is here reported. Figure 59a depicts the experimental test setup, whereas Figure 59b shows one of the specimens just before to the test. The samples were put through a four-point

bending test while being loaded quasi-statically under displacement control at a constant rate of 0.05 mm/s until failure. The end cross sections of each girder were simply supported by two rubber bearings, and the same portions were laterally restrained by L-shaped steel components. A strong steel crossbeam with two loading points and a clear distance of 850 mm was used to transmit the vertical force, creating a shear-span length of 2875mm.

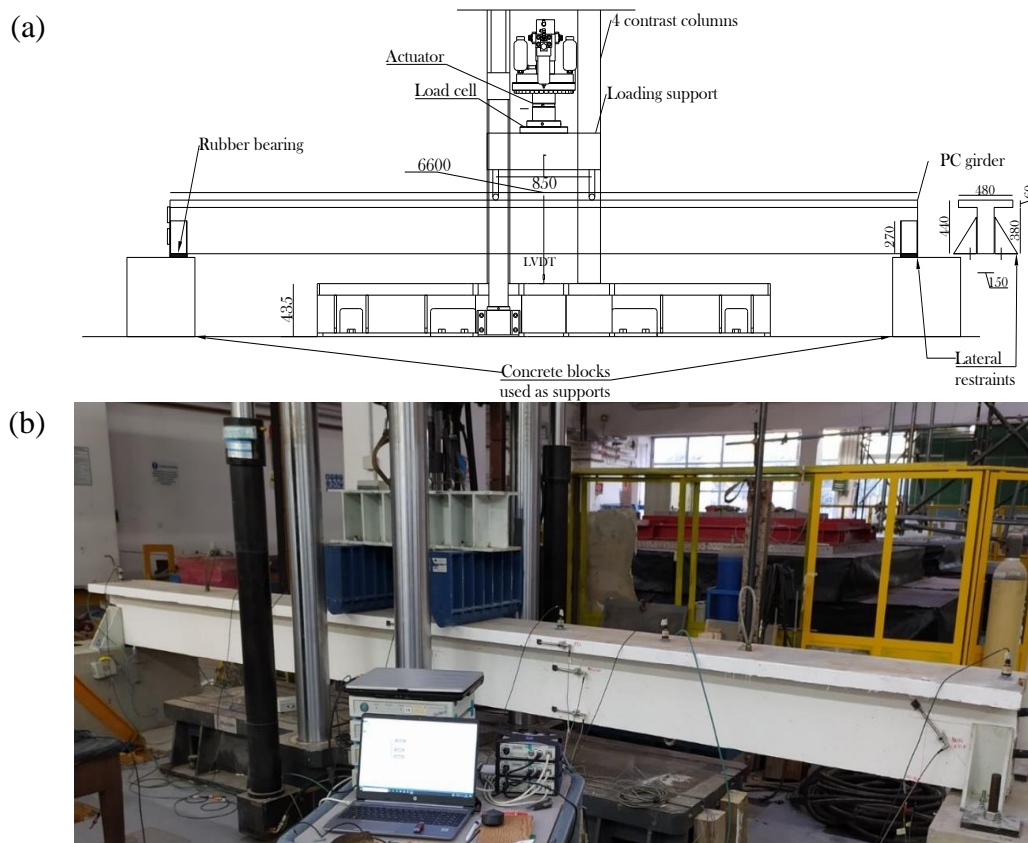


Figure 59. (a) specimens after casting, (b) geometry of the generic tested samples (longitudinal view and cross sections, measures are in mm)(Galano et al. 2023).

In both Abaqus and ELS, a non-linear static analysis is set up to replicate the test method: first, prestressing is applied through the tendon, and then the four-point bending test is reproduced by displacing the crossbeam/pins downward (i.e. displacement-control approach) up to flexural failure of the girder (Galano et al. 2023).

Figure 60 depicts the global response of each PC girder, along with an experimental-numerical comparison of force-displacement response curves and bending moment (shown in secondary vertical axis). The numerical results were collected for the girders' whole flexural response, including the post-peak (i.e. softening and/or collapse). As a result, Figure 60 includes an estimation of the

girders' behaviour beyond the maximum experimental displacements. For all of the numerical techniques used, there was high experimental - numerical agreement. Each numerical model's response perfectly reproduces the experimental curves, from the initial linear response through the end non-linear behaviour of both girders. As reported in Galano et al. (Galano et al. 2023) maximum percentage difference between experimental test and numerical results were about 7% only.

The numerical models yielded the initial cracking as vertical force values where the tensile strength is attained in the midspan cross section. Considering the peak vertical forces of the girders, the accuracy of the experimental-numerical comparison continues to increase. The study conducted by Galano et al (Galano et al. 2023) shows how numerical simulations may predict the peak response of prestressed girders with a maximum percentage deviation of 3%.

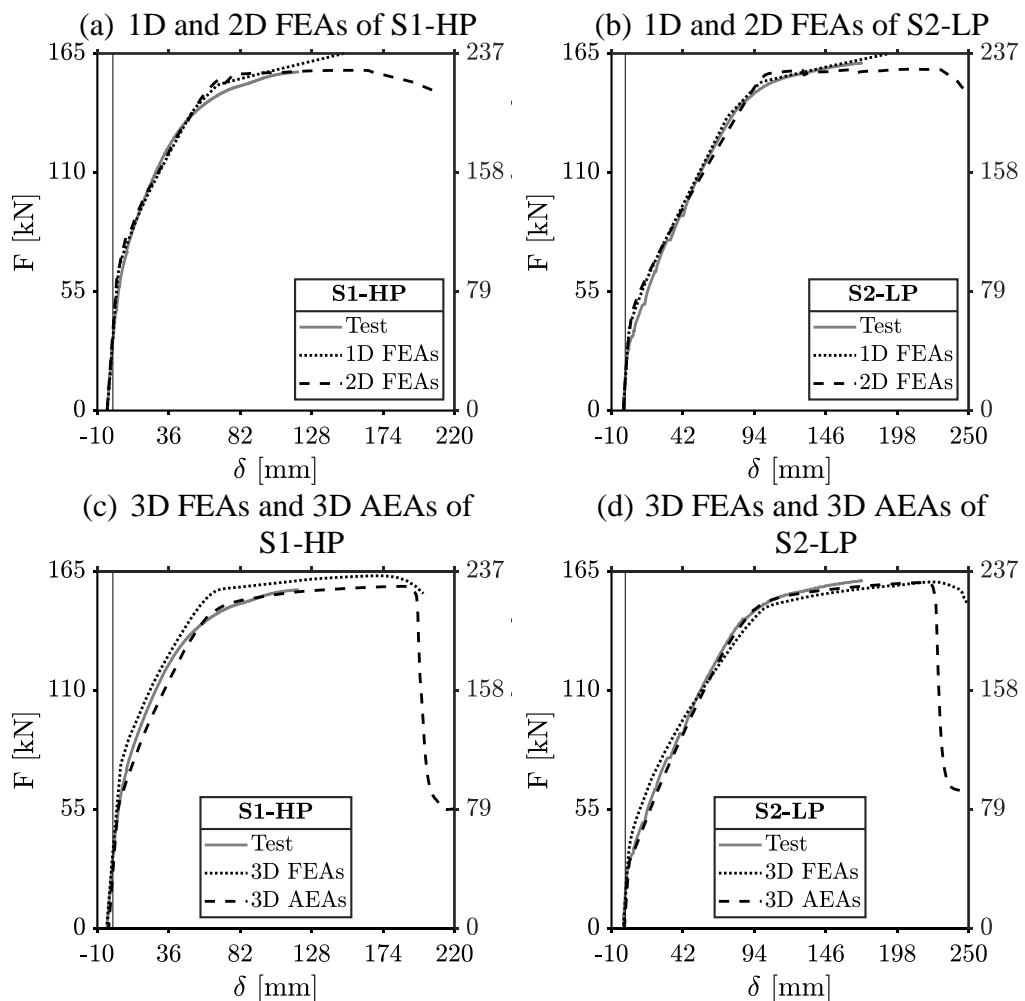
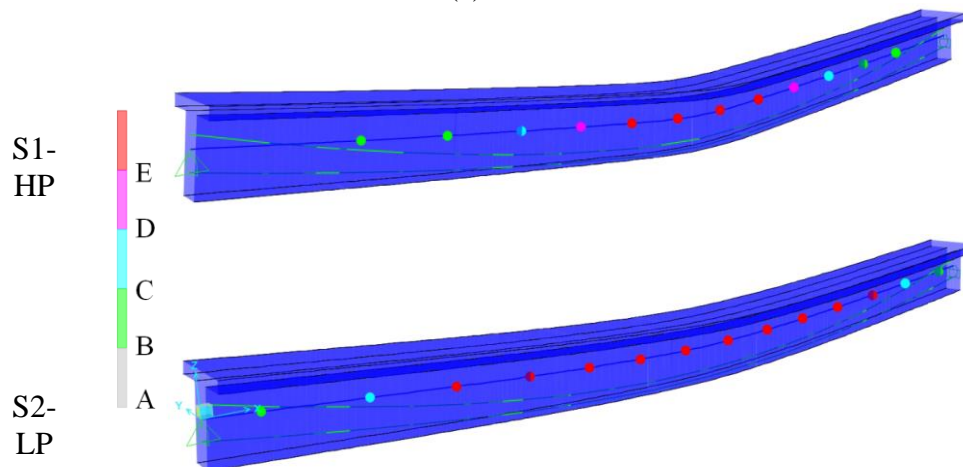


Figure 60. Experimental-numerical comparison: force-displacement curves (Galano et al. 2023).

Figure 61 displays the girders' ultimate numerical response. In 1D FEAs, progressive vertical deformation gradually activated the plastic hinges in the girder's various positions. The plastic hinges situated around the midspan cross section achieved the highest bending moment for S1-HP, while the ultimate non-linear response was also achieved outside the loaded component for low prestress (Figure 61a). The axial stresses in each shell were provided by 2D FEAs (Figure 61b), providing information on the tensile and compressive response of the generic section. In Abaqus, tensile damage contour plots (Figure 61c) offer a good depiction of the cracking patterns on the element at a general vertical displacement threshold (Figure 61c and Figure 61c, d). As can be observed, the S1-HP specimen has a discrete path for the separate fractures, but the S2-LP specimen exhibits more extensive damage across the tensile bottom portion. By using axial tensile strains, this was also discovered in 3D AEAs (Figure 61d), where there was a greater concentration of the maximum tensile values between the two loaded points for S2-HP initial prestress. As a result, the initial prestress impacts the local reaction of the girder, according to results from 1D FEAs on plastic hinges (Galano et al. 2023).

(a) 1D FEAs



(b) 2D FEAs

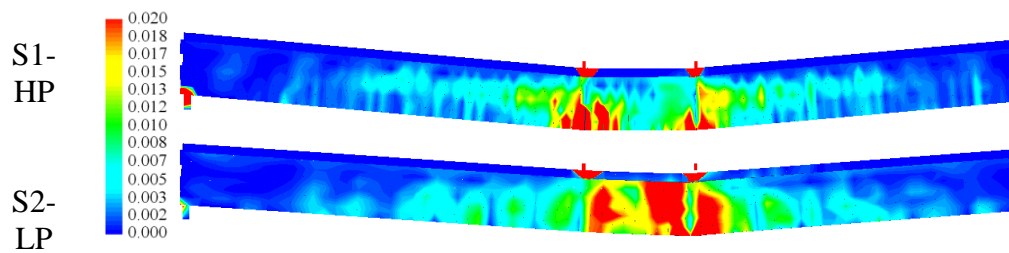
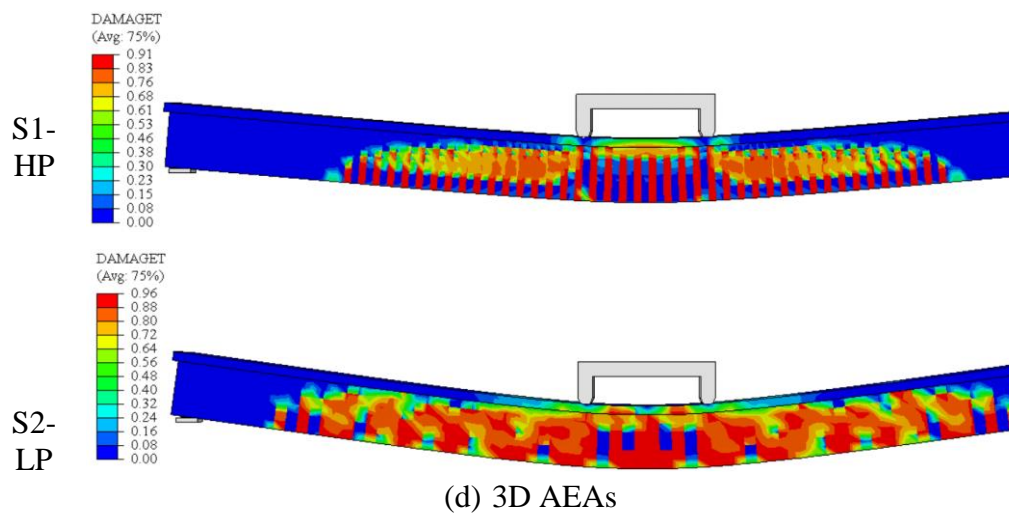
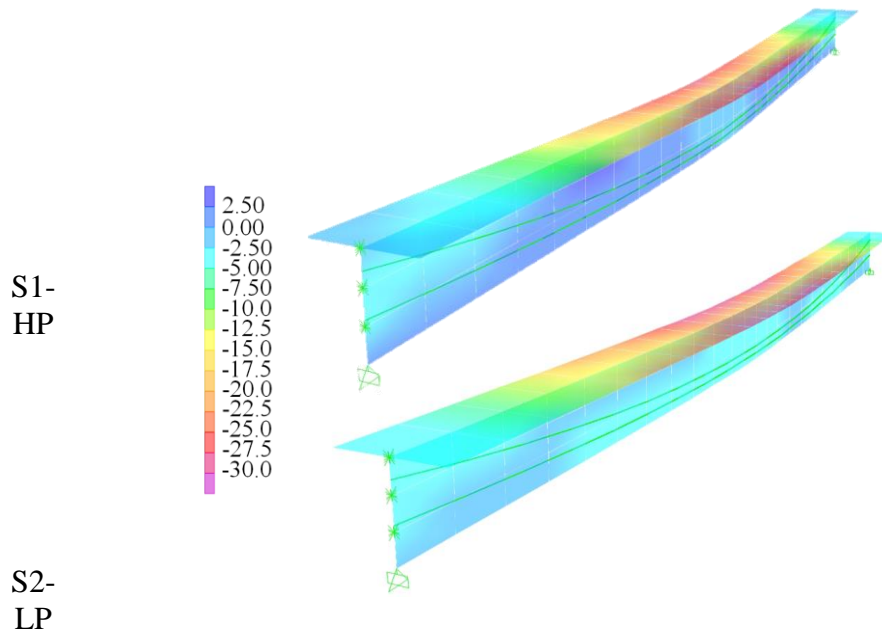


Figure 61. Contours plots at ultimate response of the girders: (a) plastic hinges response for 1D FEAs, (b) stresses in the shells for 2D FEAs, (c) tension damages for 3D FEAs, (d) axial tensile strains in 3D AEAs (Galano et al. 2023).

The global accuracy of each numerical model is evaluated using the error coefficient, defined as:

$$E_{num,i} = \frac{F_{e,num,i}^\delta - F_{e,exp,i}^\delta}{F_{e,exp,i}^\delta} \quad (23)$$

where $F_{num,i}^\delta$ and $F_{exp,i}^\delta$ are the numerical (“num.” is referred to a generic analysis type) and experimental forces at a generic level of total vertical deformation δ . Then, the average values of the n error coefficients is evaluated and the global error coefficient $E_{num} = \sum_{i=1}^n E_{num,i} / n$ is obtained. The numerical analysis accuracy is higher when E_{num} reduces, i.e. the numerical curve matches the experimental one with better approximation. The percentage error coefficients are reported in Figure 62, where the discretization of the experimental curves (i.e. each 5 mm of total vertical displacement) are also shown. Moreover, the values of the standard deviations of these values are also reported, being obtained as:

$$\sigma_{num} = \sqrt{\frac{1}{n} \sum_{i=1}^n (E_{num,i} - E_{num})^2} \quad (24)$$

The maximum percentage error is of the order of 6% and is related to 3D FEA of S1-HP with a standard deviation equal to 0.045; whereas the best accuracy is obtained for 3D AEA of S2-LP, with an error of around 2% and a standard deviation equal to 0.009.

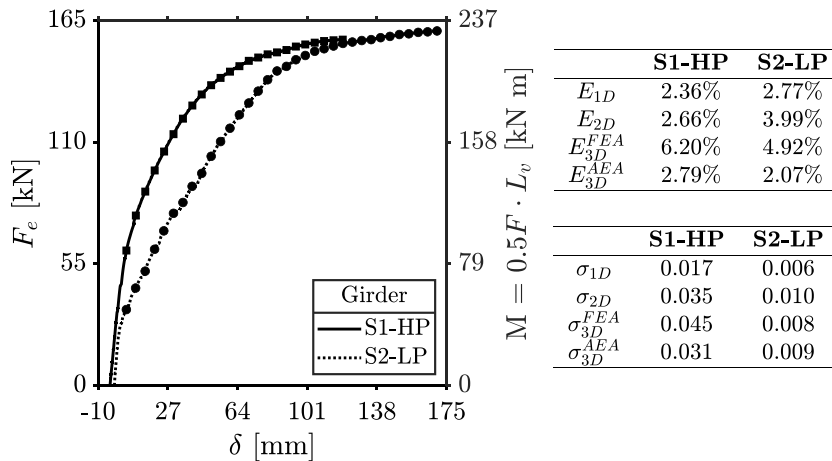


Figure 62. Numerical error coefficients and standard deviations related to each numerical model (Galano et al. 2023).

Starting from these results, the bridge deck model was built as discuss in Section 5.2 (the girders considered in the bridge deck model were the S1-HP specimens). A nonlinear static analysis with displacement control was carried out by applying

a vertical displacement on loading plates (Figure 57) up to the collapse of the deck. The ELS software (ASI 2020) uses the PARDISO direct sparse solver (Schenk and Gärtner 2004) technique with a modified Cholesky decomposition (ASI 2020) to solve the system of equations (ASI 2020). In the analyses 2000 steps were considered with an increment of $5 \cdot 10^{-4}$ m for each step.

First of all, the PC bridge deck model was validated by comparing the results obtained for the beam (S1-HP) and bridge deck by applying a centred load on it (i.e., in this way the loads were uniformly distributed in all beams' deck). The bridge deck curve was obtained by dividing the total force by the number of the beams, giving the response curve of one beam of the deck. Figure 63 depicts the results, which exhibit force-displacement response curves and underlie a high level of agreement, particularly during the early elastic and post yielding phases up to the collapse. Moreover, the maximum force reached in both models is 150kN.

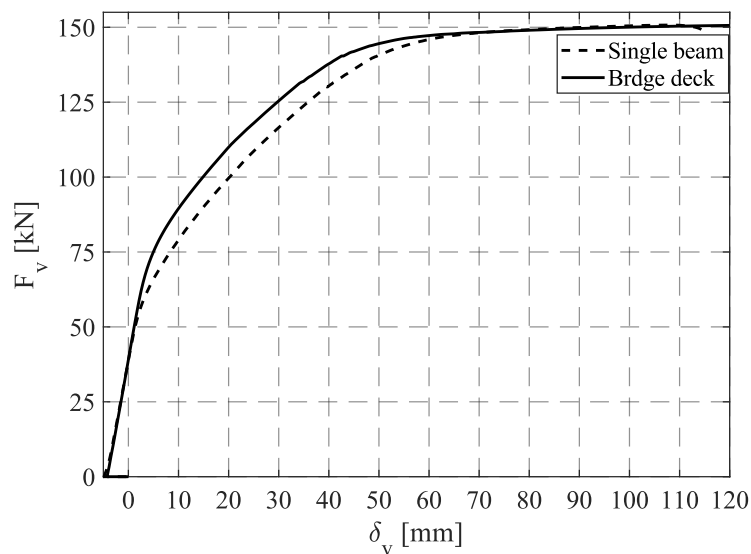


Figure 63. Comparison between single beam and bridge deck (divided by the number of beams' deck) force-displacement response curves.

As discussed in Section 5.1 three types and models of PC bridge deck were considered by varying the type of cross girders:

- (i) PC bridge deck with prestressed cross girders separated from RC slab
- (ii) PC bridge deck with cross girders separated from RC slab (i.e., not prestressed)
- (iii) PC bridge deck with cross girders connected to RC slab (i.e., not prestressed)

The cross girders play a fundamental role in the collapse of bridge deck as well as in the type of collapse due to the fact that the cross girder could be considered as the element that allows to define the bridge deck cross section as rigid if it is accurately designed (Cestelli Guidi n.d.; Raithel 1977, 1978).

Figure 64 depicts the force-displacement response curves for all types of PC bridge deck models in order to investigate the influence of cross girders on the PC bridge deck behaviour. Moreover, the Courbon-Engesser analysis (Cestelli Guidi n.d.; Raithel 1977, 1978) was carried out to define the distance between the maximum capacity (i.e., in terms of maximum vertical force F_v) of the deck evaluated with a simplified approach and a complex 3D model (i.e., 3D AEM model).

Figure 64 shows that the PC bridge deck with prestressed cross girders separated from RC slab could reach a higher vertical force than the other two types. In this regard, a maximum vertical force of 550kN was achieved. F_v values of 475kN and 497kN were obtained for the PC bridge deck with cross girders separated and connected to RC slab, respectively. In this regard, a decrease of 14% and 10% was observed for the F_v , respectively. Indeed, prestressed cross girders allowed the redistribution of loads and stresses on the structural elements of the deck much more than the other two types. In addition, the first drop of PC bridge deck with prestressed cross girders force-displacement curves is almost vertical comparing with the others. Moreover, the maximum forces reached after the drop were higher than other two types due to the fact that the PC bridge deck cross section is rigid thanks to the prestressed cross girder, thus, they allowed the redistribution of stresses in the other structural elements.

The PC bridge deck with cross girders connected to the RC slab presents a force-displacement curve (Figure 64) with a softer drop branch and a similar trend to the bridge deck with prestressed cross girders in the post drop phase. In this regard, the connection between cross girders and RC slab allowed a slight redistribution of stresses in the structural elements after the drop. Therefore, similar force values to the prestressed cross girders type were attained in this phase. On the other hand, the PC bridge deck with cross girders separated from RC slab and not prestressed presents not only the lowest value of F_v (i.e., 475kN), but also vertical forces similar to the single beam after the drop (i.e., 150kN). Therefore, the bridge deck cross section cannot be considered as rigid and after

the drop phase the loads were applied on the edge beam only without any redistribution on the other structural elements.

Moreover, the Courbon-Engesser analysis (Cestelli Guidi n.d.; Raithel 1977, 1978) was carried out and the vertical force that led to the failure of edge girder was obtained (i.e., the vertical force that develops the maximum bending moment in the edge girder). A value of 196 kN was evaluated and a decrease between 140% and 180% was observed respect than the 3D AEM model. Indeed, the Courbon-Engesser analysis does not take into account loads and stresses redistributions that lead to a higher deck capacity. Thus, this simplified approach is good for a preliminary analysis or a fragility analysis where a huge computational effort is required (i.e., hundred thousand models to analyse). On the other hand, a 3D complex model (e.g., 3D AEM model) could be useful for a detailed analysis of a single bridge deck with much more accurate results.

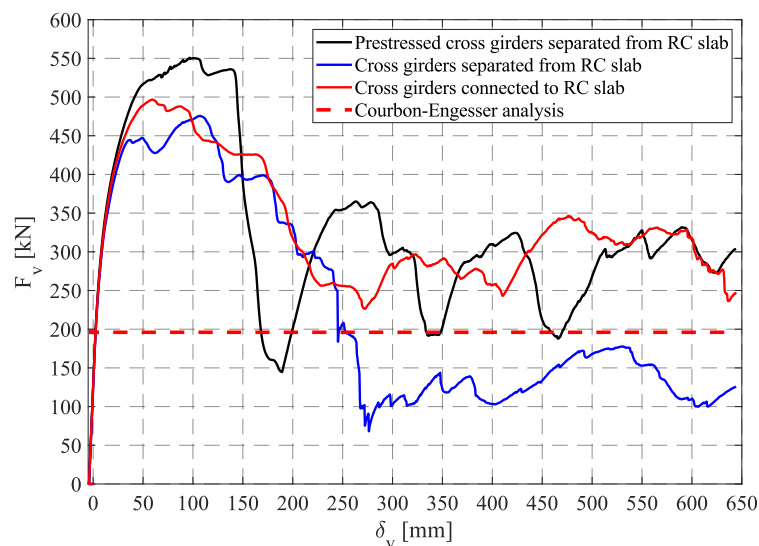


Figure 64. PC bridge deck force-displacement response curve.

In order to investigate the structural behaviour of all types of PC bridge decks, in the following figures the force-displacement and bending moment-displacement curves are shown for the RC slab and cross girders. Moreover, the pictures of the ELS (ASI 2020) bridge deck model when the first drop and collapse occurred are shown. Figure 65 depicts the sections considered in the RC slab to derive the envelope of the bending moments. These sections were chosen because they were the most stressed and well describe the behaviour of the entire RC slab. On the other hand, all cross girders were taken into account to derive the bending moment envelope.

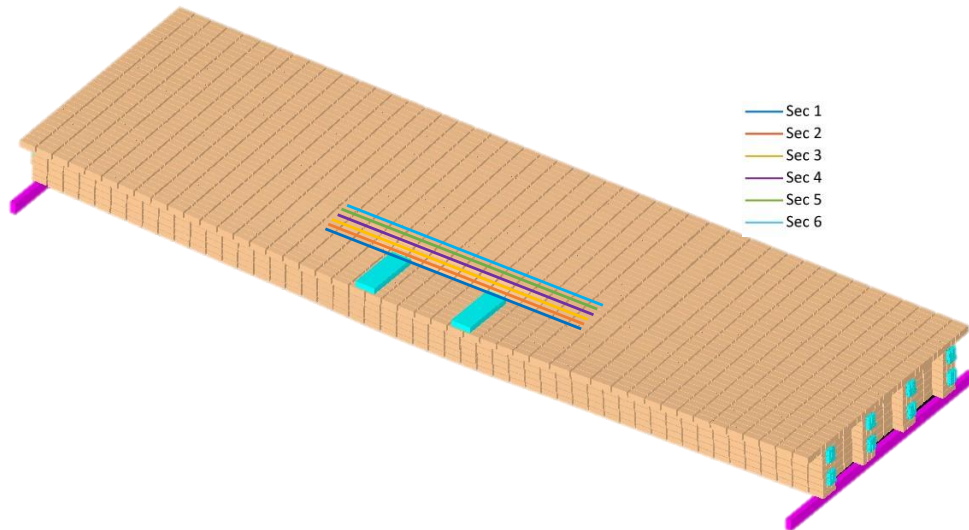
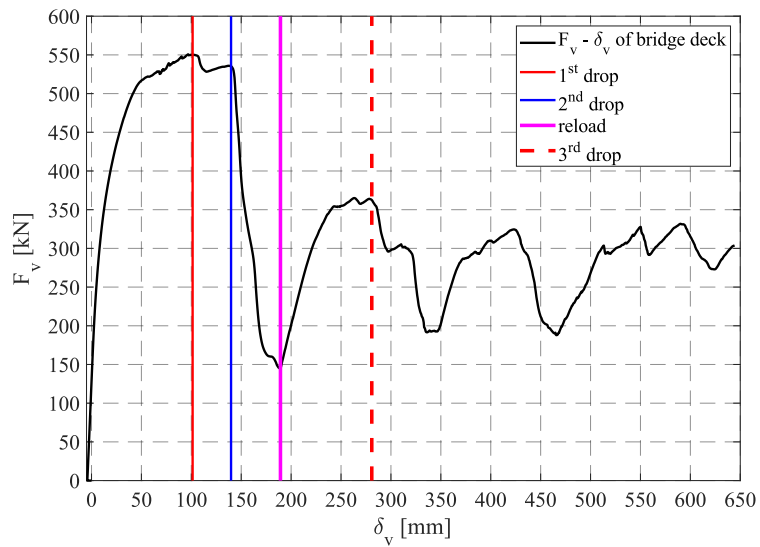


Figure 65. RC slab sections to derive the bending moment envelope.

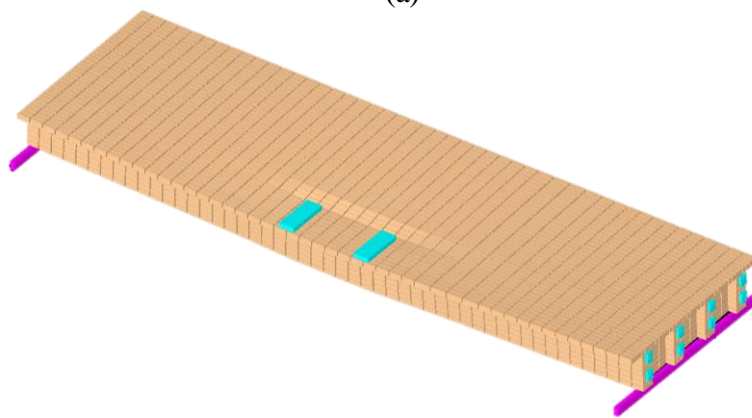
Figure 66 shows the force-displacement curve (Figure 66a), the 3D model when the first drop (i.e., the first drop in the F_v - δ_v curve) and the collapse occur in the bridge deck model (Figure 66a-b) and the normalised F_v - δ_v and M - δ_v envelope curves (for RC slab and cross girders) (Figure 66d). The normalisation of F_v was obtained by dividing the F_v by the maximum value of F_v . On the other hand, M was normalised by dividing the bending moment by the maximum capacity of cross section (M_{rd}) (of RC slab or cross girder).

Figure 66a highlights three main drops and one reload phase (i.e., before the deck started to have big displacements). The first drop was caused by an initial damage of RC slab near the loading plates (i.e., the most stressed area of slab) (Figure 66b). Furthermore, in Figure 66d is depicted the drop of the F_v - δ_v and M - δ_v curves for PC bridge deck and RC slab, respectively, although the cross girders appear to be unaffected by the drop influence. Then, the second drop was attained and the vertical force dropped to 150 kN (i.e., the maximum load of single beam (Figure 63)). Therefore, the prestressed cross girders started to be loaded thanks to the redistribution of stresses into the bridge deck (i.e., rigid bridge deck cross section) (Figure 66d). Then, the stresses redistribution led to reload the RC slab, as well as the F_v - δ_v curve (i.e., magenta line in Figure 66a-d), whereas the M - δ_v curve for cross girders exhibited a sub horizontal branch. When the third drop occurred both RC slab and cross girders reached their maximum capacity, thus, all curves present the drop (Figure 66d) and the PC bridge deck continues to have a residual capacity.

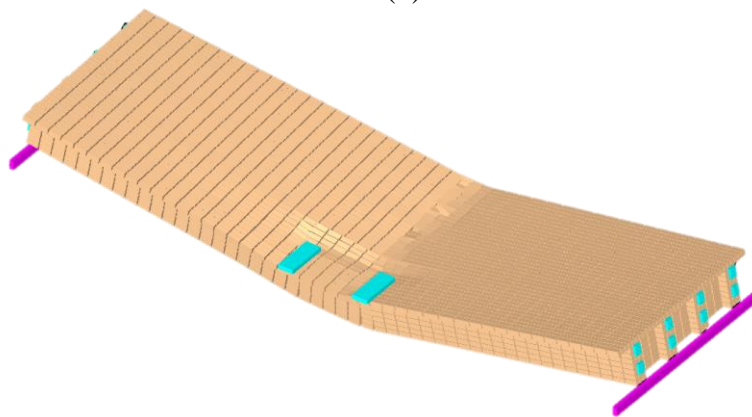
Therefore, the collapsed 3D PC bridge deck model is depicted in Figure 66c. It is worth underlying that the PC bridge deck cross section was still rigid in the collapse condition, thus, the prestressed cross girders allowed the collaboration among the structural elements of the deck (e.g., beams) in order to perform a higher capacity.



(a)



(b)



(c)

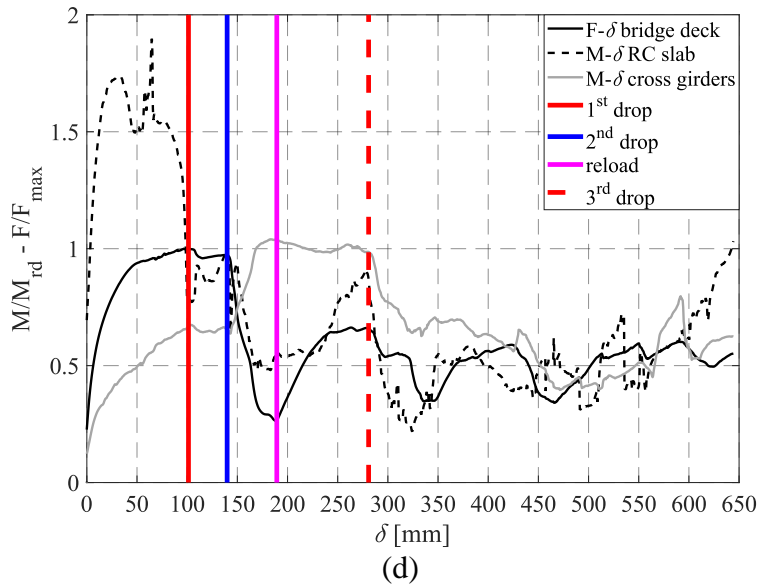
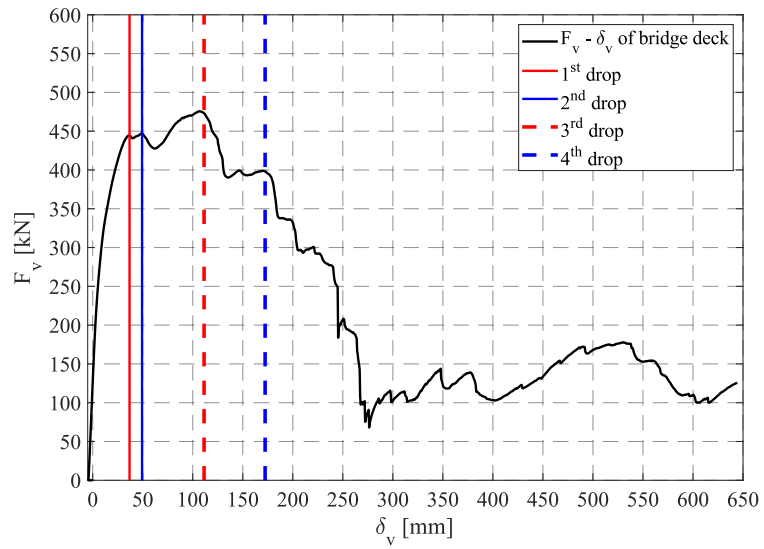


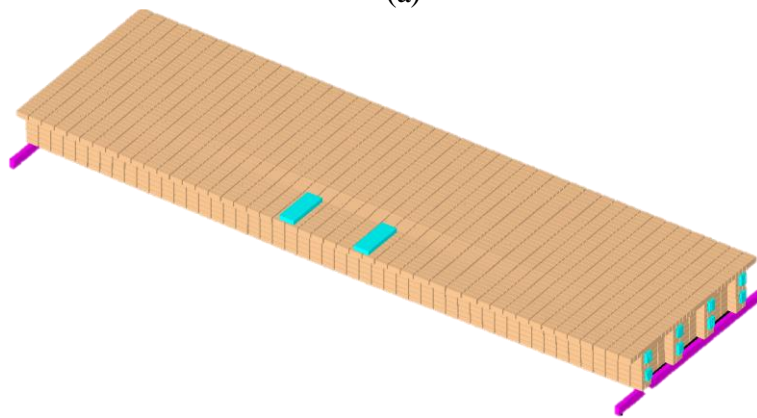
Figure 66. PC bridge deck with prestressed cross girders separated from RC slab (a) force-displacement curve, (b) 3D model when the first drop (i.e., the first drop in the F_v - δ_v curve) occurs, (c) 3D model when the collapse occurs and (d) normalised F_v - δ_v and M - δ_v envelope curves.

Figure 67a depicts four major drops (i.e., before the deck started to have big displacements). The first drop was produced by an early RC slab damage at the loading plates (the most stressed section of the slab) (Figure 67b). Furthermore, the drop of the F_v - δ_v and M - δ_v curves for the PC bridge deck and RC slab is shown in Figure 67d, but the cross girders appear to be unaffected by the drop influence. As a result of the redistribution of stresses into the bridge deck, the cross girders began to be loaded (Figure 67d). Then, the stresses redistribution caused the RC slab and the F_v - δ_v curves to be reloaded, however the curve for cross girders showed a degraded branch. When the third drop started, both the RC slab and the cross girders reached their full capacity and dropped as well (Figure 67d). Then, during the last drop, the RC slab and cross girders were failed, thus, no more redistribution was allowed in the PC bridge deck. Indeed, the F_v - δ_v curve represents the edge girder behaviour (Figure 67a-d). In this regard, the Figure 67c shows the collapsed 3D PC bridge deck model and it is possible to see the RC slab on the edge girder separated from the remaining part of the bridge deck. Therefore, the cross girders were not able to define a rigid deck cross section and no stress redistribution it was allowed from the third drop. It is worth mentioning that the fundamental difference between this bridge deck type and the preceding one is a lower maximum capacity (i.e., the maximum F_v is greater

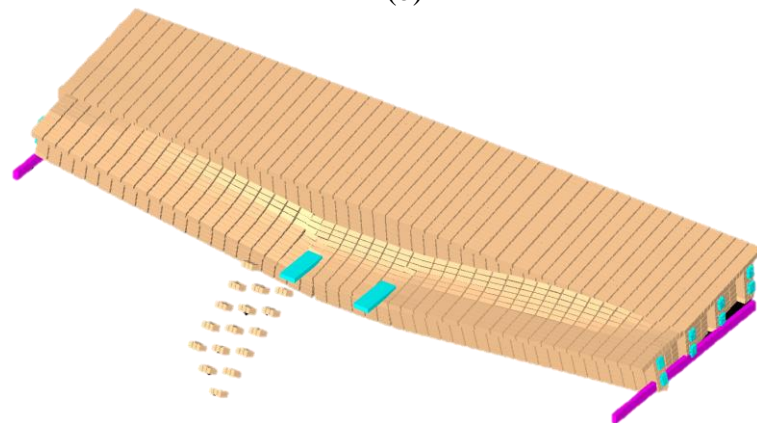
when prestressed cross girders are considered) as well as a lower capacity in the damaged condition of the PC bridge deck.



(a)



(b)



(c)

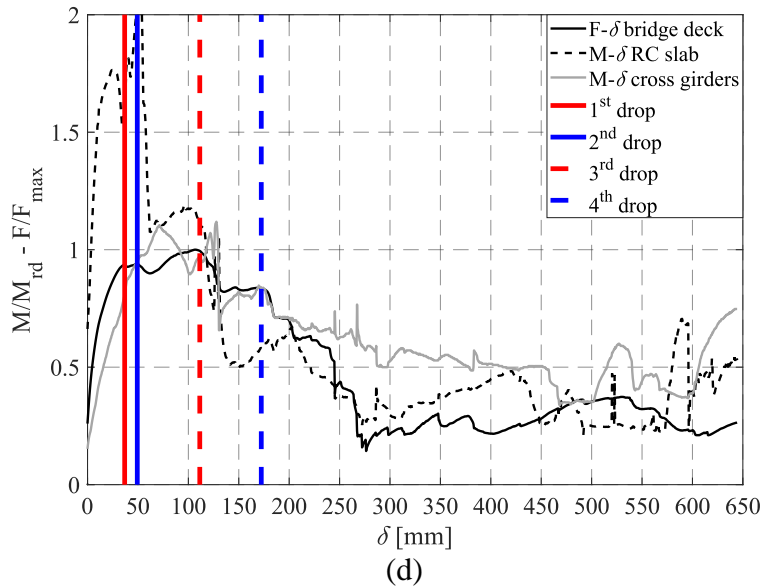
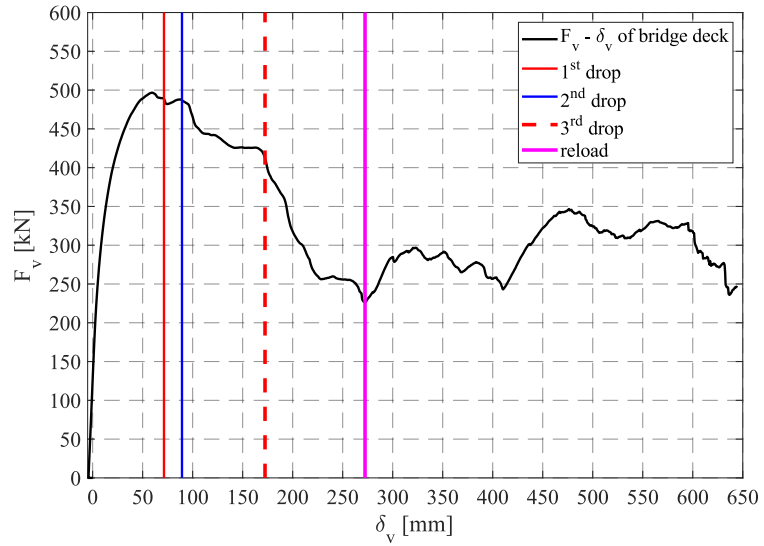


Figure 67. PC bridge deck with cross girders separated from RC slab (not prestressed) (a) force-displacement curve, (b) 3D model when the first drop (i.e., the first drop in the F_v - δ_v curve) occurs, (c) 3D model when the collapse occurs and (d) normalised F_v - δ_v and M - δ_v envelope curves.

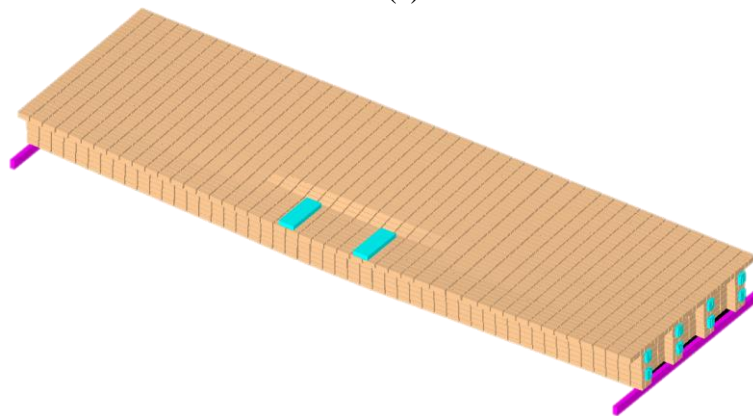
Figure 68a depicts three major drops and one slight reload (i.e., before the deck started to have big displacements). The first drop was produced by an early RC slab damage at the loading plates (the most stressed section of the slab) (Figure 68b) as for the first two types of PC bridge deck. Furthermore, the drop of the F_v - δ_v and M - δ_v curves for the PC bridge deck and RC slab is shown in Figure 68d, but the cross girders, connected to the RC slab, appear to be unaffected by the drop influence. As a result of the redistribution of stresses into the bridge deck, when the second drop occurred, the RC slab and the F_v - δ_v curves were reloaded, however the curve for cross girders showed a degrading branch. In contrast, when the third drop started, both the RC slab and the cross girders dropped (Figure 67d) and the cross girders had a slight reloading up to a sub-horizontal branch. Then, during the reload branch of the F_v - δ_v curve, the RC slab started to reload thanks to stresses redistribution into the bridge deck, whereas the cross girders were failed, thus, a degrading branch is observed in Figure 68d.

Figure 68c shows the collapsed 3D PC bridge deck model and it highlights that this type of cross girders (i.e., cross girder connected to the RC slab) allowed a partial stresses redistribution in the bridge deck. In this regard, the cross girders allowed the collaboration between the first two beams of the deck, whereas the remaining two are separated due to the RC slab failure. Indeed, the deck behaviour can be assumed as a middle way between the bridge deck with

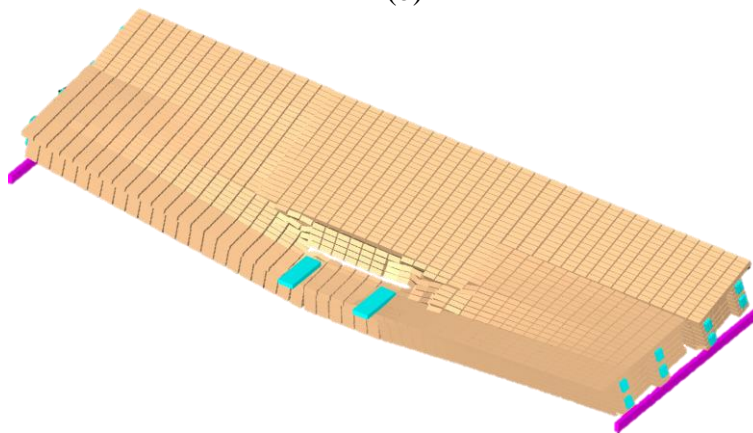
prestressed girders and the deck with cross girders separated from RC slab. Therefore, the cross girders were not able to define a perfect rigid deck cross section and no stress redistribution it was allowed from the last reload (i.e., magenta line in Figure 68d).



(a)



(b)



(c)

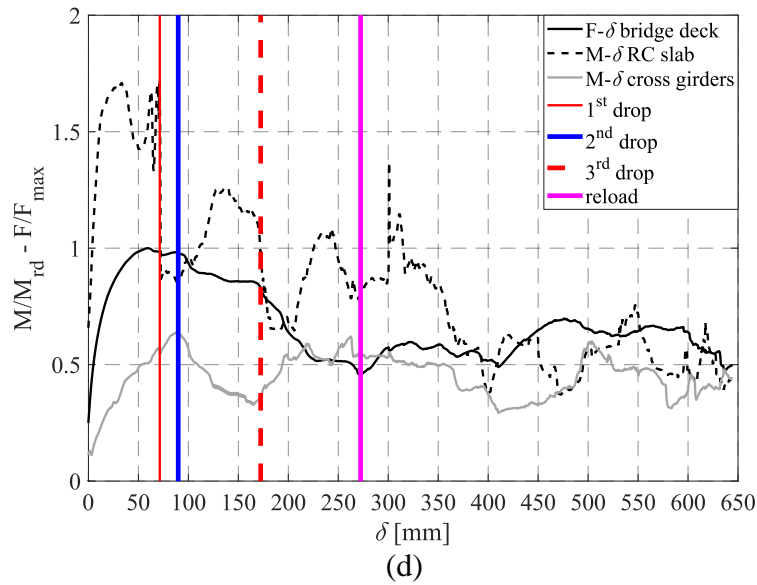


Figure 68. PC bridge deck with cross girders connected to RC slab (not prestressed) (a) force-displacement curve, (b) 3D model when the first drop (i.e., the first drop in the F_v - δ_v curve) occurs, (c) 3D model when the collapse occurs and (d) normalised F_v - δ_v and M - δ_v envelope curves.

As described above, the PC concrete bridge deck structural behaviour is highly influenced by cross girder types. In some cases they can be used as fuses in the bridge deck to bring the entire deck to a specific type of collapse. These analyses can be used in order to design a 1:5 simply supported post tensioned PC bridge decks with four beams, four cross girders and a continuous RC slab experimental test and validate these results.

Conclusions and future perspectives

This study was aimed at evaluating the traffic-load fragility of existing Italian, simply supported, beam-type, prestressed concrete bridges built between 1970 and 1980, which was an extraordinary time for construction of highway bridges. After that traffic load models prescribed in past and current Italian codes were reviewed, a statistical analysis of data collected by the authors from the literature and on real bridges was carried out. The analysis focused on girder bridge decks, performing their geometric and capacity modelling according to current Italian codes.

Based on statistics for model variables, a sensitivity analysis was first conducted to identify the geometric and mechanical properties that mostly influence the performance of selected bridge decks under traffic loading. According to uncertainty modelling of bridge decks, sensitivity analysis accounted for correlation between random variables, assuming lower and/or upper bounds based on engineering judgement. Sensitivity analysis results allow the following conclusions to be drawn:

- The flexural capacity of the case-study bridge decks is mostly influenced by span length of longitudinal girders, conventional yield strength of prestressing steel, and deck width.
- The effect of the variability in prestressing ratio on shear capacity depends on the shear capacity model being used, but a higher accuracy of the shear capacity model for PC elements in uncracked condition was detected.
- Shear capacity was found to be more sensitive to prestressing ratio and concrete compressive strength.
- The effects of different variables on structural performance were measured through flexural and shear demand-to-capacity ratios. The former is more sensitive to span length, slab thickness and yield strength of prestressing steel, whereas the shear demand-to-capacity ratio has a significant sensitivity to the prestressing ratio, with lower impact of other variables such as concrete compressive strength, deck width and yield strength of prestressing steel. The

reinforcing steel ratio has a negligible influence, motivating the assumption of a deterministic value in subsequent probabilistic assessment.

A simulation of design process according to code provisions in force at the time of construction confirmed the representativeness of bridge models used in sensitivity analysis.

Then, fragility analysis of a class of existing Italian concrete bridge decks, which were built between 1970 and 1980 and were subjected to different traffic load patterns, has been presented. Monte Carlo sampling technique was applied into a fully automated MATLAB procedure, generating 10^4 samples of bridge deck models and carrying out both structural analysis and performance assessment for traffic-load fragility computation and modelling. The scale factor α of first-lane tandem load on bridge deck was considered as intensity measure in order to scale the TLM intensity from 0 to 5 times a nominal value of traffic loads provided by Italian regulations for existing bridges. Then, the bridge deck performance was evaluated based on the ultimate limit state of edge girders, considering both flexural and shear failure modes. The large number of random samples allowed the estimation of collapse fragility according to a frequentist approach, which however was validated through demand-capacity convolution at multiple load intensities; hence fitting lognormal probability distributions to fragility data sets for derivation of fragility curves. Moreover, the occurrence of flexure and shear failure modes was first probabilistically assessed separately and then considered altogether to develop the collapse fragility curve of the selected bridges.

Based on sensitivity of flexural capacity model to tensile strength of prestressing steel, the authors performed additional fragility analysis under varying mean or coefficient of variation of that mechanical property. The main findings of fragility analysis can be summarised as follows:

- The case-study bridges subjected to code-compliant traffic loads are significantly more vulnerable to flexural failure than its shear counterpart; the conditional probability of shear failure reduces under increasing prestressing ratio.
- Traffic-load fragility models have been derived for the limit state of collapse, assuming a lognormal distribution function with very high fitting accuracy. Fragility curves are characterised by a median traffic load equal to 1.68 times the design load and dispersion equal to 0.30.

- Sensitivity analysis of fragility parameters has shown a significant influence of the mean prestressing steel strength on median traffic load, with very low impact on dispersion. Furthermore, the coefficient of variation of prestressing steel strength does not influence the traffic-load fragility parameters.

The NTC-TLM fragility curve leads to a failure probability (i.e., related to the nominal value of traffic loads) equal to $5.7 \cdot 10^{-2}$, whereas the failure probability due to heavy traffic loads prescribed by new Italian guidelines for existing bridges (denoted as heavy GL-TLMs) reduces to $4.9 \cdot 10^{-3}$.

Results of fragility analysis have highlighted that traffic load limitations, i.e., the adoption of recently proposed traffic load models by new Italian guidelines, would always provide lower fragility levels in comparison to those resulting from traffic loads complying with the 2018 Italian building code (here denoted as NTC-TLMs). Usage limitations of the carriageway in terms of number and/or position of traffic load lanes allow a significant fragility mitigation of existing PC bridge decks to values between 10^{-6} and 10^{-4} .

Then, some considerations on the unconditional failure probability corresponding to different load patterns were also presented. Based on some data from the literature, the collapse probability corresponding to heavy GL-TLMs has been found to be of the same order of magnitude of that resulting from the 2018 Italian technical code. Annual collapse probabilities estimated through the fragility analysis procedure presented in this study are fully in line with annual collapse rates available in the literature, hence providing a validation of the proposed approach to the probabilistic assessment of existing bridges under traffic loads.

A more accurate evaluation of the collapse probability could be obtained once probabilistic models of traffic loads will be developed on the basis of, for instance, a large amount of WIM data. This study is expected to provide support to the ongoing testing and revision of new Italian guidelines for existing bridges, as well as to road management companies for the definition of risk-informed traffic/use limitations for high-risk bridges.

On the basis of these outcomes, it can be inferred that flexural behaviour has a remarkable effect on the vulnerability of the considered class of existing bridges, providing important information on structural retrofitting of existing bridge decks against traffic loads. The fragility models presented in this study might be used

by engineers, roadway management companies and decision-makers in national/regional risk assessment of highway bridges, which provides quantitative data for subsequent prioritization schemes where most critical bridges are identified for more refined analysis and, if any, structural retrofitting.

Further studies are required to improve the accuracy of uncertainty and capacity modelling, collecting more data on real bridges (particularly on prestressing steel strength) when they will be made available in the framework of future research projects. Other developments of this study might account for progressive deterioration of materials (which is of paramount importance especially in post-tensioned PC bridges), possible failure of girder bearings (e.g., dapped-end joints/corbels) and WIM-inferred traffic load models for collapse risk assessment based on the convolution of bridge fragility and traffic-related hazard.

Moreover, a more accurate characterization of the hazard contribution after site-specific traffic load distributions will be measured through WIMs. This task aims to provide useful suggestions to improve current TLMs and corresponding safety factors to be emended in a revised version of the Italian guidelines on existing bridges.

Among several advances, this study is also being used for the development and testing of a software that allows quick safety checks and fragility analysis of existing bridge decks under different traffic load models. Road management companies will benefit from that software to make a risk-informed classification of their bridge portfolios, and subsequently, to perform detailed inspections and structural safety checks. Moreover, the multi-level analysis is used to derive fragility curves for a portfolio of bridges or a specific bridge through a bridge-class fragility analysis or a bridge-specific fragility analysis, respectively. All software modules allow the user to build the own bridge deck portfolios by importing own data about bridge deck parameters and derive proper probability distributions or regression models that can be imported to carry out fragility analyses.

In the end, a 1:5 simply supported post tensioned PC bridge decks with four beams, four cross girders and a continuous RC slab is modelled through the applied element method (AEM). The AEM assumes that the two elements are linked by pairs of normal and shear springs arranged at contact sites and uniformly spaced along the components' edges. As a result, even if two

components share just a piece of the same surface (partially overlapped elements), AEM generates connection springs. Each spring in AEM completely represents the loads, stresses, deformations, and failure of a given section of the structure. The main advantage of this system is its capacity to follow structural behaviour from early loading phases through final collapse in a tolerable amount of CPU time. The 3D bridge deck model is implemented into the Extreme Loading for Structures (ELS) software in order to evaluate the influence of cross girders on the structural behaviour. A nonlinear analysis with displacement control is carried out by considering three types of cross girders: (i) prestressed cross girders separated from RC slab, (ii) cross girders separated from RC slab (not prestressed), (iii) cross girders connected to RC slab (not prestressed). The analysis results show that the first type of cross girders allows to reach a higher capacity (in terms of maximum vertical force) due to the stress redistribution in the structural elements. All beams are involved in the collapse mechanism (i.e., rigid bridge deck cross section is allowed thanks to prestressed cross girders). On the other hand, the cross girders separated from the RC slab (not prestressed) are not able to develop a rigid cross section, indeed, the bridge deck collapse mechanism involves the edge beam only (i.e., the loaded beam) and a lower capacity is attained. The third type of cross girders (i.e., connected to the RC slab) are a middle way between the first and second type, thus, the collapse mechanism involves two out of four beams and the maximum vertical force reached is between the first two types of PC bridge deck. Therefore, the cross girders type play a fundamental role on the structural behaviour and its collapse mechanism, indeed, in some cases they can be used as fuses in the bridge deck to bring the entire deck to a specific type of collapse. In conclusion, these analyses can be also used in order to design a 1:5 simply supported post tensioned PC bridge decks with four beams, four cross girders and a continuous RC slab experimental test and validate these results.

References

- Allaix, D. L., Botte, W., Diamantidis, D., Engen, M., Faber, M., Hendriks, M., et al. (2016). *fib Bulletin 80. Partial factor methods for existing concrete structures*. (R. Caspeele, R. Steenbergen, & M. Sýkora, Eds.). fib. The International Federation for Structural Concrete. <https://doi.org/10.35789/fib.BULL.0080>
- American Association of State Highway and Transportation Official (AASHTO). (2001). Recommended LRFD Guidelines for the Seismic Design of Highway Bridges. Based on: NCHRP 12-49, Comprehensive Specification for the Seismic Design of Bridges, Revised LRFD Design Specifications, (Seismic Provisions), Third draft of specifications and.
- ASI. (2020). Extreme Loading for Structures. v9. *Applied Science International, LLC*.
- Associazione italiana tecnico-economica del cemento. (1929). L'Industria Italiana del Cemento (in Italian).
- Associazione italiana tecnico-economica del cemento. (1962). Applicazioni del cemento armato precompresso sull'Autostrada del Sole (in Italian).
- Associazione nazionale italiana cemento armato precompresso. (1956). Giornate ANICAP (in Italian).
- Associazione nazionale italiana cemento armato precompresso. (1962). Realizzazioni italiane in cemento armato precompresso anni '50. IV congresso internazionale del precompresso (F.I.P.).
- Associazione nazionale italiana cemento armato precompresso. (1966). Realizzazioni italiane in cemento armato precompresso 1962-1966. V congresso internazionale del precompresso (FPI).
- Associazione nazionale italiana cemento armato precompresso. (1970). Realizzazioni italiane in cemento armato precompresso 1966-1970. 6° congresso internazionale del precompresso (FIP).
- Associazione nazionale italiana cemento armato precompresso. (1974). Realizzazioni italiane in cemento armato precompresso 1970-1974. 6° congresso internazionale del precompresso (FIP).
- Astaneh-Asl, A. (2008). PROGRESSIVE COLLAPSE OF STEEL TRUSS BRIDGES, THE CASE OF I-35W COLLAPSE.
- Ataei, N., & Padgett, J. E. (2013). Probabilistic Modeling of Bridge Deck Unseating during Hurricane Events. *Journal of Bridge Engineering*, 18(4), 275–286. [https://doi.org/10.1061/\(ASCE\)BE.1943-5592.0000371](https://doi.org/10.1061/(ASCE)BE.1943-5592.0000371)
- Aviram, A., Mackie, K., & Stojadinovic, B. (2008). EPISTEMIC UNCERTAINTY OF SEISMIC RESPONSE ESTIMATES FOR REINFORCED CONCRETE BRIDGES.
- Baggio, C., & Trovalusci, P. (1998). Limit Analysis for No-Tension and Frictional Three-Dimensional Discrete Systems*. *Mechanics of Structures*

- and Machines*, 26(3), 287–304.
<https://doi.org/10.1080/08905459708945496>
- Bai, Y., Burkett, W. R., & Nash, P. T. (2006). Rapid Bridge Replacement under Emergency Situation: Case Study. *Journal of Bridge Engineering*, 11(3), 266–273. [https://doi.org/10.1061/\(ASCE\)1084-0702\(2006\)11:3\(266\)](https://doi.org/10.1061/(ASCE)1084-0702(2006)11:3(266))
- Baltzopoulos, G., Baraschino, R., Iervolino, I., & Vamvatsikos, D. (2018). Dynamic analysis of single-degree-of-freedom systems (DYANAS): A graphical user interface for OpenSees. *Engineering Structures*, 177(September), 395–408. <https://doi.org/10.1016/j.engstruct.2018.09.078>
- Banerjee, S., & Shinozuka, M. (2008). Mechanistic quantification of RC bridge damage states under earthquake through fragility analysis. *Probabilistic Engineering Mechanics*, 23(1), 12–22. <https://doi.org/10.1016/j.probengmech.2007.08.001>
- Belletti, B., Rodríguez, J., Andrade, C., Franceschini, L., Sánchez Montero, J., & Vecchi, F. (2020). Experimental tests on shear capacity of naturally corroded prestressed beams. *Structural Concrete*, 21(5), 1777–1793. <https://doi.org/10.1002/suco.202000205>
- Belletti, B., Vecchi, F., Bandini, C., Andrade, C., & Montero, J. S. (2020). Numerical evaluation of the corrosion effects in prestressed concrete beams without shear reinforcement. *Structural Concrete*, 21(5), 1794–1809. <https://doi.org/10.1002/suco.201900283>
- Bhattacharya, S., Dash, S. R., & Adhikari, S. (2008). On the mechanics of failure of pile-supported structures in liquefiable deposits during earthquakes. *CURRENT SCIENCE-BANGALORE*-, 94, 605.
- Biezma, M. V., & Schanack, F. (2007). Collapse of Steel Bridges. *Journal of Performance of Constructed Facilities*, 21(5), 398–405. [https://doi.org/10.1061/\(ASCE\)0887-3828\(2007\)21:5\(398\)](https://doi.org/10.1061/(ASCE)0887-3828(2007)21:5(398))
- Billah, K. Y., & Scanlan, R. H. (1991). Resonance, Tacoma Narrows bridge failure, and undergraduate physics textbooks. *American Journal of Physics*, 59(2), 118–124. <https://doi.org/10.1119/1.16590>
- Billington, D. P. (1976). Historical Perspective on Prestressed Concrete. *PCI Journal*, 21(5), 48–71. <https://doi.org/10.15554/pcij.09011976.48.71>
- Boonyapinyo, V., Yamada, H., & Miyata, T. (1994). Wind-Induced Nonlinear Lateral-Torsional Buckling of Cable-Stayed Bridges. *Journal of Structural Engineering*, 120(2), 486–506. [https://doi.org/10.1061/\(ASCE\)0733-9445\(1994\)120:2\(486\)](https://doi.org/10.1061/(ASCE)0733-9445(1994)120:2(486))
- Borzi, B., Ceresa, P., Franchin, P., Noto, F., Calvi, G. M., & Pinto, P. E. (2015). Seismic Vulnerability of the Italian Roadway Bridge Stock. *Earthquake Spectra*, 31(4), 2137–2161. <https://doi.org/10.1193/070413EQS190M>
- Botte, W., Vereecken, E., Taerwe, L., & Caspeele, R. (2021). Assessment of posttensioned concrete beams from the 1940s: Large-scale load testing, numerical analysis and Bayesian assessment of prestressing losses. *Structural Concrete*, 22(3), 1500–1522.

<https://doi.org/10.1002/suco.202000774>

- Cardone, D., Perrone, G., & Sofia, S. (2011). A performance-based adaptive methodology for the seismic evaluation of multi-span simply supported deck bridges. *Bulletin of Earthquake Engineering*, 9(5), 1463–1498. <https://doi.org/10.1007/s10518-011-9260-8>
- Castaldo, P., Gino, D., Bertagnoli, G., & Mancini, G. (2018). Partial safety factor for resistance model uncertainties in 2D non-linear finite element analysis of reinforced concrete structures. *Engineering Structures*, 176, 746–762. <https://doi.org/10.1016/j.engstruct.2018.09.041>
- Castaldo, P., Gino, D., & Mancini, G. (2019). Safety formats for non-linear finite element analysis of reinforced concrete structures: discussion, comparison and proposals. *Engineering Structures*, 193, 136–153. <https://doi.org/10.1016/j.engstruct.2019.05.029>
- Castaldo, P., Palazzo, B., Alfano, G., & Palumbo, M. F. (2018). Seismic reliability-based ductility demand for hardening and softening structures isolated by friction pendulum bearings. *Structural Control and Health Monitoring*, 25(11), e2256. <https://doi.org/10.1002/stc.2256>
- Cestelli Guidi. (n.d.). *Cemento armato precompresso (in Italian)*. (Hoepli, Ed.) (7th ed.). Milano.
- Chen, Q., Wang, L., & Zhao, H. (2009). Hydrodynamic Investigation of Coastal Bridge Collapse during Hurricane Katrina. *Journal of Hydraulic Engineering*, 135(3), 175–186. [https://doi.org/10.1061/\(ASCE\)0733-9429\(2009\)135:3\(175\)](https://doi.org/10.1061/(ASCE)0733-9429(2009)135:3(175))
- Chen, S.-Z., Wu, G., & Feng, D.-C. (2019a). Development of a bridge weigh-in-motion method considering the presence of multiple vehicles. *Engineering Structures*, 191, 724–739. <https://doi.org/10.1016/j.engstruct.2019.04.095>
- Chen, S.-Z., Wu, G., & Feng, D.-C. (2019b). Damage detection of highway bridges based on long-gauge strain response under stochastic traffic flow. *Mechanical Systems and Signal Processing*, 127, 551–572. <https://doi.org/10.1016/j.ymsp.2019.03.022>
- Chen, S.-Z., Wu, G., Feng, D.-C., & Zhang, L. (2018). Development of a Bridge Weigh-in-Motion System Based on Long-Gauge Fiber Bragg Grating Sensors. *Journal of Bridge Engineering*, 23(9), 1–18. [https://doi.org/10.1061/\(asce\)be.1943-5592.0001283](https://doi.org/10.1061/(asce)be.1943-5592.0001283)
- Cheng, J., Jiang, J.-J., Xiao, R.-C., & Xiang, H.-F. (2002). Advanced aerostatic stability analysis of cable-stayed bridges using finite-element method. *Computers & Structures*, 80(13), 1145–1158. [https://doi.org/10.1016/S0045-7949\(02\)00079-2](https://doi.org/10.1016/S0045-7949(02)00079-2)
- Clemente, P. (2020). Monitoring and evaluation of bridges: lessons from the Polcevera Viaduct collapse in Italy. *Journal of Civil Structural Health Monitoring*, 10(2), 177–182. <https://doi.org/10.1007/s13349-020-00384-6>
- Comité Européen de Normalisation. (2003). EN1991-2. Eurocode 1: Actions on structures – Part 2: Traffic loads on bridges. Brussels, Belgium.

- Comité Européen de Normalisation. (2004a). EN1992-1-1. Eurocode 2: Design of concrete structures – Part 1-1: General rules and rules for buildings. Brussels, Belgium.
- Comité Européen de Normalisation. (2004b). Eurocode 8 Design of structures for earthquake resistance-Part 2: Bridges, DRAFT No 3.
- Comité Européen de Normalisation. (2006). EN1990. Eurocode: Basis of design. Brussels, Belgium.
- Consolazio, G. R., & Cowan, D. R. (2005). Numerically Efficient Dynamic Analysis of Barge Collisions with Bridge Piers. *Journal of Structural Engineering*, 131(8), 1256–1266. [https://doi.org/10.1061/\(ASCE\)0733-9445\(2005\)131:8\(1256\)](https://doi.org/10.1061/(ASCE)0733-9445(2005)131:8(1256))
- Conti, E., Malerba, P. G., Quagliaroli, M., & Scaperrotta, D. (2020). Residual capacity of a reinforced concrete grillage deck exposed to corrosion. *Structure and Infrastructure Engineering*, 16(1), 202–218. <https://doi.org/10.1080/15732479.2019.1624786>
- Cook, W., Barr, P. J., & Halling, M. W. (2015). Bridge Failure Rate. *Journal of Performance of Constructed Facilities*, 29(3), 1–8. [https://doi.org/10.1061/\(asce\)cf.1943-5509.0000571](https://doi.org/10.1061/(asce)cf.1943-5509.0000571)
- Correia, J. A. F. O., Montenegro, P., & Zhu, S.-P. (2019). Editorial on reliability and safety of structures and infrastructures. *Proceedings of the Institution of Civil Engineers - Forensic Engineering*, 172(4), 123–124. <https://doi.org/10.1680/jfoen.2019.172.4.123>
- Cosenza, E., & Losanno, D. (2021). Assessment of existing reinforced-concrete bridges under road-traffic loads according to the new Italian guidelines. *Structural Concrete*, 22(5), 2868–2881. <https://doi.org/10.1002/suco.202100147>
- Crespi, P., Zucca, M., Longarini, N., & Giordano, N. (2020). Seismic Assessment of Six Typologies of Existing RC Bridges. *Infrastructures*, 5(6), 52. <https://doi.org/10.3390/infrastructures5060052>
- Cui, P., Zhu, Y., Han, Y., Chen, X., & Zhuang, J. (2009). The 12 May Wenchuan earthquake-induced landslide lakes: distribution and preliminary risk evaluation. *Landslides*, 6(3), 209–223. <https://doi.org/10.1007/s10346-009-0160-9>
- Daniels, J., Hughes, D., Ramey, G. E., & Hughes, M. L. (2007). Effects of Bridge Pile Bent Geometry and Levels of Scour and P Loads on Bent Pushover Loads in Extreme Flood/Scour Events. *Practice Periodical on Structural Design and Construction*, 12(2), 122–134. [https://doi.org/10.1061/\(ASCE\)1084-0680\(2007\)12:2\(122\)](https://doi.org/10.1061/(ASCE)1084-0680(2007)12:2(122))
- De Matteis, G. De, Zizi, M., & Prete, A. Del. (2018). Conservation state and structural deficiencies of typical Italian bridges. *BEYOND ALL LIMITS 2018: International Congress on Sustainability in Architecture, Planning, and Design, 17-19 October 2018, Ankara, Turkey.*, (October), 17–19.
- De Matteis, G., Zizi, M., & Prete, A. (2019). Structural Features of Typical Italian

Bridges Built in the '50s: Four Case Studies in the Province of Caserta. *7th Structural Engineers World Congress*, (May), 1–12.

- Deng, L., Wang, W., & Yu, Y. (2016). State-of-the-Art Review on the Causes and Mechanisms of Bridge Collapse. *Journal of Performance of Constructed Facilities*, *30*(2), 1–13. [https://doi.org/10.1061/\(asce\)cf.1943-5509.0000731](https://doi.org/10.1061/(asce)cf.1943-5509.0000731)
- Di Prisco, M. (2019). Critical infrastructures in Italy: State of the art, case studies, rational approaches to select the intervention priorities. *fib Symposium*, 49–58.
- Di Sarno, L., da Porto, F., Guerrini, G., Calvi, P. M., Camata, G., & Prota, A. (2019). Seismic performance of bridges during the 2016 Central Italy earthquakes. *Bulletin of Earthquake Engineering*, *17*(10), 5729–5761. <https://doi.org/10.1007/s10518-018-0419-4>
- Diaz, E. E. M., Moreno, F. N., & Mohammadi, J. (2009). Investigation of Common Causes of Bridge Collapse in Colombia. *Practice Periodical on Structural Design and Construction*, *14*(4), 194–200. [https://doi.org/10.1061/\(ASCE\)SC.1943-5576.0000006](https://doi.org/10.1061/(ASCE)SC.1943-5576.0000006)
- Ding, Y. (2016). Severe accident blocked Zhonghuan line. http://english.eastday.com/Shanghai/u1ai8547264_K23558.html
- Elsharkawy, H. A., Elafandy, T., EL-Ghandour, A. W., & Abdelrahman, A. A. (2013). Behavior of post-tensioned fiber concrete beams. *HBRC Journal*, *9*(3), 216–226. <https://doi.org/10.1016/j.hbrcj.2013.08.006>
- Estes, A. C., & Frangopol, D. M. (2001). Bridge Lifetime System Reliability under Multiple Limit States. *Journal of Bridge Engineering*, *6*(6), 523–528. [https://doi.org/10.1061/\(ASCE\)1084-0702\(2001\)6:6\(523\)](https://doi.org/10.1061/(ASCE)1084-0702(2001)6:6(523))
- Fan, W., Yuan, W., Yang, Z., & Fan, Q. (2011). Dynamic Demand of Bridge Structure Subjected to Vessel Impact Using Simplified Interaction Model. *Journal of Bridge Engineering*, *16*(1), 117–126. [https://doi.org/10.1061/\(ASCE\)BE.1943-5592.0000139](https://doi.org/10.1061/(ASCE)BE.1943-5592.0000139)
- Faravelli, L. (2001). Modelling the response of an elastomeric base isolator. *Journal of Structural Control*, *8*(1), 17–30. <https://doi.org/10.1002/stc.4300080102>
- Fotopoulou, S. D., & Pitilakis, K. D. (2017a). Vulnerability assessment of reinforced concrete buildings at precarious slopes subjected to combined ground shaking and earthquake induced landslide. *Soil Dynamics and Earthquake Engineering*, *93*, 84–98. <https://doi.org/10.1016/J.SOILDYN.2016.12.007>
- Fotopoulou, S. D., & Pitilakis, K. D. (2017b). Probabilistic assessment of the vulnerability of reinforced concrete buildings subjected to earthquake induced landslides. *Bulletin of Earthquake Engineering*, *15*(12), 5191–5215. <https://doi.org/10.1007/S10518-017-0175-X>
- Frangopol, B. D. M., Kong, J. S., & Gharaibeh, E. S. (2001). Reliability -Based Life -Cycle Management. *Journal of Computing in Civil Engineering*,

- (January), 27–34.
- Fu, G., & Hag-Elsafi, O. (2000). Vehicular Overloads: Load Model, Bridge Safety, and Permit Checking. *Journal of Bridge Engineering*, 5(1), 49–57. [https://doi.org/10.1061/\(ASCE\)1084-0702\(2000\)5:1\(49\)](https://doi.org/10.1061/(ASCE)1084-0702(2000)5:1(49))
- Fu, Z., Ji, B., Cheng, M., & Maeno, H. (2012). Statistical Analysis of the Causes of Bridge Collapse in China. In *Forensic Engineering 2012* (pp. 75–83). Reston, VA: American Society of Civil Engineers. <https://doi.org/10.1061/9780784412640.009>
- Galano, S., Losanno, D., Miluccio, G., & Parisi. (2023). Experimental tests and multi-dimensional numerical simulations of two scaled post-tensioned prestressed concrete bridge girders. Under review.
- Galano, S., Losanno, D., & Pecce, M. R. (2020). Prestressed reinforced concrete bridges : state of art of the Italian existing stock.
- GARDONI, P., MOSALAM, K. M., & KIUREGHIAN, A. DER. (2003). PROBABILISTIC SEISMIC DEMAND MODELS AND FRAGILITY ESTIMATES FOR RC BRIDGES. *Journal of Earthquake Engineering*, 7(sup001), 79–106. <https://doi.org/10.1080/13632460309350474>
- Ge, Y. J., & Tanaka, H. (2000). Aerodynamic flutter analysis of cable-supported bridges by multi-mode and full-mode approaches. *Journal of Wind Engineering and Industrial Aerodynamics*, 86(2–3), 123–153. [https://doi.org/10.1016/S0167-6105\(00\)00007-6](https://doi.org/10.1016/S0167-6105(00)00007-6)
- Ghali, A., & Tadros, G. (1997). Bridge Progressive Collapse Vulnerability. *Journal of Structural Engineering*, 123(2), 227–231. [https://doi.org/10.1061/\(ASCE\)0733-9445\(1997\)123:2\(227\)](https://doi.org/10.1061/(ASCE)0733-9445(1997)123:2(227))
- Ghobarah, A., & Ali, H. M. (1988). Seismic performance of highway bridges. *Engineering Structures*, 10(3), 157–166. [https://doi.org/10.1016/0141-0296\(88\)90002-8](https://doi.org/10.1016/0141-0296(88)90002-8)
- Gilbert, M. (2007). *Limit analysis applied to masonry arch bridges: State-of-the-art and recent developments*.
- Gino, D., Castaldo, P., Giordano, L., & Mancini, G. (2021). Model uncertainty in non-linear numerical analyses of slender reinforced concrete members. *Structural Concrete*, 22(2), 845–870. <https://doi.org/10.1002/suco.202000600>
- Han, Q., Du, X., Liu, J., Li, Z., Li, L., & Zhao, J. (2009). Seismic damage of highway bridges during the 2008 Wenchuan earthquake. *Earthquake Engineering and Engineering Vibration*, 8(2), 263–273. <https://doi.org/10.1007/s11803-009-8162-0>
- Hao, S. (2010). I-35W Bridge Collapse. *Journal of Bridge Engineering*, 15(5), 608–614. [https://doi.org/10.1061/\(ASCE\)BE.1943-5592.0000090](https://doi.org/10.1061/(ASCE)BE.1943-5592.0000090)
- Harajli, M. H. (n.d.). Effect of Span-Depth Ratio on the Ultimate Steel Stress in Unbonded Prestressed concrete members. *ACI Structural Journal*, 87(3). <https://doi.org/10.14359/2631>

- Harik, I. E., Shaaban, A. M., Gesund, H., Valli, G. Y. S., & Wang, S. T. (1990). United States Bridge Failures, 1951–1988. *Journal of Performance of Constructed Facilities*, 4(4), 272–277. [https://doi.org/10.1061/\(ASCE\)0887-3828\(1990\)4:4\(272\)](https://doi.org/10.1061/(ASCE)0887-3828(1990)4:4(272))
- Hashimoto, K., & Chouw, N. (2003). Investigation of the effect of Kobe earthquake on a three-dimensional soil–structure system. *JSCE Journal of Earthquake Engineering*, 27, 1–8.
- Heyman, J. (1982). *The masonry arch*. (Ellis Horwood, Ed.). Chichester, U.K.
- Hong, J.-H., Chiew, Y.-M., Lu, J.-Y., Lai, J.-S., & Lin, Y.-B. (2012). Houfeng Bridge Failure in Taiwan. *Journal of Hydraulic Engineering*, 138(2), 186–198. [https://doi.org/10.1061/\(ASCE\)HY.1943-7900.0000430](https://doi.org/10.1061/(ASCE)HY.1943-7900.0000430)
- Huber, P., Vill, M., Schweighofer, A., & Kollegger, J. (2018). Full-scale shear tests on post-tensioned bridge girders of existing bridges. *Structural Concrete*, 19(1), 5–15. <https://doi.org/10.1002/suco.201700123>
- Hughes, D., Ramey, G. E., & Hughes, M. L. (2007). Bridge Pile Bent Number of Piles and X-Bracing System: Impact on Pushover Capacity as Scour Increases. *Practice Periodical on Structural Design and Construction*, 12(2), 82–95. [https://doi.org/10.1061/\(ASCE\)1084-0680\(2007\)12:2\(82\)](https://doi.org/10.1061/(ASCE)1084-0680(2007)12:2(82))
- Hussien, O. F., Elafandy, T. H. K., Abdelrahman, A. A., Abdel Baky, S. A., & Nasr, E. A. (2012). Behavior of bonded and unbonded prestressed normal and high strength concrete beams. *HBRC Journal*, 8(3), 239–251. <https://doi.org/10.1016/j.hbrj.2012.10.008>
- Hwang, H., Jernigan, J. B., & Lin, Y.-W. (2000). Evaluation of Seismic Damage to Memphis Bridges and Highway Systems. *Journal of Bridge Engineering*, 5(4), 322–330. [https://doi.org/10.1061/\(ASCE\)1084-0702\(2000\)5:4\(322\)](https://doi.org/10.1061/(ASCE)1084-0702(2000)5:4(322))
- Italian High Council of Public Works. (1933). Normale n.8 15/09/1933 (in Italian). Rome, Italy.
- Italian High Council of Public Works. (1945). Normale n.6018 09/06/1945 (in Italian). Rome, Italy.
- Italian High Council of Public Works. (1962). Circ. CSLLPP 14/02/1962. Norme relative ai carichi per il calcolo dei ponti stradali (in Italian).
- Italian High Council of Public Works. (1972). DM 30/05/1972. Norme tecniche alle quali devono uniformarsi le costruzioni in conglomerato cementizio normale e precompresso ed a struttura metallica. (in Italian). Rome, Italy.
- Italian High Council of Public Works. (1974). DM 29/07/1974. Norme tecniche per il calcolo, l' esecuzione, ed il collaudo delle strutture in conglomerato cementizio armato normale. (in Italian). Rome, Italy.
- Italian High Council of Public Works. (1976). DM 16/06/1976. Norme tecniche per l' esecuzione delle opere in cemento armato normale e precompresso e per le strutture metalliche. (in Italian).
- Italian High Council of Public Works. (1985). DM 27/07/1985. Norme tecniche per l' esecuzione delle opere in cemento armato normale e precompresso e

- per le strutture metalliche. (in Italian).
- Italian High Council of Public Works. (1992). D.M. 14/2/1992 - Norme tecniche per l'esecuzione delle opere in cemento armato normale e precompresso e per le strutture metalliche.
- Italian High Council of Public Works. (2020). Linee guida per la classificazione e gestione del rischio, la valutazione della sicurezza ed il monitoraggio dei ponti esistenti. (in Italian). Rome, Italy.
- Italian Ministry of Infrastructures and Transportation. (1980). Criteri Generali E Prescrizioni Tecniche Per La Progettazione , Esecuzione E Collaudo Dei Ponti (in Italian). Rome, Ital.
- Italian Ministry of Infrastructures and Transportation. (1990). DM 04/05/1990. Aggiornamento delle norme tecniche per la progettazione, la esecuzione e il collaudo dei ponti stradali (in Italian).
- Italian Ministry of Infrastructures and Transportation. (1992). Codice della Strada. D.Lgs. 30.04.1992, n. 295. (in Italian). Rome, Italy.
- Italian Ministry of Infrastructures and Transportation. (2018). DM 17/01/2018. Aggiornamento delle Norme tecniche per le costruzioni. (in Italian). Rome, Ital.
- Italian Ministry of Infrastructures and Transportation. (2019). Circ. 21 gennaio 2019, n. 7. Istruzioni per l'applicazione dell'«Aggiornamento delle “Norme tecniche per le costruzioni”» di cui al decreto ministeriale 17 gennaio 2018. Supplemento ordinario n. 35 alla Gazzetta ufficiale del 11 febbraio 2019. (in Italian. Rome, Italy).
- Italian Ministry of Infrastructures and Transportation. (2020). DM 17/12/2020, n. 578. Adozione delle linee guida per la gestione del rischio dei ponti esistenti e per la definizione di requisiti ed indicazioni relativi al sistema di monitoraggio dinamico. (in Italian). Rome, Italy.
- Iverson, R. M. (2000). Landslide triggering by rain infiltration. *Water Resources Research*, 36(7), 1897–1910. <https://doi.org/10.1029/2000WR900090>
- Jacinto, L., Pipa, M., Neves, L. A. C., & Santos, L. O. (2012). Probabilistic models for mechanical properties of prestressing strands. *Construction and Building Materials*, 36, 84–89. <https://doi.org/10.1016/j.conbuildmat.2012.04.121>
- Jalayer, F., Ebrahimian, H., Miano, A., Manfredi, G., & Sezen, H. (2017). Analytical fragility assessment using unscaled ground motion records. *Earthquake Engineering & Structural Dynamics*, 46(15), 2639–2663. <https://doi.org/10.1002/eqe.2922>
- Kappos A, M. J. (2006). *Documented classification of bridges in Greece. Technical Report*,.
- Kawai, T. (1980). Some consideration on the finite element method. *International Journal for Numerical Methods in Engineering*, 16(1), 81–120. <https://doi.org/10.1002/nme.1620160108>

- KAWAI, Y., SIRINGORINGO, D., & FUJINO, Y. (2014). FAILURE ANALYSIS OF THE HANGER CLAMPS OF THE KUTAI-KARTANEGARA BRIDGE FROM THE FRACTURE MECHANICS VIEWPOINT. *Journal of JSCE*, 2(1), 1–6. https://doi.org/10.2208/journalofjsce.2.1_1
- Kawashima, K., Aydan, Ö., Aoki, T., Kishimoto, I., Konagai, K., Matsui, T., et al. (2010). Reconnaissance Investigation on the Damage of the 2009 L'Aquila, Central Italy Earthquake. *Journal of Earthquake Engineering*, 14(6), 817–841. <https://doi.org/10.1080/13632460903584055>
- Khosravikia, F. (2020). Machine-learning-based Models, Methods, and Software for Intensity, Vulnerability, and Risk Assessment of Central U.S. Induced Earthquakes. <https://repositories.lib.utexas.edu/handle/2152/83059>
- Kikuchi, A., Kawai, T., & Suzuki, N. (1992). The rigid bodies—spring models and their applications to three-dimensional crack problems. *Computers & Structures*, 44(1–2), 469–480. [https://doi.org/10.1016/0045-7949\(92\)90269-6](https://doi.org/10.1016/0045-7949(92)90269-6)
- Kim, J., & Song, J. (2019). A Comprehensive Probabilistic Model of Traffic Loads based on Weigh-in-Motion Data for Applications to Bridge Structures. *KSCE Journal of Civil Engineering*, 23(8), 3628–3643. <https://doi.org/10.1007/s12205-019-2432-9>
- Kim, S., Frangopol, D. M., & Soliman, M. (2013). Generalized Probabilistic Framework for Optimum Inspection and Maintenance Planning. *Journal of Structural Engineering*, 139(3), 435–447. [https://doi.org/10.1061/\(ASCE\)ST.1943-541X.0000676](https://doi.org/10.1061/(ASCE)ST.1943-541X.0000676)
- Kim, S. J., Holub, C. J., & Elnashai, A. S. (2011). Analytical Assessment of the Effect of Vertical Earthquake Motion on RC Bridge Piers. *Journal of Structural Engineering*, 137(2), 252–260. [https://doi.org/10.1061/\(ASCE\)ST.1943-541X.0000306](https://doi.org/10.1061/(ASCE)ST.1943-541X.0000306)
- Kong, J. S., & Frangopol, D. M. (2005). Probabilistic Optimization of Aging Structures Considering Maintenance and Failure Costs. *Journal of Structural Engineering*, 131(4), 600–616. [https://doi.org/10.1061/\(ASCE\)0733-9445\(2005\)131:4\(600\)](https://doi.org/10.1061/(ASCE)0733-9445(2005)131:4(600))
- Kunnath, S. K., Erduran, E., Chai, Y. H., & Yashinsky, M. (2008). Effect of Near-Fault Vertical Ground Motions on Seismic Response of Highway Overcrossings. *Journal of Bridge Engineering*, 13(3), 282–290. [https://doi.org/10.1061/\(ASCE\)1084-0702\(2008\)13:3\(282\)](https://doi.org/10.1061/(ASCE)1084-0702(2008)13:3(282))
- Lapidus, L. and Pinder, G. F. (1982). Numerical Solution of Partial Differential Equations in Science and Engineering. *John Wiley and Sons*.
- LeBeau, K. H., & Wadia-Fascetti, S. J. (2007). Fault Tree Analysis of Schoharie Creek Bridge Collapse. *Journal of Performance of Constructed Facilities*, 21(4), 320–326. [https://doi.org/10.1061/\(ASCE\)0887-3828\(2007\)21:4\(320\)](https://doi.org/10.1061/(ASCE)0887-3828(2007)21:4(320))
- Lee, G. C., Mohan, S. B., Huang, C., & Fard, B. N. (2013). A study of US bridge failures (1980–2012). *MCEER Technical Rep*, 1–148.

- Lee, J., Lee, Y. J., Kim, H., Sim, S. H., & Kim, J. M. (2016). A new methodology development for flood fragility curve derivation considering structural deterioration for bridges. *Smart Structures and Systems*, 17(1), 149–165. <https://doi.org/10.12989/sss.2016.17.1.149>
- Lee, S.-B. (1996). Fatigue failure of welded vertical members of a steel truss bridge. *Engineering Failure Analysis*, 3(2), 103–108. [https://doi.org/10.1016/1350-6307\(96\)00003-9](https://doi.org/10.1016/1350-6307(96)00003-9)
- Lichtenstein, A. G. (1993). The Silver Bridge Collapse Recounted. *Journal of Performance of Constructed Facilities*, 7(4), 249–261. [https://doi.org/10.1061/\(ASCE\)0887-3828\(1993\)7:4\(249\)](https://doi.org/10.1061/(ASCE)0887-3828(1993)7:4(249))
- Lin, C., Bennett, C., Han, J., & Parsons, R. L. (2010). Scour effects on the response of laterally loaded piles considering stress history of sand. *Computers and Geotechnics*, 37(7–8), 1008–1014. <https://doi.org/10.1016/j.compgeo.2010.08.009>
- Lin, C., Han, J., Bennett, C., & Parsons, R. L. (2014). Case History Analysis of Bridge Failures due to Scour. In *Climatic Effects on Pavement and Geotechnical Infrastructure* (pp. 204–216). Reston, VA: American Society of Civil Engineers. <https://doi.org/10.1061/9780784413326.021>
- Liu, Y.-J., Gao, Y.-M., Zhou, X.-H., Zhang, Z.-J., & Zhang, Z.-F. (2017). Technical and Economic Analysis in Steel-concrete Composite Girder Bridges with Small and Medium Span. *Zhongguo Gonglu Xuebao/China Journal of Highway and Transport*, 30, 1–13.
- Livesley, R. K. (1992). A computational model for the limit analysis of three-dimensional masonry structures. *Meccanica*, 27(3), 161–172. <https://doi.org/10.1007/BF00430042>
- Lou, L., & Zerva, A. (2005). Effects of spatially variable ground motions on the seismic response of a skewed, multi-span, RC highway bridge. *Soil Dynamics and Earthquake Engineering*, 25(7–10), 729–740. <https://doi.org/10.1016/j.soildyn.2004.11.016>
- Lu, Y. E., & Zhang, L. M. (2013). Progressive collapse of a drilled-shaft bridge foundation under vessel impact. *Ocean Engineering*, 66, 101–112. <https://doi.org/10.1016/j.oceaneng.2013.04.007>
- M.C. Kunde, & R.S. Jangid. (2003). Seismic behavior of isolated bridges: A state-of-the-art review. *Electronic Journal of Structural Engineering*, 3, 140–170. <https://doi.org/10.56748/ejse.335>
- Maekawa, K., & Okamura, H. (1983). DEFORMATIONAL BEHAVIOR AND CONSTITUTIVE EQUATION OF CONCRETE USING THE ELASTO-PLASTIC AND FRACTURE MODEL. *Journal of the Faculty of Engineering, University of Tokyo, Series B*, 37, 253–328.
- Maljaars, J. (2020). Evaluation of traffic load models for fatigue verification of European road bridges. *Engineering Structures*, 225, 111326. <https://doi.org/10.1016/j.engstruct.2020.111326>
- Manos, G. C., Mitoulis, S. A., & Sextos, A. G. (2012). A knowledge-based

- software for the preliminary design of seismically isolated bridges. *Bulletin of Earthquake Engineering*, 10(3), 1029–1047. <https://doi.org/10.1007/s10518-011-9320-0>
- Marsaglia, G., W. Tsang, and J. W. (2003). Evaluating Kolmogorov's Distribution. *Journal of Statistical Software*, 8(18).
- Massey, F. J. (1951). The Kolmogorov-Smirnov Test for Goodness of Fit. *Journal of the American Statistical Association*, 46, 68–78.
- MATLAB and Statistics Toolbox Release R2022b. The MathWorks Inc., Natick, Massachusetts. (2022).
- Mavrouli, O., Fotopoulou, S., Pitilakis, K., Zuccaro, G., Corominas, J., Santo, A., et al. (2014). Vulnerability assessment for reinforced concrete buildings exposed to landslides. *Bulletin of Engineering Geology and the Environment*, 73(2), 265–289. <https://doi.org/10.1007/S10064-014-0573-0>
- McKenna, F., Fenves, G.L. and Scott, M. H. (2003). Open System for Earthquake Engineering Simulation. Pacific Earthquake Engineering Research Center, University of California, Berkeley. <http://opensees.berkeley.edu>
- Meguro, K., & Tagel-Din, H. (1997). A new simplified and efficient technique for fracture behavior analysis of concrete structures. *Fracture Mechanics of Concrete Structures Proceedings FRAMCOS-3*, 911–920.
- Meguro, Kimiro, & Tagel-Din, H. (2001). Applied Element Simulation of RC Structures under Cyclic Loading. *Journal of Structural Engineering*, 127(11), 1295–1305. [https://doi.org/10.1061/\(ASCE\)0733-9445\(2001\)127:11\(1295\)](https://doi.org/10.1061/(ASCE)0733-9445(2001)127:11(1295))
- Meguro, Kimiro, & Tagel-Din, H. S. (2002). Applied Element Method Used for Large Displacement Structural Analysis. *Journal of Natural Disaster Science*, 24(1), 25–34.
- Meguroi, K., & Tagel-Din, H. (2000). APPLIED ELEMENT METHOD FOR STRUCTURAL ANALYSIS: THEORY AND APPLICATION FOR LINEAR MATERIALS.
- Miller, L. H. (1956). Table of Percentage Points of Kolmogorov Statistics. *Journal of the American Statistical Association*, 51, 111–121.
- Montalvo, C., Cook, W., & Keeney, T. (2020). Retrospective Analysis of Hydraulic Bridge Collapse. *Journal of Performance of Constructed Facilities*, 34(1). [https://doi.org/10.1061/\(ASCE\)CF.1943-5509.0001378](https://doi.org/10.1061/(ASCE)CF.1943-5509.0001378)
- Monteiro, R., Zelaschi, C., Silva, A., & Pinho, R. (2019). Derivation of Fragility Functions for Seismic Assessment of RC Bridge Portfolios Using Different Intensity Measures. *Journal of Earthquake Engineering*, 23(10), 1678–1694. <https://doi.org/10.1080/13632469.2017.1387188>
- Morandi, R. (1954). *Strutture (in Italian)*. (L. Dedalo., Ed.).
- Morgese, M., Ansari, F., Domaneschi, M., & Cimellaro, G. P. (2020). Post-collapse analysis of Morandi's Polcevera viaduct in Genoa Italy. *Journal of Civil Structural Health Monitoring*, 10(1), 69–85.

<https://doi.org/10.1007/s13349-019-00370-7>

- Mosleh, A., Jara, J., Razzaghi, M. S., & Varum, H. (2020). Probabilistic Seismic Performance Analysis of RC Bridges. *Journal of Earthquake Engineering*, 24(11), 1704–1728. <https://doi.org/10.1080/13632469.2018.1477637>
- National Transportation Safety Board (NTSB). (2007). Collapse of I-35W Highway Bridge Minneapolis, Minnesota August 1, 2007. *Highway Accident Report*, (NTSB/HAR-08/03), 178. http://www.nts.gov/news/events/2008/minneapolis_mn/
- Nuti, C., Briseghella, B., Chen, A., Lavorato, D., Iori, T., & Vanzi, I. (2020). Relevant outcomes from the history of Polcevera Viaduct in Genova, from design to nowadays failure. *Journal of Civil Structural Health Monitoring*, 10(1), 87–107. <https://doi.org/10.1007/s13349-019-00371-6>
- Okamura, H., & Maekawa, K. (1990). *Non-linear Analysis and Constitutive Models of Reinforced Concrete*.
- Orduña, A., & Lourenço, P. B. (2005). Three-dimensional limit analysis of rigid blocks assemblages. Part I: Torsion failure on frictional interfaces and limit analysis formulation. *International Journal of Solids and Structures*, 42(18–19), 5140–5160. <https://doi.org/10.1016/j.ijsolstr.2005.02.010>
- Ozsarac, V., Monteiro, R., & Calvi, G. M. (2021). Probabilistic seismic assessment of reinforced concrete bridges using simulated records. *Structure and Infrastructure Engineering*, 1–21. <https://doi.org/10.1080/15732479.2021.1956551>
- Padgett, J., DesRoches, R., Nielson, B., Yashinsky, M., Kwon, O.-S., Burdette, N., & Tavera, E. (2008). Bridge Damage and Repair Costs from Hurricane Katrina. *Journal of Bridge Engineering*, 13(1), 6–14. [https://doi.org/10.1061/\(ASCE\)1084-0702\(2008\)13:1\(6\)](https://doi.org/10.1061/(ASCE)1084-0702(2008)13:1(6))
- PAPAZOGLU, A. J., & ELNASHAI, A. S. (1996). ANALYTICAL AND FIELD EVIDENCE OF THE DAMAGING EFFECT OF VERTICAL EARTHQUAKE GROUND MOTION. *Earthquake Engineering & Structural Dynamics*, 25(10), 1109–1137. [https://doi.org/10.1002/\(SICI\)1096-9845\(199610\)25:10<1109::AID-EQE604>3.0.CO;2-0](https://doi.org/10.1002/(SICI)1096-9845(199610)25:10<1109::AID-EQE604>3.0.CO;2-0)
- Parisi, F., Scalvenzi, M., & Brunesi, E. (2019). Performance limit states for progressive collapse analysis of reinforced concrete framed buildings. *Structural Concrete*, 20(1), 68–84. <https://doi.org/10.1002/suco.201800039>
- Payá-Zaforteza, I., & Garlock, M. E. M. (2012). A numerical investigation on the fire response of a steel girder bridge. *Journal of Constructional Steel Research*, 75, 93–103. <https://doi.org/10.1016/j.jcsr.2012.03.012>
- Pearson, C., & Delatte, N. (2006). Collapse of the Quebec Bridge, 1907. *Journal of Performance of Constructed Facilities*, 20(1), 84–91. [https://doi.org/10.1061/\(ASCE\)0887-3828\(2006\)20:1\(84\)](https://doi.org/10.1061/(ASCE)0887-3828(2006)20:1(84))
- Pelle, A., Briseghella, B., Bergami, A. V., Fiorentino, G., Giaccu, G. F., Lavorato, D., et al. (2022). Time-dependent cyclic behavior of reinforced

- concrete bridge columns under chlorides-induced corrosion and rebars buckling. *Structural Concrete*, 23(1), 81–103. <https://doi.org/10.1002/suco.202100257>
- Peng, G.-F., Bian, S.-H., Guo, Z.-Q., Zhao, J., Peng, X.-L., & Jiang, Y.-C. (2008). Effect of thermal shock due to rapid cooling on residual mechanical properties of fiber concrete exposed to high temperatures. *Construction and Building Materials*, 22(5), 948–955. <https://doi.org/10.1016/j.conbuildmat.2006.12.002>
- Peng, W., Dai, F., & Taciroglu, E. (2014). Research on Mechanism of Overturning Failure for Single-Column Pier Bridge. In *Computing in Civil and Building Engineering (2014)* (pp. 1747–1754). Reston, VA: American Society of Civil Engineers. <https://doi.org/10.1061/9780784413616.217>
- Peng, W., Zhao, H., Dai, F., & Taciroglu, E. (2017). Analytical Method for Overturning Limit Analysis of Single-Column Pier Bridges. *Journal of Performance of Constructed Facilities*, 31(4). [https://doi.org/10.1061/\(ASCE\)CF.1943-5509.0000999](https://doi.org/10.1061/(ASCE)CF.1943-5509.0000999)
- Perdomo, C., Abarca, A., & Monteiro, R. (2022). Estimation of Seismic Expected Annual Losses for Multi-Span Continuous RC Bridge Portfolios Using a Component-Level Approach. *Journal of Earthquake Engineering*, 26(6), 2985–3011. <https://doi.org/10.1080/13632469.2020.1781710>
- Pereira, S. S. R., Carvalho, H., Mendes, V. R. V., & Montenegro, P. A. (2020). Assessment of the 2014 structural collapse of Batalha dos Guararapes viaduct, Brazil. *Proceedings of the Institution of Civil Engineers-Forensic Engineering*, 172(4), 150–157.
- Pinto, P. E., & Franchin, P. (2010). Issues in the Upgrade of Italian Highway Structures. *Journal of Earthquake Engineering*, 14(8), 1221–1252. <https://doi.org/10.1080/13632461003649970>
- Priestley, M. J. N. (1988). The Whittier Narrows, California Earthquake of October 1, 1987—Damage to the I-5/I-605 Separator. *Earthquake Spectra*, 4(2), 389–405. <https://doi.org/10.1193/1.1585481>
- Priestley, M. J. N., Verma, R., & Xiao, Y. (1994). Seismic Shear Strength of Reinforced Concrete Columns. *Journal of Structural Engineering*, 120(8), 2310–2329. [https://doi.org/10.1061/\(ASCE\)0733-9445\(1994\)120:8\(2310\)](https://doi.org/10.1061/(ASCE)0733-9445(1994)120:8(2310))
- Pujol M.E.; Monical, J.D.; and Schultz, A.E., S. . K. (n.d.). Investigation of the Collapse of the Chirajara Bridge. *Concrete International*, 41(6).
- R., M. K., & G., N. B. (2022, November 26). Uncertainty Quantification in Analytical Bridge Fragility Curves. *TCLÉE 2009*. [https://doi.org/doi:10.1061/41050\(357\)9](https://doi.org/doi:10.1061/41050(357)9)
- Raithel. (1977). *Costruzioni di ponti (in Italian)* (Liguori ed.). Napoli.
- Raithel. (1978). *Ponti a travata (in Italian)*. (Liguori editore, Ed.). Napoli.
- RD 16/11/1939, n. 2229. Norme per l'esecuzione delle opere in conglomerato cementizio semplice od armato (in Italian). (1939). Rome, Italy.

- Robertson, I. N., Riggs, H. R., Yim, S. C., & Young, Y. L. (2007). Lessons from Hurricane Katrina Storm Surge on Bridges and Buildings. *Journal of Waterway, Port, Coastal, and Ocean Engineering*, 133(6), 463–483. [https://doi.org/10.1061/\(ASCE\)0733-950X\(2007\)133:6\(463\)](https://doi.org/10.1061/(ASCE)0733-950X(2007)133:6(463))
- Salem, H. M., & Helmy, H. M. (2014). Numerical investigation of collapse of the Minnesota I-35W bridge. *Engineering Structures*, 59, 635–645. <https://doi.org/10.1016/j.engstruct.2013.11.022>
- Sanabra-loewe, M., & Capellà-llovera, J. (2014). The four ages structures. *PCI Journal*, 59(4), 93–121.
- Santarsiero, G., Masi, A., Picciano, V., & Digrisolo, A. (2021). The Italian Guidelines on Risk Classification and Management of Bridges: Applications and Remarks on Large Scale Risk Assessments. *Infrastructures*, 6(8), 111. <https://doi.org/10.3390/infrastructures6080111>
- Scanlan, R. H. (1998). Bridge Flutter Derivatives at Vortex Lock-In. *Journal of Structural Engineering*, 124(4), 450–458. [https://doi.org/10.1061/\(ASCE\)0733-9445\(1998\)124:4\(450\)](https://doi.org/10.1061/(ASCE)0733-9445(1998)124:4(450))
- Schenk, O., & Gärtner, K. (2004). Solving unsymmetric sparse systems of linear equations with PARDISO. *Future Generation Computer Systems*, 20(3), 475–487. <https://doi.org/10.1016/j.future.2003.07.011>
- Shome, N., & Cornell, C. A. (2000). Structural seismic demand analysis: Consideration of collapse. *8th ACSE Specialty Conference on Probabilistic Mechanics and Structural Reliability*, (3), PMC2000-119. http://www.rms-group.org/rms_papers/pdf/nilesh/pmc.pdf
- Silva V, Crowley H, C. M. (2014). Fragility function manager tool. In *In: SYNER-G: typology definition and fragility functions for physical elements at seismic risk*, Springer. <https://doi.org/10.1007/978-94-007-7872-6>
- SMITH, D. (1976). BRIDGE FAILURES. *Proceedings of the Institution of Civil Engineers*, 60(3), 367–382. <https://doi.org/10.1680/iicep.1976.3389>
- Smith, M. (2009). *ABAQUS/Standard User's Manual*.
- Starossek, U. (2007). Typology of progressive collapse. *Engineering Structures*, 29(9), 2302–2307. <https://doi.org/10.1016/j.engstruct.2006.11.025>
- Stefanidou, S. P. (2017). Software for Bridge-Specific Fragility Analysis. *MOJ Civil Engineering*, 3(5), 351–357. <https://doi.org/10.15406/mojce.2017.03.00081>
- Stefanidou, S. P., & Kappos, A. J. (2017). Methodology for the development of bridge-specific fragility curves. *Earthquake Engineering and Structural Dynamics*, 46(1), 73–93. <https://doi.org/10.1002/eqe.2774>
- Stefanidou, S. P., & Kappos, A. J. (2021). Fragility-informed selection of bridge retrofit scheme based on performance criteria. *Engineering Structures*, 234(February), 111976. <https://doi.org/10.1016/j.engstruct.2021.111976>
- Stefanidou, S. P., Paraskevopoulos, E. A., Papanikolaou, V. K., & Kappos, A. J.

- (2022). An online platform for bridge-specific fragility analysis of as-built and retrofitted bridges. *Bulletin of Earthquake Engineering*, 20(3), 1717–1737. <https://doi.org/10.1007/s10518-021-01299-3>
- Strade & Autostrade. La messa in sicurezza dei ponti italiani. (2021). <https://www.stradeeautostrade.it/ponti-e-viadotti/la-messa-in-sicurezza-dei-ponti-italiani/>
- Structures, C. and. (n.d.). SAP2000: integrated finite element analysis and design of structures: basic analysis reference.
- Sun, Z., Wang, D., Guo, X., Si, B., & Huo, Y. (2012). Lessons Learned from the Damaged Huilan Interchange in the 2008 Wenchuan Earthquake. *Journal of Bridge Engineering*, 17(1), 15–24. [https://doi.org/10.1061/\(ASCE\)BE.1943-5592.0000210](https://doi.org/10.1061/(ASCE)BE.1943-5592.0000210)
- TAGEL-DIN, H., & MEGURO, K. (2000). NONLINEAR SIMULATION OF RC STRUCTURES USING APPLIED ELEMENT METHOD. *Doboku Gakkai Ronbunshu*, 2000(654), 13–24. https://doi.org/10.2208/jscej.2000.654_13
- Takahashi, T. (1978). Mechanical Characteristics of Debris Flow. *Journal of the Hydraulics Division*, 104(8), 1153–1169. <https://doi.org/10.1061/JYCEAJ.0005046>
- Torbol, M. (2011). Effect of Directionality of Multi-Component Ground Motions on Bridge Fragility Curves.
- Veletzos, M. J., & Restrepo, J. I. (2011). Modeling of Jointed Connections in Segmental Bridges. *Journal of Bridge Engineering*, 16(1), 139–147. [https://doi.org/10.1061/\(asce\)be.1943-5592.0000112](https://doi.org/10.1061/(asce)be.1943-5592.0000112)
- Vereecken, E., Botte, W., Lombaert, G., & Caspeele, R. (2021). Assessment of corroded prestressed and posttensioned concrete structures: A review. *Structural Concrete*, 22(5), 2556–2580. <https://doi.org/10.1002/suco.202100050>
- Vu, N. A., Castel, A., & François, R. (2010). Response of post-tensioned concrete beams with unbonded tendons including serviceability and ultimate state. *Engineering Structures*, 32(2), 556–569. <https://doi.org/10.1016/j.engstruct.2009.11.001>
- Walton, C. M., Yu, C., & S, S. R. (n.d.). an Assessment of Recent State Truck Size and Weight Studies Summary Report 241-4 (S), (July 1982), 3–5.
- Wang, Z., Dueñas-Osorio, L., & Padgett, J. E. (2013). Seismic response of a bridge-soil-foundation system under the combined effect of vertical and horizontal ground motions. *Earthquake Engineering & Structural Dynamics*, 42(4), 545–564. <https://doi.org/10.1002/eqe.2226>
- Wardhana, K., & Hadipriono, F. C. (2003). Analysis of Recent Bridge Failures in the United States. *Journal of Performance of Constructed Facilities*, 17(3), 144–150. [https://doi.org/10.1061/\(asce\)0887-3828\(2003\)17:3\(144\)](https://doi.org/10.1061/(asce)0887-3828(2003)17:3(144))
- Warn, G. P., & Whittaker, A. S. (2008). Vertical Earthquake Loads on Seismic Isolation Systems in Bridges. *Journal of Structural Engineering*, 134(11),

- 1696–1704. [https://doi.org/10.1061/\(ASCE\)0733-9445\(2008\)134:11\(1696\)](https://doi.org/10.1061/(ASCE)0733-9445(2008)134:11(1696))
- Werner, S. D., Taylor, C. E., Cho, S., Lavoie, J., Huyck, C., Eitzel, C., et al. (2006). Redars 2 Methodology and software for seismic risk analysis of highway systems. *Special Report MCEER-06-SP08*, 148.
- Wiśniewski, D. F., Cruz, P. J. S., Henriques, A. A. R., & Simões, R. A. D. (2012). Probabilistic models for mechanical properties of concrete, reinforcing steel and pre-stressing steel. *Structure and Infrastructure Engineering*, 8(2), 111–123. <https://doi.org/10.1080/15732470903363164>
- Witzany, J., Cejka, T., & Zigler, R. (2008). Failure Resistance of Historic Stone Bridge Structure of Charles Bridge. II: Susceptibility to Floods. *Journal of Performance of Constructed Facilities*, 22(2), 83–91. [https://doi.org/10.1061/\(ASCE\)0887-3828\(2008\)22:2\(83\)](https://doi.org/10.1061/(ASCE)0887-3828(2008)22:2(83))
- Xu, F. Y., Zhang, M. J., Wang, L., & Zhang, J. R. (2016). Recent Highway Bridge Collapses in China: Review and Discussion. *Journal of Performance of Constructed Facilities*, 30(5). [https://doi.org/10.1061/\(ASCE\)CF.1943-5509.0000884](https://doi.org/10.1061/(ASCE)CF.1943-5509.0000884)
- Yang, J., & Lee, C. M. (2007). Characteristics of vertical and horizontal ground motions recorded during the Niigata-ken Chuetsu, Japan Earthquake of 23 October 2004. *Engineering Geology*, 94(1–2), 50–64. <https://doi.org/10.1016/j.enggeo.2007.06.003>
- Yi, R., Zhou, R., & Huang, X. (2015). Reason and risk of bridge collapse in recent 15 years. *Transp. Sci. Technol*, 5, 61–64.
- Yi, Z., Agrawal, A. K., Ettouney, M., & Alampalli, S. (2014a). Blast Load Effects on Highway Bridges. I: Modeling and Blast Load Effects. *Journal of Bridge Engineering*, 19(4). [https://doi.org/10.1061/\(ASCE\)BE.1943-5592.0000547](https://doi.org/10.1061/(ASCE)BE.1943-5592.0000547)
- Yi, Z., Agrawal, A. K., Ettouney, M., & Alampalli, S. (2014b). Blast Load Effects on Highway Bridges. II: Failure Modes and Multihazard Correlations. *Journal of Bridge Engineering*, 19(4). [https://doi.org/10.1061/\(ASCE\)BE.1943-5592.0000548](https://doi.org/10.1061/(ASCE)BE.1943-5592.0000548)
- Zhang, G., Liu, Y., Liu, J., Lan, S., & Yang, J. (2022). Causes and statistical characteristics of bridge failures: A review. *Journal of Traffic and Transportation Engineering (English Edition)*, 9(3), 388–406. <https://doi.org/10.1016/j.jtte.2021.12.003>
- Zhang, X., Wang, L., Zhang, J., Ma, Y., & Liu, Y. (2017). Flexural behavior of bonded post-tensioned concrete beams under strand corrosion. *Nuclear Engineering and Design*, 313, 414–424. <https://doi.org/10.1016/j.nucengdes.2017.01.004>
- Zhao, S. J., Tang, X. B., & Ren, W. X. (2017). The Statistical Characteristics Analysis of Bridge Accidents and Prevention Principle of Security Risk. *Journal of Railway Engineering Society*, 34(05), 59–64.
- Zorzi. (1981). *Ponti e Viadotti (in Italian)*. (D. L. E. D'arte., Ed.).